THIAPORPHYRINS AND METALLOTHIAPORPHYRINS ; SYNTHESIS AND SPECTROSCOPIC STUDIES IN GROUND, EXCITED SINGLET AND TRIPLET STATES

A Thesis Submitted
in Partial Fulfilment of the Requirements
for the Degree of
DOCTOR OF PHILOSOPHY

By

R. PUTHISIGAMANI PANDIAN

to the

DEPARTMENT OF CHEMISTRY

INDIAN INSTITUTE OF TECHNOLOGY KANPUR

APRIL, 1993

Dedicated
to
my
Parents

STATEMENT

I hereby declare that the matter embodied in this thesis, "Thiaporphyrins and Metallothiaporphyrins; Synthesis and Spectroscopic Studies in Ground, Excited Singlet and Triplet States", is the result of investigations carried out by me in the Department of Chemistry, Indian Institute of Technology, Kanpur, India under the supervision of Dr. T.K. Chandrashekar.

In keeping with the general practice of reporting scientific observations, due acknowledgement has been made wherever the work described is based on the findings of other investigators.

R. Puthisigamani Pandian

R. PUTHISIGAMANI PANDIAN

Kanpur

April, 1993

CERTIFICATE

It is certified that the work contained in the thesis entitled, "**Thiaporphyrins and Metallothiaporphyrins; Synthesis and Spectroscopic Studies in Ground, Excited Singlet and Triplet States**", by **R. PUTHISIGAMANI PANDIAN**, has been carried out under my supervision and same has not been submitted elsewhere for a degree.

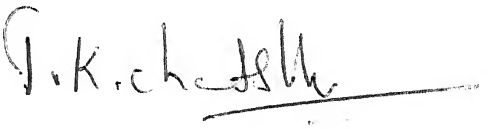

(T.K. Chandrashekar)
Thesis Supervisor
Department of Chemistry
Indian Institute of Technology
Kanpur-208016, India

Kanpur
April, 1993

DEPARTMENT OF CHEMISTRY

INDIAN INSTITUTE OF TECHNOLOGY KANPUR, INDIA

CERTIFICATE OF COURSE WORK

This is to certify that **R. PUTHISIGAMANI PANDIAN** has satisfactorily completed all the courses required for the Ph.D. degree. The courses include:

CHM 605	Principles of Organic Chemistry
CHM 624	Modern Physical Methods in Chemistry
CHM 625	Principles of Physical Chemistry
CHM 645	Principles of Inorganic Chemistry
CHM 646	Bio-Inorganic Chemistry
CHM 668	Advanced Inorganic Chemistry II
CHM 800	General Seminar
CHM 801	Special Seminar
CHM 900	Post-graduate Research

R. Puthisigamani Pandian was admitted to the candidacy of the Ph.D. degree in March 1990 after he successfully completed the written and oral qualifying examinations.

P. K. Ghosh

(P.K. Ghosh)
Head
Department of Chemistry
I.I.T. Kanpur

Y.D. Vankar

(Y.D. Vankar)
Convenor
Departmental Post-graduate
Committee, Dept. of Chemistry
I.I.T. Kanpur

ACKNOWLEDGEMENTS

I take this opportunity to place on record my deep sense of gratitude to my thesis supervisor, Dr. T.K. Chandrashekar, for guiding me and giving constant encouragement throughout the course of this work. It is my privilege and pleasure to be a member of his research group. His novel ideas and concepts have helped me in shaping my attitude towards the subject and carrying out this small piece of work.

I thank,

.....Dr. V. Chandrasekhar, for kind words during my times of trouble,

.....Profs. G. Sivasubramaniam, Sevaga pandian, Sivasamy Alagappan and Dr. Kannan, ANJAC College, Sivakasi for encouraging me to take up a chemistry carrier,

.....Dr. N.S. Gajbhiye, for his keen interest in my work and kind help,

.....Prof. S. Sarkar and Dr. R.N. Mukherjee for allowing me to do cyclic voltammetric measurements,

.....Prof. Hans van Willigen, Department of Chemistry, University of Massachusetts, Harbor Campus, Boston, USA for providing me the photoexcited triplet ESR spectra of thiaporphyrins.

.....Prof. N. Periasamy, Chemical Physics group, TIFR, Bombay, for his help in doing all the fluorescence life time measurements.

.....Prof. A.L. Verma, NEHU, Shillong, for providing me the Resonance Raman spectra of thiaporphyrins,

.....Mr. Visvakarma, CDRI, Lucknow, for recording the fluorescence spectra.

.....Dr. N. Chidambaram, for his help at the initial stages of this work.

.....My labmates Damodar Reddy, Ravi Kanth, Ravi Kumar, Kuljeet Singh, Immie and Justin for their cooperation and pleasant association,

.....Drs. P.K. Chaudhury, Z. Shirin and K. Ramesh for their help in cyclic voltammetric measurements.

.....Drs. A. Ramamoorthy and S.R. Pandian, for all the help rendered by them,

.....Messrs Ilango, Govind, Murali, Sampath, Srinivasan, Mano Ravi, Ramesh Rao, Sivakumar, Punniya Murthy,Kannan and Navaneetha Krishnan, for their cooperation in organizing the thesis in its final form,

.....all my colleagues and friends, for their co-operation during the course of this investigations,

.....my Appa, Amma and Annan for their unfailing love, encouragement and the trouble taken by them to make me what I am today,

.....and the Government of India for financing my education all these years.

Pandian

TABLE OF CONTENTS

SYNOPSIS

The thesis entitled, **"THIAPORPHYRINS AND METALLO-THIAPORPHYRINS ; SYNTHESIS AND SPECTROSCOPIC STUDIES IN GROUND, EXCITED SINGLET AND TRIPLET STATES"**, has been divided into six chapters.

An overview of the literature work on various aspects such as synthesis, X-ray structure, spectral characterization and electronic structure are described in chapter one. In addition, the similarities between the spectral behaviour of the metallothiaporphyrins and metallo N-substituted Porphyrins are highlighted.

The second chapter describes the general experimental techniques and methods employed for the evaluation of physical parameters. There are four sections. Section 1 gives the details of the chemicals and purification methods employed. Section 2 describes the synthesis of precursor compounds for various porphyrins reported in this thesis. In section 3, a brief outline of the physico-chemical techniques employed and details of the instruments used are given. In section 4, the methods of calculation of physical parameters are given.

The third chapter describes the spectroscopic studies on thiaporphyrins and their protonated derivatives. This has been divided into two parts. Part A describes the ground state properties of thiaporphyrins and their protonated derivatives. The excited state properties of the thiaporphyrins measured using Resonance Raman, fluorescence and photoexcited triplet ESR methods are described in Part B. A brief summary of the results obtained in this chapter is given below.

Electronic absorption spectra of these macrocycles show porphyrin like behaviour with strong soret band and weak Q bands. Substitution of the -NH groups of tetraphenylporphyrin ($TPPH_2$) by sulfur causes a red shift of all the absorption bands and the magnitude of the red shift depends on the number of sulfur atoms substituted. The dications of both mono and dithiaporphyrins show larger bathochromic shift of Q bands relative to $TPPH_2$, indicating a stronger resonance interaction with the phenyl groups. Electrochemical data indicate harder oxidations and easier reductions of thiaporphyrins relative to $TPPH_2$. ^1H NMR studies reveal the presence of two fold axis of symmetry in dithiaporphyrins while the reduced symmetry of monothiaporphyrin are reflected in inequivalence of pyrrole signals.

The Resonance Raman spectra show shifts of various structurally sensitive Raman modes to both higher and lower frequencies upon protonation. An analysis of these shifts reveal that the dications have predominantly an A_{2u} ground state. A linear correlation has been obtained between structurally sensitive Raman bands (ν_2, ν_4, ν_{10}, ν_{11}) with energy of the lowest Q band. The emission data indicate considerable quenching of fluorescence of thiaporphyrins and the magnitude of quenching and the red shift of emission bands are shown to be depend on the number of sulfur atoms in the porphyrin core. The estimated excited state potentials suggest that thiaporphyrins are better electron donors in the first singlet excited state. A comparison of magnitude of Zero Field Splitting (ZFS) parameters (D and E) of neutral thiaporphyrins with $TPPH_2$ indicates no significant alterations in the triplet spin density. However, the protonated derivatives show large decrease in D(30-40 %) and E(40-50 %)

values. The Electron Spin Polarization (ESP) pattern indicate dominance of in-plane spin sublevel with respect to population and decay process for neutral species while a redirection of spin sublevel activity is observed for protonated species. The structural change accompanying the protonation process accounts for most of these observations.

Chapter four describes the synthesis and characterization of two water soluble thiaporphyrins; tetrakis (4-sulfonato phenyl)-21-thiaporphyrin and tetrakis (4-sulfonato phenyl)-21-23-dithiaporphyrin (S_2TPPS) and Cu^{2+} and Ni^{2+} derivatives of STPPS (CuSTPPSCl and NiSTPPSCl). Both STPPS and S_2TPPS show aggregation in aqueous solution. Addition of cation and crown ether to a dilute monomeric solution of STPPS and S_2TPPS results in a cofacial dimer formation similar to those observed for normal anionic water soluble porphyrins. The electronic absorption spectra of both metal derivatives show split soret band and a complex pattern of Q bands due to reduced symmetry. Both the metal derivatives are paramagnetic. The fluorescence of STPPS and S_2TPPS are quenched considerably and the magnitude of quenching depends on the number of sulfur atoms in the porphyrin core. Electrochemical studies indicate harder oxidations and easier reductions for STPPS and S_2TPPS relative to H_2TPPS (Tetrakis (4-sulfonato phenyl) porphyrin). The first electron addition to CuSTPPSCl and NiSTPPSCl results in the reduction of the metal center suggesting that the metal $d_{x^2-y^2}$ orbital is lower in energy than the empty porphyrin $e_g(\pi^*)$ orbitals in contrast to those observed for CuTPPS and NiTPPS.

Triplet state characteristics such as Zero Field Splitting (ZFS) parameters (D and E) and Electron Spin Polarization (ESP)

pattern of STPPS and S_2TPPS remain same as in analogous H_2TPPS. This is possibly due to similarities in the structure of the porphyrin core of STPPS, S_2TPPS and H_2TPPS. However, there is a strong dimerization effect on the D value similar to those observed for dimerization of H_2TPPS. The exciton model with some contribution from charge transfer can account for the observed dimerization induced changes in the ZFS parameters for thiaporphyrins.

Chapter five describes the synthesis, characterization and spectral behaviour of a unique diporphyrin containing a normal porphyrin subunit with N_4 core and thiaporphyrin subunit containing a N_3S core linked via (pentoxy) chain (Figure). This unique diporphyrin offers an opportunity to synthesise bimetallic derivatives having same metal and different metals in the porphyrin cores. The free base diporphyrin (H_2-H) and Zn^{+2} - free base thiaporphyrin (Zn-H), Zn^{+2} - Cu^{+2} thiaporphyrin (Zn-Cu) and

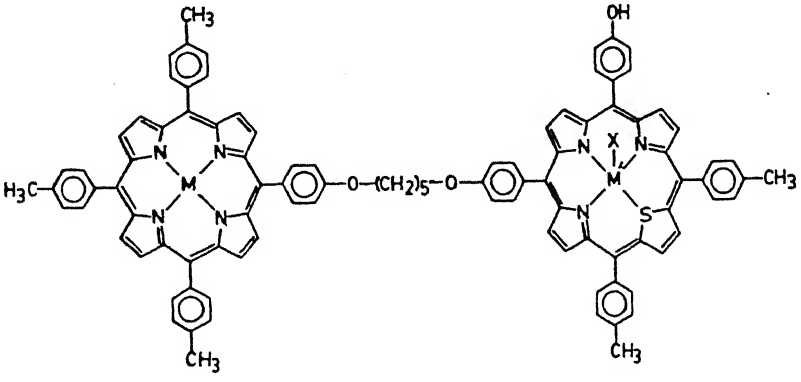

M = 2H ; M′= H ; H_2 – H Diporphyrin 3
M = Zn^{+2}; M′= H ; Zn – H Diporphyrin 4
M = Zn^{+2}; M′= Cu^{+2}; X=Cl ; Zn-Cu Diporphyrin 5
M = Ni^{+2} ; M = Ni^{+2}; X=Cl ; Ni-Ni Diporphyrin 6

Ni^{2+} - Ni^{+2} thiaporphyrin (Ni-Ni) diporphyrins have been characterized using ^{1}HNMR, FAB Mass, EPR, optical absorption and fluorescence spectroscopy. The absorption spectral data and electrochemical data show only weak interactions between porphyrin

subunits in Zn-H and H_2-H diporphyrins. However, a blue shift and quenching of absorbance of both Q and soret bands of bimetallic diporphyrins (Zn-Cu), a positive shift for oxidation and reduction potentials of zinc normal porphyrin subunit in Zn-Cu diporphyrin indicate substantial interaction between normal and thiaporphyrin subunits. The electrochemical data of the bimetallic diporphyrins (Zn-Cu and Ni-Ni) shows that first reduction is metal centered (the metal present in thiaporphyrin subunit) suggesting the reversal of order of energy levels of metal $d_{x^2-y^2}$ and the porphyrin $e_g(\pi^*)$ orbitals similar to that observed for monomeric metallothiaporphyrins. The first electron addition in Zn-Cu and Ni-Ni bimetallic diporphyrins results in the reduction of the metal center corresponding to the formation of Zn^{2+}-Cu^{+1} and Ni^{2+}-Ni^{+1} diporphyrins. This offers an opportunity to stabilise the two different oxidation states of the same metal in single diporphyrin unit. Preliminary results on chemical reduction using mild reducing agents are quite encouraging.

Chapter six gives the summary of the investigations carried out in this thesis.

CHAPTER 1

1.1.0 GENERAL INTRODUCTION

Studies on porphyrins and metalloporphyrins have received attention of many investigators because of their involvement in diverse biological systems. In particular, heme proteins have been investigated on multi-and interdisciplinary levels. These proteins, all containing an iron porphyrin as the prosthetic group, are responsible for oxygen transport and storage (hemoglobin and myoglobin)[1], electron transport (cytochrome b,c)[2], oxygen reduction (cytochrome oxidase)[3] and hydrogen peroxide utilization and destruction (peroxidases and catalases)[4]. In each of these cases, the nitrogens of the porphyrin ring (usually protoporphyrin) are coordinated to iron essentially in a planar core. Therefore their diversity of function must be dictated by the number and the nature of the axial ligands, the spin and oxidation states of the iron and nature of the polypeptide chain.

Biological oxidations by heme enzymes can be classified as follows: oxygenations of organic substrates catalysed by cytochrome P_{450}[5], oxidations by peroxidases[6], oxidative halogenations by chloroperoxidases[7] and hydrogen peroxide dismutation[8,4] by catalase.

A considerable effort has been put in towards the developments of new generation of synthetic porphyrins which are able to reproduce and mimic different heme enzyme mediated reactions such as oxygenation, oxidation, oxidative chlorination and dismutation.[5,7]

Among the synthetic porphyrins, meso tetraarylporphyrins ($TPPH_2$) and their metal derivatives have been extensively used as catalyst for oxidation reactions mediated by PhIO. This is because the flat porphyrins such as protoporphyrin IX, or octaethylporphyrin with no substituents at meso positions are more reactive towards meso cleavage via the formation of a meso-hydroxyporphyrin derivative.[9] Not only iron, but also chromium[10] and manganese TPP complexes[11,12] are capable of catalyzing the oxygen atom transfer from PhIO to an olefin or an alkane.

The metal derivatives of $TPPH_2$ constitute the first generation of metalloporphyrin catalysts used in oxygenation reactions. The second generation of tetraarylporphyrins is represented by meso-tetrakis (pentafluorophenyl) porphyrin (H_2TPFPP)[13], mesotetra mesityl porphyrin (H_2TMP)[14,15] and mesotetrakis (2,6-dichlorophenyl) porphyrin (H_2TDCPP)[16,17] and related ligands where alkyl or halogen substituents have been introduced at ortho, meta or para positions of the phenyl groups. This will not only provide steric effect (cage effect) to avoid the formation of catalytically inactive μ-oxo complexes but also will enhance the electrophilicity of the metal-oxo entity.

The third generation is an extension of the previous idea by having bromine, chlorine or fluorine at the β-position of pyrroles such as meso tetrakis (2,6-dichloro phenyl)-β-octabromo porphyrin (H_2Br_8TDCPP)[18], meso-tetrakis (2,6-dichloro phenyl)β-octa chloro porphyrin (H_2Cl_8TDCPP)[19], meso-tetramesityl-β-octabromo porphyrin H_2Br_8TMP[20],meso-tetrakis (2,4,6-trimethyl-3-chloro phenyl)-β-octa-chloro porphyrin ($H_2Cl_{12}TMP$)[20a] and meso-tetrakis (penta fluorophenyl)-β-octafluoro porphyrin (H_2F_8TPFPP).[21]

Nature prefers unsymmetrical arrangement of substituents in nearly all cases. Thus, the preparation and study of unsymmetrical porphyrins and expanded porphyrins remain of interest. Some examples of expanded porphyrins are sapphyrins and samaragdrins by Broadhurst, Grigg and Sessler[22], pentaphyrins and hexaphyrins by Gossauer et al[23], expanded phthalocyanines by Wachter et al[24], platyrins by LeGoff et al[25], vinylogous porphyrins by Franck et al[26], stretched porphycenes by Vogel et al[27], texaphyrins by Sessler[28] and non-aromatic large pyrrole containing macrocycles by Acholla et al.[29a,b] These expanded porphyrins could provide important information on the fundamental and interrelated questions of ring size, aromaticity and effective macrocycle stability as well as providing an important entry into the development of improved photosensitizers etc.

Another attractive modification in the TPP molecule would be to change the immediate environment around the central metal atom, which means to replace the nitrogens by other hetero atoms such as sulfur, oxygen, selenium, tellurium etc. This provides an attractive core modification and their insertions into the porphyrin core is expected to change the electronic environment of the porphyrin π-system. Further substitution of nitrogen by bigger heteroatoms reduces the porphyrin ring core size. Thus a series of sulfur containing porphyrins mono- di- and tetra thiaporphyrins constitute a group of core modified porphyrins where the core size is systematically varied. These core modified thiaporphyrins provide an opportunity to study the coordination abilities of the thiophene moiety, the geometric constrains imposed by macrocycle as well as the multiplicity of possibilities (S-bound or η^5 bound) available for metal/thiophene

coordination. Moreover, thiophene-transition metal bond appears to be relatively weak but very important to the process of hydro desulfurization.[29c,d] Therefore, it is of interest to examine the effect of the thiophene ring substitution in the porphyrin ring on the coordination of metal ions.

These core modified thiaporphyrins are the subject of this thesis.Specifically, mono- and di- thiaporphyrins have been synthesised and characterized. Their ground state and excited state properties are systematically studied to understand the effect of core modification on the electronic structure of the porphyrin core. This thesis is divided into three parts as follows. Part I describes the ground state properties measured by electronic absorption and electrochemical methods in the non aqueous solvents. Furthermore the excited singlet and triplet state properties measured by fluorescence and photoexcited triplet ESR methods in nonaqueous medium are also included. In order to evaluate the behaviour of the thiaporphyrins in the aqueous medium, water soluble thiaporphyrins have been synthesised and characterized for the first time. Part II of this thesis describes the synthesis, characterization, ground and excited state properties of these porphyrins in the aqueous medium. Part III of this thesis describes synthesis, characterization, and spectral properties of a unique diporphyrin in which normal porphyrin unit is covalently linked through the meso phenyl rings to a monothiaporphyrin. This unique diporphyrin contains two different hetero cores (N_4 and N_3S) and this provides an opportunity to coordinate different metal ions to two different porphyrin cores. Thus for example Zn^{+2} ion can be introduced to the normal porphyrin subunit while Cu^{+2} or Ni^{+2} can be introduced

to the thiaporphyrin subunit resulting in a Zn^{+2} - Cu^{2+} or Zn^{+2}-Ni^{+2} diporphyrin.

Before a detailed discussion of the results of this thesis is presented, a brief survey of various aspects of thiaporphyrin chemistry reported in literature is presented in the following sections. It is pertinent to point out here that most of the work reported on different aspects of thiaporphyrin chemistry in literature overlaps with our studies since we started the work described in this thesis in 1988.

1.2.0 Development of synthetic methodology of hetero atom substituted porphyrins

The general synthesis of unsymmetrically substituted TPP molecules have been given by Adler and coworkers[30] and the conditions for optimal yield[31] and purity have been studied. Synthesis of unsymmetrical phenyl substituted TPP molecules were reported by Little et al[32]. In this work a mixture of aldehydes were reacted with pyrrole in propionic acid to give a mixture of three porphyrins (two symmetrically phenyl substituted porphyrins and one unsymmetrically phenyl substituted porphyrin) which were then separated by chromatography. A step wise synthesis of unsymmetrical porphyrins was described by Haris et al. for meso porphyrins, rhodoporphyrins and γ-phyloporphyrins.[33] However there were no reports on the synthesis of core modified heteroatom porphyrins till 1971.

In 1971, the first synthesis of heteroatom substituted porphyrins was reported by Broadhurst and Grigg[34]. They used a [3+1] cyclisation approach to prepare the heteroatom substituted porphyrins. A number of general methods are available for

construction of the porphyrin ring.[35] These are based on the combination of two units, each containing two pyrrole rings to give a linear (uncyclised) tetrapyrrole rings, which is then either isolated and cyclised to a porphyrin in a separate step, or allowed to undergo spontaneous cyclisation to a porphyrin.

Broadhurst et. al. selected two approaches for the incorporation of furan and thiophene rings into porphyrin: (i) known as oxidative cyclisation of 1,19-dideoxy-1,19-biladienes-ac (I)[33,36] and (ii) modification of a MacDonald porphyrin synthesis.[37]

In the first method, 2-formyl furans (R=H, or Me) (II) and dipyrromethane 5,5'-dicarboxylic acid (III) (Fig. 1.1) are condensed in the presence of a variety of acidic catalysts. The visible spectra of crude products of this method resemble those of 1,19-dideoxy biladienes ac salts. Then attempts were made to cyclise the crude product directly using formic acid or formic acid and Cu(II) acetate but in both cases the required macrocycle was not isolated. Similar results were obtained from analogous reactions in the thiophene series.[36]

$$\text{II} + \text{III} \xrightarrow{\text{acid catalyst}} \text{IV} \xrightarrow[\text{Complex mixture}]{\text{attempted cyclisation}} \text{No products}$$

Synthesis of 1,19-dideoxy biladiene-ac containing one furan ring (V) (Fig. 1.1) was attempted by a $SnCl_4$-catalysed Friedal-Crafts coupling using the bromo methyl dipyrromethene (VI) (Fig. 1.1) with the furyl pyrro methane (VII) but again complex mixture of products were isolated.

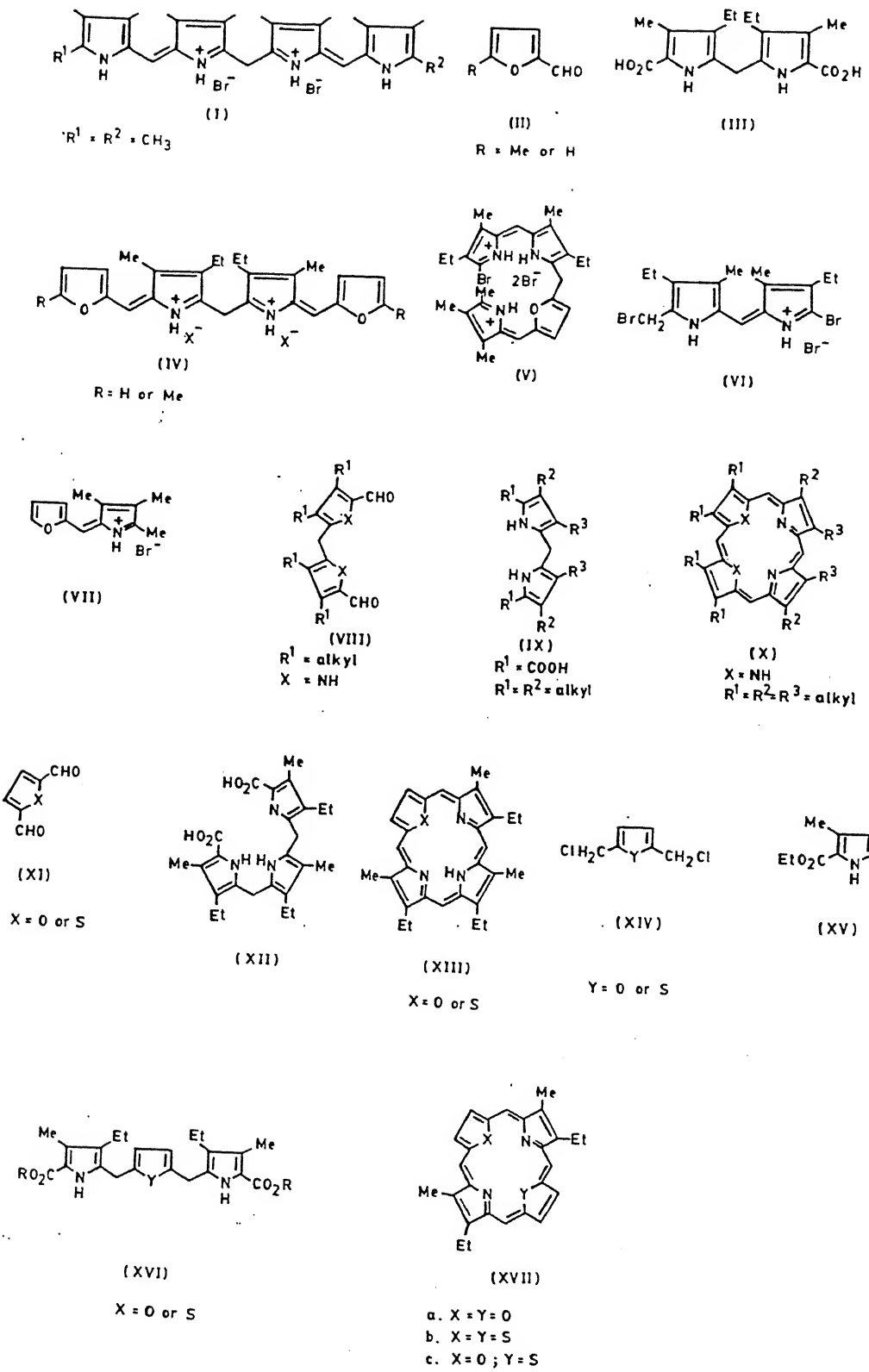

Fig.1.1 Molecular structure of porphyrins and some intermediate

$$VI + VII \xrightarrow[SnCl_4\text{-Friedal-Craft coupling}]{} V \text{ complex mixture} \xrightarrow{\text{attempted cyclization}} \text{No products}$$

1,19-dideoxy biladiene-ac method fail to form a hetero atom substituted porphyrins. Then, Broadhurst et al[34] extended the modified MacDonald[37] porphin synthesis.

MacDonald synthesis[37] involves the acid catalysed condensation of 5,5'-diformyl dipyrromethane (VIII) (X=NH, R^1 = alkyl) (Fig. 1.1) and dipyrromethane (IX) (R^1 = H or COOH, R^2 = R^3= alkyl) (Fig. 1.1) to give the corresponding porphin (X) (Fig. 1.1). Same strategy was used to make the dioxaporphyrins (X= O, $R^1 = R^2 = R^3$ = alkyl)

$$VIII + IX \xrightarrow[2)\ [O]]{1)\ H^+} X$$

Broadhurst et al[34] selected a [3+1] approach to the synthesis of porphins containing one or two furan and / or thiophene rings. Eventhough the method was developed by them[34], it was an extension of the MacDonald route synthesis.[37]

$$XI + XII \xrightarrow[2.\ [O]]{1.\ H^+} XIII$$

The tripyrrane diacid (XII) (Fig. 1.1) generated in situ reacts with diformyl compounds (XI) (X = O or S) (Fig. 1.1) to yield 21-oxa (25%) or 21-thiaporphyrin (12%) (XIII) (X = O or S) (Fig. 1.1). Same MacDonald synthetic strategy was used to make dioxaporphyrins or dithiaporphyrins.

The same [3+1] approach was used to synthesise dioxa- and dithiaporphyrins using two furan or two thiophene rings.[34] In this method, bischloromethyl heterocycle (XIV) (Y = O or S) and two

moles of pyrrole ester (XV) (Fig. 1.1) undergo Friedal-Craft coupling in the presence of $SnCl_4$ to form a three ring unit (XVI) (Fig. 1.1) containing a furan or thiophene.

$$\text{XIV} + \text{XV} \xrightarrow{SnCl_4} \text{XVI}$$

Three ring unit was condensed separately with the diformyl compounds (XI) to give a macrocycle containing two hetero atoms (XVII a-c) (Fig. 1.1)

$$\text{XVI} + \text{XI} \longrightarrow \text{XXVII}$$

In 1975, Ulman and coworkers[38] described another easy synthetic strategy, which is applicable not only to thiophene derivatives but also for the other ring systems such as Se, Te rings. This was based on the general synthesis of $TPPH_2$ reported by Adler and coworkers.[30,31] In this method,acid catalysed condensation of pyrrole and benzaldehyde gives the $TPPH_2$

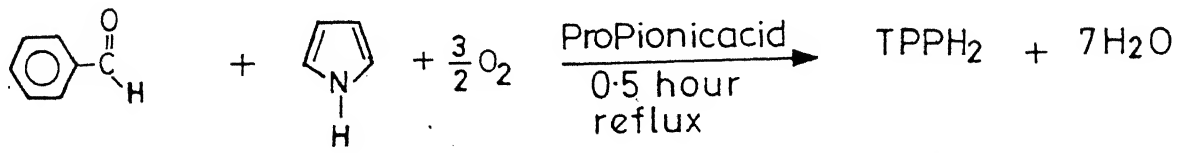

It has been proposed that the initial step is commonly assumed to be the acid-catalysed addition of pyrrole to benzaldehyde.

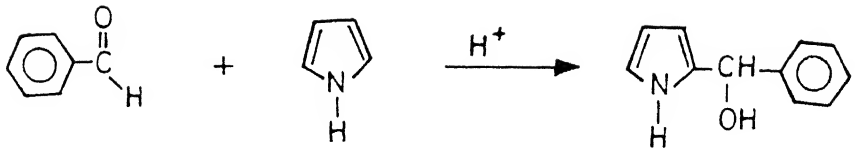

It is not clearly understood yet, how this intermediate proceeds further, one can assume four possibilities

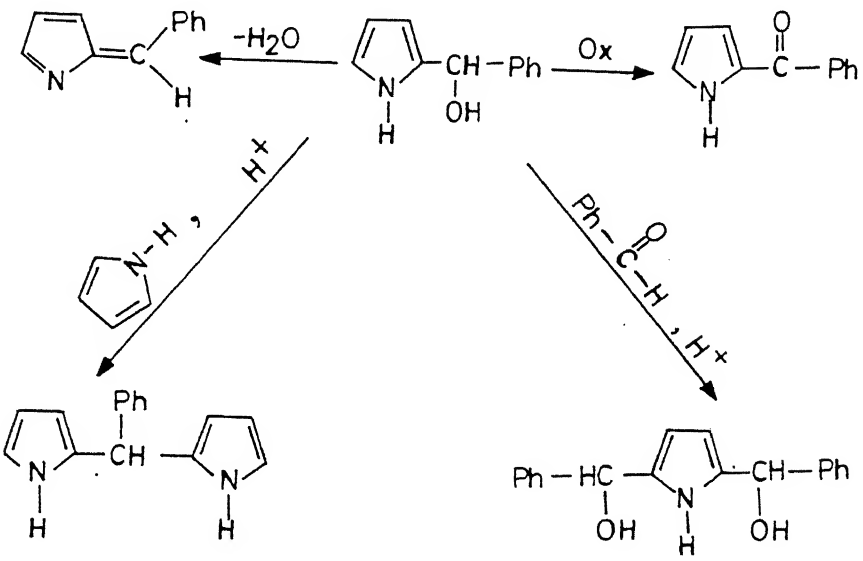

One can assume that the reaction proceeds via dialcohol intermediates (XVIII) (Fig. 1.2) which can further react with pyrrole under oxidising conditions to give the $TPPH_2$

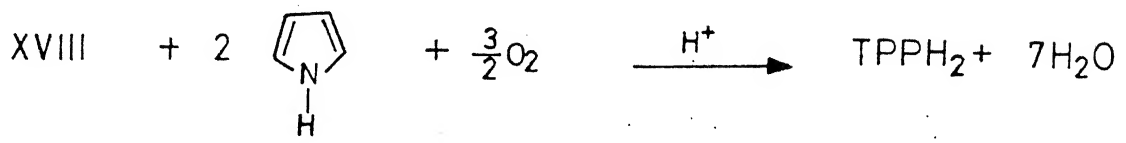

Ulman[38] made use of this method to synthesise the hetero atom substituted porphyrins as follows: the first step in this method involved a synthesis of corresponding dialcohols containing heteroatoms. The condensation of the dialcohol with pyrrole in an acid medium to give the corresponding heteroatom porphyrins forms the second step.

(a) Synthesis of heteroatom dialcohols

Scheme-I

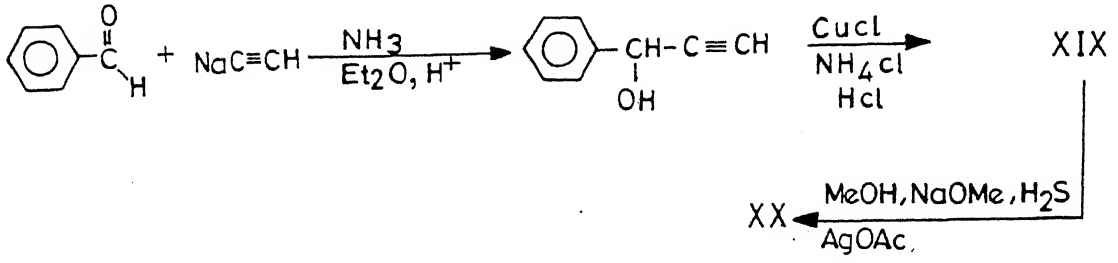

The yield of 2,5-bis(phenyl hydroxy methyl) thiophene (XX) is 25%. Similar synthetic procedure was used to make 2,5-bis(phenyl hydroxy methyl) selenophene (XXI)[39] and 2,5-bis(phenyl hydroxy methyl) tellurophene (XXII)[40]

$$\text{XIX} \xrightarrow[\substack{CH_3OH \\ AgOAc}]{NaHSe} \text{(XXI)}$$

The yield of 2,5-bis (phenyl hydroxy methyl) selenophene is 21%.

$$\text{XIX} \xrightarrow[\substack{CH_3OH \\ AgOAc}]{NaHTe} \text{XXII}$$

The yield of 2,5-bis (phenyl hydroxy methyl) tellurophene (XXII)

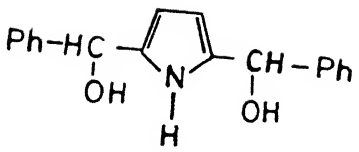

XVIII

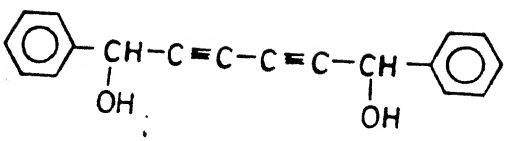

XIX

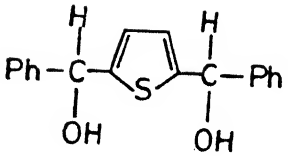

XX

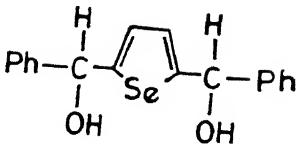

XXI

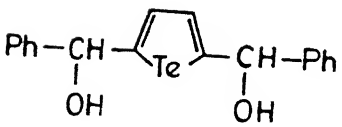

XXII

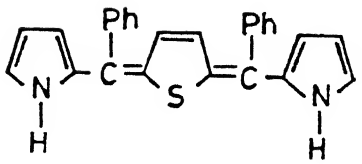

XXIII

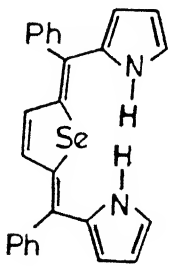

XXIV

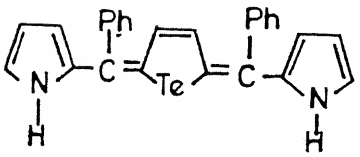

XXV

Fig.1.2 Molecular structure of some intermediates

(Fig. 1.2) is 52%.

Scheme II

A better method which is simple and gives higher yield is the synthesis of 2,5-bis (phenyl hydroxy methyl) thiophene from 2,5-dilithio thiophene.[41]

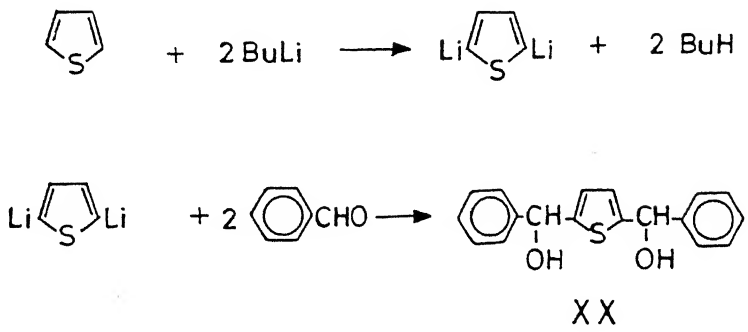

XX

1.2.1 Condensation of dialcohols to form heteroatom porphyrins

(a) Synthesis of dithiaporphyrins[38]

2,5-bis (phenyl hydroxy methyl) thiophene (XX) (Fig.1.2) and pyrrole were condensed in the presence of acid to yield tetraphenyl dithiaporphyrins (S_2TPP).

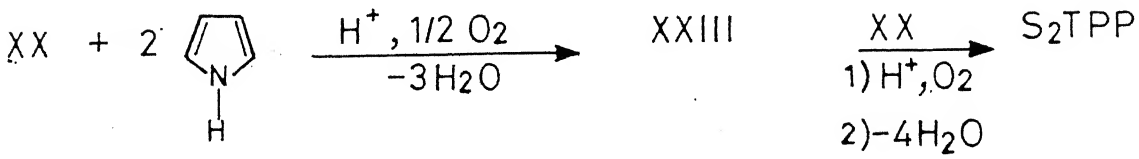

The yield of tetraphenyl dithiaporphyrin is 10%. Similar synthetic strategy was used to synthesise diselenaporphyrin[39] and yield of tetraphenyl diselenaporphyrin (Se_2TPP) is 10%.

b) Synthesis of tetraphenyl-21-Selena-23-thiaporphyrin[39]

2,5-bis(phenyl hydroxy methyl) selenophene (XXI) (Fig. 1.2) and pyrrole were condensed in the presence of chloroacetic acid to give 2,5-bis (α-phenyl pyrryl methylene) selenophene (XXIV) (Fig.1.2). This was reacted with XX (Fig. 1.2) to give tetraphenyl-21-selena-23-thiaporphyrin with 10 % yield.

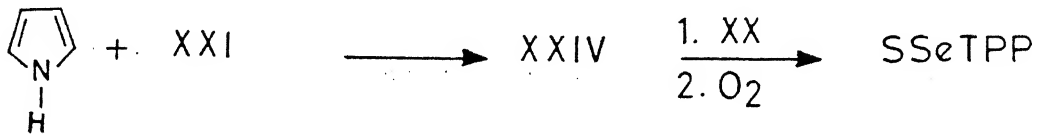

c) Synthesis of tetraphenyl-21-telura-23-thiaporphyrin[40]

2,5-bis(phenyl hydroxy methyl) tellurophene (XXII) (Fig. 1.2) and pyrrole were refluxed in the presence of chloroacetic acid to give 2,5-bis(α-phenyl pyrryl methylene) telluorophene (XXV) (Fig.1.2). This was reacted with XX (Fig. 1.2) to give tetraphenyl-21-telura-23-thiaporphyrin (STeTPP).

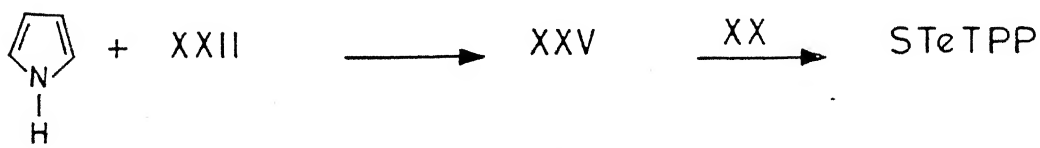

The yield of tetraphenyl-21-telura-23-thiaporphyrin (STeTPP) 0.067%.

d) Synthesis of Tetraphenyl monothiaporphyrin

The first synthesis of tetraphenyl-21 thiaporphyrin was reported by Latos-Grazynski and coworkers[42] in 1987. This was

based on the mixed aldehyde synthesis. Thus one mole of 2,5-bis (phenyl hydroxy methyl) thiophene (XX) (Fig. 1.2), two moles of benzaldehyde and three moles of pyrrole were condensed in the propionic acid to give a mixture of STPPH, S_2TPP and $TPPH_2$.

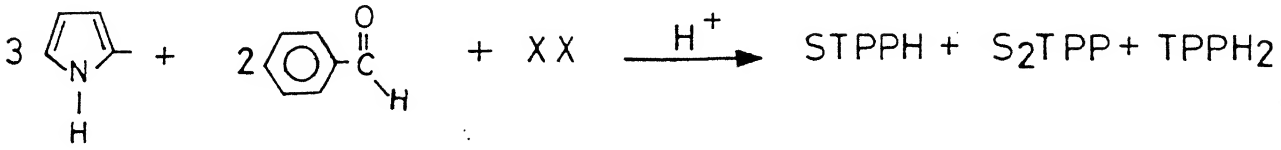

STPPH was separated from mixture in 5% yield.

1.2.3 Synthesis of Tetraoxa- and Tetrathiaporphyrin dications

In 1988, Vogel and coworkers[43,44] followed the MacDonald condensation of 5,5'-methylene-di-2-furaldehyde (VIII) (X= 0, R^1= H) (Fig. 1.1) and difuryl methane XXVI (Fig. 1.3) in CH_2Cl_2 in the presence of trifluoro acetic acid to get tetraoxaporphyrinogen (XXVIII) (Fig.1.3). Further reaction with HNO_3 and $HClO_4$ gave tetraoxaporphyrin dication (XXVII) (Fig. 1.3) in 8% yield.

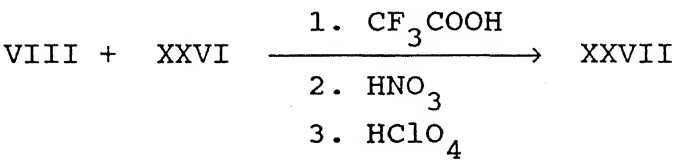

The above procedure was modified in 1989 by Vogel and coworkers, using furfuryl alcohol as the starting material to synthesise the

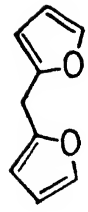

XXVI

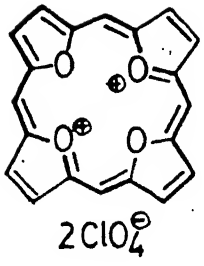

XXVII

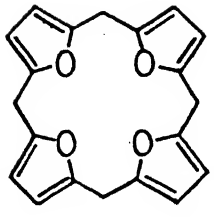

XXVIII

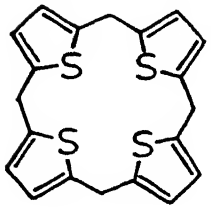

XXIX

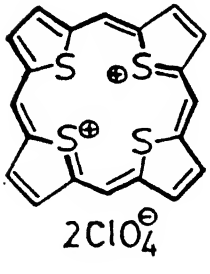

XXX

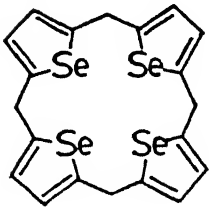

XXXI

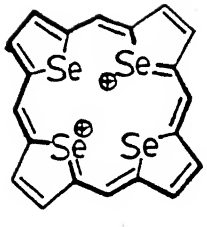

XXXII

Fig.1.3 Molecular structure of some porphyrins and intermediates

tetraoxaporphyrinogen (XXVIII) (Fig. 1.3).

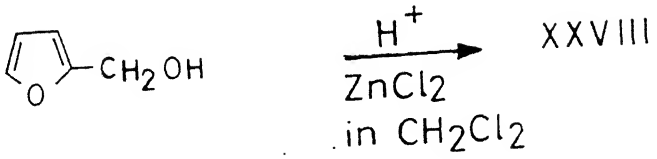

The tetraoxaporphyrinogen (XXVIII) (Fig. 1.3) was oxidised with DDQ in benzene solution and the resulting product was treated with HNO_3. The addition of $HClO_4$ yields tetraoxaporphyrin dication (XXVII) (Fig. 1.3) in 86%.

$$\text{XXVIII} \xrightarrow[\text{2. } HNO_3 \\ \text{3. } HClO_4]{\text{1. DDQ}} \text{XXVII}$$

When H_2S and HCl gases were passed simultaneously into a solution of tetraoxaporphyrinogen in ethanol for 2 hours at 0^oC and 3 hours at room temperature to give tetrathiaporphyrinogen[45] (XXIX). It was oxidised with DDQ and $HClO_4$ to form a tetrathiaporphyrin dication (XXX) (Fig. 1.3) in 25% yield

$$\text{XXVIII} \xrightarrow{H_2S/H^+} \text{XXIX} \xrightarrow[\text{2. } HClO_4]{\text{1. DDQ}} \text{XXX}$$

Tetraselena dication[45] was also prepared from tetraoxaporphyrinogen passing the H_2Se as above in 45% yield.

$$\text{XXVIII} \xrightarrow{H_2Se/H^+} \text{XXXI} \xrightarrow[\text{2. } H_2SO_4]{\text{1. DDQ}} \text{XXXII}$$

1.3.0 Structural aspects of heteroatom substituted porphyrins

X-ray structures of few thiaporphyrins have been reported recently. The general effect of heteroatom substitution is to alter the interior of the porphyrin skeleton while the external shape which is responsible for crystal packing remains relatively unaffected as long as the thiophene rings remain near the porphyrin plane. The decrease in core size upon substitution of hetero atoms was clearly reflected from the X-ray structure. Table 1.1 below lists intramolecular distance (A^{o}) observed between chalcogen atoms for a few heteroatom porphyrins.[48,56b] It is apparent from the table that the distance between the two hetero atoms (for example, S.....S distance in S_2TPP) is much shorter than the sum of the Van der waals radii of hetero atoms, clearly reflecting the shrinkage in the core size and thus invoking possibility of the bonding interaction between the hetero atoms.

Table 1.1 : Intra molecular distances (A^{o}) in chalcogens

Atom Pair	Macrocycle	Observed in hetero substituted porphyrins	Sum of Van der waals radii[49]	Sum of single bond covalent radii[50]
N....N[46]	$TPPH_2$	4.20	3.00	1.40
N....S[47]	STPPH	3.547	-	-
S....S[48]	S_2TPP	3.069	3.7	2.08
S....Se[48]	SSeTPP	2.89	3.85	2.21
Se...Se[48]	Se_2TPP	2.85	4.00	2.34
S....Te[48]	STeTPP	2.65	3.95	2.41
S....S[45]	TTP^{2+}	3.532	-	-

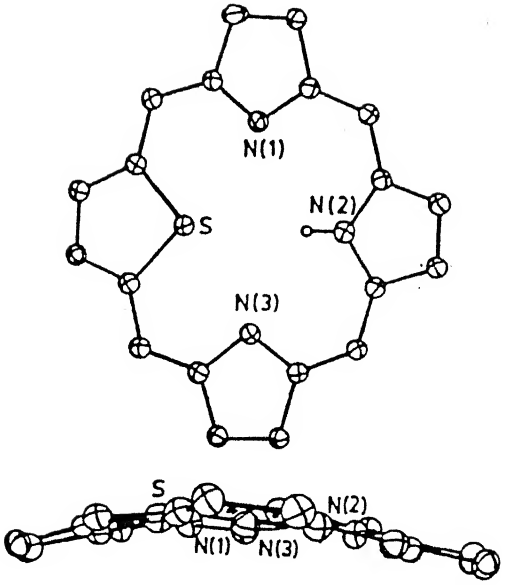

(a)

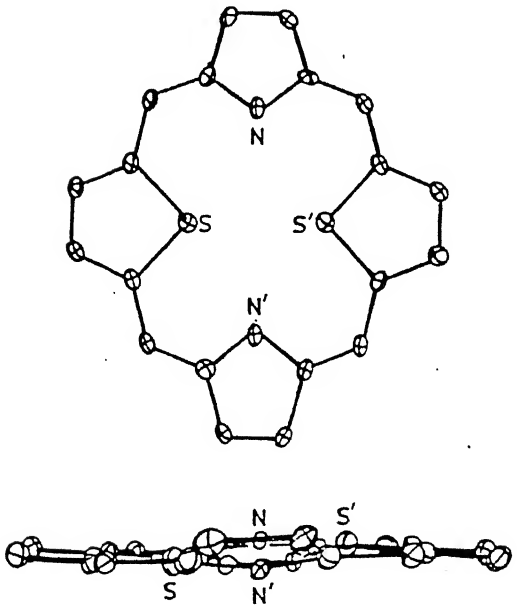

(b)

Fig.1.4 (a) X-ray structure of tetraphenyl-21-thiaporphyrin (top), bottom: a view emphasizing the planar aspects of the thiaporphyrin

(b) X-ray structure of tetraphenyl-21-23-dithiaporphyrin (top), bottom: a view emphasizing the planar nature of dithiaporphyrin

The structure of STPPH[47] (Fig. 1.4) indicates that porphyrin plane is almost planar with a small distortion. This is expressed by considering the dihedral angle between the plane of the four meso carbons and the planes of the four membered rings. The dihedral angle in STPPH are: thiophene, 14.1°; pyrrole (N(1)), -11.5°; pyrrole (N(2)), 10.0°; pyrrole (N(3)), - 7.4°. Because of sulfur atom, the core size of the macrocycle is restricted. The non-bonded S....N(2) distance is 3.547 Å while the non-bonded N(1).....N(3) distance (4.40 Å) is some what longer than that in tetragonal form (4.108 A°) or in the triclinic form(4.06,4.20 A°) of tetraphenyl porphyrin.[46]

Surprisingly even the structure of S_2TPP (Fig. 1.4) shows a small deviation from the planarity of the porphyrin core. The dihedral angle between the plane of the four meso carbons and the planes of four-membered rings are thiophene 4.9°, pyrrole 12.9°. The non-bonded N.....N′ distance is 4.65 A°, while S....S distance is 3.06 A° (S.....S′ distance of 3.05 A° was quoted[52] from an unpublished structure which gave no other information on the macrocycle and an attractive S....S interaction was proposed for this molecule[52]). Notice that the S.....S′ distance would be slightly shortened if the dithiaporphyrin was strictly planar. The S....S′ distance is considerably shorter than the sum of the Van der Waals radii for two sulfur atoms (3.70 A°)[49] but longer than that of a typical S——S single bond (2.08 A°).[50]

Table 1.2 : Bond distance (A^o) relating to delocalization pattern in Thiaporphyrins

Macrocycle	Pyrrole			Thiophene		
	$N-C_\alpha$	$C_\alpha-C_\beta$	$C_\beta-C_\beta$	$S-C_\alpha$	$C_\alpha-C_\beta$	$C_\beta-C_\beta$
$ST(NO_2)_2PPH$	1.369	1.445	1.347	1.74	1.421	1.365
S_2TPP	1.362	1.461	1.353	1.748	1.408	1.367
TTP^{2+} 45				1.725	1.412	1.363
Thiophene[51]				1.714	1.370	1.423

Balch et al[47] have shown that there is an appreciable effect on the aromatic character of the macrocycle of the thiophene portion by relating the bond distances observed in the X-ray structure with the delocalisation pattern. Table 1.2 shows some of the C-C, C-N and C-S distances of pyrrole and thiophene rings in few porphyrins. Inspection of the table indicates that the bond distances within the thiophene are altered. Thus the $C_\alpha-C_\beta$ bond lengths in 21-thiaporphyrin ($ST(NO_2)_2PPH$), dithiaporphyrin (S_2TPP) and tetrathiaporphyrin dication (TTP^{2+}) are longer than the C_β - C_β distances whereas the reverse is true for thiophene.[53] The C_α-S bond remains practically unchanged in all these porphyrins. These changes suggest that π-electron density has been altered within the thiophene portion such that it is increased in the $C_\beta-C_\beta$ bond, decreased in the $C_\alpha-C_\beta$ bonds and unchanged in the C_α-S bonds.

Ulman and coworkers[48] have reported the structures of heteroatoms substituted TPP molecules in which the two heteroatom substituted were different. The distance between the heteroatoms

are as follows: S....S 3.02 A^{o}, S....Se 2.89 A^{o}, Se....Se 2.85 A^{o}, S.....Te 2.65 A^{o}. They proposed that the bonding interaction between the hetero atoms follows the order S....N < S.....S< S....Se < S.....Te. It was assumed that the non-bonded electrons on pyrrolidine nitrogens are also involved in the bonding interaction within the core of porphyrin. These interactions are crucial for the stability of the molecule. Even traces of CF_3COOH,which protonate the nitrogens are sufficient to decompose STeTPP molecule.

Gouterman and coworkers[52] from the theoretical calculations on few chalcogen porphyrins suggest that the bonding interaction between the two heteroatoms can be explained by invoking the participation of empty d-orbitals of the hetero atoms. A bond order analysis in comparison with d-orbital populations shown in table 1.3 clearly suggest that the existence of the bonding interaction between the hetero atoms.

The data in table 1.3 clearly show that the bond order between the group 6 atoms in the chalcogen porphyrins are negative if the participation of d-orbitals are not included and upon inclusion of the d orbital participation the bond order becomes positive and increases in the order of S....S < S....Se < Se...Se which is in agreement with the X-ray data. Thus the iterative extended Hückel (IEH) bond order calculations supports that the bonding interaction exists between the hetero atoms in the porphyrin core. Further experimental evidence for the bonding interaction also comes from the recent Resonance Raman[55] and NMR study.[56]

Table 1.3 : Bond orders and d-orbital populations[a]

Molecule	Atoms	$B.O_{kl}^{b}$	$\tau_{B.O\ kl}^{b}$	$N(d)^{c}$
S_2TPP	S...S	0.122(-0.046)	0.22(0.077)	0.192
SSeTPP	S...Se	0.182(-0.078)	0.041(0.010)	0.307
Se_2TPP	Se...Se	0.320(-0.121)	0.061(0.017)	0.382

a - LCAO;MO covalent bond order between two atoms S and Se calculated using Cohen relation[54], b - Bond order with d orbitals (in parentheses, without d orbitals), c - orbital populations.

The structure of tetraoxaporphyrin dication (Fig. 1.5) was reported by Vogel and coworkers[43] in 1988. The structure indicates square planar dispositions of oxygen like in metalloporphyrins and the structure resembles that of a planar porphyrin. However, the C_α - C_β bond lengths are slightly shorter than the observed for the porphyrin. O...O distances (O....O', 2.869 A^o, O....O"' 2.9 A^o) are similar to the N....N distances (2.87, 2.91 A^o) observed for porphyrins.

The X-ray structure of tetrathiaporphyrin dication[45] (Fig. 1.5) however shows the non-planar structure. It is centro symmetric and the meso-methine carbon atoms lie in the plane with respect to which the hetero five membered rings are inclined by 3.7^o and 22.8^o, respectively. The bond length is in the order C_α-C_β > C_β-C_β, typical for porphyrins (opposite to that in parent heterocycle pyrrole, furan and thiophene). Consistent with the symmetry of the molecule, the sulfur atoms also lie in a plane.

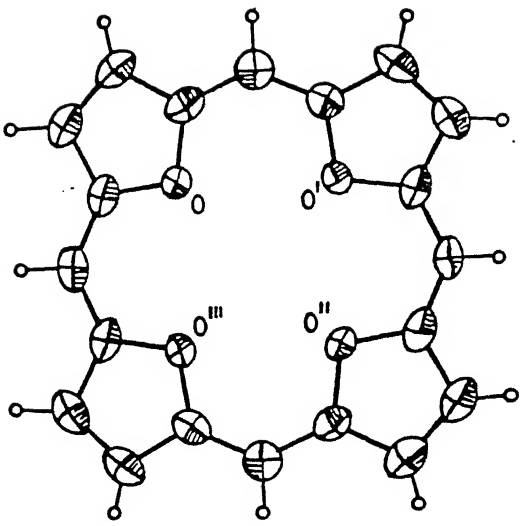

(a)

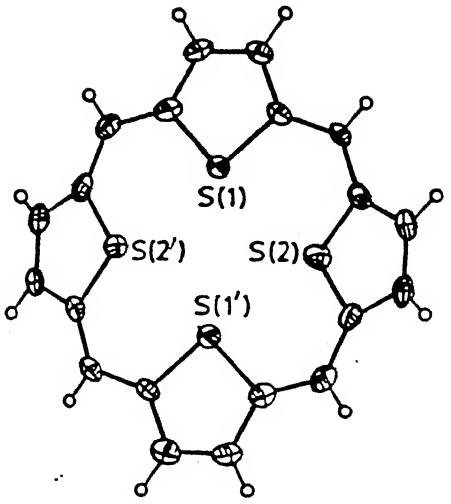

(b)

Fig.1.5 (a) X-ray structure of tetraoxaporphyrin dication
(b) X-ray structure of tetrathiaporphyrin dication

The distance between neighbouring sulfur atoms (2.78 and 2.80 A^{o} respectively) thereby falls about $1A^{o}$ short of double the Van der waals radius, so that it can be assumed that there are attractive interactions between these atoms. Thus upon introduction of large size heteroatoms, the conformation of ring changes from slightly puckered to highly puckered.

1.3.1 Structure of Metallothiaporphyrins

The complexation behaviour of monothiaporphyrins with transition metals has been explored recently by Balch and Grazynski.[57a] Many of the metal complexes have been characterized by X-ray structure. The Cu^{+2}, Ni^{+2}, Fe^{+2} monothiaporphyrin complexes have a number of common features. All these three metal ions form a five coordinate complex in an approximate square pyramidal geometry around the metal. The metal ion is bonded to three nitrogen atoms and one thiophene sulfur with an axial chloride ligand. All the three complexes are high spin in nature. The structures shown in Fig. 1.6 suggest that the thiophene ring is sharply bent out of the N_3 pyrrole core while the pyrrole rings are only slightly tipped away from the plane. The thiophene sulfur is co-ordinated to pyramidal fashion with η^1 coordination. Table 1.4 lists characteristics of metal-ligand distances. Also the metal ion distances of FeN-CH_3TPPCl complex is included for comparison. Inspection of the table reveals that M-N bond distance decreases in the order $Fe^{+2} > Ni^{+2} > Cu^{+2}$. This has been accounted interms of nuclear screening effect on going from iron to copper. These bond distances are similar to those observed for the five co-ordinate complexes of iron porphyrins and the Ni-N bond lengths are similar to high spin complexes of Ni^{+2}

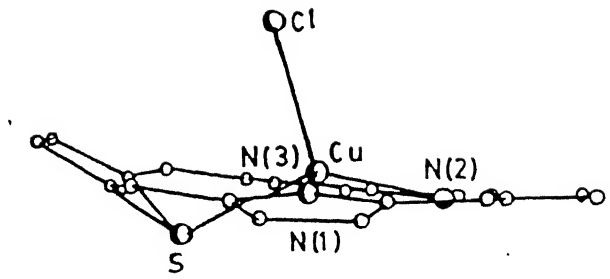

(a)

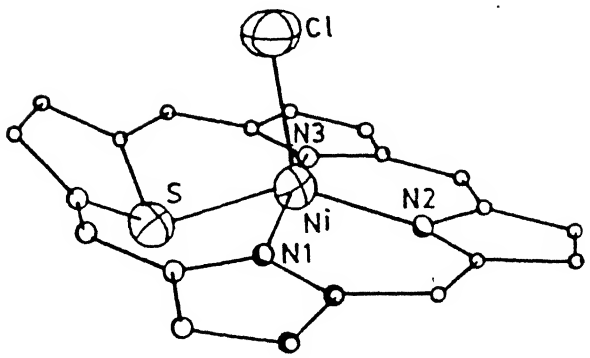

(b)

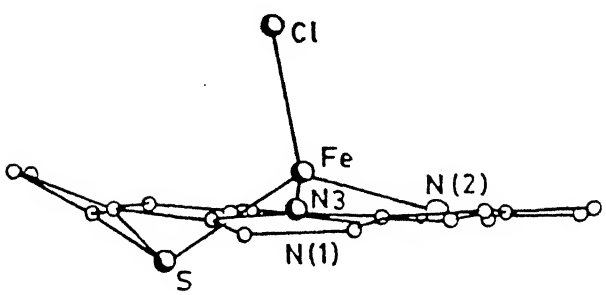

(c)

Fig.1.6 (a) X-ray structure of Cu(II) derivative of tetraphenyl-21-thiaporphyrin (view of the inner core), (b) X-ray structure of Ni(II) derivative of tetraphenyl -21-thiaporphyrin (view of the inner core) (c) X-ray structure of Fe(II) derivative of tetraphenyl-21-thiaporphyrin (view of the inner core). In all the structures phenyl groups are omitted.

porphyrins.

Table 1.4 Characteristic Metal - Ligand Distances (A^o)

	FeSTPPCl	NiSTPPCl	CuSTPPCl	$Fe(N\text{-}CH_3TPP)Cl$ [57b]
M-Cl	2.215	2.275	2.373	2.244
M-N(1)	2.127	2.094	2.055	2.155
M-N(2)	2.064	1.963	1.962	2.118
M-N(3)	2.138	2.084	2.057	2.156
M-S	2.388	2.296	2.335	2.329
$M\text{-}N_3^a$	0.538	0.295	0.274	0.620

a - distance from the metal to plane of the three nitrogen atoms.

In contrast to the behaviour of the M-N bonds, there is a systematic lengthening of the M-Cl bonds for the same series. The larger effect, the 0.1 A^o increase on going from Ni(II) to Cu(II), can be readily be ascribed to the filling of the out of plane σ^* orbital in the Cu(II) complex. The M-S distances show an irregular trend within the series. Iron atom in Fe^{+2} complex is relatively much away from N_3 plane as compared to Cu^{+2}, Ni^{+2}, Fe^{+2} complexes.

The thiaporphyrin ring has had to distort from its intrinsic planar geometry to accommodate the co-ordination of these metal ions. The bending of the thiophene ring allows this group to co-ordinate the metal ion in η^1 fashion through the sulfur atoms, which acquires a pyramidal geometry. The limited core size of the macrocycle needs to accommodate the metal ion in folding environment. Thus the crystal structures of tetraphenyl monothiaporphyrin metal complexes show severe nonplanarity, with thiophene ring tipped out of the plane. The thiophene sulfur is η^1

bonded to metal ion in a pyramidal fashion.

Recently structure of Ni(I) complex of monothiaporphyrin has been reported [58] The structure shown in Fig. 1.7 is similar to those of other metal complexes of thiaporphyrin, i.e. thiophene ring tipped 52.3^{o} out of the plane and pyramidal coordination of thiophene sulfur. A comparison of the crystal data of Ni(I) complex with corresponding Ni^{+2} and Cu^{+2} complexes are made in table 1.5.

The Ni-N and Ni-S bond lengths are shorter than five co-ordinate complexes of Ni(II)STPPCl and Cu(II)STPPCl and six co-ordinate complexes of Ni(II) porphyrins. Moreover, Ni(I)-N(2) distances are also shorter than diamagnetic four co-ordinated complex in Ni(II) porphyrins and Cu(II) porphyrins but Ni(I)-N(1) and Ni(II)-N(3) bond lengths are longer than four co-ordinated complexes of Ni(II) porphyrins and Cu(II) porphyrins. The dramatic shortening of Ni-S bond that occurs upon reduction may reflect increased π back donation. This type of back donation is reported in the literature for Cu-S bonds.[59]

Table 1.5 : Characteristic Distance (A^{o})

	Ni(I)SDPDTP	NI(II)STPPCl[57]	Cu(II)STPPCl[57]
M-N(1)	2.015	2.094	2.055
M-N(3)	2.014	2.084	2.057
M-N(2)	1.910	1.963	1.962
M-S	2.143	2.296	2.335
$M-N_3^a$	0.042	0.295	0.274

a - distance of the metal from the N_3 plane.

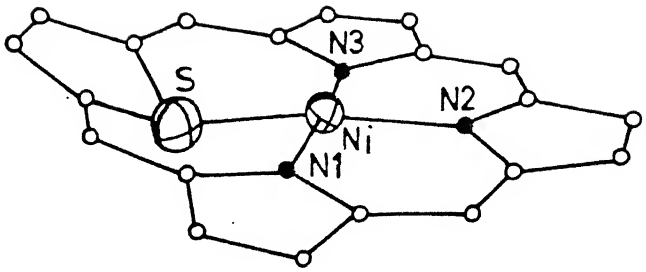

(a)

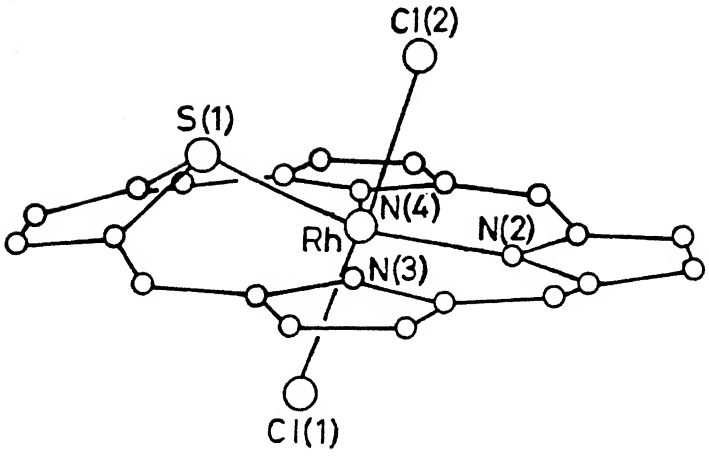

(b)

Fig.1.7 (a) X-ray structure of Ni(I) derivative of tetraphenyl-21-thiaporphyrin (view of the inner core) (b) X-ray structure of Rh(III) derivative of tetraphenyl-21-thiaporphyrin (view of the inner core). In all structures phenyl groups are omitted.

Recently Latos-Grazynski et al[60] reported the six co-ordinate complexes of rhodium monothiaporphyrins ($RhSTPPCl_2$) (Fig. 1.7). The crystal structure analysis shows that $RhSTPPCl_2$ is nonplanar and nearly octahedral with thiophene ring severely bent out of the N_3 plane and lesser the degree of tipping of the pyrrole rings from that plane. The dihedral angle between $C_\alpha C_\beta C_\beta C_\alpha$ plane and the $C_\alpha S\ C_\alpha$ plane is 26.4° which is larger than found in the five co-ordinate complexes[57] of Cu(II) STPPCl (15.2°), NiSTPPCl (13.4°) and Fe(II)STPPCl (11.8°) and much larger than STTPH[42] (2.4°). The geometry of sulfur bonded in $RhSTPPCl_2$ is similar to that established for other η^1-thiophene complexes. The two Rh-Cl bonds are nearly equal [2.333 and 2.346 A°] and are of normal length. The major difference between the five and six co-ordinated complexes of 21-thiaporphyrin is the movement of the metal towards N_3 plane. In $RhSTPPCl_2$, Rh to N_3 plane distance is only 0.033 A° while in the five co-ordinate complexes this distance is much larger [0.274 A° in Cu(II)STPPCl, 0.295 A° in Ni(II) STPPCl, 0.538 A° in Fe(II) STPPCl]. The folding of thiophene ring allows carbon atoms of the thiophene ring to be nearly co-planar with the rest of the thiophene ring core so that the π-conjugation is not disrupted.

Thus the crystal structure analysis shows that 5 and 6 co-ordinate complexes of monothiaporphyrin are nonplanar with the thiophene ring is sharply bent out of the plane of the porphyrin ring, and the thiophene sulfur bonded to the metal in η^1 fashion.

1.4.0 Miscellaneous Reports

Recently a detailed NMR studies were made on Ni(II) tetraphenyl 21-thiaporphyrin to elucidate the molecular and electronic structure. It has been proposed that Ni(II)STPPCl and related systems are quite flexible in solution. Replacement of axial chloride by perchlorate results in the formation of low spin diamagnetic complex, (Ni(II)STPPClO_4). Imidazole replaces the axial halide to produce five coordinate derivatives, and the NMR signals from the co-ordinated imidazole has also been assigned. The formation of six coordinate form was also established. The pyrrole shift pattern is related to Ni(II) coordination number. The isotropic shifts of pyrrole and thiophene resonance are shown to be dominated by σ contact mechanism. To account for the sulfur contribution and geometry of 21-thiaporphyrin, semi quantitative Fenske-Hall-LCAO method[51] has been used to determine molecular orbitals that are involved in the distribution of spin densities via π-orbitals.

Very recently the paramagnetic σ-bonded phenyl Ni(II) thiaporphyrin systems[62] have been characterized by NMR. Addition of phenyl Grignard reagent to toluene or CH_2Cl_2 solution of Ni(II) monohalide complexes of 5, 20-diphenyl-10, 15-bis(p-tolyl) 21-thiaporphyrin and N-methyl tetraphenyl porphyrin at $-70^{o}C$ resulted in the formation of paramagnetic σ-phenyl Ni(II) derivatives. A coordination of the phenyl ligand has been proven by unique down field pattern of three phenyl resonances in ^{2}H NMR spectra. It has been shown that the σ-phenyl Ni(II) derivatives are in the high spin paramagnetic electronic state, $d^{2}_{xy}d^{2}_{xz}$ d^{2}_{yz} $d^{1}_{z^2}d^{1}_{x^2-y^2}$. The protons of nickel bound phenyl group display

substantial hyperfine shifts which are dominated by σ-contact contribution. A contact shift pattern established for the phenyl ligand resembles that of pyridine in a variety of Ni(II) pyridine complexes[63], probably due to the isoelectronic structure of the both the ligands. Homolytic cleavage of Ni(II)-C bonds has been observed in toluene with the formation of Ni(I) thiaporphyrin.

1.5.0 Similarities between Metal derivatives of thiaporphyrins and N-alkyl porphyrins

The structural data outlined so far for the metal derivatives of monothiaporphyrins have revealed similarities between the structures of metallothiaporphyrins with that of metal derivatives of N-alkyl porphyrins. In view of this, a brief survey of similarities observed between these two kinds of porphyrins are discussed in the following section.

The studies on N-alkyl or N-aryl[64] N-oxide[65] octaethyl and tetraphenyl porphyrins and their insertion products[66] have attracted attention of researchers because of their biochemical significance. The reaction of alkylating agents with heme proteins leads to the formation of N-substituted porphyrins via an intermediate.[67] The N-oxide porphyrin complexes have been treated as alternative models for oxidized forms of heme proteins (particularly cytochrome P_{450} and peroxidases) as intermediates in heme catabolism.[68]

Monothiaporphyrins and N-methylporphyrins co-ordinate as monoanions facilitating the formation of five coordinate structures for neutral complexes. They incorporate an anionic additional axial ligand perpendicular to the plane. Thus the thiaporphyrin ligand differs from the porphyrin and N-oxide

porphyrin ligands which coordinate as dianions and forms metal complexes that have nearly planar four coordinate geometry.

Both monothiaporphyrins and N-methyl porphyrins have decreased core size in the porphyrin cavity relative to normal porphyrins and the co-ordination of the metal ions results in a five coordinate geometry with the severe nonplanarity around the metal center.[57a] This is reflected in the UV-visible spectrum of the metal derivatives which show split soret band and a complex pattern of Q bands in contrast to normal metalloporphyrins where only two Q bands are observed Q(0,0) and Q(1,0) and one soret band are generally observed. For example, UV-spectra of $CuNCH_3TPPCl$[69] (371, 451, 564, 617 and 672 nm) and CuSTPPSCl (440, 465, 570, 610 and 690 nm) have the same number of bands with comparable wavelengths, but are different from CuTPP.

The electrochemical reduction of CuNMeTPPX (X = $-ClO_4^-$, Br^-)[69] and CuSTPPCl[70] indicates reduction of the metal center corresponding to Cu(II)$\longrightarrow$ Cu(I) around -0.1 volts. This is in contrast to CuTPP, where the first electron reduction results in the formation of monoanion of CuTPP. Thus this reversal of energy levels is an account of severe distorted geometry around the metal center in monothiaporphyrin and N-methyl porphyrin.

The Fe(II) STPPCl[57a] and Fe(II)NMeTPPCl[57b] are found to be resistant to oxidation by oxygen while Fe(II) porphyrins are sensitive to oxygen and forms a μ-oxo dimer. The structures of Fe(II)STPPCl (Fig. 1.6) and Fe(II) N-MeTPPCl (Fig. 1.8) reveal many common features. Both complexes are five coordinate with Iron out of the plane with an axial chloride. Thiophene ring in Fe(II)STPPCl and N-methylated pyrrole ring in Fe(II)N-MeTPPCl are bent out of the porphyrin plane on the same side. The Fe-N, Fe-Cl

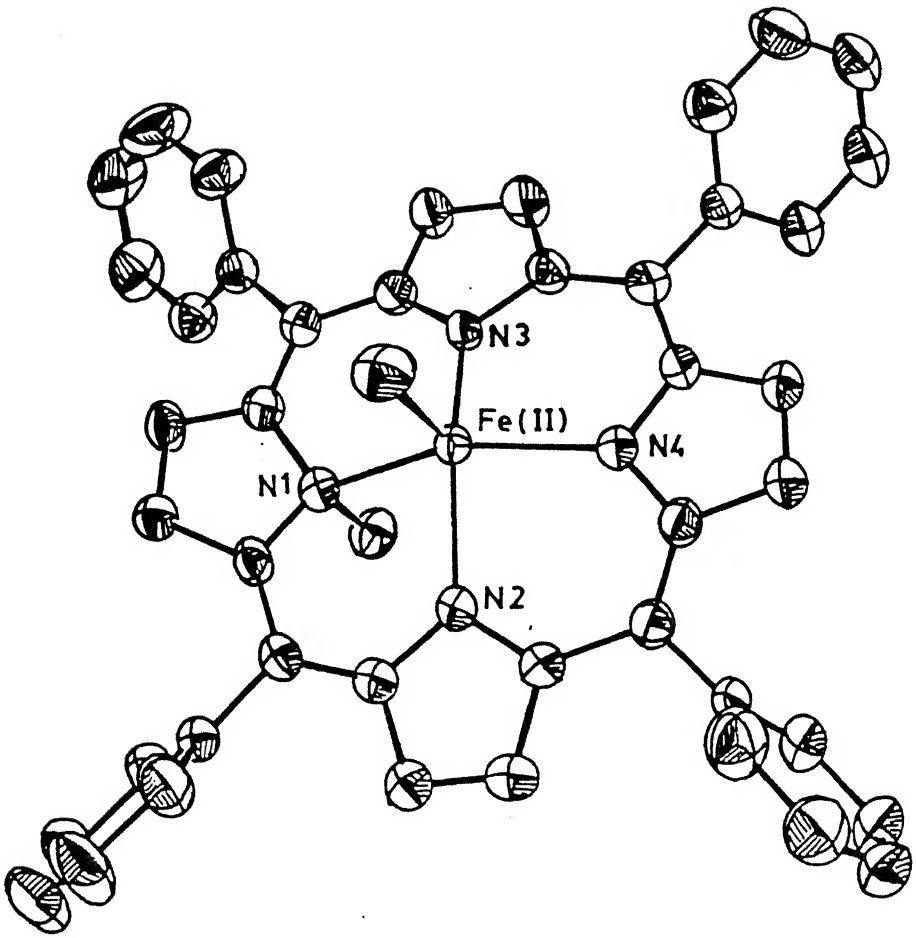

Fig.1.8 X-ray structure of Fe(II) derivative of N-methyl tetraphenyl porphyrin.

bond lengths are similar and their spectroscopic and magnetic properties are also identical. For example, Mossbauer spectral parameters and magnetic moments are shown below.

	Fe(II) N-MeTPPCl[71]	Fe(II) STPPCl[57a]
Isomer shift	0.88 mm/s	0.84 mm/s
Quardrupole splitting	3.93 mm/s	3.74 mm/s

Thus the metallothiaporphyrins and metallo N-methyl porphyrins have many similarities interms of spectral and magnetic properties probably attributed to the similarity in the structure.

1.6.0 Scope of the Present Thesis

From the forgoing discussion it is clear that the studies on thiaporphyrins in literature are limited to their synthetic methodologies and X-ray structures. There are no systematic studies available to compare the spectral properties and electrochemical properties to understand the effect of hetero atom substitution on the electronic structure of the porphyrin ring. In this thesis an effort has been made to systematically measure the spectroscopic and electrochemical properties of a variety of monothia- and dithia porphyrins and their metal derivatives both in ground and excited singlet and triplet states. A comparison of these measured properties of thiaporphyrins with the normal porphyrins have revealed many similarities and differences with respect to the electrochemical behaviour and magnetic behaviour.For the first time the triplet state properties of thiaporphyrins have been looked into by photoexcited triplet ESR

method. In order to evaluate the spectral and electrochemical properties in the aqueous medium, we have synthesised water soluble thiaporphyrins and their properties are studied in detail. The linking of a normal porphyrin unit with the thiaporphyrin results in a unique diporphyrin with different electronic structures. Specific metallations of the normal porphyrin and the thiaporphyrin subunits result in unique bimetallic diporphyrins both with similar metals and dissimilar metals. The results of this thesis have been divided into the following chapters.

Chapter 1 describes general introduction on various aspects of porphyrins and thiaporphyrins that are reported in literature. The purification of chemicals, solvents and synthesis of some of the starting materials and the details of the various experimental methods employed are described in Chapter 2. Chapter 3 describes the studies on mono- and di- thiaporphyrins in non-aqueous media in the ground, excited singlet and triplet states. The behaviour of thiaporphyrins and their metal derivatives in aqueous medium with respect to aggregation, magnetic properties, singlet and triplet excited state properties are described in Chapter 4. Fifth chapter deals with synthesis, characterization and photophysical properties of novel diporphyrins containing N_4 and N_3S cores, and various bimetallic diporphyrins containing same and different metals are also synthesised and characterized. The results obtained during the course of investigation are summarised in Chapter 6.

CHAPTER 2

GENERAL EXPERIMENTAL METHODS AND TECHNIQUES

In this chapter, the materials employed at different stages of the investigation are listed. Besides, a description of the methods used to synthesize the precursor compounds for various thiaporphyrins and normal porphyrins, and the purification procedure of all the chemicals and solvents are given. A brief outline of the physico chemical techniques employed and details of the instruments used are given.

2.1.0 Materials employed:

The common solvents used for synthesis were purified according to the reported procedure.[72]

Pyrrole was procured from Aldrich Chemicals (USA) and was distilled over KOH (129^{o}-131^{o}C) before use.

Thiophene,P-anisaldehyde and P-tolualdehyde were procured from Aldrich Chemicals (USA) and were distilled before use. 18-Crown-6, chlorosulphonic acid, 1,5-dibromopentane and P-hydroxy benzaldehyde were obtained from Aldrich Chemicals (USA) and were used as received. Tetrabutyl ammonium bromide and n-Butyl lithium (15% in hexane), Trifluoro acetic acid were procured from E.Merck (W. Germany) and were used as received.

Solvents for NMR measurements, $CDCl_3$, $DMSOd_6$ and TFAd were also obtained from Aldrich Chemicals, USA and were used as received.

Andydrous potassium carbonate, anhydrous sodium sulphate, anhydrous calcium chloride were obtained from Qualigens Fine

Chemicals, Bombay, India.

Aluminum oxide (basic) and silicagel (60-120 mesh) were purchased from Acme Laboratory Chemicals, Bombay, India.

N,N,N',N'-Tetramethyl ethylene diamine was procured from Loba Chemicals, India and was distilled over KOH before use.

Dimethyl formamide (DMF) and Dimethyl sulphoxide (DMSO) (A.R. Grade) were procured from Qualigens Fine Chemicals, Bombay, India and were used as received.

KCl, NH_4Cl, NaCl were purchased from B.D.H., India and were used as received.

n-hexane and Tetrahydrofuran (THF) were distilled and stored over sodium.

Benzaldehyde (A.R. grade), glycerol, propionic acid (L.R. Grade), chloroform, dichloromethane, Methanol,Petroleum ether (60-80^{o}C) ethylacetate, Toluene, Benzene, diethyl ether, acetone, Conc. H_2SO_4, Conc. HCl and Conc. HNO_3 were procured from S.D. Fine Chemicals, India.

2.1.1 Metal Salts Employed

Zinc acetate dihydrate, copper chloride dihydrate and nickel hexa hydrate were of A.R. grade obtained from S.D. Fine Chemicals, Bombay, India.

2.1.2 Solvents Employed for Spectroscopic Measurements

The following solvents were used for spectroscopic measurements:

(a) Chloroform (A.R. grade) from S.D. Fine Chemicals (India) was

distilled over P_2O_5.[72]

(b) Dichloromethane (L.R. grade) from S.D. Fine Chemicals (India) was washed twice with 10% aqueous Na_2CO_3 solution, twice with water, dried over anhydrous calcium chloride for 6 hours and distilled over P_2O_5 and stored over molecular sieves ($4A^{o}$).

(c) Toluene (spectroscopic grade) from S.D.Fine Chemicals (India) was used as received.

(d) Dimethyl formamide (DMF) (A.R. grade) was distilled under reduced pressure of 36 mm of Hg at $80^{o}C$ and stored over molecular sieves ($4A^{o}$).

(e) Dimethyl sulfoxide (A.R. grade) was distilled under reduced pressure of 12 mm of Hg at $80^{o}C$ before use.

(f) Double distilled water used for all studies in aqueous medium.

2.2.0 Preparation of Tetrabutyl ammonium perchlorate (TBAP)

50 g (0.16 mole) of tetrabutyl ammonium bromide was dissolved in 600 cm^3 of water and 31.2 cm^3 (99.9%) of perchloric acid (31.16 g, 0.31 mole) was added to get the white precipitate. The precipitate was filtered and the crude product was washed with large excess of water to remove excess perchloric acid. It was then recrystallised from minimum amount of ethanol to get the crystalline tetrabutyl ammonium perchlorate (TBAP). Yield 90% (49.5 g).

2.2.1 Synthesis of 2,5 bis (phenyl hydroxy methyl) thiophene[41]

To a solution of N,N,N′,N′-tetra methyl ethylene diamine (6.906 g; 59.425 mmol, 9 cm^3) in dry n-hexane (90 cm^3), n-butyl

lithium (3.806 g, 59.425 mmol, 37.1 cm^3) was added followed by thiophene (2g, 23.7 mmol, 1.9 cm^3) under argon atmosphere. The reaction mixture was stirred at room temperature for an hour and later heated under reflux for two hours. The reaction mixture was then allowed to attain the room temperature. Benzaldehyde (6.2g, 59.425 mmol, 6 cm^3) in dry tetrahydrofuran (THF) (25 cm^3) was added dropwise to the ice-cooled reaction mixture . After addition was over the reaction mixture was allowed to attain the room temperature and saturated ammonium chloride solution was added and it was then extracted with ether or chloroform (100 cm^3). The organic layers were combined and washed with brine (100 cm^3) and dried over anhydrous Na_2SO_4. The crude product obtained on evaporation of the solvent was purified by flash chromatography over silicagel (ethylacetate: petroleum ether (60-80^oC),4:6) afforded the diol as a pale yellow solid. This was recrystallised from dry toluene, m.p. 135^oC, Yield: 59% (4.1 g).

IR (KBr) : 3320, 3080, 3050, 2910, 1605, 1495, 1455, 1200, 1040, 1020, 970 cm^{-1}

IR : 3450,3060, 3030, 2922, 2852, 1605, 1490, 1305, 1280, 1250, 1190, 950 cm^{-1} .[41]

^1H NMR ($CDCl_3$): 1.17 (S, 2H), 5.14 (S, 2H), 6.06 (S, 2H), 6.75 (m, 10H).

2.2.2 Synthesis of 2,5, bis (p-tolyl hydroxy methyl) thiophene

Thiophene (6.0 g,71.1 mmol, 5.7cm^3), N,N,N',N'-tetramethyl ethylene diamine (20.718, 178.28 mmol, 27 cm^3) and p-tolualdehyde (21.42, 178.28 mmol, 21 cm^3) under similar reaction conditions as

mentioned above ($ 2.2.1) afforded 2,5,-bis (p-tolyl hydroxy methyl) thiophene. m.p. 83-85^{o}C, Yield: 60% (13.82 g).

IR (KBr) : 3350,3055, 2925, 1605, 1515, 1265, 1040, 1025, 1010 cm^{-1}.

^{1}H NMR ($CDCl_3$): 1.94 (br, 2H), 2.35 (S, 6H), 5.90 (S, 2H), 6.68 (S, 2H), 7.2 (q, 8H).

2.2.3 Synthesis of 2,5-bis (p-anisyl hydroxy methyl) thiophene[41]

Thiophene (2.0 g, 23.7 mmol, 1.9 cm^3), N,N,N',N'-tetramethyl ethylene diamine (6.906 g, 59.425 mmol, 9 cm^3), n-butyl lithium (3.806 g, 59.425 mmol, 37.1 cm^3) and p-anisaldehyde (8.1 g, 59.425 mmol, 7.2 cm^3) under similar reaction as above ($ 2.2.1), afforded 2,5-bis (P-anisyl hydroxy methyl) thiophene. m.p. 152-4^{o}C. Yield 50% (4.2 g).

IR (KBr) : 3345, 3020, 2965, 2855, 1615, 1515, 1255, 1035, 1005 cm^{-1}

^{1}H NMR ($CDCl_3$): 1.83 (br, 2H), 3.84 (S, 6H), 5.94 (S, 2H), 6.71 (S, 2H), 6.87 (d, 4H, J_{AB} = 8.3 Hz), 7.36 (d, 4H, J_{AB} = 8.3 Hz).

^{1}H NMR ($CDCl_3$): 2.3 (S, 2H), 3.79 (S, 6H), 5.90 (S, 2H), 6.68 (S, 2H), 7.09 (8H, J_{AB} = 8.5 Hz) (Lit.)[41].

2.2.4 Prepartion of Monohydroxy phenyl tritolyl porphyrin (I)[32]

Pyrrole (2.68 g, 2.77 cm^3, 0.04 mol) was added to the refluxing propionic acid (500 cm^3) containing (3.96 g (3.53 cm^3,0.0297 mol) of p-tolylaldehyde and 1.230 g (0.01 mol) of

p-hydroxy benzaldehyde. The mixture was refluxed for 45 minutes and left overnight. The propionic acid was removed from the reaction mixture under reduced pressure leaving behind a black violet residue. It was washed with hot water and solvent extracted using $CHCl_3$. It was chromatographed on a basic alumina column using $CHCl_3$ as the eluent to remove meso-tetrakis (p-tolyl) porphyrin. The polarity of the solvent was changed to $CHCl_3$:CH_3OH (100 : 5 V/V) to elute the mono (hydroxy phenyl) tritolyl porphyrin (Fig.2.1). Evaporation of the solvent from the eluent under reduced pressure yielded violet colored compound. Yield 5.8% (0.39 g).

^1H NMR: 8.84 (S, 8H), 8.15 (d, 6H), 7.6 (d, 6H), 7.3 (m), 7.12 (m), 2.75 (s, 9H).

^1H NMR: 8.83 (S, 8H), 8.05 (d, 6H), 7.49 (d, 6H) 7.15 (m),7.00 (m), 2.68 (S, 9H).[32]

2.2.5 Preparation of 5-(4-(5-bromo-1-pentoxy) phenyl-10,15,20-tritolyl porphyrin[73]

A mixture of 0.500 g ($7.4x10^{-4}$ mol) of (monohydroxy) phenyl tritolyl porphyrin and 1.5 g of anhydrous potassium carbonate and 1,5-dibromopentae (2.272 g, 1.34 cm^3) were stirred magnetically with 25 cm^3 of dry DMF for 48 hours. The reaction mixture was then poured into 85 cm^3 of water and 15 cm^3 of methanol. The precipitated porphyrin was filtered off using a Buchner funnel and washed with methanol (10 cm^3). The porphyrin was dried, in an oven at 100°C. The excess dibromopentane was removed under reduced pressure at 120°C. It was chromatographed over basic

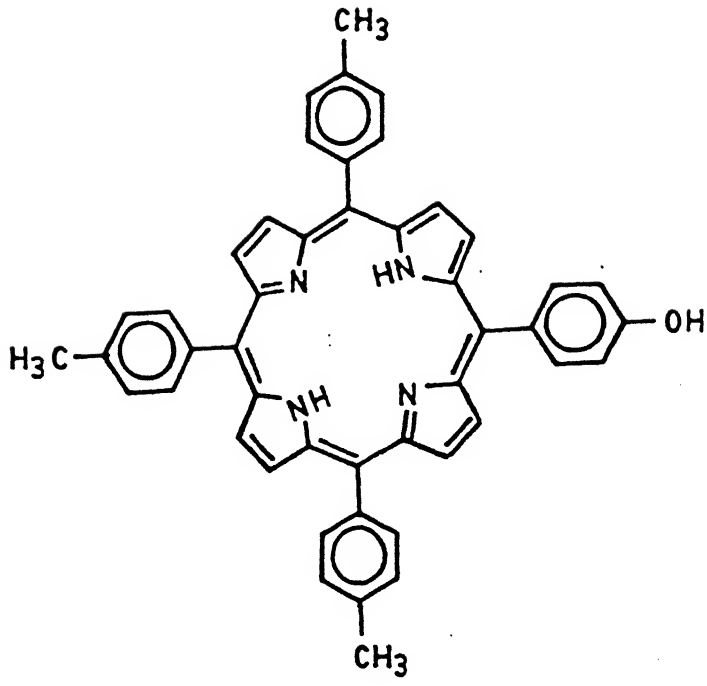

I

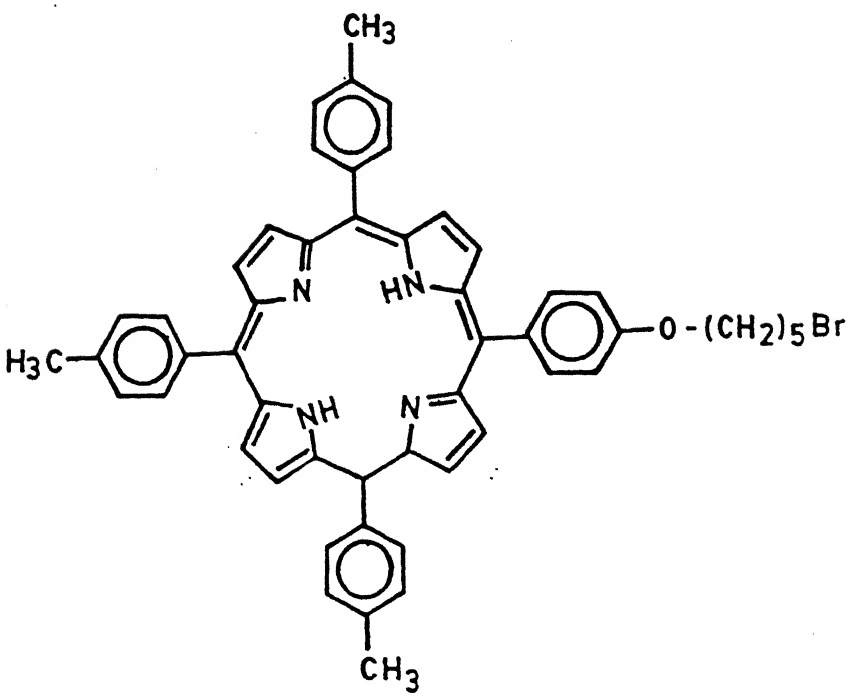

II

Fig. 2.1 Molecular structure of (I) p-mono hydroxy phenyl tritolyl porphyrin, (II) 5-(4-bromo-1-pentoxy) phenyl-10, 15, 20-tritolylporphyrin.

alumina column using toluene as the eluent. The first fraction (pink colour) obtained was 5-(4-(5-bromo-1-pentoxy)phenyl-10,15, 20-tritolyl porphyrin (II) (Fig. 2.1) and the unreacted monohydroxy phenyl tritolyl porphyrin (I) remained on the column as a slow moving purple band. Yield 87% (0.532 g).

^{1}H NMR ($CDCl_3$): 8.75 (S, 8H), 8.11 (d,8H), 7.55 (d, 6H), 7.22 (d,2H), 4.20 (t, 3H), 3.5 (t, 2H), 2.65 (S, 9H), 1.43 (m, 6H).

^{1}H NMR ($CDCl_3$): 8.83 (S, 8H), 8.05 (d, 8H), 7.46 (d, 6H), 7.10 (d, 2H), 4.08 (t, 2H), 3.41 (t, 2H), 2.13 (S,9H), 1.16 (m, 6H) (Lit.).[73]

2.3.0 Physico-chemical Techniques

The details of the instruments used for characterization and evaluation of spectroscopic data are given below.

The optical absorption spectra were recorded on a SHIMADZU UV-160 spectrometer with an adjustable temperature unit. ESR measurements were done on a Varian E-109, X-band spectrometer at liquid nitrogen temperature. IR spectra were recorded on a Perkin-Elmer model 580 Infrared spectrometer. The FAB mass spectra were recorded using a Jeol SX-120/DA-6000 mass spectrometer using Argon (6 KV, 10 mA) as the FAB gas. The accelerating voltage was 10 KV and the spectra were recorded at room temperature with m-nitrobenzyl alcohol as the matrix unless specified otherwise. The proton NMR spectra were recorded on Bruker WP-80 FT NMR spectrometer (80 MHz) and Bruker WM-400 FT NMR

spectrometer (400 MHz).

Raman spectra were recorded with the help of a SPEX Ramalog 1403 double monochromator equipped with a cooled RCA 31034A photomultiplier and photon counting detection system. Different excitation lines were provided by a Liconix model 4240 He-Cd and Spectra-Physics Model 165 Argon ion lasers. Samples were placed in a rotating Raman cell to avoid local heating and photo decomposition. The position of Raman peaks were calibrated with known lines of Indene.

Cyclic voltammetric studies were made with a BAS Model CV-27 polarographic analyser utilizing the three electrode configuration consisting of a Glassy carbon (working electrode), Pt wire (auxillary electrode) and a Ag/AgCl (reference electrode) electrodes. An Omnigraphic Model 100 X-Y recorder was used to record the current voltage output and / or cyclic voltammetric experiments were conducted on a PAR Model 370 Polarographic analyser utilizing the three electrode configuration of a Pt (BAS) as the working electrode, a Pt mesh counter electrode and a commercially available saturated colomel electrode (SCE) as the reference electrode. A RE 0074 X-Y recorder was used to record the curent-voltage output. Half-wave potentials were measured as the average of the cathodic and anodic peak potentials.

Fluorescence spectra were recorded on Jobin Yvon spectrofluorimeter JY-3 CS and a Perkin-Elmer LS 50B Luminescence spectrofluorimeter using the 1x1 cm quartz cell. The data analysis were done using the fluorescence data Manager Programme supplied by Perkin-Elmer. The lifetime apparatus uses a CW mode

locked Nd-YAG/synchronously pumped, cavity dumped dye laser (Rhodamine dissolved in ethylene glycol-ethanol mixture) as the excitation source. The lifetime were measured by picosecond time correlated single photon counting technique.

The triplet ESR measurements of various thiaporphyrins and their dications (chloroform: toluene (2:1)) were made on Varian E-9 X-band spectrometer. All the triplet ESR spectra were recorded with and without field modulation at -150°C. The pulsed laser (wavelength 560 nm) source was used for photo excitation. In method (A) the field modulation used was 100 KHz and light intensity modulation of 80 Hz with the detection system employing a pair of lock-in-amplifier tuned to the modulation frequencies.[74] The field modulation amplitude employed was 40 G and the microwave power about 5 mW. The ESR signals were measured 0.5 μs after laser excitation. The spectra were recorded in the derivative form and by using light modulation a doublet radical signal in the centre of the spectrum was removed. Also, this detection method has the advantage of signal enhancement provided by spin polarization.[75] In method B, no field modulation was used and the signal was detected after 1 μs of the laser excitation. With this technique the signal to noise ratio is improved because of the large spin polarization in the triplet shortly after their formation.[76] The spectra were recorded in absorption mode.

All the triplet spectra of water soluble thiaporphyrins were recorded in frozen H_2O : glycerol (1:1) at about 100K. The conditions of triplet ESR spectra recorded were: temperature at -150°C using excitation at 560 nm (unless noted otherwise),1.5

mJ/pulse, pulse repetition rate 40 Hz, spectra measured 0.5 micro seconds after excitation (laser pulse width 15 ns) for a period of 50 ns, microwave power 5 mW, number of sweeps 5, sweep time 1.5 minute, sweep width 1000 Gauss.

2.4.0 Methods for data analysis:

The fluorescence quantum yield (ϕ_f) was calculated from the emission and the absorption spectra by a comparative method, the following the equation:[52]

$$\phi_f = \frac{[F(\text{sample})])A(TPPH_2)]}{[F(TPPH_2)][(A(\text{sample})]} \times \phi_f\ (TPPH_2) \qquad (2.1)$$

where the [F(sample)] and [F($TPPH_2$)] are the integrated fluorescence intensities of the sample and 5,10,15,20 tetraphenyl porphyrin ($TPPH_2$).

[A(sample)] and[A($TPPH_2$)] are the absorbance of the sample and $TPPH_2$ at excitation of the same wavelength. ϕ_f ($TPPH_2$) is the quantum yield of $TPPH_2$ which is taken as 0.11.[77] The natural radiative lifetime (τ^o) was calculated by two methods: (i) using the relation

$$\tau^o = \frac{\tau_{fluo}}{\phi_f} \qquad (2.2)$$

where τ_{fluo} is the measured fluorescence lifetime and ϕ_f is the quantum yield of the sample. (ii) from the absorption and the emission spectra using Birks-Dyson[78] modification of Strickler-Berg[79] equation which is based on mirror symmetry

between the absorption and emission spectra, using the following equation:

$$\frac{1}{\tau^o} = 2.88\times10^{-9}\ \eta^2 < \bar{\nu}_f^{-3} >_{av}^{-1} \int \varepsilon(\bar{\nu})\ \bar{\nu}^{-1}\ d\nu \qquad (2.3)$$

where η is the refractive index of the solvent used.

$< \bar{\nu}_f^{-3} >_{av}^{-1}$ is the reciprocal of the mean value of ν^{-3} in the fluorescence spectrum, and this is defined by the following relation:

$$< \bar{\nu}_f^{-3} >_{av}^{-1} = \int F(\bar{\nu})\ d\bar{\nu} \ /\ F(\bar{\nu})\ \bar{\nu}^{-3}\ d\bar{\nu} \qquad (2.4)$$

where $\int F(\bar{\nu})d\bar{\nu}$ is the integrated fluorescence intensity and was evaluated directly from fluorescence spectrum by calculating the area under the curve of $F(\bar{\nu})$ versus $\bar{\nu}$.

$\int F(\bar{\nu})\bar{\nu}^{-3}\ d\bar{\nu}$ was evaluated from modified fluorescence spectrum by calculating the area under the curve of $F(\bar{\nu})\ \bar{\nu}^{-3}$ versus $\bar{\nu}$.

$\int \varepsilon(\bar{\nu})\ \bar{\nu}^{-1}\ d\bar{\nu}$ was calculated by evaluating area under the absorption [Q(x) (0,0) and Q_y (0,0)] curve of $\varepsilon(\bar{\nu})\bar{\nu}^{-1}$ versus $\bar{\nu}$ where $\varepsilon(\bar{\nu})$ is the molar extinction coefficient as a function of wave number ($\bar{\nu}$) and $F(\bar{\nu})$ is the fluorescence intensity as a function of wave number ($\bar{\nu}$).

The rate of fluorescent radiative decay (K_f) and rate of intersystem crossing (K_{isc}) were calculated using the relations

$$K_f = \frac{1}{\tau^o} \qquad (2.5)$$

$$K_{isc} = [\ K_f\ (1 - \phi_f)/\phi_f)\ ] \qquad (2.6)$$

The excited state redox potentials were estimated from the

emission spectra and the ground state redox potentials following the relation:[80]

$$^{*}E^{o}(P^{+}/^{*}P) = E^{o}(P^{+}/P) - E_{O-O}(P - ^{*}P) \qquad (2.7)$$

$$^{*}E^{o}(^{*}P/P^{-}) = E^{o}(P/P^{-}) + E_{O-O}(P - ^{*}P) \qquad (2.8)$$

where the E_{O-O} $(P - ^{*}P)$ is the energy of the Q(0,0) transition of the emitting excited state of the porphyrin, $^{*}E^{o}(^{*}P/P^{-})$ and $^{*}E^{o}(P^{+}/^{*}P)$ are the excited state reduction and oxidation potentials respectively and E^{o} (P^{+}/P) and E^{o} (P/P^{-}) refer to the ground state oxidation and reduction potentials respectively.

The solution magnetic susceptibility measurements were made by the usual NMR method[81] with a JEOL PMX-60(60 MHz) spectrometer and made use of the paramagnetic shift of water proton and using the equation

$$\text{Mass susceptibility } \chi_M = \frac{3\Delta f}{2\pi f m} + \chi_o + \frac{\chi_o (d_o - d_s)}{m} \qquad (2.9)$$

where Δf is the frequency separation between two water peaks in Hz, f is the frequency at which the proton resonances are being studied in Hz, m is the mass of the substance contained in 1 mL of solution, χ_o is the mass susceptibility of the solvent, d_o is the density of the solvent and d_s is the density of solution. The last term in the equation (2.9) is negligible for highly paramagnetic substances and hence can be ignored.

The magnetic moment was calculated using the equation

$$\mu = 2.84 \sqrt{\chi_M T} \qquad (2.10)$$

where χ_M is the molar magnetic susceptibility and T is the temperature of the NMR probe used.

The solvent susceptibilities were taken from literature.[82]

2.5.0 Summary

A brief account of various solvents, chemicals and methods of preparation of the different starting materials used in the synthesis is given here. This chapter also describes the different spectrometers and other physical methods used in the present study.

CHAPTER 3

SPECTRAL AND ELECTROCHEMICAL CHARACTERISTICS OF THIAPORPHYRINS AND THEIR DICATIONS IN GROUND AND EXCITED STATES IN NONAQUEOUS MEDIA

3.1.0 Introduction

Although, the synthetic procedures for the preparation of thiaporphyrins were developed some time back[34], systematic studies to understand the changes in the electronic structure of the porphyrin ring upon sulfur substitution began only about 5-6 years back mainly from the research groups of Latos Grazynski[42,61] in collaboration with Alan Balch, and Manassen and Ulman[55,56] in collaboration with Martin Gouterman and Thomas Spiro. The main purpose of these studies were to understand the structural aspects of the thiaporphyrins and their coordination abilities with transition metals. A considerable progress has been made in this direction and the details of the work done are discussed in the first chapter of this thesis. However, more work remains to be done for a complete understanding of the electronic structure of thiaporphyrins and some of the pertinent questions which need clarifications are about bonding interactions between two sulfur atoms in dithiaporphyrins, participation of empty d-orbitals available on sulfur atoms with the π-system of the porphyrin ring, the effect of heavy sulfur atoms on the spin-orbit coupling and behaviour of these thiaporphyrins in the excited singlet and triplet state. Keeping some of these questions in mind, we have embarked on this thiaporphyrin project with a hope of contributing significantly towards an understanding of ground and excited state properties. Specifically four thiaporphyrin;5,10,15,20-tetraphenyl

21-thiaporphyrin (STPPH), 5,10,15,20-tetraphenyl-21,23-dithiaporphyrin (S_2TPP) and to understand the effect of substituents, methoxy and methyl substituted dithiaporphyrins $(CH_3)_4S_2TPP$ and $(OCH_3)_4S_2TPP$ are chosen for study in this chapter (Fig.3.1). This chapter is divided into two parts. Part A describes the studies on the ground state properties evaluated using absorption spectra, ^1H NMR and Electro Chemical methods. The excited states were probed using Resonance Raman, fluorescence and photoexcited triplet ESR methods. Furthermore, from a knowledge of ground state redox properties and the energies of the first singlet excited state, the excited state redox potentials have been evaluated. The excited state studies are presented as Part B in this chapter. It has been shown that the energies of the highest occupied molecular orbitals (HOMO) (A_{2u} orbital) and the lowest unoccupied molecular orbitals (LUMO) $e_g(\pi^*)$ changes upon sulfur substitution with respect to normal porphyrins thus altering light absorption properties and the redox properties. The protonation experiments show the expected structural change due to steric crowding and triplet ESR data clearly reflect the changes in the kinetics of triplet formation and decay which is manifested in the change in the polarization pattern from ea ea ea to aa ae ee for monothiaporphyrins. To the best of our knowledge, this represents the first study on photoexcited triplet ESR of thiaporphyrins.

3.2.0 Experimental

Purification of solvents for spectral studies and synthesis of 2,5-bis(phenylhydroxy methyl) thiophene, 2,5,bis(p-tolyl hydroxymethyl) thiophene and 2,5,bis(p-anisyl hydroxymethyl) thiophene have been described in Chapter 2.

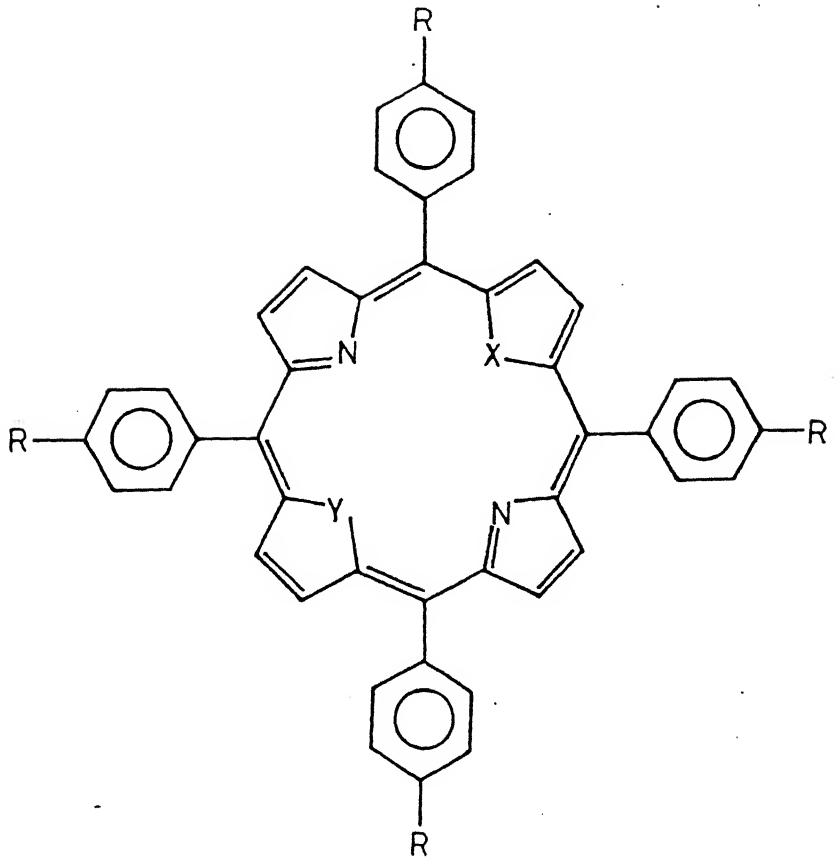

1	X = S ;	Y = NH ;	R = H	STPPH
2	X = S ;	Y = S ;	R = H	S_2TPP
3	X = S ;	Y = S ;	R = CH_3	$(CH_3)_4S_2TPP$
4	X = S ;	Y = S ;	R = OCH_3	$(OCH_3)_4S_2TPP$

Fig.3.1 Molecular structure of various thiaporphyrins

3.2.1 Preparation of STPPH[42]

2,5-bis(phenylhydroxymethyl) thiophene (0.7g, 2.5mmol), benzaldehyde (0.53g, 0.5 cm^3, 5.0 mmol) and pyrrole (0.50g, 0.52 cm^3, 7.5 mmol) were dissolved in freshly distilled propionic acid (250 cm^3). The mixture was refluxed for an hour and left at room temperature for 24 hours. The solvent was removed under reduced pressure. The crude product was thoroughly washed with hot water and was dissolved in chloroform and washed with 25% ammonia solution (100 cm^3) followed by water and dried over anhydrous sodium sulphate. The solvent was removed and the crude product was purified by column chromatography over basic alumina column using CCl_4 and CCl_4-$CHCl_3$ as the eluents. A pink band which was eluted with CCl_4 was identified as $TPPH_2$. Another yellowish orange band eluted with CCl_4:$CHCl_3$ (19 : 1 V/V) was identified as STPPH. This was followed by another small slow moving orange band identified as S_2TPP. The fraction containing STPPH was twice rechromatographed over basic alumina column using the CCl_4:$CHCl_3$ (19 : 1 V/V) as the eluent. STPPH was recrystallised from chloroform: n-hexane mixture. Yield of STPPH 4.5% (71 mg)

3.2.2 Preparation of S_2TPP[38]

2,5-bis(phenyl hydroxy methyl)thiophene (6g, 21.4 mmol) and pyrrole (1.43g, 1.48 cm^3, 21.4 mmol) were dissolved in freshly distilled propionic acid (500 cm^3) containing 2% acetic anhydride. The reaction mixture was refluxed for an hour and left for over night. The solvent was removed under reduced pressure. The crude product obtained was thoroughly washed with hot water and was dissolved in chloroform and washed with 25% ammonia solution (100

cm^3) several times with water and dried over anhydrous sodium sulphate. The crude product obtained on evaporation of the solvent was purified by column chromatography over basic alumina using benzene as the eluent. A yellow colour fraction which was eluted with benzene: $CHCl_3$ (3:1 V/V) was identified as S_2TPP. It was twice rechromatographed over basic alumina using benzene, and benzene : $CHCl_3$ (3:1 V/V) as the eluents. It was recrystallised from chloroform: n-hexane mixture. Yield of S_2TPP 10%.

3.2.3 Preparation of $(CH_3)_4\ S_2TPP$

2,5,-bis (p-tolyl hydroxymethyl)thiophene (6g, 1.95 mmol) and pyrrole (1.43g, 1.48 cm^3, 21.4mmol) under similar reaction conditions as above (§ 3.2.2) afforded $(CH_3)_4S_2TPP$. Yield 10%.

3.2.4 Preparation of $(OCH_3)_4S_2TPP$[41]

2,5-bis (p-anisylhydroxy methyl) thiophene (6g, 17.6 mmol) and pyrrole (1.18 g, 1.23 cm^3, 17.6 mmol) were dissolved in freshly distilled propionic acid (500 cm^3) containing acetic anhydride 2% V/V. The reaction mixture was refluxed for an hour. When the reaction mixture attained room temperature, the solvent was removed under reduced pressure. The crude product obtained was dissolved in chloroform and washed successively with 25% ammonia solution (3x100 cm^3), water and dried over anhydrous sodium sulphate. The crude product was obtained on evaporation of the solvent, was purified by column chromatography over basic alumina using benzene as the eluent. The orange fraction eluted with benzene:chloroform (1:3 V/V) was identified as $(OCH_3)_4S_2TPP$. It was twice rechromatographed over basic alumina using benzene:

$CHCl_3$ (3 : 1 V/V) as the eluent. It was recrystallised from chloroform: n-hexane mixture. Yield of $(OCH_3)_4S_2TPP$) is 8.2%.

PART A

3.3.0 GROUND STATE PROPERTIES OF THIAPORPHYRINS AND THEIR DICATIONS

RESULTS

3.3.1 Electronic Spectra

The electronic spectral data of different thiaporphyrins and their dications are listed in table 3.1. For comparison, the data of free base tetraphenylporphyrin ($TPPH_2$) and its dication are also included.[38] The observed effects upon substitution of nitrogen by sulfur are (i) a red shift of the soret band relative to $TPPH_2$. The magnitude of red shift depends on the number of pyrrole nitrogens replaced as well as on para substituents of the phenyl ring (ii) a red shift of the Q-bands; the Q-bands I and II experience a larger shift relative to Q bands III and IV. (iii) A reduction in intensity of soret bands and Q-bands relative to free base $TPPH_2$ and the magnitude of decrease is a function of number of sulfur atoms in the porphyrin core. (iv) the change in the intensity pattern of Q-bands; Q I is more intense than Q II in all thiaporphyrins in contrast to $TPPH_2$. Furthermore, the soret bands are more intense than Q bands in all the thiaporphyrins similar to those observed for normal porphyrins.

The absorption spectra of $(CH_3)_4S_2TPP$ and its mono and dications in $CHCl_3$ is shown in Fig. 3.2. The mono and dications were generated by careful titration of dilute solution of

Table 3.1 Electronic spectral data of thiaporphyrins and their mono- and dications in $CHCl_3$[a]

Porphyrin	Soret band λ_{max}(nm)(εx10^{-4})	Q bands, λ_{max}(nm) (εx10^{-3})					
		IV		III	II		I
S_2TPP	435(25)	514(26)		547(7.0)	633(2.2)		696(4.5)
S_2TPPH^+	449(14.4)		598(5.8)			697(7.0)	
$S_2TPPH_2^{2+}$	463(28)		697(31.5)			735(29.7)	
$(CH_3)_4S_2TPP$	437(27)	516(26)		550(8.9)	634(1.9)		698(5.5)
$(CH_3)_4S_2TPPH^+$	459(18)		609(11.8)			708(15.0)	
$(CH_3)_4S_2TPPH_2^{2+}$	468(26.5)		722(41.4)			760(40.2)	
$(OCH_3)_4S_2TPP$	440(25.1)	518(20.8)		555(11.3)	639(1.6)		703(5.8)
$(OCH_3)_4S_2TPPH^+$	474(16)		772(36.7)				
$(OCH_3)_4S_2TPPH_2^{2+}$	472(14.4)		783(55.7)				
STPPH	429(18.7)	513(17.1)		547(4.4)	618(1.9)		675(3.0)
[b]$STPPH_3^{2+}$	456(19.0)		699(24)				
[c]$TPPH_2$	419(46.4)	515(18.7)		548(8.6)	592(5.5)		647(3.9)
[c]$TPPH_4^{2+}$	448(43.6)		608(9.0)			659(50.9)	

[a]Mono- and dications are generated by titrating a dilute solution of TFA in $CHCl_3$;

[b]Monocation could not be generated in this case in $CHCl_3$;

[c]Data taken from Ref.38.

trifluoro acetic acid ~1x10^{-3}M in $CHCl_3$. The monocation of STPPH in $CHCl_3$ was not observed probably due to very close P^k values of mono and dications. It is seen from Fig. 3.2 that upon protonation the four-banded Q-band structure is changed to a simple two banded pattern. Furthermore, the Q-band and soret bands are shifted to red upon monocation formation relative to the neutral species and the formation of dications results in the further red shift of the Q and soret bands. A similar effect was observed for structurally similar $TPPH_2$ upon protonation.

3.3.2 ^{1}H NMR Spectra

The ^{1}H NMR spectra of thiaporphyrins were recorded in $CDCl_3$ and the dications were generated by addition of appropriate amounts of deuterated trifluoro acetic acid to $CDCl_3$ solution. Fig. 3.3 shows the ^{1}H NMR spectra of $(CH_3)_4S_2TPP$ and its dication. All the proton chemical shifts and coupling constants are listed in table 3.2. The ^{1}H NMR spectrum of monothiaporphyrin (STPPH) shows a doublet for thiophene protons and a singlet and an AB quartet[70] for two kinds of pyrrole protons marked as A and B in the figure 3.4 and the multiplet for meso phenyl protons. The ^{1}H NMR spectrum of dithiaporphyrins shows two separate sharp singlets for pyrrole and thiophene protons. The phenyl protons in unsubstituted S_2TPP[56] appear as two multiplets centered around 8.26 and 7.874 ppm due to ortho and meta and para protons, respectively. The phenyl protons in parasubstituted $(CH_3)_4S_2TPP$ and $(OCH_3)_4S_2TPP$ appear as AB quartet. The methyl protons in $(CH_3)_4S_2TPP$ and methoxy protons in $(OCH_3)_4S_2TPP$ appear as a singlet at 2.75 and 4.12 ppm respectively essentially indicating the symmetrical substitution. The formation of dications of

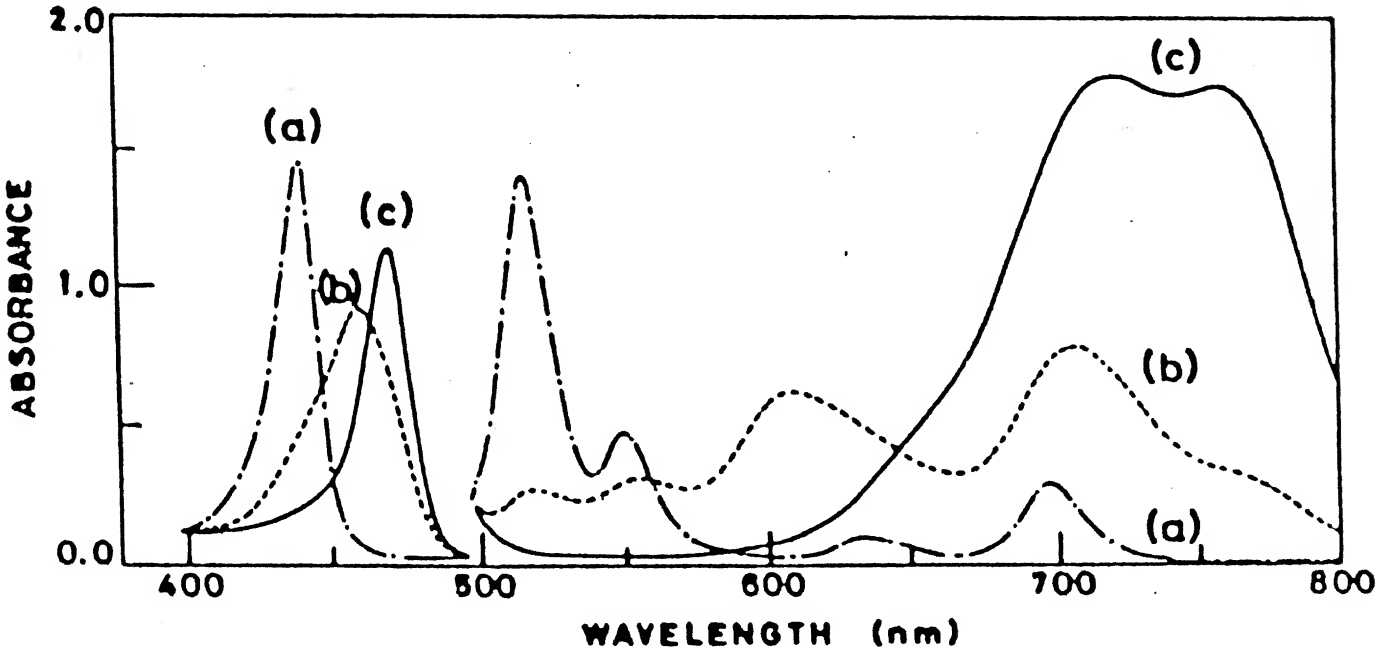

Fig.3.2 Electronic spectra of (a) $(CH_3)_4S_2TPP$ (b) $(CH_3)_4STPPH^+$ and (c) $(CH_3)_4S_2TPPH_2^{2+}$ in $CHCl_3$ (concentration used $\simeq 1x10^{-5}M$)

Table 3.2 ^{1}H NMR of thiaporphyrin and their dications* in $CDCl_3$

Porphyrin	Pyrrole	Thiophene	Phenyl		p-Substituent
S_2TPP	8.69(s)	9.61(s)	8.26(o)(M)	7.874(m,p)(M)	-
$S_2TPPH_2^{2+}$	9.08(s)	9.74(s)	8.64(o)(M)	8.16(m,p)(M)	-
$(CH_3)_4S_2TPP$	8.78(s)	9.80(s)	8.23(o)d	7.68(m)d	2.75(s)
			J_{AB}=7.5 Hz	J_{AB}=7.5 Hz	
$(CH_3)_4S_2TPPH_2^{2+}$	9.13(s)	9.77(s)	8.64(o)d	8.05(m)d	2.91(s)
			J_{AB}=8.8 Hz	J_{AB}=8.8 Hz	
$(OCH_3)_4S_2TPP$	8.72(s)	9.72(s)	8.21(o,d)	7.42(m,d)	4.12(s)
			J_{AB}=8.8 Hz	J_{AB}=8.8 Hz	
$(OCH_3)_4S_2TPPH_2^{2+}$	8.95(s)	9.58(s)	8.68(o,d)	7.76(m,d)	4.31(s)
			J_{AB}=8.8Hz	J_{AB}=8.8 Hz	
STPPH	8.96(d)	9.78(s)	8.32(o,M)	7.64(m,p)(M)	
	8.70(q)				
$STPPH_3^{2+}$	9.15(d)	9.63(s)	8.75[b](M)	8.12(m,p)(M)	
$TPPH_2$[a]	8.72(s)	---	8.30(o,M)	7.80(m,p)(M)	
$TPPH_2^{2+}$	8.67(s)	---	8.59(o,M)	8.01(m,p)(M)	

* Dications are generated by titrating appropriate amounts of TFA to $CDCl_3$ solution;

s,d,M refers to singlet, doublet and multiplet;

o,p,m refers to ortho, meta and para protons of phenyl rings;

a taken from Ref. 56c.

b - ortho hydrogens of phenyl and one kind of pyrrole protons are merged.

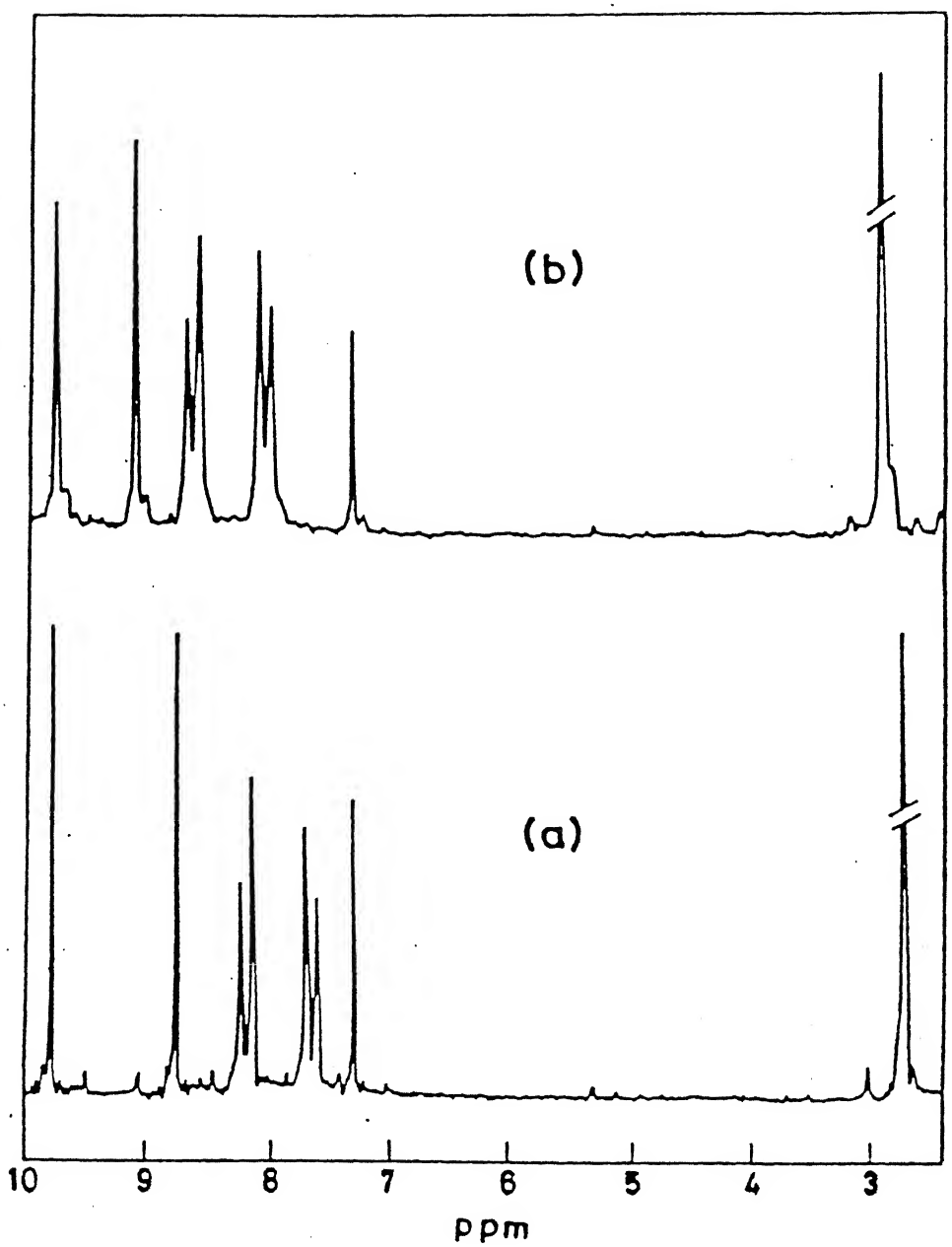

Fig.3.3 ^{1}H NMR spectra of (a) $(CH_3)_4S_2TPP$ and (b) $(CH_3)_4S_2TPPH_2^{2+}$ in $CDCl_3$

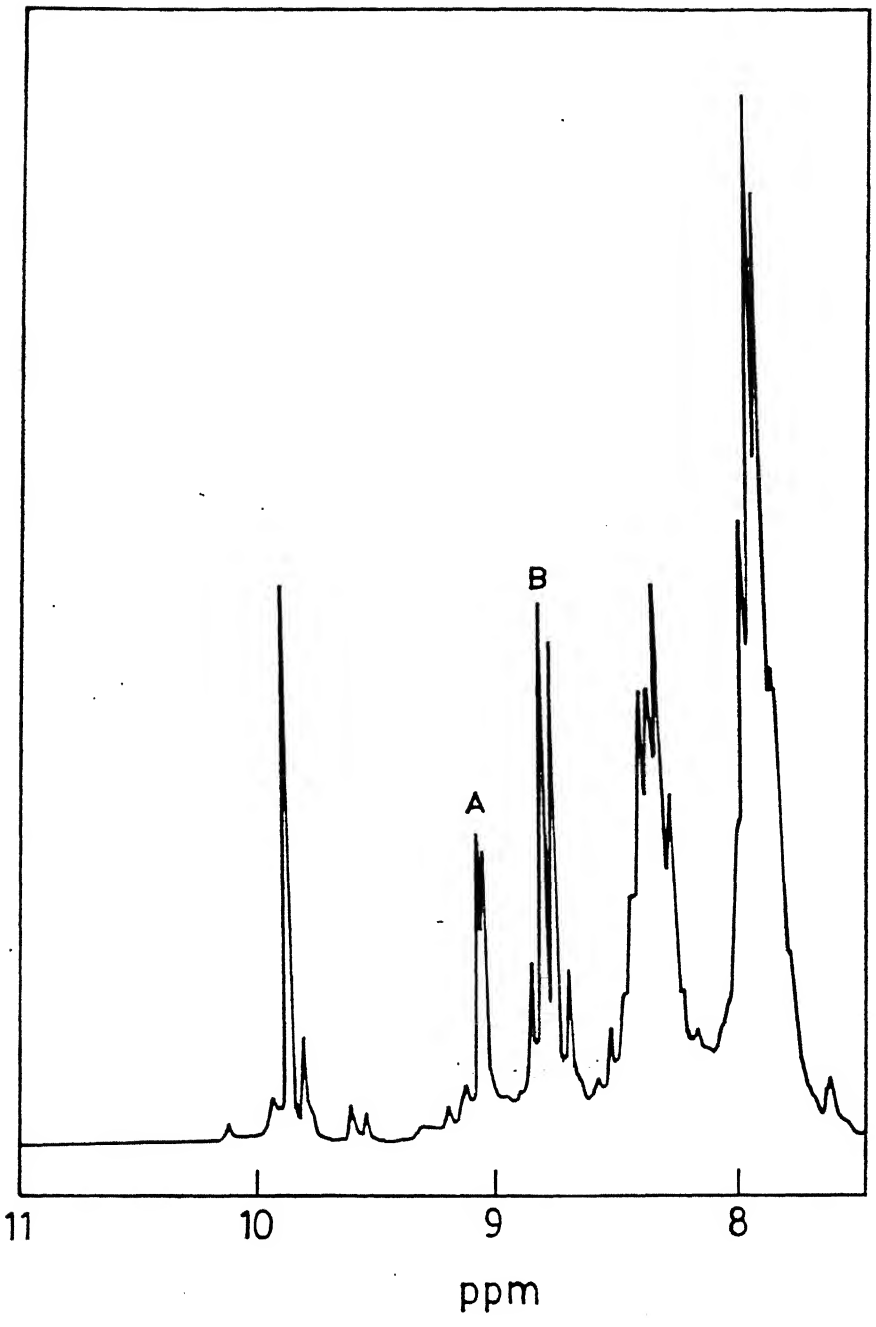

Fig.3.4 ^{1}H NMR spectrum of STPPH in $CDCl_3$ (Two kinds of pyrrole protons are marked as A and B).

thiaporphyrins result in a large down field shift (0.23-0.39 ppm) of pyrrole protons while the thiophene protons experience a negligible shift. All the phenyl protons experience a considerable downfield shift (0.32 - 0.47 ppm) with coupling constants remaining unaltered. The methyl protons in $(CH_3)_4S_2TPPH_2^{2+}$ and methoxy protons in $(OCH_3)_4S_2TPPH_2^{2+}$ experience a small downfield shift (0.16 - 0.19 ppm).

3.3.3 Electro Chemistry

Electro chemical data of various thiaporphyrins along with $TPPH_2$ in CH_2Cl_2 are listed in table 3.3. Typical cyclic voltammograms of $(CH_3)_4S_2TPP$ and $(OCH_3)_4S_2TPP$ in methylene chloride are shown in Fig. 3.5. Both S_2TPP and $(CH_3)_4S_2TPP$ show one redox couple (I) for oxidation and two couples (II and III) for the reduction process. Further, oxidation was accompanied by decomposition in these two cases. However, in the case of $(OCH_3)_4S_2TPP$ the second oxidation was achieved in the potential range scanned. The first oxidation process in $(CH_3)_4S_2TPP$ is quasi reversible (ΔE_p = 70 mV, $\frac{i_p}{i_c} \simeq 1$). The first and second reduction process in $(CH_3)_4S_2TPP$ is quasi reversible (ΔE_p = 76-100 mV, $\frac{i_p}{i_c} \simeq 1$). The first reduction process in $(OCH_3)_4S_2TPP$ is reversible (ΔE_p = 60 mV, $i_p/i_c \simeq 1$). The redox potential data in table 3.3 indicate the following effects upon replacement of -NH by sulfur atom: (i) both oxidation and reduction potentials experience a slight positive shift (~ 140 mV for oxidation and 290-320 mV for reduction) relative to $TPPH_2$ (ii) electron donating groups at the para position of the phenyl rings of S_2TPP shift the oxidation potentials to less positive values

Table 3.3 Half-wave potentials of thiaporphyrins in CH_2Cl_2 ($E_{1/2}$ in V vs SCE)

Porphyrin	I^*_{ox}	II_{ox}	$I_{Red.}$	$II_{Red.}$	Δ_{redox}
S_2TPP	1.17	---	-0.94	-1.23	2.11
$(CH_3)_4S_2TPP$	1.09	---	-0.95	-1.27	2.04
$(OCH_3)_4S_2TPP$	0.98	1.17	-0.97	-1.28	1.95
$(CH_3)_4STPPH$	1.035	---	-1.065	---	2.10
$TPPH_2$[a]	1.03	---	-1.23	-1.55	2.26

$\Delta_{redox} = E_{1/2}(I_{ox}) - E_{1/2}(I_{red.})$;

a - taken from Ref.87b.

*Ox - Oxidation, Red - reduction

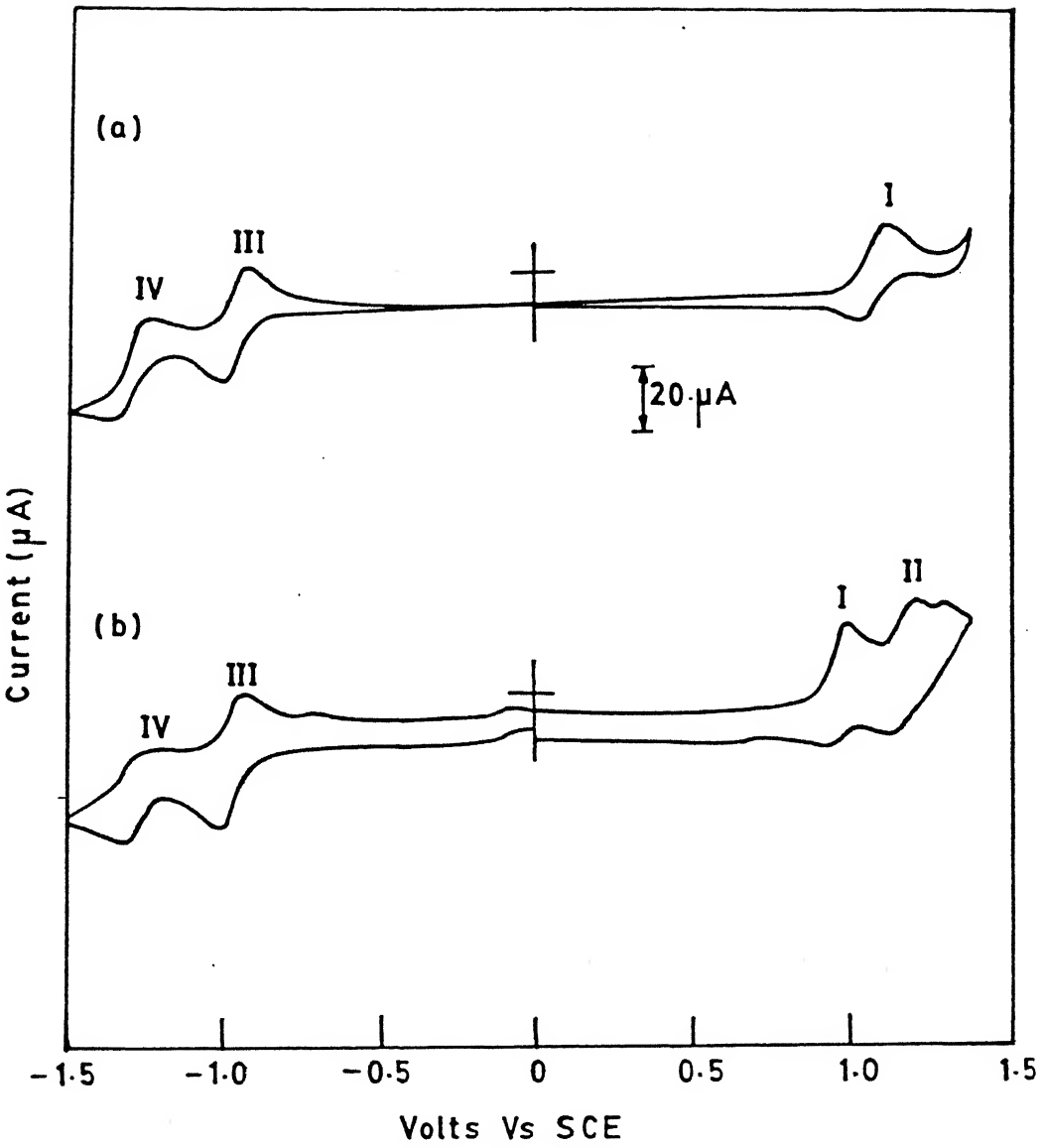

Fig.3.5 Cyclic voltammogram of (a) $(CH_3)_4S_2TPP$ (b) $(OCH_3)_4S_2TPP$ i
CH_2Cl_2 and 0.1 M TBAP. Scan rate (ν) for (a) is 50 mV/
and (b) is 100 mV/s.

(80-190 mV) while slightly more negative shifts are observed for reduction potentials. (iii) a linear decrease (30mV) of Δ_{redox} upon substitution of sulfur atom.

DISCUSSION

3.3.1 Electronic Spectra

Many of the qualitative features of the electronic absorption spectra of porphyrins have been interpreted interms of Gouterman's four orbital model.[83] The model focusses on the importance of the highest filled molecular orbitals (HOMO) and the lowest unfilled molecular orbitals (LUMO) (Fig. 3.6). According to the four orbital model, the soret band can be assigned to the excitation from ground to B state while Q-band transition corresponds to the excitation to E states in the porphyrins. Configuration interaction (CI) mixes the two excited configurations in such way that one observes the weak transition (Q-band), corresponding to a destructive CI interference and a strong transition (soret band), corresponds to a constructive CI interference. The visible absorption spectrum of free base porphyrin shows the four bands. This has been attributed to a break down of a symmetry (D_{4h}) of the porphyrin ring by central protons. Thus Q(0,0) splits into Q_x(0.0) and Q_y(0,0). Each band has a vibronic transition Q_x (1,0) and Q_y(1,0) respectively.

The absorption spectra of thiaporphyrins show the red shift of the soret band and Q-bands relative to $TPPH_2$ indicating the changes in the energy levels of E and B states upon substitution of sulfur. The sulfur atom being larger in size, reduces the size

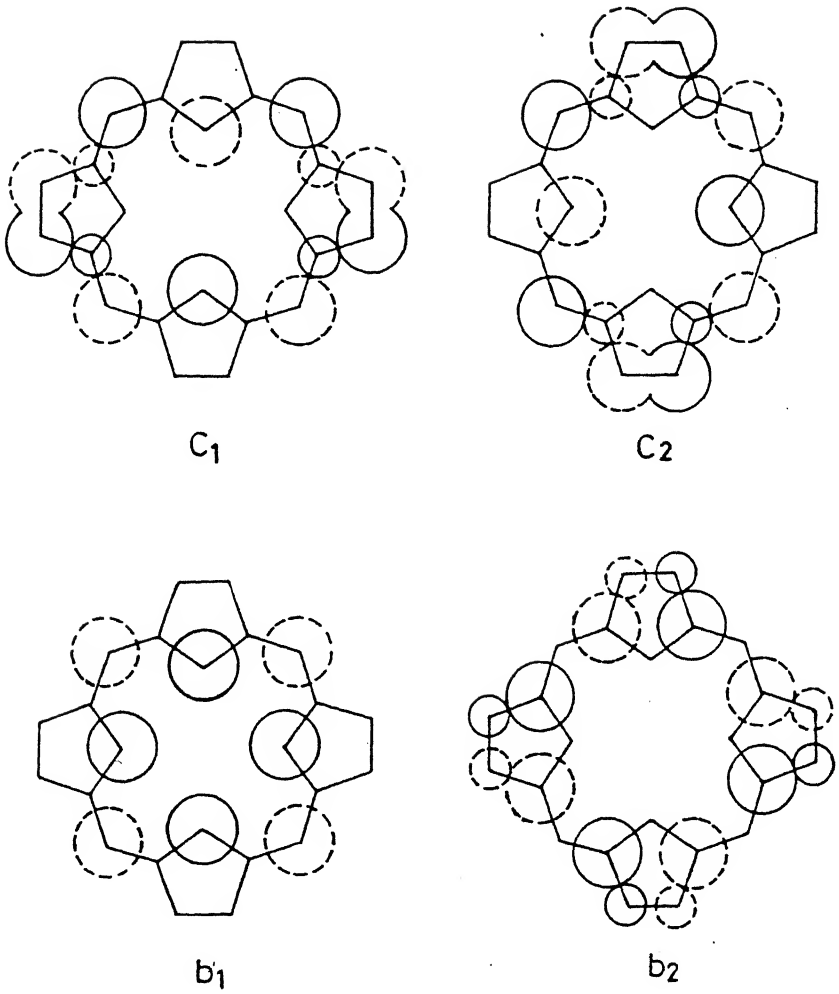

Fig.3.6 The four orbitals of the Gouterman Model, representing the two HOMO's and the two LUMO's of a porphyrin with D_{4h} symmetry. The atomic orbital coefficients are proportional to the circles and solid and dashed circles indicate the sign of wave function. In D_{4h} or D_{2h} symmetry, the symmetries of four orbitals are $b_1 = a_{2u}$ or $b_{1u} = a_{1u}$ or a_u, $c_1 = e_g$ or b_{2g} and $c_2 = e_g$ or b_{3g} respectively.

of the porphyrin core and in dithiaporphyrins this decreased core size can induce bonding interaction between sulfur atoms.[56] Indeed, molecular orbital (MO) energy calculations by Gouterman[52] and coworkers and Resonance Raman studies by Spiro et al[55] on dithiaporphyrin clearly provide evidence for the presence of bonding interaction between hetero atoms, thus altering the energy levels of porphyrin. Furthermore, electrochemical studies by Ulman and coworkers reveal that both HOMO and LUMO are stabilized upon sulfur substitution, thus reducing the energy gap between HOMO and LUMO (vide infra). This decreased energy gap is responsible for the observed red shift in the optical spectra. The higher magnitude of red shift for dithiaporphyrins relative to monothiaporphyrins is consistent with this observation.

It is well known that the meso aryl porphyrins upon protonation exhibit red shift of soret and Q-bands.[84] This has been attributed to the structural change in the porphyrin core accompanying the protonation. The meso-phenyl ring is expected to be tilted with respect to the porphyrin plane with a tilt angle between 60 and 70^{o} because of the steric interaction between the ortho hydrogens of the phenyl rings and the protons of adjacent pyrrole rings. The protonation of the porphyrin is expected to release this repulsive interaction by tilting the pyrrole and the thiophene rings out of the porphyrin plane inducing significant nonplanarity and thus making the phenyl rings more coplanar with porphyrin plane. This would facilitate the delocalisation of π-electrons into phenyl ring by a resonance interaction. Such a structural change is supported by earlier spectroscopic studies and the X-ray structure of structurally similar tetraphenyl porphyrin dication.

The X-ray structure of dithiaporphyrin[47] has revealed that the porphyrin core is almost planar with a very small deviation(the deviation, expressed as the dihedral angle between the meso carbons and the planes of the four membered rings are thiophene 4.9° and pyrrole 12.9°]. In view of the similarities in the structure, it is reasonable to expect similar structural change upon protonation in the thiaporphyrins. Furthermore, the magnitude of red shift observed in thiaporphyrins is much larger, (the Q1 band shifts 12 nm in $TPPH_2$, while the same band shifts 39, 62 and 80 nm for S_2TPP, $(CH_3)_4S_2TPP$ and $(OCH_3)_4S_2TPP$, respectively) as compared to that of tetraphenylporphyrin indicating an increased resonance interaction between phenyl rings and porphyrin plane. However, the magnitude of red shift observed for the soret band upon protonation in $TPPH_2$ and thiaporphyrins remains more or less constant (29 nm for $TPPH_2$, 27, 28, 31 and 32 nm for STPPH, S_2TPP, $(CH_3)_4S_2TPP$ and $(OCH_3)_4S_2TPP$, respectively).

3.3.2 ^1H NMR spectra

The appearance of two separate sharp singlets for thiophene and pyrrole protons indicate the presence of a two-fold axis of symmetry in dithiaporphyrins which is in accordance with structure. However, in monothiaporphyrins, the symmetry is reduced and this is reflected in the inequivalence of pyrrole protons. It is interesting to note that $TPPH_2$ shows only a singlet for pyrrole protons (8.72 ppm) and this has been accounted interms of rapid tautomeric equilibrium between the pyrrole rings.[85] However, the spectrum recorded at - 80°C shows two peaks for the two kinds of pyrrole protons (8.90 and 8.61 ppm) due to

decrease in rate of exchange. In dithiaporphyrins such a tautomerism is not possible since the NH groups are replaced by sulfur and hence all the pyrrole protons are equivalent. Furthermore, sulfur substitution does not effect the chemical shift of these protons as evident from the table 3.2. However, inspection of the table 3.2 indicates that thiophene protons are shifted down field (0.71 ppm in S_2TPP). This has been explained using a simple valence bond model.[56] Assuming a pd^2 hybridization of the filled p_z orbital with empty d_{xz} and d_{yz} orbitals of sulfur, three pd^2 orbitals can be described as follows:

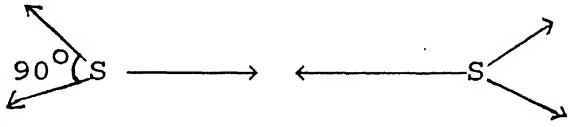

pd^2 hybridization of sulfur atoms

Two of these orbitals are orthogonal, third is in right direction to explain S-S interaction. The average electron density in each of the pd^2 orbitals is 2/3 of an electron and as they are originated from d-orbitals situated in the xz and yz planes and they can interact with molecular π-system. The shorter the S....S distance, stronger is the attractive interaction and more effective overlap between the two pd^2 orbitals involved. Thus for greater S....S interaction, less electron density is available on the heteroatoms of the inner aromatic pathway (16 membered structure).[56] This results in the greater statistical weight of the outer aromatic pathway (18-membered structure).[56] Because thiophene protons are closer to the outer aromatic pathway which results in down field shift (9.61 ppm) in the NMR spectrum.

The protonation results in larger shift of pyrrole protons in dithiaporphyrins [0.39 ppm for S_2TPP, 0.35 ppm for $(CH_3)_4S_2TPP$, 0.23 ppm for $(OCH_3)_4S_2TPP$)] relative to the thiophene protons [0.13 ppm for S_2TPP, -0.03 ppm for $(CH_3)_4S_2TPP$ and -0.14 ppm for $(OCH_3)_4S_2TPP$] suggesting the protonation of pyrrole nitrogens.[56] The observed downfield shift of the pyrrole, phenyl protons and substituents methyl, methoxy groups upon dication formation can be ascribed to the following two effects: (i) the introduction of two extra positive charges into the porphyrin core (ii) the nonplanarity of the dications leading to greater resonance interaction between phenyl rings and porphyrin plane. Based on the spectral data a schematic representation of the protonation process is depicted in Fig. 3.7 for dithiaporphyrins.

3.3.3 Electro Chemical Studies

The direction of the shifts for oxidation (140 mV for S_2TPP)and reduction (290, 320 mV for S_2TPP) potentials for thiaporphyrins suggest harder oxidations and easier reductions relative to $TPPH_2$ (table 3.3). These shifts in the redox potentials indicate changes in the energies of the HOMO's and LUMO's such that the energy gap between the HOMO's and LUMO's decreases as a function of number of sulfur atoms (Δ_{redox}). A linear correlation has been observed for the energies of the soret maxima and Δ_{redox}.[86] It has been pointed out earlier that both HOMO and LUMO are stabilized in thiaporphyrins by different mechanisms.[86] The stabilization of the HOMO, which occurs on substitution of NH groups by sulfur atoms has been explained by assuming the participation of the empty d-orbitals of the sulfur

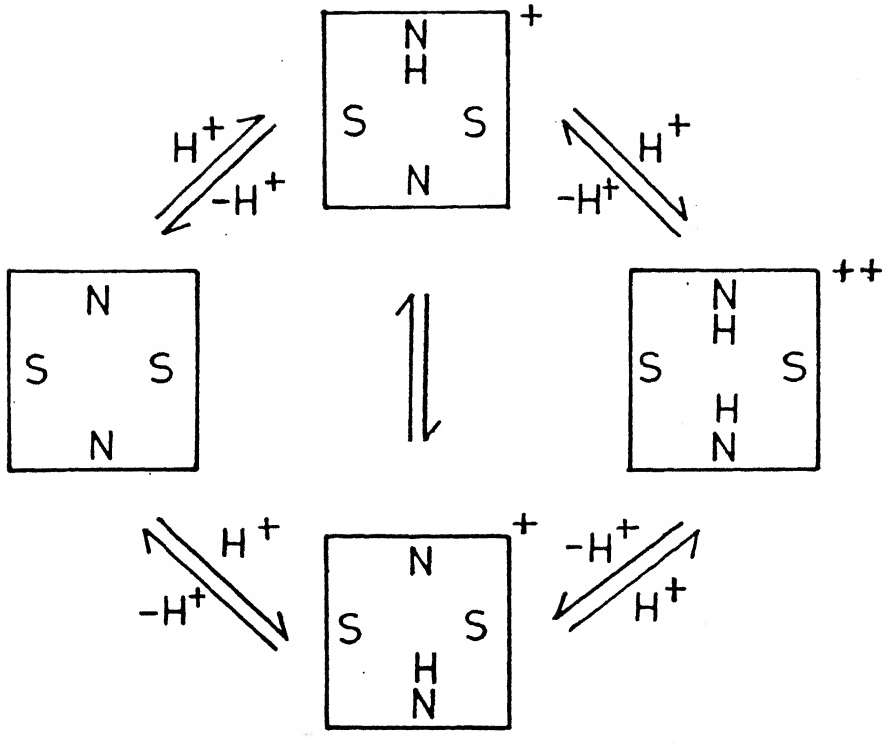

Fig.3.7 Proposed protonation scheme for dithiaporphyrins.

atoms. This mechanism is valid only when the bonding interaction is considered. The X-ray studies[48] indicate that S.....S distance is 3.02 A^{o} compared to a Van der Waal's radii of 3.70 A^{o}. This short distance demands definition of four $d\pi$ - $d\pi$ orbitals

$$\phi_{1,2} = d_{xz}\ (1) \pm d_{xz}\ (2) \qquad (3.1)$$

$$\phi_{3,4} = d_{yz}\ (1) \pm d_{yz}\ (2) \qquad (3.2)$$

These new orbitals have the right symmetry to interact with the outer porphyrin orbitals, and MO calculations show indeed that a considerable stabilization is achieved by this d-orbital participation.[52] Thus without the participation of the empty d orbitals a repulsion is found between the sulfur atoms. The LUMO stabilization has been explained as folows: the high resolution NMR results suggested that the bonding interactions between the chalcogen atoms act as an electron drain on the molecular π-system, as a result large down field shift of the proton resonances were observed. This electron drain effect can be compared to the effect which transition metals have on the electrochemical behaviour of metalloporphyrins and is called "the inductive effect" by Fuhrhop.[87a] Thus, it is concluded that replacement of nitrogen by sulfur is to reduce the energy gap between the HOMO and LUMO and this inturn affects the net absorption and redox potentials.

Part B

3.4.0 EXCITED STATE PROPERTIES OF THIAPORPHYRINS AND THEIR DICATIONS

RESULTS

3.4.1 Resonance Raman Studies

Figures 3.8 and 3.9 compare the Resonance Raman spectra obtained with 457 nm excitation of a representative $(OCH_3)_4S_2TPP$ and its dication in the high and low frequency region. A detailed analysis of the vibrational modes of S_2TPP and few other chalcogen porphyrins has recently been done by Spiro and coworkers[55] and in the present study the Raman bands were assigned following this work and taking into account the latest normal mode analysis of metallo-TPP.[88] However, for STPPH, which has a lower symmetry, only few modes have been assigned by comparison with S_2TPP. The Resonance Raman data along with the shifts observed upon protonation of all the thiaporphyrins are listed in table 3.4. The following major changes were noted upon protonation: (a) the phenyl modes shift to slightly lower frequencies. (b) the modes of porphyrin skeletal vibrations, ν_2, ν_{11}, ν_{10} and ν_{13} also experience a considerable shift to lower frequencies while the ν_4 mode which is primarily associated with the pyrrole symmetric half-ring stretch shifts to higher frequency side[89]; (c) the modes directly involving the S-atoms (C_α - S stretching) and ν_{16} (symmetric deformation of the porphyrin ring) undergo a small positive and negative shift, respectively; (d) the ν_{cm-ph} mode at 1250 cm^{-1} in S_2TPP experiences a small shift to higher frequency; (e) the relative intensities of Raman bands also change; for example, ν_2 and ν_{10} modes gain intensity while the ν_{cm-ph} mode loses intensity upon protonation. Literature studies often reveal

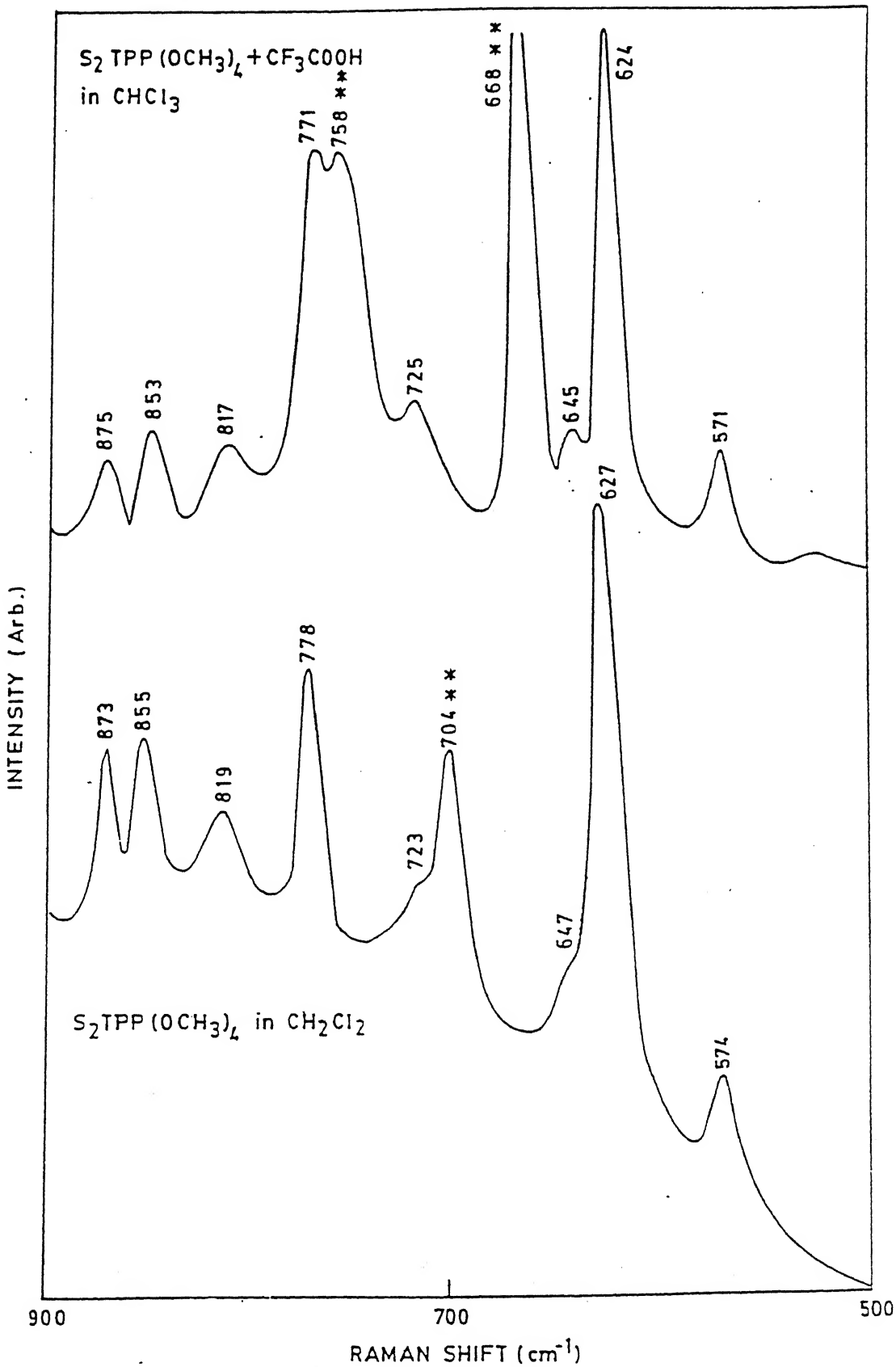

Fig.3.8 Resonance Raman spectra of $(OCH_3)_4S_2TPP$ and its dicat in the low frequency region. ** Peak corresponds to solvent.

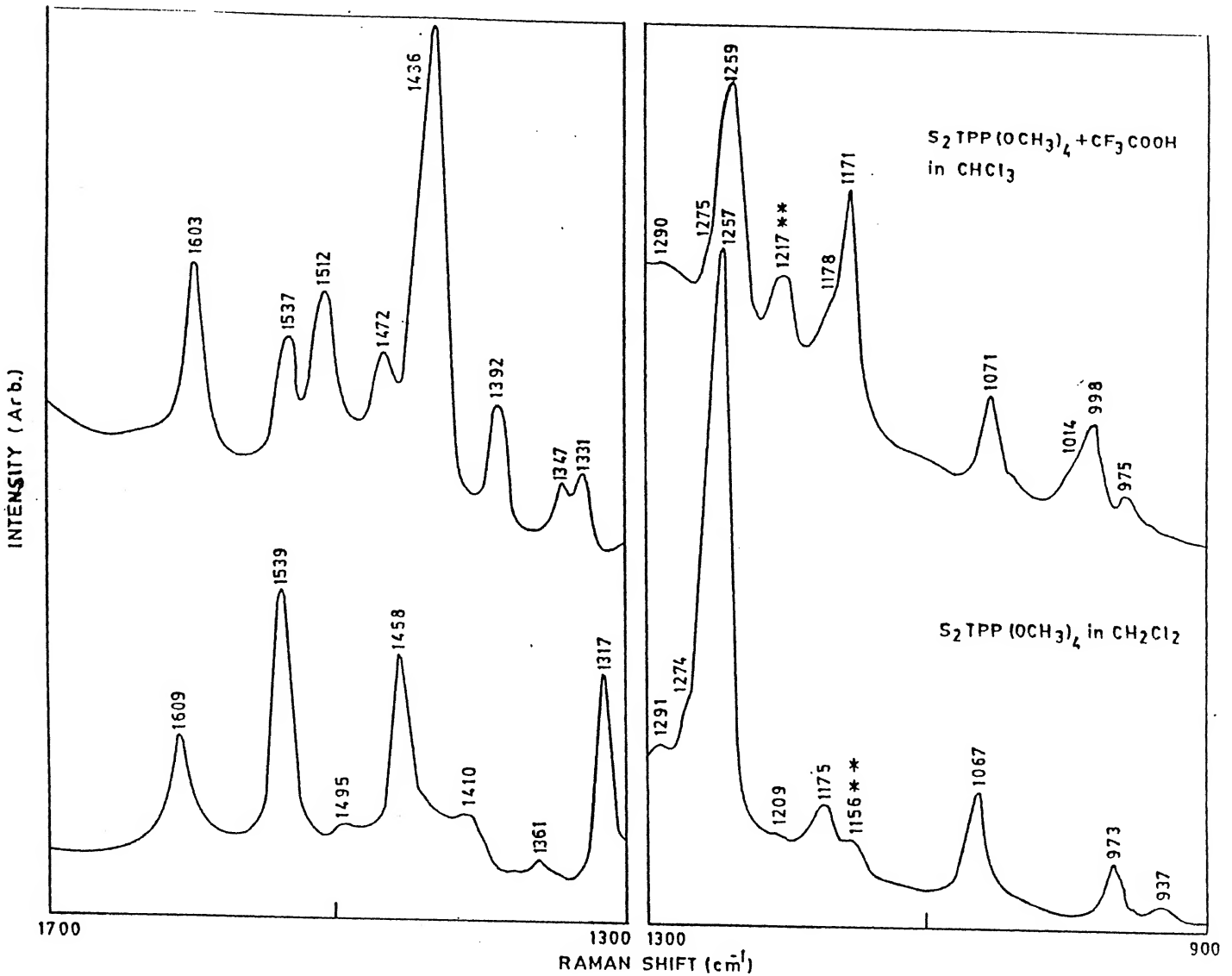

Fig.3.9 Resonance Raman spectra of $(OCH_3)_4S_2TPP$ and its dication in the high frequency region. ** Peak corresponds to the

Table 3.4 Observed Resonance Raman Frequencies (cm^{-1}) of thiaporphyrins and their dications (only major bands)

S_2TPP	$\Delta\nu$	$(CH_3)_4S_2TPP$	$\Delta\nu$	$(OCH_3)_4S_2TPP$	$\Delta\nu$	STPPH	$\Delta\nu$	Mode NO and assignment[a]
1599 (1596)*	-3	1612 (1611)	-1	1609 (1603)	-6	- (-)	-	Φ_4; $\nu_{(C-C)phenyl}$
1409 (1395)	-14	1402 (1394)	-8	1410 (1392)	-18	1408 (1397)	-11	$\nu_{10}(B_{1g})$; $\nu_{(C_\alpha-C_m)asym}$
1538 (1524)	-14	1535 (1512)	-23	1539 (1512)	-27	1544 (1531)	-13	$\nu_2(A_{1g})$; $\nu_{(C_\beta-C_\beta)sym}$
- (1542)	--	-- (1540)	--	-- (1537)	--	-- (1543)	-	$\nu_{19}(A_{2g})$; $\nu_{(C_\alpha-C_m)asym}$
1457 (1442)	-15	1457 (1443)	-14	1458 (1436)	-22	1459 (1455)	-4	$\nu_{11}(B_{1g})$; $\nu_{(C_\beta-C_\beta)asym}$
1361 (1349)	-12	1360 (1348)	-12	1361 (1347)	-14	1361 (1356)	-5	$\nu_{29}(B_{2g})$; $\nu_{(Pyr\ quarter\ ring)}$ Mainly $(C_\beta-H + (C_\alpha-C_\beta)$
1314 (-)	-	1315 (1332)	+17	1317 (1331)	+14	1318 (1330)	+12	$\nu_4(A_{1g})$; $\nu_{(Pyr.half\ ring)sym}$
- (1290)	-	- (1289)	-	- (1290)	-	- (1287)	-	δ (N-H)-
1250 (1257)	+7	1254 (1255)	+1	1257 (1259)	+2	1254 (1254)	0	$\nu_1(A_{1g})$: $\nu_{(Cm-Ph)}$
1182 (1173)	-9	1168 (1163)	-5	1175 (1171)	-4	1191 (-)	-	$\nu_{13}(B_{1g})$; $\delta_{(Cm-H)sym}$
1071 (1074)	+3	1067 (1072)	+5	1067 (1071)	+4	1075 (1076)	+1	$\nu_9(A_{1g})$: $\delta_{(C_\beta-H)sym}$
972 (982)	+10	974 (976)	+2	973 (975)	+2	968 (983)	+15	$\nu_6(A_{1g})$; $\nu_{(Pyr.breathing)}$ Mainly $(C_\alpha-C_\beta)$ + (C_N-C_α)
869 (876)	+7	874 (875)	+1	873 (875)	+2	870 (870)	0	$\nu_7(A_{1g})$; $\delta_{(Pyr.def)sym.}$
837 (841)	+4	854 (855)	+1	855 (853)	-2	838 (842)	+4	$\nu_{16}(B_{1g})$; $\delta_{(Pyr.def)}$
628 (622)	-6	626 (623)	-3	627 (624)	-3	628 (631)	+3	$\nu_{(C_\alpha-X)}$

a - Mode numbering system and assignment as per reference of 88

$\Delta\nu$ - is the frequency shift upon dication with respect to neutral species

(+) and (-) corresponds to shifts to higher and lower frequencies respectively upon dication formation

* - represents frequency for corresponding dication.

a correlation between the structurally sensitive Raman modes with the energy of the Q-band transitions for a variety of OEP and TPP complexes.[90] Such a plot shown in Fig. 3.10 reveal a linear correlation between the frequencies of four structurally sensitive[89] Raman modes (ν_2, ν_4, ν_{10} and ν_{11}) with the lowest energy Q bands both in neutral and dicationic forms.

3.4.2 Fluorescence Studies

The room temperature fluorescence spectra of a few representative thiaporphyrins (STPPH, S_2TPP and $(OCH_3)_4S_2$TPP) with $TPPH_2$ is shown in Fig. 3.11. The emission spectral data of thiaporphyrins are listed in table 3.5. The general features of these findings are as follows: (a) the fluorescence intensity are quenched considerably and the emission maxima are shifted to red. The magnitude of red shift and the intensity decrease are linearly related to the number of sulfur atoms in the porphyrin core. (b) The singlet lifetimes measured and the relative quantum yield calculated are generally much lower than that of the parent $TPPH_2$ consistent with the earlier observations on some dithiaporphyrins.[52] (c) The rate of fluorescence decay (K_f) and rate of intersystem crossing (K_{isc}) decreases and increases respectively for the thiaporphyrins relative to $TPPH_2$.

The fluorescence spectra of a few thiaporphyrin dications ($STPPH_3^{2+}$, $S_2TPPH_2^{2+}$) with tetraphenylporphyrin dication ($TPPH_4^{2+}$) are shown in Fig. 3.11 (inset). The table 3.5 shows that emission maxima of thiaporphyrins are shifted to red. The magnitude of red shift depends upon the number of sulfur atoms in the porphyrin core. A comparison of ground (P^+/P, P/P^-) and excited (P^*/P^-,

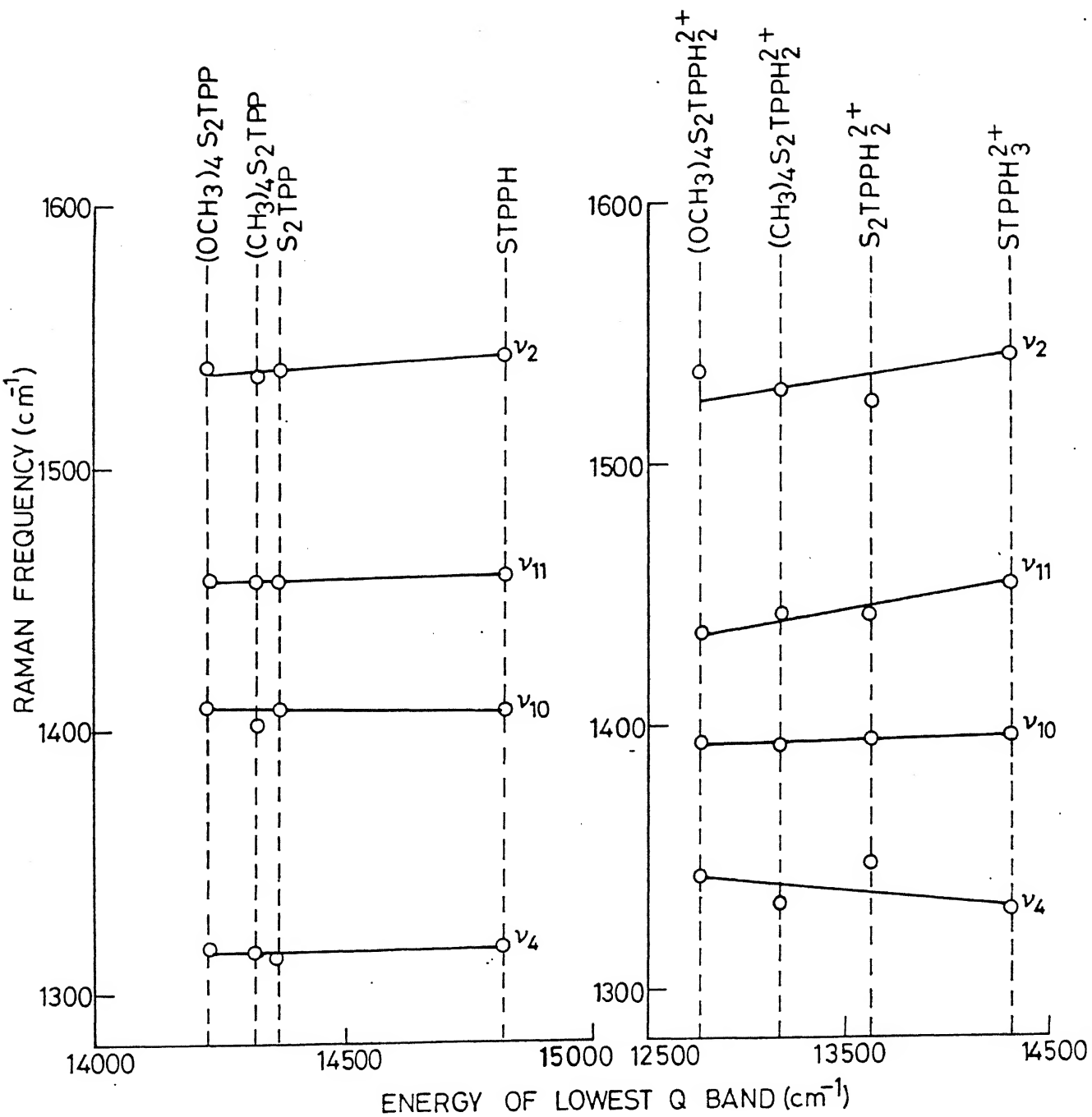

Fig.3.10 A plot of the lowest energy Q band versus selected structurally sensitive Raman vibrational modes for various thiaporphyrins and their dications.

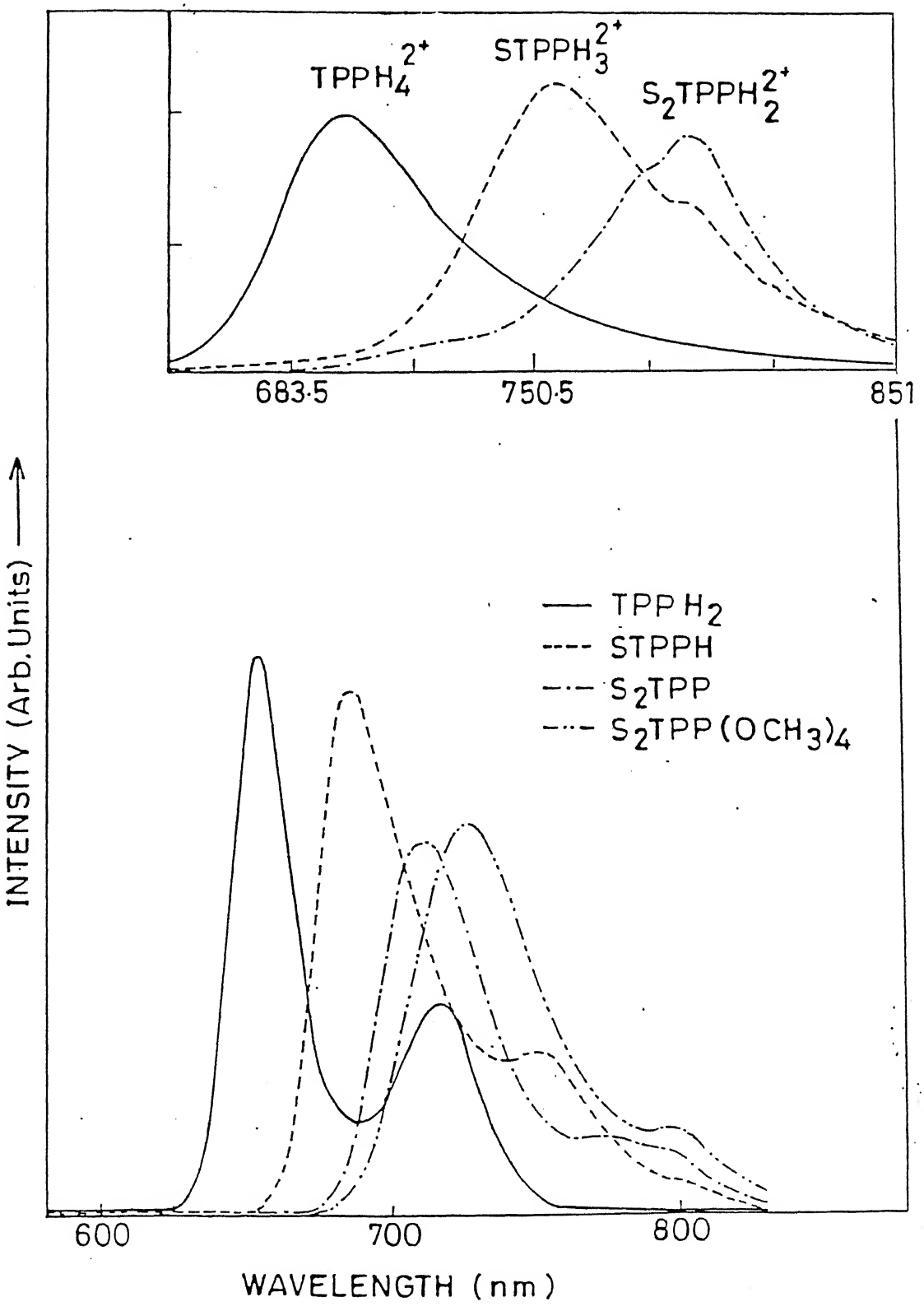

Fig.3.11 Emission spectra of $TPPH_2$, STPPH, S_2TPP and $(OCH_3)_4S_2TPP$ in $CHCl_3$. Inset shows the emission spectra of $TPPH_4^{2+}$, $STPPH_3^{2+}$, $S_2TPPH_2^{2+}$ in $CHCl_3$.

Table 3.5 Singlet excited state parameters of thiaporphyrins and their dications

Porphyrin	Red shift relative to $TPPH_2/TPPH_4^{2+}$		Quantum yield	Singlet lifetime	$k_f x10^{-7}$	$k_{isc} X 10^{-7}$	E_{o-o}	E^{*o}	E^{*o}
	Q(0,0)	Q(0,1) nm	ϕ_f	(ns)	s^{-1}	s^{-1}	(P-*P) eV	$P^+/{}^*P$ (V)	${}^*P/P^-$ (V)
STPPH	28(59*)	38	0.01683	1.36	1.24	72.30	1.821	-0.741	+0.747
S_2TPP	53(98)	67	0.00764	1.25	0.61	79.40	1.756	-0.586	+0.816
$(CH_3)_4S_2TPP$	60(118)	75	0.00653	1.15	0.57	86.40	1.739	-0.649	+0.789
$(OCH_3)_4S_2TPP$	69(152)	83	0.01513	1.13	-	-	1.717	-0.737	+0.747
$TPPH_2$ $	-	-	0.11	9.5	1.16	9.36	1.900	-0.870	+0.670

* - This corresponds to shift in dications.

$ - Taken from Ref. 52

P^+/P^*) states redox potentials of thiaporphyrins with $TPPH_2$ is shown in Fig. 3.12. The table 3.5 shows that excited state oxidation potentials and excited state reduction potentials of thiaporphyrins are shifted to less positive values (129 mV to 284 mV) and more negative values (77 mV to 146 mV) with respect to $TPPH_2$ suggesting that the thiaporphyrins are better oxidants and poor reductants in the first singlet excited state relative to $TPPH_2$.

DISCUSSION

3.4.1 Resonance Raman Studies

A major feature to be considered in the interpretation of the frequency shifts in the Raman spectra is based on the structural change in the porphyrin core accompanying the protonation. Porphyrin skeletal mode frequencies in the Raman spectra are known to be sensitive to the core size as well as to the electronic effects.[91] Earlier studies on nonplanar hemes have indicated that the porphyrin skeletal vibrations are significantly shifted to lower frequencies relative to the planar derivative presumably due to the loss of π-conjugation at the methine bridges.[92] Both core expansion and the pyrrole tilting contribute to the frequency decrease. Thus the observed shifts for most of the skeletal vibrations to lower frequencies upon protonation is attributed to the extension of the π-electron delocalisation to the meso phenyl rings which would decrease the electron density and force constants of the porphyrin skeletal modes. The shift of the ν_{cm-ph} mode to the higher frequency in the protonated form supported this contention. This is also

consistent with the previous Resonance Raman studies on several meso arylporphyrins, their dications and metalloporphyrins.[93] Furthermore, it is well established that the core size of the porphyrin ring shows an inverse relationship with the higher frequency vibrational modes.[89] Thus, the direction of the shift of the higher frequency modes (table 3.4) indicate the core expansion upon protonation.

The site of protonation is obviously on the pyrrolidiene nitrogens since the pyrrole nitrogens are replaced by sulfur in dithiaporphyrins. This is clearly reflected in the significant shift of the C_α-N stretching frequency to higher side upon protonation. The fact that the C_α-S stretching mode experience only a small shift also supports this observation. On the basis of SCF-MO calculations[94], the porphyrin radicals with predominantly a_{2u} character have higher electron densities located on the C_m and N atoms and this orbital is bonding with respect to the C_β - C_β and C_α - C_m bonds while it is slightly antibonding with respect to the C_α -N and C_α -C_β bonds. Removal of electrons upon protonation should weaken the C_β - C_β and C_α - C_m bonds and decrease their frequencies while it should enhance the bonding character of the C_α -N bonds with concomitant increase in their frequencies. This is what we have observed experimentally as is clear from table 3.4 and Fig. 3.9 indicating that the dication of these thiaporphyrins have predominantly a_{2u} ground state. Moreover, removal of electrons from the a_{2u} orbital upon protonation would raise the energy of this orbital reducing the energy gap from the $e_g(\pi^*)$ orbital which explains directly the red shift of the visible absorption bands upon protonation.

It is evident from Fig.3.10 that the vibrational frequencies of the ring stretching modes are nearly proportional to the transition energy. A similar correlation was observed previously for a series of metallo octaethylporphyrins.[90] This observation strongly suggests that the electronic absorption reflects the core expansion upon protonation in the excited state. It is also inferred from the plot that larger the red shift of the Q-bands in the optical spectrum upon protonation the stronger is the conjugation between the porphyrin plane and the phenyl rings and greater is the delocalization of the π-electrons. The intensity changes observed in general indicate the differences in the enhancement mechanism of Raman bands between the neutral and protonated forms. Specifically, the gain in intensity of the $\nu_2(C_\beta\text{-}C_\beta)$ stretching and ν_{11} $(C_\alpha - C_m)$ modes indicate larger mixing of these modes in the protonated species relative to the neutral species. This is consistent with the large body of the data on metalloporphyrin radical cations where even a greater mixing of these modes has been observed.[95,89b]

3.4.2 Fluorescence Studies

The fluorescence spectral data (table 3.5) show that fluorescence maxima of thiaporphyrins are red shifted relative to $TPPH_2$ is consistent with the decreased energy gap between the HOMO and LUMO upon sulfur substitution.[52] The calculated relative quantum yield data indicate a strong fluorescence quenching in thiaporphyrins which vary as STPPH $\simeq (OCH_3)_4S_2TPP > S_2TPP \simeq (CH_3)_4S_2TPP$. This decrease in quantum yield can be ascribed, in part,to the internal heavy atom effect of sulfur atoms. The empty d-orbitals (d_{xz} and d_{yz}) of sulfur atoms have appropriate

symmetry to interact with porphyrin π-system affecting the spin orbit coupling which serve as a mechanism for intersystem crossing (isc).[96] The increase in intersystem crossing rate (K_{isc}) and decrease in measured fluorescent lifetime upon sulfur substitution is in accordance with this conclusion. In the absence of Φ_T (triplet quantum yield) values, estimates of contribution of internal conversion to S_1 state decay is difficult. Nevertheless, contribution from internal conversion to S_1 state decay is expected because theoretical calculations by Gouterman and coworkers[52] predict the absence of any low lying charge transfer states for S_2TPP and such states are shown to be present in selenium containing porphyrin.

As pointed out earlier the red shift upon dication formation is attributed to the increased resonance interaction between the meso phenyl ring and the porphyrin plane. The much larger red shifts (59 nm for STPPH, 98 nm for S_2TPP) relative to $TPPH_2$ upon protonation suggest a greater resonance interaction in thiaporphyrins. Ground state studies also reveal the same.

The singlet excited state potentials estimated assuming that the excited states are not very much distorted relative to the ground state vary with the number of sulfur atoms in the porphyrin core (Fig. 3.12). Among the thiaporphyrin, S_2TPP is a better electron donor and poor electron acceptor in the excited state. Thus, it appears that the introduction of sulfur atoms into the porphyrin core makes it better oxidant with excited state oxidation potential getting 284 mV (for S_2TPP), 221 mV (for $(CH_3)S_2$TPP), 133 mV (for $(OCH_3)_4S_2$TPP) and 129 mV (for STPPH) less negative relative to $TPPH_2$.

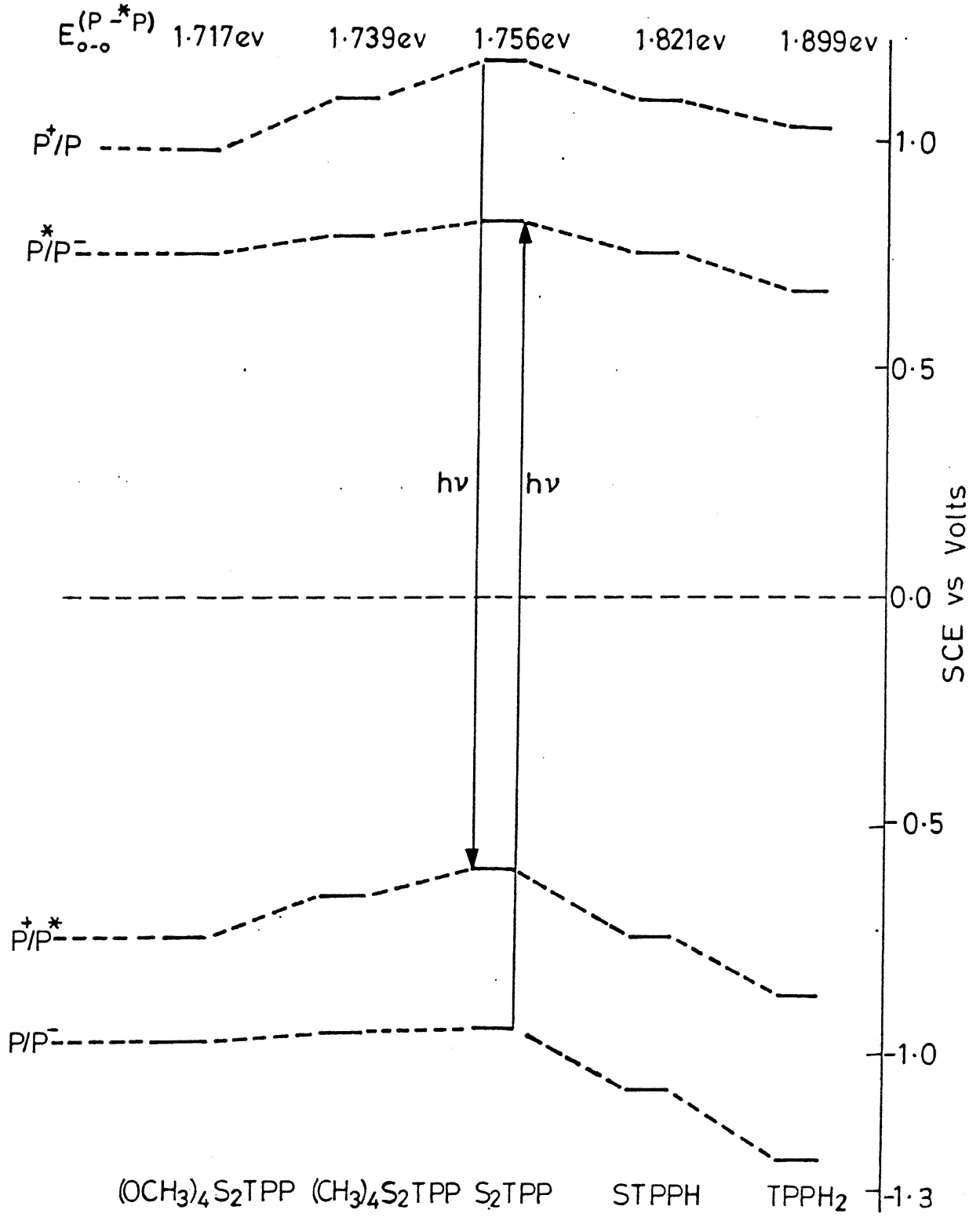

Fig.3.12 Comparison of ground (P^+/P, P/P^-) and excited state (P^+/P^*, P^*/P^-) redox potentials of thiaporphyrins with $TPPH_2$.

3.4.5 Triplet ESR Studies

In this section a brief outline of the general principles of the photoexcited triplet ESR are described before a detailed discussion on the results obtained on the thiaporphyrins are disucssed for the sake of clarity.

Consider a typical organic triplet state which is formed via intersystem crossing (isc) from the singlet manifold.[75] The degeneracy removal in the absence of an external magnetic field is mainly due to the dipolar interaction between two unpaired electrons[97]

$$\mathcal{H}_d = S.\hat{D}.S. \qquad (3.3)$$

where S is the spin operator and $\hat{D}$ is the dipolar tensor operator which is traceless and transforms like a second-rank spherical tensor.Expansion of equation 3.3 gives rise to different representations of the dipolar Hamiltonian. For example, in terms of a co-ordinate system which diagonalizes dipolar tensor:

$$\mathcal{H}_d = -\left(X S_x^2 + Y S_y^2 + Z S_z^2\right) \qquad (3.4)$$

where X, Y and Z are the expectation values of the principal axes between the spatial wave functions:

$$\begin{aligned} X &= -\tfrac{1}{2} g^2 \beta^2 \left\langle \frac{r^2 - 3X^2}{r^5} \right\rangle \\ Y &= -\tfrac{1}{2} g^2 \beta^2 \left\langle \frac{r^2 - 3Y^2}{r^5} \right\rangle \\ Z &= -\tfrac{1}{2} g^2 \beta^2 \left\langle \frac{r^2 - 3Z^2}{r^5} \right\rangle \end{aligned} \qquad (3.5)$$

Since X + Y + Z = 0, the equation 3.4 can be replaced by another common representation:

$$H_d = D \left[S_z^2 - \frac{1}{3} S^2 \right] + E \left[S_x^2 - S_y^2 \right] \qquad (3.6)$$

where D and E are the zero-field splitting (ZFS) parameters, which are expressed in terms of X,Y and Z as

$$D = - \frac{3}{2} Z \qquad (3.7)$$

$$E = - \frac{1}{2} (Y - X) \qquad (3.8)$$

To solve the dipolar spin-Hamiltonian at zero magnetic field it is convenient to employ the zero-field wave functions $\tilde{T} \equiv |T_x>$, $|T_y>$, $|T_z>$. The resulting energy levels are shown in Fig. 3.13. Some useful aspects can be enumerated at this point regarding the dipolar Hamiltonian.

The ZFS parameters and the corresponding energy levels depend strongly on the average distance between the two unpaired electrons (molecular dimensions) in the photo excited triplet (eq. 3.5). The absolute signs of D and E depends on the particular choice of coordinate system, usually, D and E are assigned such that $|D| > 3 |E|$.

The molecular symmetry should affect the ZFS parameters. In cubic symmetry where all three principal axes are equivalent both D and E vanish leaving a completely degenerate system at zero field. In molecules of lower symmetry where a four fold symmetry exists, the $|E|$ value vanishes leaving a partial degeneracy at zero field. When a small rhombic contribution is introduced, $|D|$ and $|E|$ are nonvanishing, thus lifting completely the degeneracy at zero field.

The ZFS parameters range approximately between 0.1 and 0.01 cm^{-1} and are thus amenable to microwave spectroscopy.

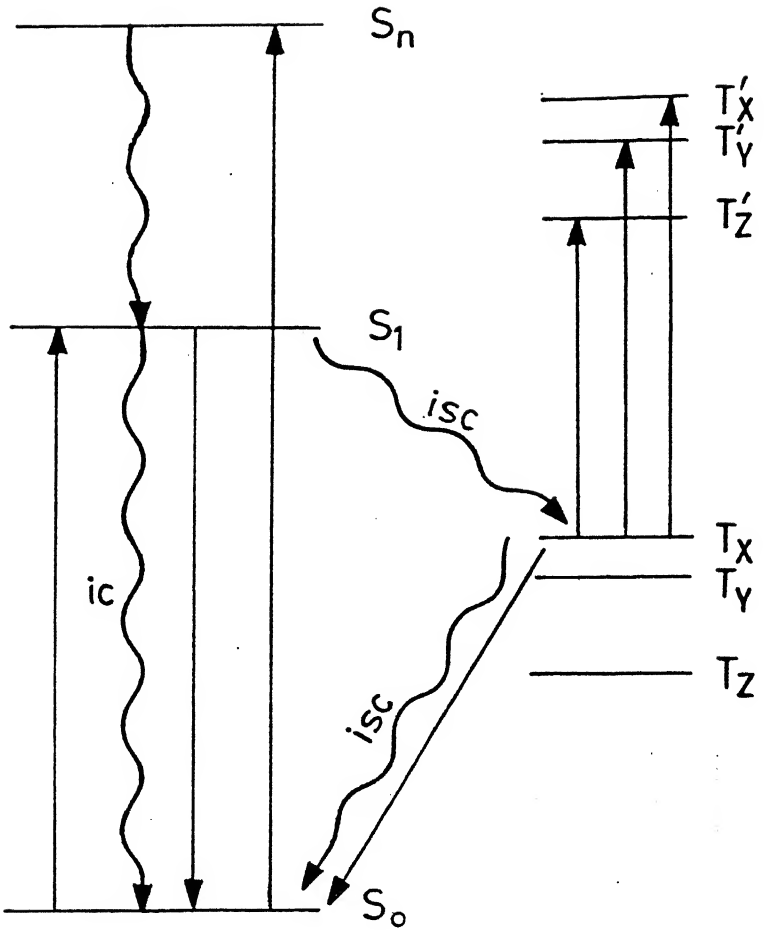

Fig.3.13 A simplified representation of Jablonski diagram. The singlet and triplet manifolds are represented by S and T, respectively. (The vibrational structure is omitted). The spin parts are represented by T_x, T_y, T_z for first excited triplet and T'_x, T'_y and T'_z for nth excited triplet.

Spin Hamiltonian in a Magnetic Field: EPR Experiments

In a magnetic field the photoexcited triplet energy will become field dependent as shown by Fig.3.14(a). The spin Hamiltonian must now include the Zeeman term

$$\mathcal{H} = \beta H \cdot \hat{g} S + \mathcal{H}_d \qquad (3.9)$$

where $\hat{g}$ is a second rank tensor where in many cases its isotropic value almost coincides with the free electron g_e factor 2.0023. The detailed analysis of the Hamiltonian will not be treated here except for summarizing the useful and relevant points.

Electron Paramagnetic Resonance (EPR) spectroscopy covers transition energies of the order of 0.3 - 1 cm^{-1}, compared to 10^4 - 5 x $10^7 cm^{-1}$ in optical spectroscopy. In addition, the conspicuous variation of EPR line widths reflects dynamic processes which may be studied over a wide range of time i.e., 10^{-4} - 10^{-10}s. These two properties make the EPR method very powerful in the unique determination of molecular structure and many inter- and intramolecular dynamic processes.

When the external magnetic field is along one of the principal axes, one state remains always stationary with respect to the field strength. The other two states diverge in opposite directions as the magnetic field increases (Fig. 3.14a).

Accordingly, the spin wave functions will transform from zero-field wave function $\tilde{T}$ to field dependent wave functions. The high field spin wave functions are $\tilde{n} \equiv | 1 >, | 0 >, | -1>$ and are related to the zero field wave functions through the transformation

$$\tilde{T} = \tilde{n} \; R \qquad (3.10)$$

where R is the matrix:

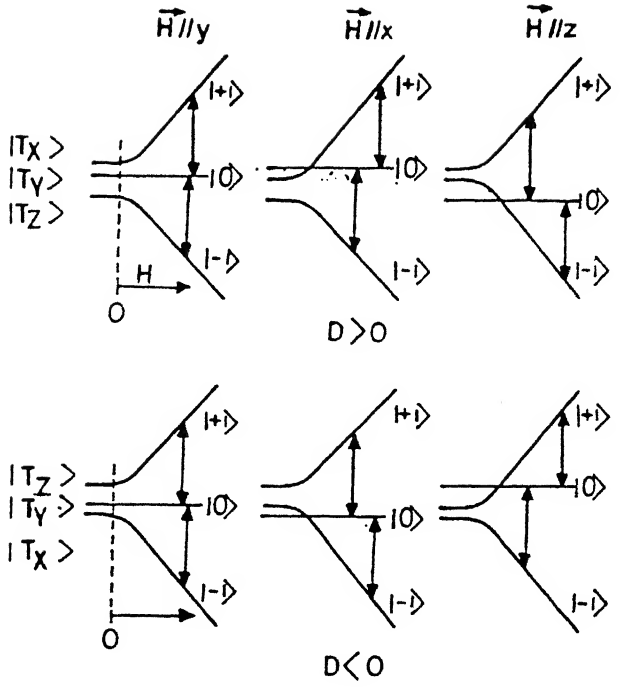

(a)

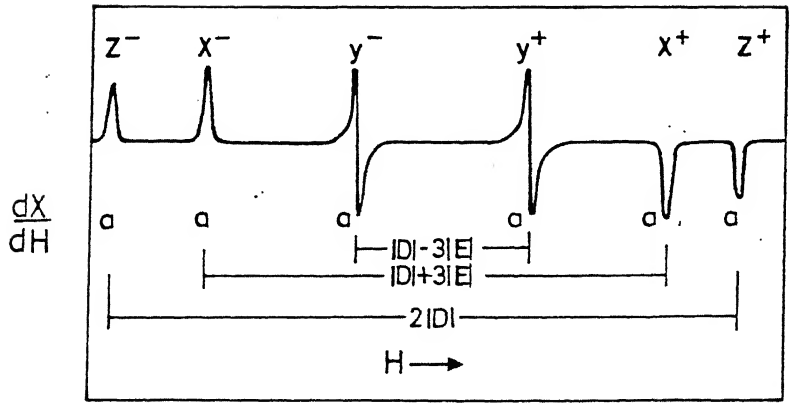

(b)

Fig.3.14 (a) Magnetic field dependence of the spin energy levels for the three canonical orientations. The upper trace is the energy level diagram for D > 0, whereas the lower trace is for D < 0, (b) First derivative of a randomly oriented triplet having $|D| > 3|E|$. The line shape and peak intensities are typical of a triplet state that is in thermal equilibrium; all signal intensities are in the absorption mode indicated by a.

$$R = \begin{bmatrix} \frac{1}{\sqrt{2}} & \frac{i}{\sqrt{2}} & 0 \\ 0 & 0 & 1 \\ -\frac{1}{2} & \frac{i}{\sqrt{2}} & 0 \end{bmatrix} \qquad (3.12)$$

It is the magnitude of |D| and |E| which determines whether one should be able to apply EPR spectroscopy to detect the triplet state. Thus, a necessary condition for EPR triplet detection is that the ZFS parameter |D|and 2|E| should be smaller than the external magnetic field. For a particular canonical orientation three transitions are possible: two at $\Delta M_s = \pm 1$ and one at the so called $\Delta M_s = \pm 2$.

For a molecule with $|D| \neq E \neq 0$, it is evident from Fig.3.14a that the overall EPR transitions around $g_e \sim 2$ ($\Delta M_s = \pm 1$) will be 6. These transitions should be observed by conventional EPR detection, i.e., the microwave field is polarized perpendicular to the external magnetic field direction. The excursion of this spectrum will be 2D centered around the free electron g_e factor.

In oriented single crystals the search for and analysis of the triplet EPR spectra are performed in the $\Delta M_s = \pm 1$ region, where the EPR transitions are most intense. This type of analysis, however, can not be carried out with compounds that could not be grown into oriented single crystals. This is the case in many porphyrin[98] and chlorophyll molecules in vitro and certainly containing in most biochemical preparations. Fortunately, much of this information can be derived by studying randomly oriented triplet states.[99] Considering the $\Delta M_s = \pm 1$ region, because of the anisotropy in the magnetic parameters, there is finite transition probability for each value of magnetic field. It can be shown, however[99], that the EPR transition at a

magnetic field parallel to one of the principal axes is well defined in the randomly oriented first derivative EPR spectrum. In a randomly oriented sample the three orientations are normally referred to as the canonical orientations. A characteristic feature of such a triplet spectrum is the occurrence of an additional transition to those already mentioned above. It appears at around g ~ 4.0 (1500 G for a ~9 GHz microwave frequency).

Figure 3.14b demonstrates schematically a conventional $\Delta M_s = \pm 1$ EPR spectrum of randomly oriented triplets. The line shape is typical of molecules with a rhombic contribution such that $|D| > 3(E) \neq 0$. It is also shown how the ZFS parameters can be evaluated from this type of spectrum. For molecules of axial symmetry (X and Y principal axes are indistinguishable), $|E|$ vanishes. This results in the coalescence of X^+, X^- and Y^+, Y^- peak intensities in the EPR spectrum.

The absolute sign of D and E depends on the choice of a molecular axis system. Conventional EPR detection prevents the sign determination from the experimental high temperature triplet spectrum. However, the application of magnetophotoselection (MPS)[100,101] method enables one to determine the signs of the ZFS parameters. This method can be applied to randomly oriented triplets whose triplet EPR spectra show distinct peaks at the canonical orientations. It is evident that these unique peaks are magnetically selected. On the other hand, the populating transitions $S_1 \longleftarrow S_o$ are polarized according to the type of transition (e.g. $\pi^* \longrightarrow \pi$ or $\pi^* \longrightarrow n$). By using plane polarized light one can select the electric field transition, and subsquently the peak intensities in the canonical orientations

will be affected accordingly. Thus, if the polarization of the optical transitions with respect to the molecular frame work are known, one can study the magnetic transitions or vice versa.

The EPR triplet detection is performed at low temperatures[102] and in the solid state phase (oriented single crystals, or randomly oriented molecules). The low temperature requirement is to increase the sensitivity (Boltzmann factor) and to prevent additional deactivation processes which will shorten the triplet life time to such an extent that the steady-state concentration of the triplet will be too small to detect. The second requirement[103] i.e., the solid state, is due to the relatively large values of the ZFS parameter (in terms of molecular reorientation correlation times) which prevent a complete averaging of the dipolar interaction, giving rise to broad EPR lines. Also, fast tumbling will result in very short SLR times as to produce severe line broadening so that the triplet spectrum in solution would escape detection.

Electron Spin Polarization:

The EPR technique enables one to elucidate details concerning the dynamics associated with the triplet manifold. The main requirement is that the kinetic parameters (population, depopulation, spin lattice relaxation rates) should lie within the time resolution and sensitivity of the detection apparatus.[104] In the high-field approximation and for $|D| << g\beta H$[105], the intersystem crossing rates are given by[106]

$$< \pm \mid K_{\pm} \mid \pm > = \frac{1}{2} (K_j + K_k)$$
$$< 0 \mid K_o \mid 0 > = K_i \text{ for } i \parallel H,\ i = X,Y,Z \qquad (3.12)$$

The same relations hold for the population rate constants A_o and $A_{\pm 1}$. For the other two perpendicular orientations, the rates are obtained using cyclic permutation.

The isc rates at zero field will be proportional to the square of matrix elements of the type[106]

$$|< S_1 \mid \mathcal{H}_{so} \mid T^1_{SP}\, T_i > |^2 \text{ for population rates } A_i$$
$$|< S_o \mid \mathcal{H}_{so} \mid T^1_{SP}\, T_i > |^2 \text{ for depopulation rate } K_i \qquad (3.13)$$

where $i = X,Y,Z$, T^1_{SP} is the spatial orbital of the triplet state, T_i is the triplet spin state and S_1 is the first excited singlet state. $\mathcal{H}_{so}$ is the spin orbit Hamiltonian.

From eq. 3.12 and eq. 3.13 it follows that isc rates are not necessarily the same. This is, in fact the case in most compounds and if the SLR rates are not very fast to cause thermalization, one should observe two types of EPR transitions between each pair of levels. One transition will be an enhanced absorption (**a**) and the other an emission (**e**). The corresponding kinetic curves will also show enhanced absorption and emission transient superimposed on relatively slow components. This effect is known as electron spin polarization.[107]

The high field EPR spectra of bacteriochlorophylls in vivo[108] exhibit a unique spin polarization pattern, in contrast to the normal spin polarization shown by the same bacteriochorophylls in vitro.[109,111] It has been claimed[109-111] that this "intriguing anomalous" in vivo spin polarization can not be interpreted in terms of the usual intramolecular selection rules. This has led to the conclusion that intermolecular mechanism such as electron transfer must be invoked.

A correlation has been obtained between the relative intensities patterns of EPR and the initial population or depopulation rates.[111] This is shown in following table 3.6.

Table 3.6 Polarization patterns predicted from relative zero field population: depopulation rates[a]

Relative Population: depopulation rate[b]			Polarization at canonical orientations[c]					
K_x	K_y	K_z	Z^-	X^-	Y^-	Y^+	X^+	Z^+
1	0	0	e	e	a	e	a	a
0	1	0	e	a	e	a	e	a
0	0	1	a	a	a	e	e	e
1	1	0	e	e	e	a	a	a
1	0	1	a	e	a	e	a	e
0	1	1	a	a	e	a	e	e
2	1	0	e	e	-	-	a	a
2	0	1	-	e	a	e	a	-
1	2	0	e	-	e	a	-	a
0	2	1	-	a	e	a	e	-
1	0	2	a	-	a	e	-	e
0	1	2	a	a	-	-	e	e

---

[a]This table gives representative population :depopulation rates for spin-orbit intersystem crossing (isc) for isolated molecules and is not all inclusive

[b]Valid if certain restrictions can be made in the value of T_{1e} (electron spin lattice relaxation time) relative to the population: dopopulation rate constants.

[c]The assignments are made assuming $D > 0$ (the usual case for $\pi\pi^*$ triplet states) and $D > -3E > 0$.

In the present study the above table 3.6 has been used to qualitatively predict the population, depopulation rates by knowing polarization pattern from the EPR experiment.

TRIPLET ESR STUDIES

RESULTS

A comparison of low temperature photo excited triplet ESR of STPPH and $(CH_3)_4S_2TPP$ and their protonated derivatives are made in Figs. 3.15 and 3.16 The zero field splitting parameters (D and E) are listed in table 3.7. All the thiaporphyrins and their dications exhibit an electron spin polarized triplet state indicating that the triplet sublevels are coupled selectively to the singlet manifold. Further, the observed polarization pattern were confirmed by recording the spectrum by pulsed laser excitation followed by detection of EPR signal at about 0.5 μs after the laser pulse without the field modulation. This will allow an unambiguous assignment of enhanced absorption (**a**) and emission (**e**) lines. All the neutral thiaporphyrins show an electron spin polarization (ESP) pattern **ea ea ea** which is essentially same as found for $TPPH_2$.[112] On the other hand, $STPPH_3^{2+}$ shows an ESP pattern **aa ae ee** and the dications of dithiaporphyrins ($S_2TPPH_2^{2+}$), ($(CH_3)_4S_2TPPH_2^{2+}$) ($(OCH_3)_4S_2TPPH_2^{2+}$ exhibit an **aa ea ee** polarization pattern. This change in the ESP pattern upon protonation indicate the difference in the specific population and decay rate constants associated with the triplet sublevels.[75,113] Furthermore, a comparison of relative intensities of the pair of peaks in each canonical orientation indicate that the absorption lines (marked (**a**) in the spectrum) are more intense than the corresponding emission (**e**) lines for neutral

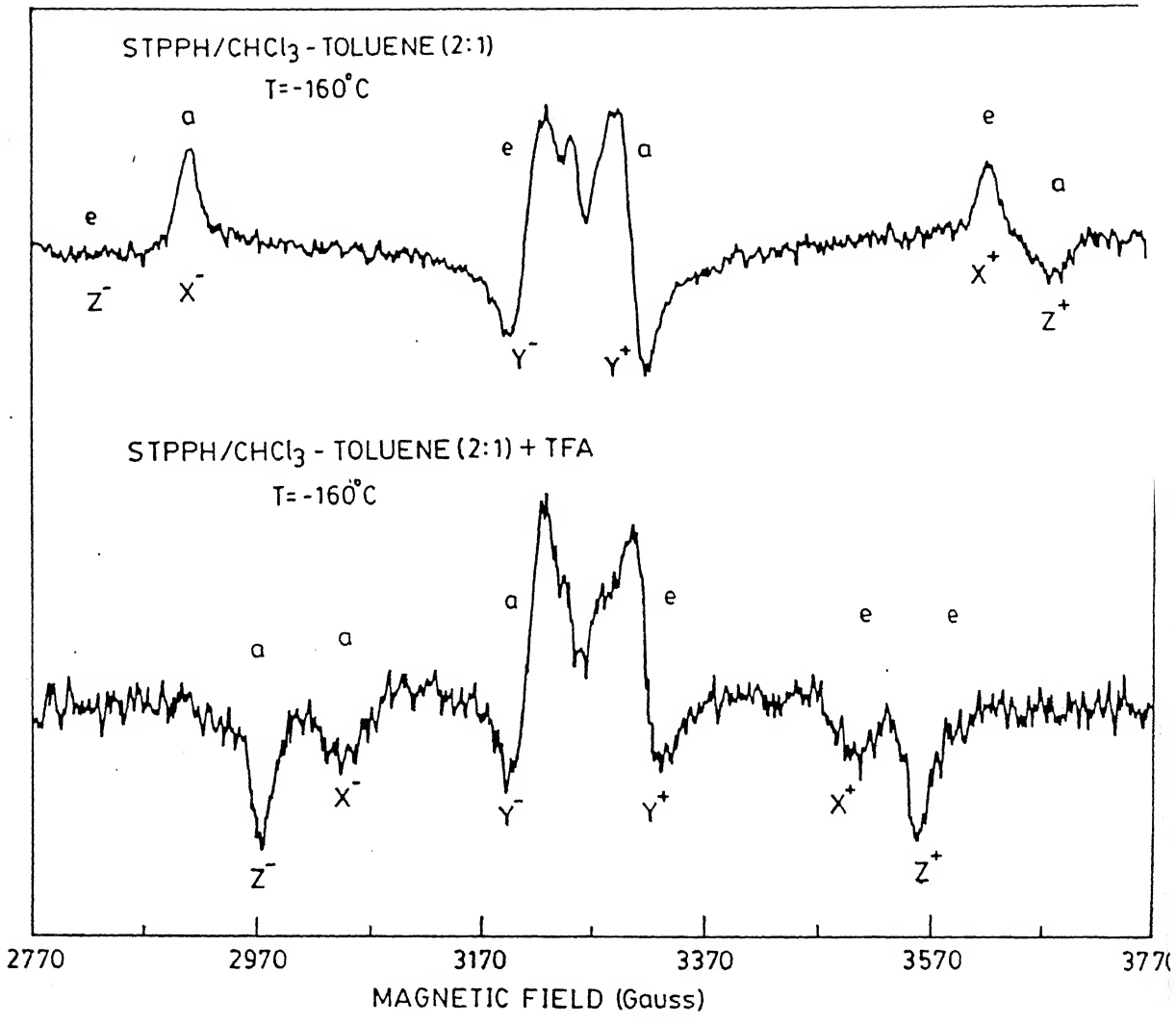

Fig.3.15 Triplet ESR spectra of STPPH and $STPPH_3^{2+}$ in $CHCl_3$-toluene [2:1] at -160°C. Microwave power 5 mW, Field modulation 20 G (100 KHz), Excitation with square wave modulated (80 Hz) light of an argon ion laser (514 nm, 0.5 W). Absorption and emission peaks have been labelled as a and e respectively. Approximately $1x10^{-4}$M solution was used for recording the spectra [note the instrumental phase shift between the spectra].

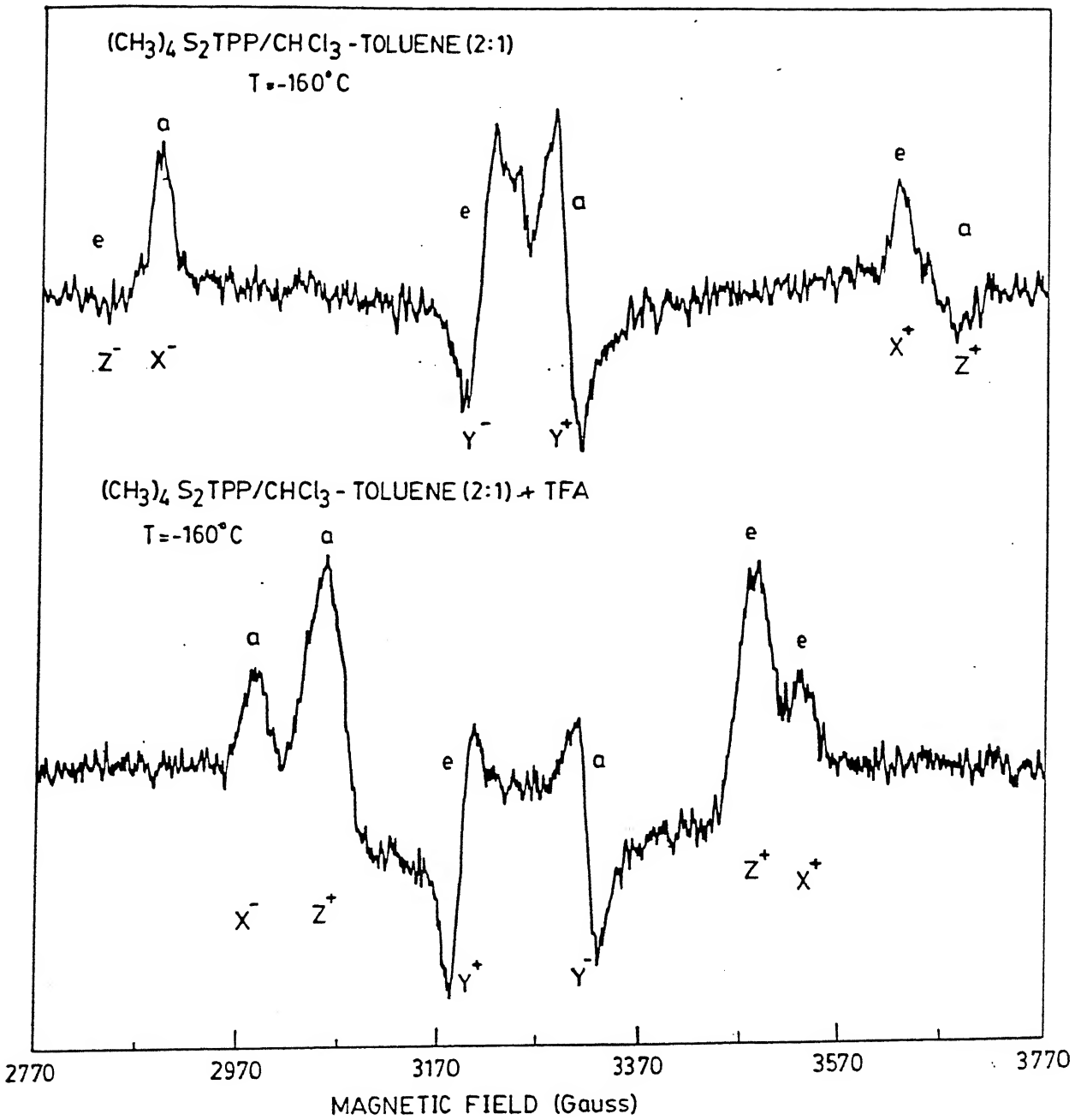

Fig.3.16 Triplet ESR spectra of $(CH_3)_4S_2TPP$ and $(CH_3)_4S_2TPPH_2^{2+}$ in $CHCl_3$ - toluene [2:1] at -160^oC. Microwave power 5 mW Field modulation 20 G (100 KHz), Excitation with square wave modulated (80 Hz) light of an argon ion laser (514 nm, 0.5 W). Absorption and emission peaks have been labelled as **a** and **e**, respectively. Approximately $1x10^{-4}M$ solution was used for recording the spectra [note the instrumental phase shift between two spectra].

Table 3.7 Zerofield splitting parameters (10^{-4} cm^{-1}) of various thiaporphyrins and their dications

Porphyrin	D	E
STPPH	375	97
$STPPH_3^{2+}$	265	55
S_2TPP	396	102
$S_2TPPH_2^{2+}$	274	53
$(CH_3)_4S_2TPP$	384	103
$(CH_3)_4S_2TPPH_2^{2+}$	254	46
$(OCH_3)_4S_2TPP$	369	101
$(OCH_3)_4S_2TPPH_2^{2+}$	230	37
$TPPH_2$	383	78

thiaporphyrins. (The average relative intensity difference is 28% for the X-components, 15% for the Y - components and about 89% for the Z-components at the modulation frequency of 80 Hz). However, for the protonated species both a and e lines of each pair have nearly equal intensity.

DISCUSSION

The steady state intensity I_h for $|0> \text{-----} > |\pm>$ transition for a given direction in the magnetic principal axis system in the absence of spin lattice relaxation (SLR) is related to the population (P_h) and the decay (K_h) rate constants by the relation[114]

$$I_h(\pm) = \pm [P_h(0)/K_h(0) - P_h(\pm) / K_h(\pm)] \qquad (3.14)$$

where h is the unit vector along the magnetic field H. If, $|o>$ level is more populated than the $|\pm>$, $I_h(+) > 0$ and $I_h(-) < 0$ and if $|\pm>$ level is more populated than $|o>$ level, then the reverse holds good. Also, absorption of microwave represent $I_h(\pm)>0$ and emission microwaves represent $I_h(\pm)>0$ with $|I_h(+)| \cong |I_h(-)|$. In the presence of fast SLR, this equation is not valid.[115] However, it is still possible to have $I_h(+) \simeq I_h(-)$ with some SLR provided $|P_h(0)(K_h)(\pm)-P_h(\pm)K_h(0)| >> W\ \delta\ [P_h(0) + 2P_h(\pm)]$, where 'W' is the rate constant for SLR between $|o>$ and $|->$ and δ is the exponent of the Boltzman factor ($\delta << 1$).[116] Even though this equation is not applicable for neutral thiaporphyrins, (since a lines are more intense than e lines for each pair), it is applicable to the spectra of dications and the nearly equal intensity of the a and e lines of each pair indicates much larger

deviation from Boltzman equilibrium for the dications at - 160°C. It is interesting to note that the triplet ESR of $H_2TPP(CN)_3$ in ethanol: CH_2Cl_2 (1:1) glasses show a similar intensity pattern.[117]

The polarization pattern observed for neutral thiaporphyrins (ea ea ea) essentially indicate that one spin component i.e. T_y (following the convention that the order of energy levels is chosen $T_x > T_y > T_z$) is most active with respect to the population and decay rate constants.[75,113] Thus, the introduction of S-atom into the porphyrin core essentially does not alter the spin dynamics relative to $TPPH_2$. The X-ray structure of STPPH and S_2TPP[47] reveals that both N_3S and N_2S_2 cores are planar like in $TPPH_2$. This structural similarity probably explains the similarity in triplet characteristics.

The ESP pattern for $STPPH_3^{2+}$ dication suggests that the active spin component is the out of plane T_z sublevel similar to that observed for ZnTPP.[113] On the other hand T_y and T_z spin sublevels are the active components for the dications of dithiaporphyrins. The observed aa ea ee pattern for the dications of dithiaporphyrins indicate one of the following two possibilities. (a) The outer pair of peaks (the largest dipolar splitting) corresponds to an orientation in which the magnetic field lies in the porphyrin plane implying that the 'Y' peaks have interchanged their position in dications. Alternatively, (b) the observed aa ea ee pattern can also be explained by assigning the largest dipolar splitting (outer peaks) to the out of plane orientation as in normal porphyrins assuming T_y and T_z sublevels are predominantly populated following the conventional order of energy levels $T_x > T_y > T_z$. The magnetophotoselection experiments[75] and an analysis of kinetics of triplet decay only can confirm either

of the above possibilities. Thus the changes observed in the spin sublevel activity in dications is attributed to the structural distortions upon protonation.

Support for such a conclusion comes from earlier literature reports. Bowman[118] has studied the triplet kinetics of normal and fully deuterated chlorophyll and pheophytin in dry and wet pyridine. In chlorophylls, the isc mechanism is achieved via a static distortion in which the central magnesium atom is forced in and out of molecular plane by magnesium-solvent interaction. In the pheophytin molecules, a dynamic model was proposed in which the isc is achieved by out of plane N-H vibrations. Furthermore, Goncalves and Burgner have identified the out of plane N-H bending as the promoting mode for isc in a free base porphyrin on the basis of spin dependent deuterium Isotope effect on the isc rate constants.[114,119]

The changes in the triplet spin density are reflected in the zero field splitting (ZFS) parameters D and E which characterize the dipolar spin Hamiltonian.[113] Comparison of D and E values of neutral thiaporphyrins with that of $TPPH_2$ (table 3.7) suggests no significant alteration in the triplet spin density. Literature studies indicate in general, that there is a substantial decrease in the ZFS parameters upon the formation of dications in porphyrin systems.[113,120] The observed decrease in the present study is consistent with these reports. In TPP systems, as pointed out by Van der Waals and coworkers[113], a lowering of D-value is expected on; (i) the extension of delocalization of π-electrons into the meso phenyl groups and (ii) when the porphyrin plane becomes nonplanar. Both these effects are operative in the present study upon protonation. Furthermore, the phenyl substituent in the

neutral dithiaporphyrins does not affect the D-values appreciably while in the dications there are significant differences in D-values; the order being $D[S_2TPPH_2]^{2+}$ > $D[(CH_3)_4S_2TPPH^{2+}_2]$ > $D[(OCH_3)_4S_2TPPH^{2+}_2]$. In the neutral compounds, since the meso phenyl ring is almost perpendicular to the porphyrin plane, the substituents on the phenyl rings are not in conjugation with porphyrin π-system. However, the phenyl rings are in conjugation upon protonation with the porphyrin π-system facilitating the electron donation from the substituents. The observed decrease in D from methyl substituent to methoxy substituent is in accord with their donating abilities to the aromatic ring. Also the magnitude of D-values of dications are comparable with those of Sapphyrin dications which are planar 22 membered aromatic π-system with five pyrrole nitrogens. (In toluene, D = -270 and E = $74x10^{-4}$ cm^{-1}). However, this dication dimerizes in polar solvents like ethanol showing further reduction in D-values.[121] The substantial reduction in E-parameter indicates that in-plane anisotropy of the triplet spin distribution decreases relative to neutral thiaporphyrins.[113]

3.5.0 Conclusions

A comparison of the spectral and electrochemical data of thiaporphyrins with the normal porphyrin reveal many similarities with respect to the molecular structure of the two porphyrin ring systems. However, the introduction of sulfur into the porphyrin core do show some differences in the electronic structures of the two ring systems and this is reflected in the altered spectroscopic properties. It has been shown that the introduction of sulfur affects the energies of the HOMO's and LUMO's relative

to normal porphyrin in such way that the energy gap between them decreases as a function of number of sulfur's substituted. This is clearly born out from absorption, fluorescence and electrochemical studies.

Upon protonation, the behaviour of thiaporphyrins is similar to those observed for meso aryl porphyrins. The expected structural change upon protonation is revealed in the large red shift of absorption and emission bands and shift of the structurally sensitive Raman bands. The linear correlation observed between the frequency of structurally sensitive bands and the lowest energy of Q-bands both in neutral and dicationic forms are interesting. The conclusion derived from the excited state redox potential data is that the thiaporphyrins are better oxidants in the first excited singlet state.

It is surprising that the introduction of the heavy S-atoms does very little to the triplet state characteristics interms of both ZFS parameters as well as the ESP pattern in the neutral thiaporphyrins. However, the structural change accompanying the protonation is clearly reflected in the reduction of ZFS parameters by a substantial amount and the redirection of the spin sub-level activity. The dominance of the in plane spin sub-level with respect to population and decay process in $(\pi\pi)^*$ triplet states of all neutral thiaporphyrins is similar to those observed for chlorophylls and other planar aromatic systems.[122] A quantitative understanding of the changes in the ESP pattern in dications is possible by measurement of actual population and decay rates for different sublevels by monitoring the decay of the peaks observed in each canonical orientation. Studies in this direction are in progress.

CHAPTER 4

WATER SOLUBLE THIAPORPHYRINS AND METALLOTHIAPORPHYRINS: SYNTHESIS, CHARACTERIZATION, GROUND AND EXCITED STATE PROPERTIES

4.1.0 Introduction

The interpretation of mechanistic studies on porphyrins requires a knowledge of the state of aggregation of the porphyrin or metalloporphyrin. In many cases, equilibria between monomers, dimers and higher species have been demonstrated[123] for synthetic water soluble porphyrins of the type meso aryl substituted porphyrins. Some typical examples are tetra 4-(3 or 2) N-methyl pyridyl porphyrin (H_2TMPyP), tetra(4-carboxyphenyl) porphyrin (H_2TCPP) and tetrakis(4-sulfonatophenyl) porphyrin (H_2TPPS). The other interest in the studies on synthetic water soluble porphyrins is their possible use as photo catalyst for splitting of water to H_2 and O_2. A considerable effort has been made in this direction using a variety of synthetic porphyrins. Some of the desired properties[124] of a good photosensitizer are (1) good solubility in water (2) intense absorption in the visible region, preferably extending into the near IR, (3) good solubility upon prolonged storage in aqueous solution, (4) no side photo reactions (5) high triplet yield (6) efficient production of separated ion products upon irradiation in the presence of an electron donor or acceptor. These points are self-explanatory but perhaps some comment is required about the need for a high triplet yield.

It has been known for a long time that the triplet state of many porphyrins and phthalocyanins will undergo net electron transfer with suitable redox couples, forming the separated ion products.[125] However, there is growing evidence that, in most cases, despite the high quenching rate constants, the singlet

excited state does not yield ion products.[126] This effect has been explained in terms of spin selection rules[127] and it appears that only in special cases[128] redox products occur from the singlet excited state of the sensitizer. Thus a necessary requirement for a good chromophore is that the triplet state is populated in high yield.

Porphyrins and phthalocyanins possess most, if not all, of the desired properties for photosensitizer for generation of H_2 from a sacrificial system.

At the present time, the most suitable system appears to consist of a chromophore(P), methyl viologen (MV^{2+}) as an electron relay, a sacrificial electron donor (such as EDTA, H_2S or cysteine) and a colloidal Pt catalyst. The principal reaction scheme may be written as

$$P^* + MV^{2+} \longrightarrow P^+ + MV^+$$

$$P^+ + EDTA \longrightarrow P + EDTA^+$$

$$EDTA^+ \longrightarrow \text{Products}$$

$$2MV^+ + 2H^+ \xrightleftharpoons{Pt} 2\,MV^{2+} + H_2$$

Although other variations are possible overall, the system produces H_2 at the expense of consuming a sacrificial electron donor. Obviously once the system has been optimised for production of H_2 it will be necessary to replace this sacrificial donor with a redox couple that is common to a corresponding system for production of O_2 from water or the system must be designed so that the ultimate electron donor is water.

$$4P^+ + 2H_2O \longrightarrow 4P + 4H^+ + O_2$$

Three separate research groups have reported that positively charged, water soluble zinc porphyrins function as efficient photosensitizer for the reduction of water to H_2. Kalyanasundaram and Gratzel[129] found that $ZnTMPyP^{4+}$ was particularly effective photosensitizer for the reduction of MV^{2+} in aqueous solution and in the presence of EDTA, as sacrificial electron donor and colloidal Pt. Irradiation of the system with visible light resulted in formation of H_2 with high yield. These findings were confirmed by McLendon and Miller[130] who also reported that H_2 production was observed when $ZnTPPS^{4-}$ was used as the photosensitizer. These reports concluded that the triplet excited state of zinc porphyrin was the active photosensitizer[129,131]; but McLendon and Miller[130] preferred a singlet-state reaction mechanism. However, flash photolysis studies[129,131] have provided strong evidence that the reaction involves the triplet excited state of the metalloporphyrins.

In view of the structural similarity of thiaporphyrins (Fig. 4.1) synthesised in the present study with the meso aryl porphyrins, we thought it is worthwhile to synthesise and study the ground and excited state properties of thiaporphyrins in aqueous medium. This chapter describes the details of the first report on the synthesis of water soluble thiaporphyrins and their ground and excited state properties.

4.2.0 EXPERIMENTAL:

Purification of solvents for spectral studies have been described in Chapter 2. Synthesis and purification of STPPH and S_2TPP have been described in Chapter 3.

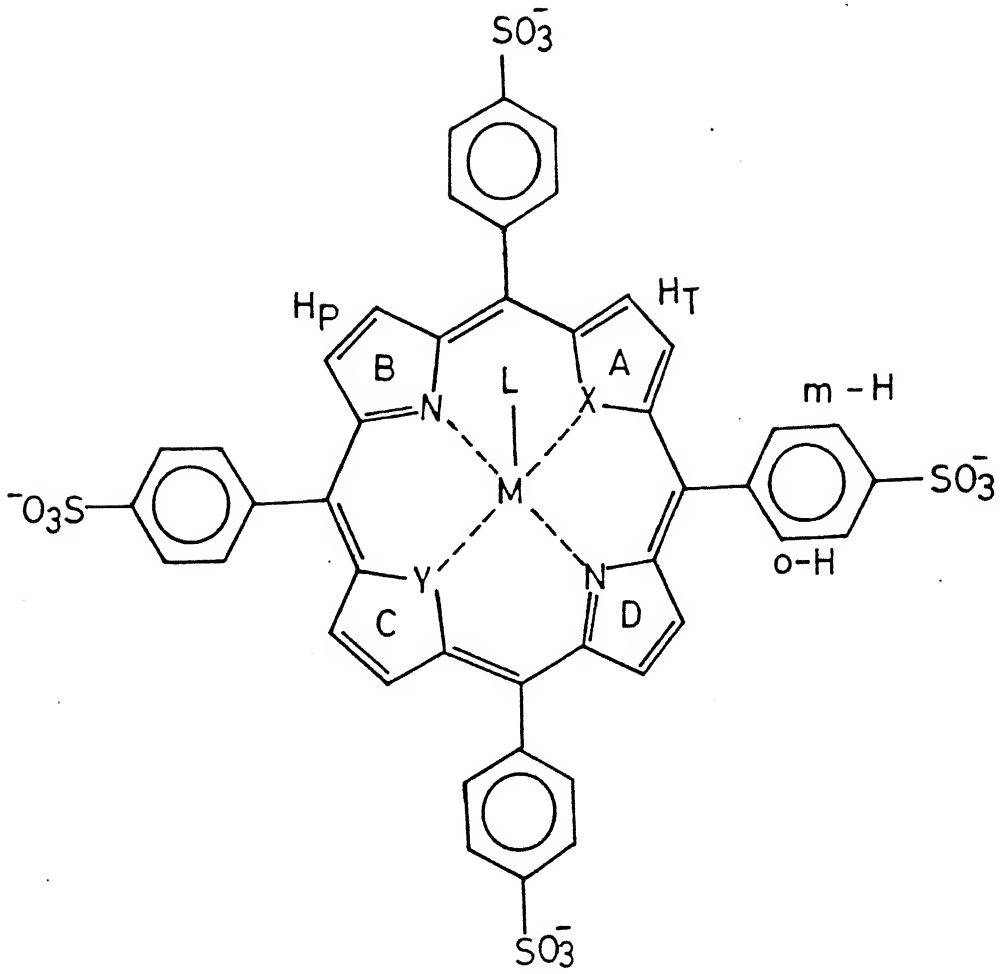

X = S ; Y = NH ; STPPS (no metal)

X = S ; Y = N ; M = Cu^{+2} ; L = Cl^- Cu STPPS Cl

X = S ; Y = N ; M = Ni^{+2} ; L = Cl^- Ni STPPS Cl

X = S ; Y = S ; S_2TPPS (no metal)

Fig.4.1 Structure of water soluble thiaporphyrins and their metallo derivatives.

4.2.1 Synthesis of STPPS:

STPPH [0.200g, 0.317 mmol] dissolved in 30 cm^3 of chloroform in a 100 cm^3 three neck flask. Chlorosulphonic acid [1.408 g, 0.8 cm^3, 12.09 mmol] was slowly added with vigorous stirring and the mixture was heated for an hour at 45°C. The stirring was continued till the evolution of HCl gas ceased. Excess chlorosulphonic acid was decomposed by addition of 20 cm^3 of ice-cold water. The mixture was cooled at 5°C for three hours and filtered. The green precipitate was washed three times with ice-cold water [3x2 cm^3] and several times with acetone and the precipitate was dried in oven at 65°C for two hours. The precipitate was dissolved in dry methanol (150 cm^3) and ammonia gas was passed till the green colour of the solution changed to yellow orange. The solution was filtered and the volume of the methanol solution was reduced to 20 cm^3 under reduced pressure. Dry acetone (70 cm^3) was added to precipitate the porphyrin. The precipitated porphyrin was purified by three successive reprecipitations from methanol with acetone. The black violet crystals (0.255 g) obtained was dried in vacuum oven at 80°C for 18 hours. Yield 79%.

4.2.2 Synthesis of S_2TPPS:

S_2TPP (0.200 g, 0.308 mmol) and chlorosulphonic acid (1.408 g, 0.8 cm^3, 12.09 mmol) under the similar reaction conditions as above ($ 4.2.1) afforded S_2TPPS. Yield 76% (0.243 g).

4.2.3 Synthesis of CuSTPPSCl:

STPPS [0.05 g, 0.0491 mmol] and $CuCl_2.2H_2O$ (0.030 g, 0.1760 mmol] in 120 cm^3 methanol was refluxed for 8 hours. The

completion of the reaction was monitored by optical absorption spectra. The solvent was evaporated under reduced pressure to 20 cm^3 and dry acetone (70 cm^3) was added to precipitate the porphyrin. The precipitated porphyrin was purified by three successive reprecipitations from methanol solution with acetone. The black crystals (0.046 g) obtained was dried in vacuum oven at 75°C for 12 hours. Yield 84%.

4.2.4 Synthesis of NiSTPPSCl

STPPS [0.05 g, 0.0491 mmol] was dissolved in 175 cm^3 of methanol and solution refluxed for 15 minutes. $NiCl_2.6H_2O$ (0.045g, 0.1893 mmol] in 25 cm^3 of methanol was added to the porphyrin solution and the refluxing was continued for a further period of 26 hours. The completion of the reaction was monitored by optical absorption spectra. The solvent was evaporated under reduced pressure to 25 cm^3 and dry acetone (90 cm^3) was added to precipitate the porphyrin. The precipitated porphyrin was washed with acetone and purified by three successive reprecipitations from methanol solution with acetone. The black crystals (0.043 g) obtained was dried in vacuum oven at 75°C for 18 hours. Yield 79%.

4.3.0 Results and Discussion

The sulfonation by chlorosulphonic acid method has many advantages over the traditional H_2SO_4 method[132] such as milder reaction conditions, shorter reaction times, higher yield and products are easy to purify. In this method the formation of mono-,di-, trisulfonated derivatives are reduced relative to H_2SO_4 method.

4.3.1 ^{1}H NMR Spectra:

The ^{1}H NMR spectra have been used to identify the product of sulfonation. ^{1}H NMR spectra of STPPS and S_2TPPS in DMSO-d_6 are shown in Fig. 4.2. The chemical shifts and coupling constants of water soluble thiaporphyrins (STPPS and S_2TPPS) are listed in table 4.1. Because of two fold axis of symmetry in S_2TPPS, the four thiophene (H_T) protons appear as a singlet at 9.78 ppm, the four pyrrole protons (H_P) appear as a singlet at 8.69 ppm. The phenyl protons appear as AB quartet (0 and m-H) (Fig. 4.2) around 8.28 and 8.13 ppm with coupling constant J_{AB} = 8.16 Hz. The coupling constants are comparable to those of para substituted benzenes. Thus the observed chemical shift values and coupling constants confirm that sulfonation occurs at the para position of the phenyl ring. On the other hand, the reduced symmetry of STPPS results in inequivalence of pyrrole protons, the two pyrrole protons (H_P) of the ring (C) resonate as a singlet at 8.98 ppm while four pyrrole protons (H_P) of the ring B and D (Fig. 4.1) resonate as AB quartet around 8.78 and 8.24 ppm with coupling constant 4.08 Hz. The thiophene protons appear as a singlet at 9.8 ppm. The phenyl protons appear as a two sets of quartets in the region 8.0-8.3 ppm with coupling constant J_{AB} = 6.12 Hz. Thus the observed chemical shift values and coupling constants confirm that sulfonation occurs at the para position of the meso phenyl ring.

4.3.2 Optical Spectra:

The electronic spectral data of water soluble thiaporphyrins (STPPS and S_2TPPS) and metallo derivatives (CuSTPPSCl and NiSTPPSCl) in aqueous solution are listed in table

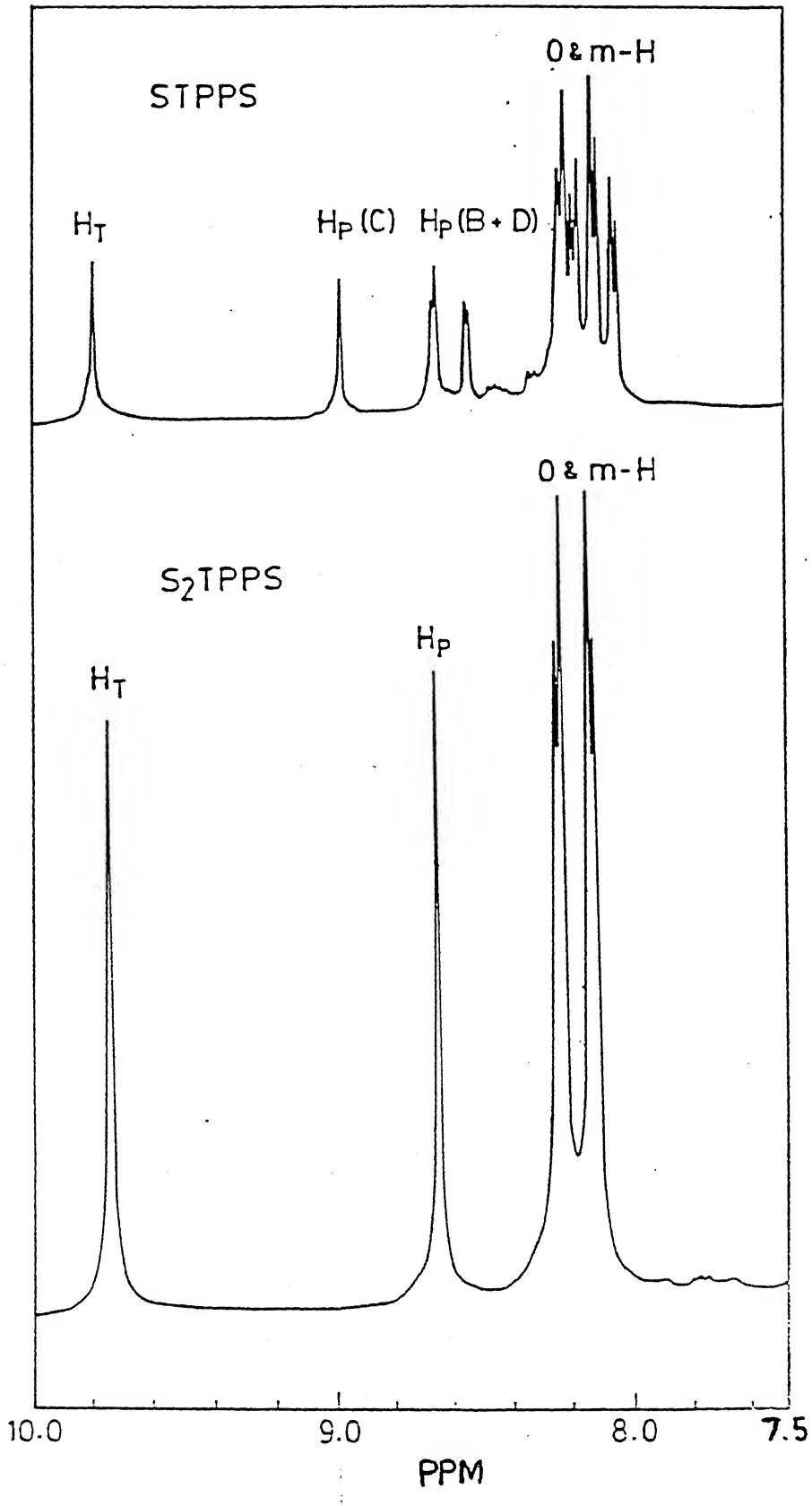

Fig.4.2 ^{1}H NMR spectra of STPPS and S_2TPPS in DMSO-d_6 at 25°C.

Table 4.1 Chemical shifts (ppm) and coupling constants (Hz) of STPPS and S_2TPPS in DMSO-d_6

Porphyrin	Thiophene		Pyrrole		Phenyl		N-H
	H_T		H_P		o-H	m-H	
		C		B&D			
STPPS	9.8(s)	8.98(s)	8.78d 8.60d J_{AB}=4.08		8.24d 8.13d J_{AB}=6.12	8.21d 8.05d J_{AB}=6.12	-2.81(s)
S_2TPPS	9.78(s)	8.69(s)			8.28d J_{AB}=8.16	8.13d J_{AB}=8.16	

s = singlet
d = doublet

Table 4.2: Electronic absorption spectral data of free base and metal thiaporphyrins

Porphyrin	Soret band	Q-bands λ_{max}(nm) ($\varepsilon \times 10^{-3}$)			
	λ_{max} (nm) ($\varepsilon \times 10^{-4}$)	IV	III	II	I
STPPS	425 (18.7)	514(14.9)	548(4.7)	608(2.5)	667(2.8)
S_2TPPS	431 (9.6)	514(11.1)	547(3.90)	625(1.4)	687(2.3)
CuSTPPSCl	434(10.0) 463 sh	--	557(5.9)	616(4.1)	686(2.6)
NiSTPPSCl	445 (6.1) 458(5.6)	--	560(5.1)	633(4.1)	690(3.2)

sh = shoulder

4.2. Fig. 4.3 shows the absorption spectra of STPPS, CuSTPPSCl and NiSTPPSCl in aqueous solution. An inspection of the data in table 4.2 shows that the sulfonation at para position of phenyl ring does not affect the peak positions and intensities of the soret and Q-bands of free base thiaporphyrins significantly. Transformation of $TPPH_2$ to H_2TPPS also show a similar trend essentially suggesting no major changes in the energies of electronic transitions upon sulfonation.

It is well known from the literature that metalloporphyrins generally show only two Q bands Q (0,0) and Q(1,0) due to D_{4h} symmetry[96] (for example CuTPPS 551 and 578 nm). However, the absorption spectra of CuSTPPSCl and NiSTPPSCl show a split soret band and a complex pattern of Q bands (Fig. 4.3). The number of bands and their positions in CuSTPPSCl are more or less similar to those encountered for symmetry reduced $CuNCH_3TPPSCl$[133] (432, 442, 552, 600 and 650 nm). X-ray structure of Cu and Ni derivatives of STPPH has revealed severe nonplanarity of the porphyrin core with thiophene tipped out of the plane of the porphyrin ring.[57] It is expected that sulfonation at the p-position of phenyl does not affect the structure of the porphyrin ring significantly. Thus the observed absorption spectra of CuSTPPSCl and NiSTPPSCl suggest a low symmetry and nonplanarity of the porphyrin core.

CuSTPPSCl is paramagnetic and shows a resolved axial EPR signal in methanol at 100 K with $g_{||} = 2.187, g_{\perp} = 2.043$, $A_{||}^{Cu} = 168$ G and $A_{\perp}^{N} = 12.0$ G. These values are more close to those observed for $CuNCH_3TPPCl$[134] ($g_{||} = 2.256$, $g_{\perp} = 2.08$, $A_{||}^{Cu} = 172$ G) rather than CuTPPS ($g_{||} = 2.197$, $g_{\perp} = 2.033$, $A_{||}^{Cu} = 188$ G). The comparison of ESR parameters of CuSTPPSCl with CuTPPS in nonaqueous media indicate a significant decrease of $A_{||}^{Cu}$ parameter. This effect

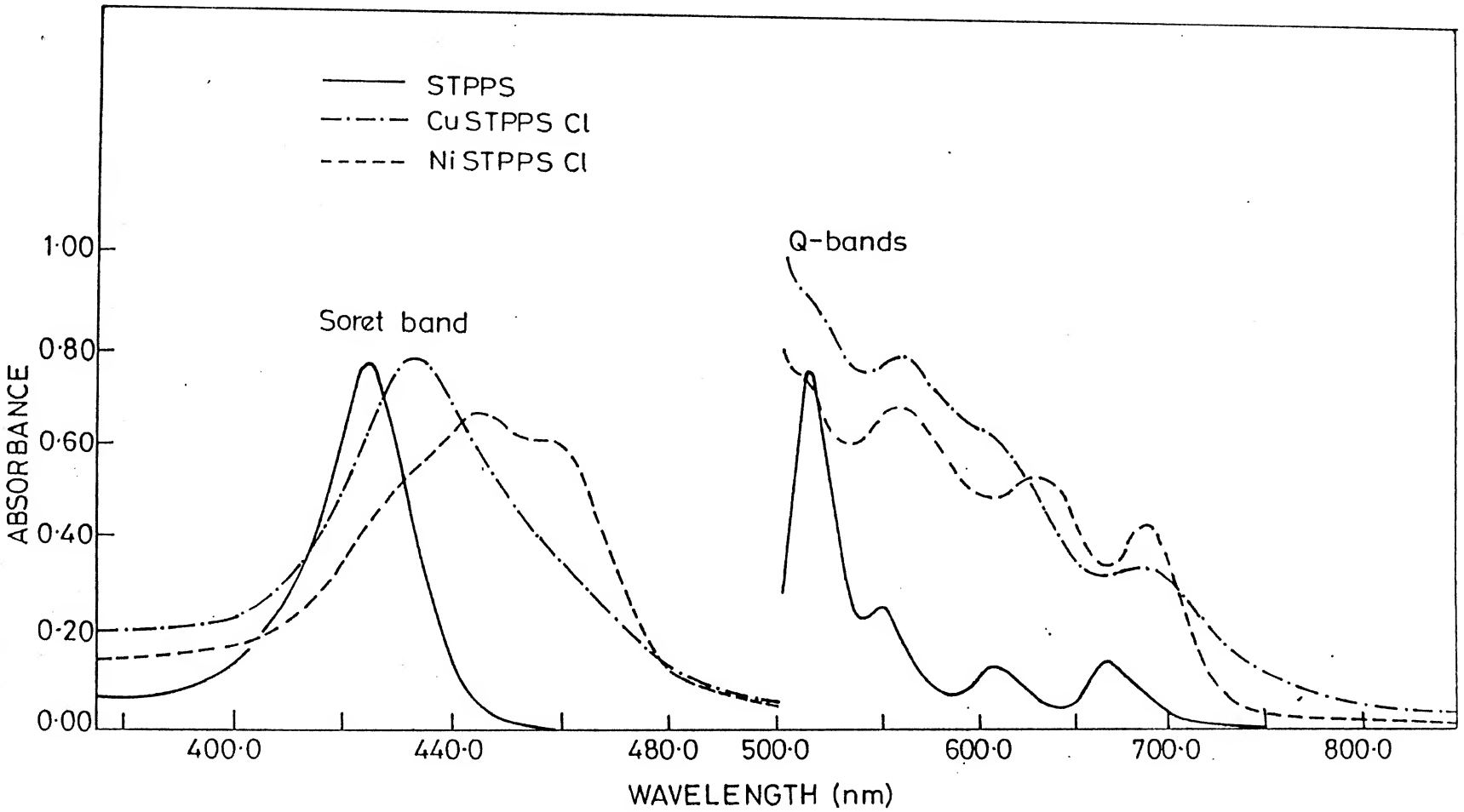

Fig.4.3 Electronic absorption spectra of STPPS (——), CuSTPPSCl (— .—.—) and NiSTPPSCl (- - -) in water (concentration used approximately $1x10^{-5}$M).

reflects pronounced changes in the symmetry of the closet surrounding of Cu(II) in CuSTPPSCl in relation to CuTPPS. CuTPPS has a planar structure with Cu^{2+} ion in the porphyrin plane. On the otherhand, Cu^{2+} ion has an approximate square pyramid symmetry with metal displaced above the thiaporphyrin plane in CuSTPPCl.[57] The structure of CuSTPPSCl should not be much different from this. Justification to such a conclusion comes from the similarity in the absorption spectral pattern and the EPR parameters. Thus, this distorted structure would favour the direct mixing of 4s metal orbital to the ground state Cu(II) caused by a symmetry lowering is responsible for the observed changes of $A_{||}^{Cu}$. A similar conclusion was offered for the decrease in $A_{||}^{Cu}$ value for $CuNCH_3TPPCl$[134] relative to CuTPP.

NiSTPPSCl is also paramagnetic and the measured magnetic moment in water at 27°C is 3.5 μ_B. This corresponds to a high spin ground state (S=1) with two unpaired electrons. NiSTPPCl whose structure is known also has a similar magnetic moment value[57] (3.3 μ_B in $CHCl_3$) indicating the high spin ground state of Ni^{+2} in the thiaporphyrin environment. This is incontrast to those observed for NiTPPS which has a planar structure. Thus the distorted structure around Ni^{+2} ion is responsible for the paramagnetic behaviour of Ni^{+2} thiaporphyrins. It should be pointed out here that Ni^{+2} derivatives of $-NCH_3TPPCl$[135] also show a similar magnetic behaviour (high spin ground state with S=1) as that observed for nickel thiaporphyrins.

4.3.3 Aggregation of STPPS and S_2TPPS:

It is well known that the water-soluble thiaporphyrins aggregate in aqueous solution and the degree of aggregation

depends on the nature of the substituents on the periphery and the structure of the porphyrin.[136] Beer's law studies indicate that the free base water soluble thiaporphyrins obey Beer's law in the concentration range, STPPS (1.5×10^{-5} to 3×10^{-4}M) and S_2TPPS (1.1×10^{-5} to 4.4×10^{-5}M). A typical Beer's law plot is shown in Fig. 4.4. At higher concentrations, the absorption spectra show small red shifts and broadened absorption bands suggesting that the thiaporphyrin do form higher aggregates in aqueous solution.

Dimerization Studies:

The dimerization of a dilute solution of water soluble porphyrin in aqueous solution in the presence of electrolytes is well documented in literature.[137] Earlier studies from this laboratory[138] have shown that upon addition of increasing amounts of K^+ ions to a dilute solution of anionic porphyrins ($\approx 10^{-5}$M) containing 18-crown-6 results in the formation of cofacial dimer in solution. In view of the structural similarity, it is expected that thiaporphyrins also show a similar behaviour. The effects of addition of K^+ and 18-crown-6 to a dilute solution of thiaporphyrins ($\approx 10^{-5}$ M) are: (a) reduction in absorbance and broadening of all the Q-bands and (b) a red shift of Q-bands with well defined isosbestic points. These results suggest the existence of an equilibrium involving the monomer and dimer of thiaporphyrins.[138] In the absence of cation and crown ether, thiaporphyrins exists as monomer and the addition of cation and crown ether strongly drives the equilibrium to the dimer. In the absence of cation the close approach of the two porphyrin monomers is not favoured due to repulsion of the negative charges on the periphery of the thiaporphyrins. The added cation reduces this

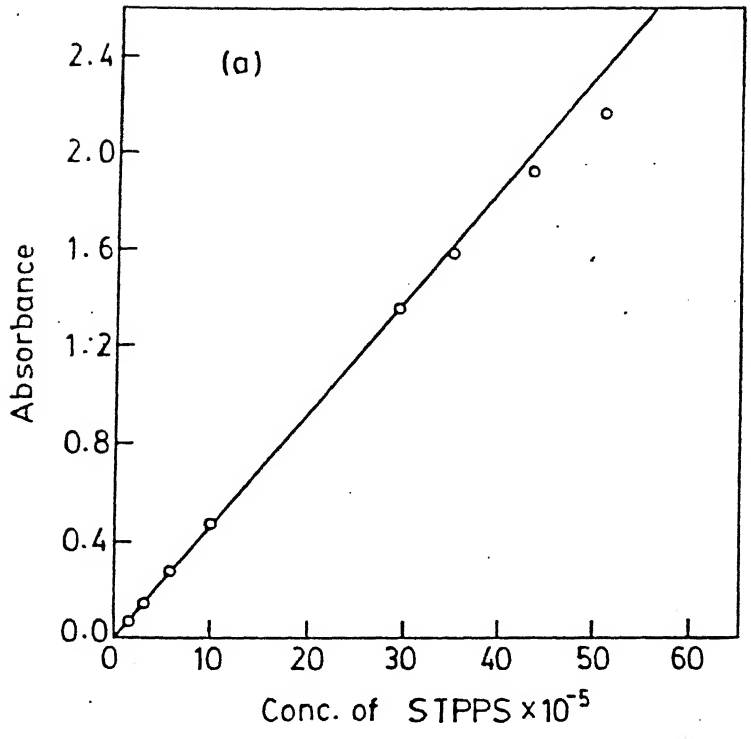

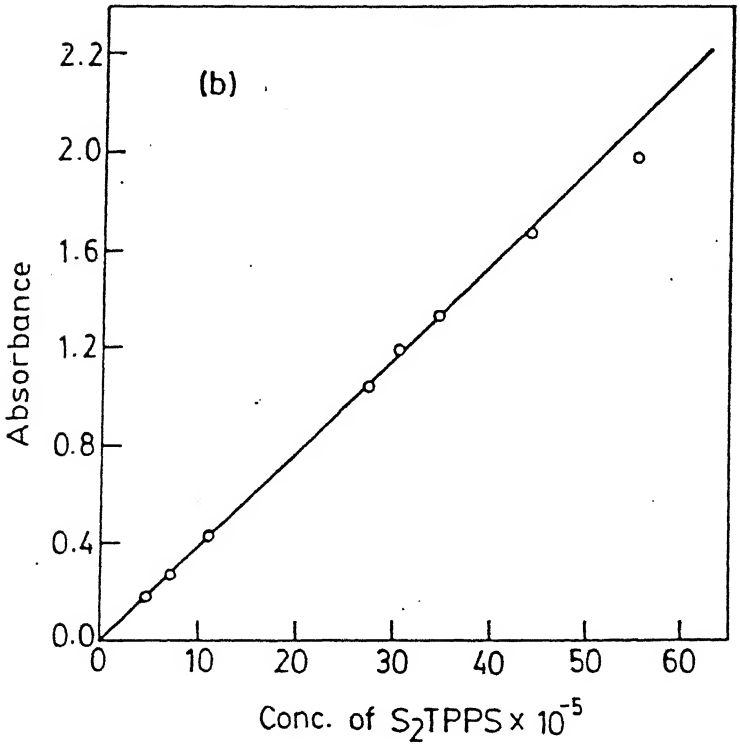

Fig.4.4 Beer's law plot for (a) STPPS and (b) S_2TPPS in aqueous solution.

electrostatic repulsion by shielding the negative charges so facilitating the close approach of the two thiaporphyrin rings to form a dimer through π-π interaction. It is observed that the cation-crown ether complex is much more effective in driving the equilibrium to the dimer side than the cation alone. This could be due to the exclusion of some water molecules from the solvation shell of the cation on complexation with the crown ether making the environment of the cation less polar and allowing the cation to approach the thiaporphyrin more closely than completely solvated cation. A comparison of the dimerization induced red shifts for STPPS and S_2TPPS with H_2TPPS indicates similar magnitudes (table 4.3) and the exciton splitting parameter calculated from the available spectral data are comparable to those observed recently for cation induced dimerization of crowned phthalocyanins[139] and porphyrins.[138] The magnitude of red shift and the intensity decrease for the CuSTPPSCl and NiSTPPSCl are much less relative to free base derivatives. This is ascribed to the nonplanarity of the porphyrin core in the metal derivatives resulting in a decreased π-π interaction (which is atleast in part responsible for red shift) between the two rings in a cofacial geometry.[140]

The effect of temperature on an aqueous solution containing S_2TPPS [5.55×10^{-5} M],18-crown-6 [0.05 M] and K^+ ions [1.96×10^{-1} M] is displayed in Fig. 4.5. The presence of well defined isosbestic points are indicative of the presence of monomer-dimer equilibrium in solution. Evidently, small changes in temperature have a large effect on the extent of dimerization with lower temperature favouring the formation of the dimer while the higher temperature shifts the equilibrium towards the monomer.

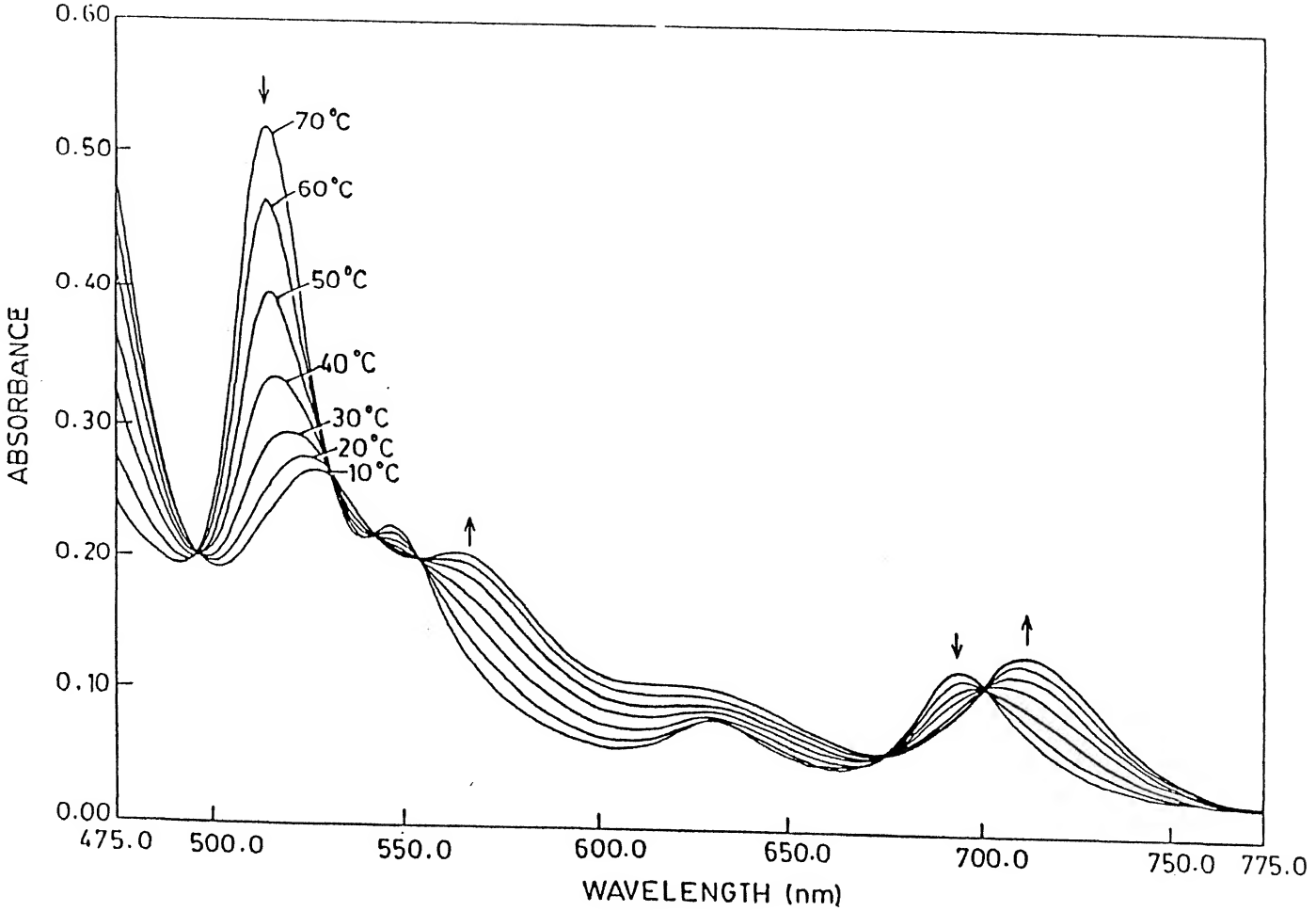

Fig.4.5 The effect of temperature on Q bands of S_2TPPS (5.55×10^{-5}M) containing 18-crown-6 (0.05 M) and K^+ (0.196 M) in water, T = 10, 20, 30, 40, 50, 60, 70°C. Arrows indicate changes of decreasing temperature.

Table 4.3 Dimerization induced absorption band shifts[a] (nm) and the exciton splitting parameter (V) for free base and metal thiaporphyrins in presence of cation and 18-crown-6 complexes

Porphyrin	Q-bands I	II	III	IV	V* (cm^{-1})
STPPS	23	11(Sh)	14	9	1025
S_2TPPS	22	5(Sh)	15	9	905
H_2TPPS	22	15(Sh)	12	9	1065
NiSTPPSCl	2	0	2		63
CuSTPPSCl	6	-3	9		232

*Calculated for Q I band

a : + red shift
- blue shift

Figure 4.6 shows the spectral titrations of K^+ ions to the dilute solution of various thiaporphyrins [$\approx 1x10^{-5}$ M] containing 18-crown-6. The shapes of the curves in Fig. 4.6 reveal that the process of formation of the dimer involves more than one step. Two types of dimers can be visualized upon addition of cation crown ether complex; a 'non-sandwich' dimer of the type porphyrin cation crown ether-porphyrin involving only one cation crown ether complex per dimer and a cofacial or sandwich dimer which involves two or more cation crown ether complexes per dimer. At lower concentrations of K^+ ions, the intensity decrease is sharp probably indicating the formation of a non-sandwich dimer with a very high formation constant. At higher concentration of K^+ ions, a transformation of non-sandwich dimer to a cofacial dimer occurs by encapsulating a second cation crown ether complex. Since two more sites are still available in the cofacial dimer for saturation, it is possible that the encapsulation continues at higher concentration until the two porphyrin units bind four cation crown ether moieties.

Evaluation of Formation Constants[138] (K) for Dimer Formation

The progressive decrease in absorbance of a prominent Q-band on increasing addition of cation-crown ether complex is made use to evaluate the extent of dimer formation using a method described previously.[141] The cation crown ether induced dimerization can be represented by equation (4.1) where P,stands for the thiaporphyrin molecule, C^+ represents the cationcrown ether

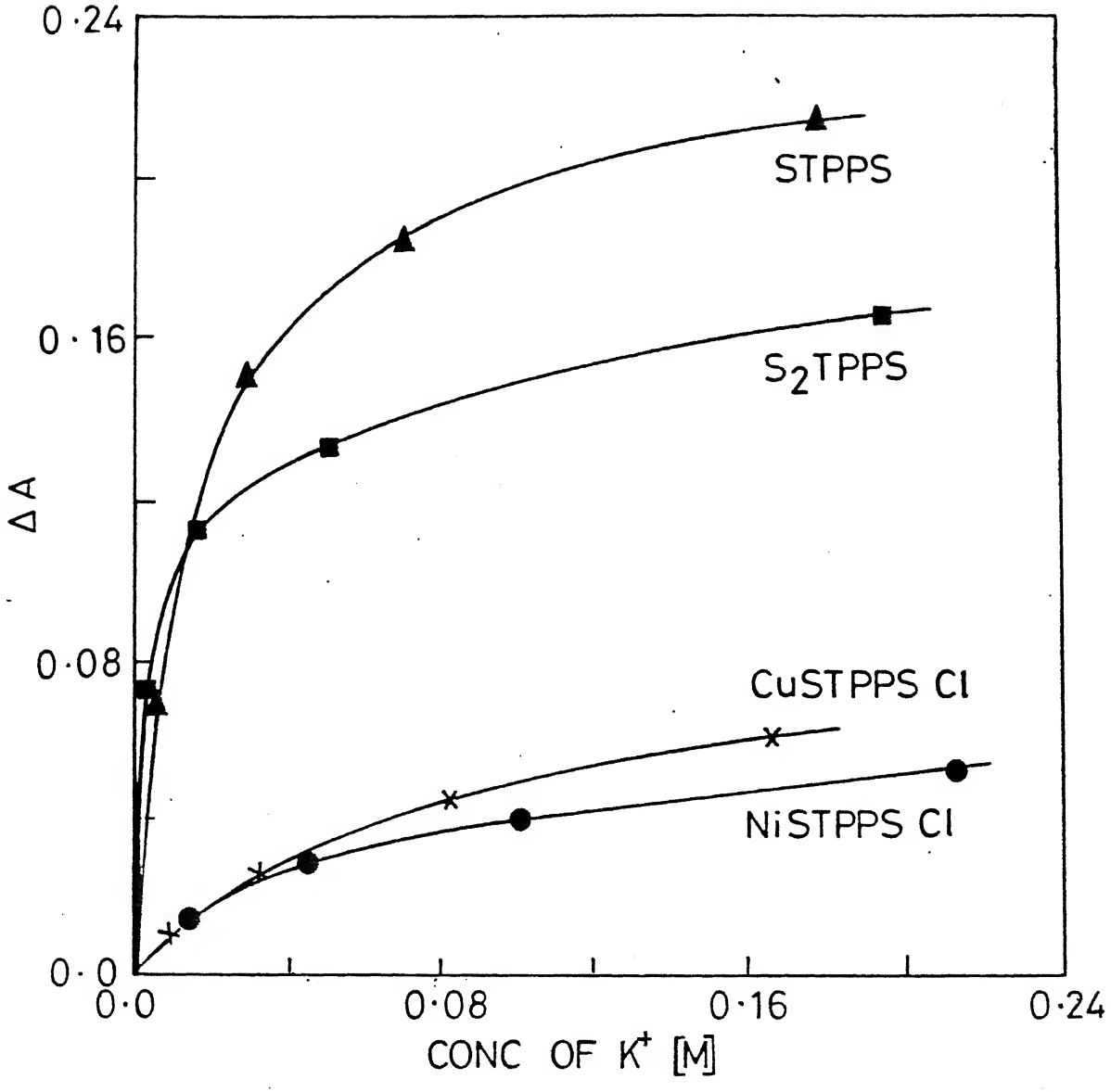

Fig.4.6 The absorbance changes of a prominent Q band of STPPS (▲), S_2TPPS (■), CuSTPPSCl (X) and NiSTPPSCl (●) in aqueous solution containing 18-crown-6 (0.05 M) upon increasing concentration of K^+ ions.

$$2P + n\ C^{+} \underset{}{\overset{K}{\rightleftharpoons}} (P_2\ C_n)^{n+} \qquad (4.1)$$

complex and n is the number of cation crown ether complexes incorporated. The value of n was varied from 1-4, the upper limit chosen was four since there are four negative groups in the periphery of porphyrin. The method adopted here assumes different values of K and computes the theoretical values of x, the amount of dimer formed and ΔA, the decrease in absorbance at each concentration of cation added using experimentally known parameters such as the thiaporphyrin concentration, the concentrations of the cations added, the decrease in absorbance at each cation concentration added and the molar absorption values of the monomer and the dimer (the absorption value for the dimer being calculated from the spectrum run at $10^{o}C$). A computer program was devised to carry out the calculations using the Newton-Raphson iterative method. Theoretical plots of ΔA versus concentration of the cation added for various values of K were constructed. The experimental points (*) were then mapped into this plot, and the best fit chosen for the overall formation constant of the dimer. Calculations were performed varying the value n from 1-4 and in all the cases the best fit was observed when n=4, suggesting that four-cation crown ether complexes are involved per dimer. A representative plot for the K^{+}, 18-crown-6 induced dimer of STPPS, for n=4 is given in Fig.4.7. The value of K for STPPS (log K = 10.6), S_2TPPS (log K = 9.5). The magnitudes of K are similar to those observed for anionic porphyrins[138] (log K = 11.0±1.5) probably suggesting that the dimerization process of anionic thiaporphyrins are similar to those observed for normal

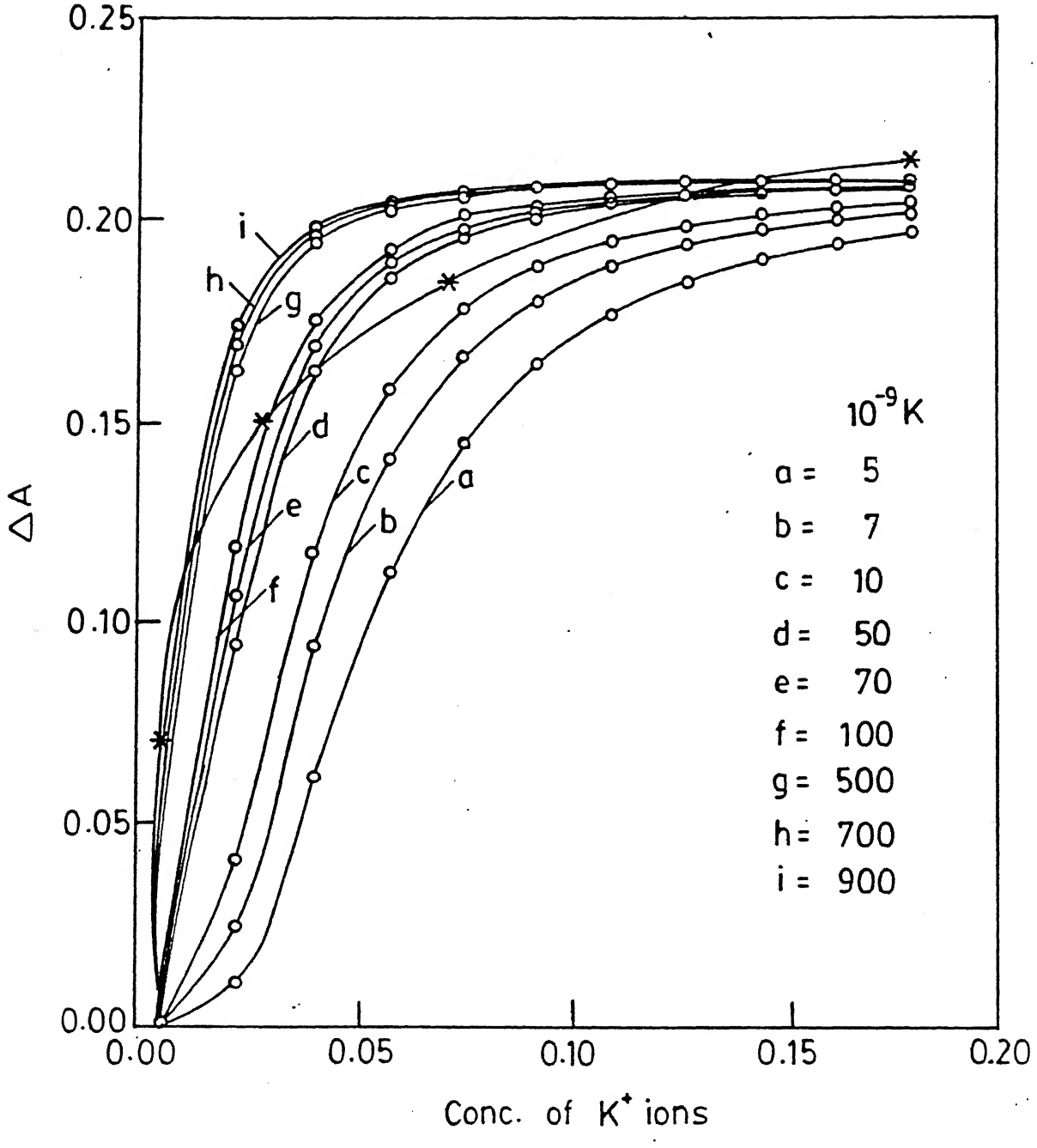

Fig.4.7 Difference in absorbance values (ΔA) versus concentration of K^+ ions added for various assumed values of K for dimerization of STPPS (for n = 4); (0) theoretical, (*) experimental.

anionic porphyrins.

4.3.4 Redox Behaviour of Water Soluble Thiaporphyrins:

Cyclic voltammetry was used to examine the redox reactions of free base and the metalloderivatives. Redox potentials of free base and metallothiaporphyrins (CuSTPPSCl and NiSTPPSCl) are listed in table 4.4. Both STPPS and S_2TPPS exhibit one electron irreversible oxidation which are shifted positively 64 mV and 140 mV respectively relative to H_2TPPS in DMF. Reductions are examined in DMF and DMSO. A typical cyclic voltammogram of S_2TPPS in DMF is shown in Fig. 4.8A. Waves 1 and 2 correspond to two one electron reductions (-0.745 V - 1.245 V). Both the reductions are chemically irreversible. STPPS in DMF also shows two one electron reductions (-0.845 V, -1.364 V) with an additional cathodic peak at -0.2 V. This peak is observed at low scan speed (20-200 mV/S) and disappears at higher potential scan speeds (> 500 mV/S) indicating a coupled chemical reaction. The two reductions observed for the free base derivatives corresponds to the formation of mono and dianions of the porphyrin ring. These results are parallel to those observed for H_2TPPS[142,143] except that potentials are shifted to more positive values with heteroatom substitution showing a regular decrease in the Δ_{redox} for the series. This is consistent with the earlier observations in the non-aqueous medium.[86]

CuSTPPSCl in DMF shows three one electron reductions (Fig. 4.8B). The first reduction (wave 3) is reversible in both DMF (ΔE_p = 72 mV and $\frac{i_{Pc}}{i_{Pa}} \approx 1$) and DMSO ($\Delta E_p$ = 63 mV and $\frac{i_{Pc}}{i_{Pa}} \approx 1$) when scanned separatelty (Fig. 4.8B inset). The $E_{1/2}$ values

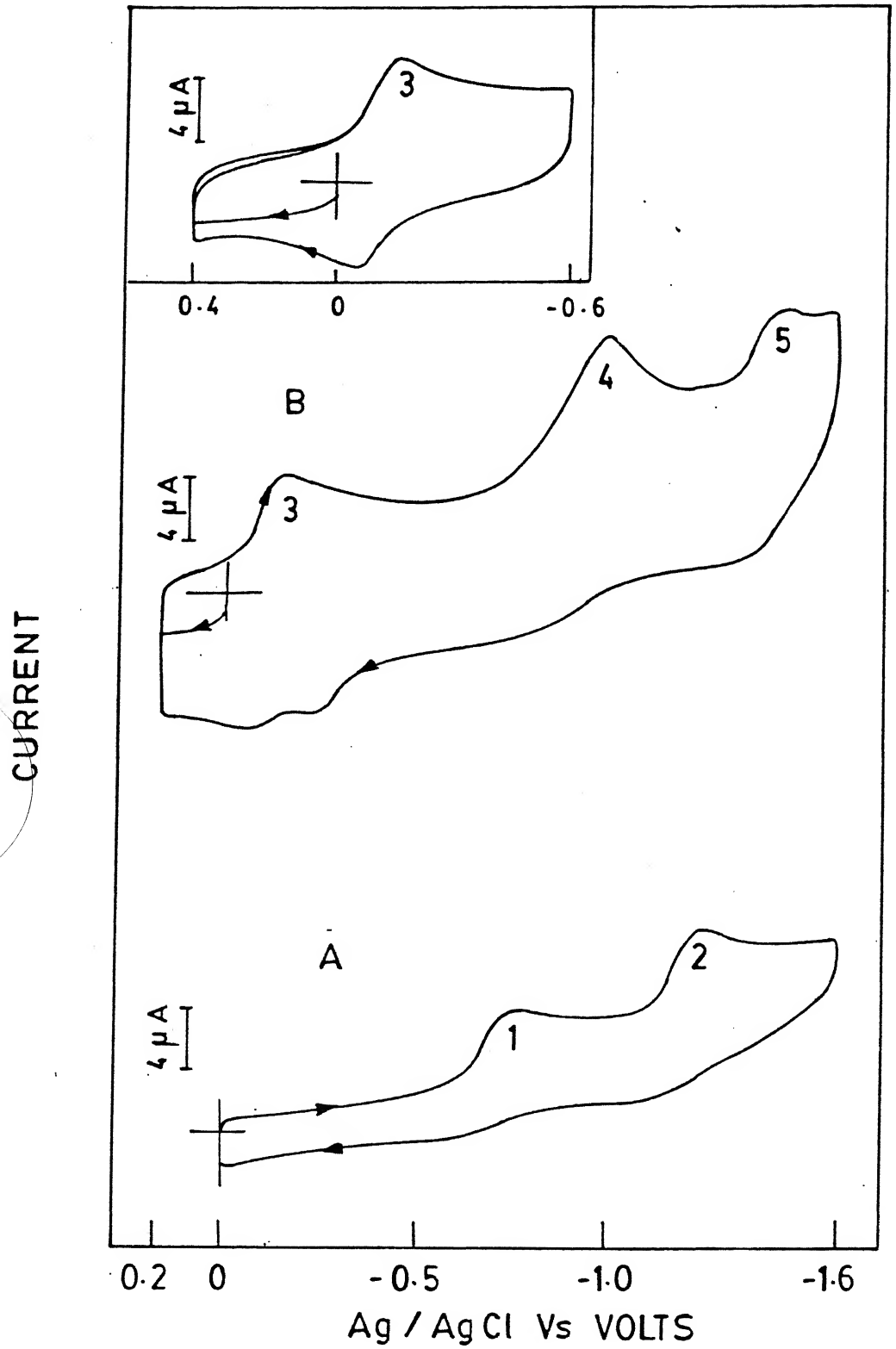

Fig.4.8 Cyclic voltammogram of (A) S_2TPPS ($\sim$6.9x10^{-4}M) in DMF, ν = 100 mV/S, (B) CuSTPPSCl (5.7x10^{-4}M) in DMF, ν = 300 mV/s (inset shows the reversible nature of Cu(II) - Cu(I) reduction).

Table 4.4 Redox potentials (V) of free base and metal thiaporphyrins

Porphyrin	Solvent	Oxidation		Reduction		
		$E_{1/2}(1)$	Metal (+2/+1)	$E_{1/2}(1)$	$E_{1/2}(2)$	Δ^*Redox
[a] H_2TPPS	DMF	+1.10(ir)	---	-0.964(ir)	-1.536(ir)	2.064
[a] STPPS	DMF	+1.164(ir)	---	-0.845(ir)	-1.364(ir)	2.009
	DMSO	---	---	-0.845(ir)	-1.382(ir)	---
[a] S_2TPPS	DMF	+1.240(ir)	---	-0.745(ir)	-1.245(ir)	1.985
	DMSO	---	---	-0.745(ir)	-1.254(ir)	---
CUSTPPSCl	DMF	---	-0.099(r)	-0.946[a](ir)	-1.40[a](ir)	---
	DMSO	---	-0.095(r)	-0.945[a](ir)	-1.382[a](ir)	---
NiSTPPSCl	DMF	---	-0.346(qr)	-0.768(r)	---	---
	DMSO	---	-0.400(qr)	-0.719(r)	-1.391[a](ir)	---

a - for these cases the $E_{1/2}$ values corresponds to peak potentials

ir - ir reversible, qr - quasireversible, r = reversible

* - $[E_{1/2}(1)(ox) - E_{1/2}(1)\ (Red)]$

corresponding to this couple is in the range completely inaccessible for free base ring centered reduction (table 4.4). Thus, this couple is assigned to the metal centered reduction corresponding to the formation of $[Cu(I)STPPSCl]^{-5}$. This is in contrast to the result observed for CuTPPS where the first electron reduction corresponds to the formation of mono anion of $[Cu(II)TPPS]^{-5}$. Addition of second electron results in the formation of monoanion $(Cu(I)STPPSCl)^{-6}$ (wave 4). Further addition of electron leads to the formation of dianion $[Cu(I)STPPSCl]^{-7}$ (wave 5). Both these reductions (-0.946 V, -1.40 V) are chemically irreversible. The absolute potential difference between the two successive ring reductions is 0.454 V in DMF and 0.437V in DMSO, which is within the range of 0.45±0.05V expected for two successive ring reductions of variety of metallo OEP and TPP complexes.[87] Furthermore, upon scan reversal, an additional cathodic peak is observed around -0.2V similar to that observed for free base STPPS. On repetitive scans at constant scan speed, there is an enhancement of peak current. This is ascribed to the instability of the dianion resulting in the demetallation of copper from porphyrin. Copper monothiaporphyrin also is known to undergo demetallation upon $2e^-$ reduction in non-aqueous media.[70] The schematic representation of electrode process are shown below:

$$[Cu(II)\ STPPSCl]^{-4} \underset{-e}{\overset{+e}{\rightleftharpoons}} [Cu(I)\ STPPSCl]^{-5}$$

$$[Cu(I)\ STPPSCl]^{-5} \xrightarrow{+e} [Cu(I)STPPSCl]^{-6} \xrightarrow{+e} [Cu(I)STPPSCl]^{-7} \xrightarrow[-Cl^-]{+H^+} Cu + STPPS^{4-}$$

The cyclic voltammogram of NiSTPPSCl in DMF and DMSO are shown in Fig. 4.9C and D. Two well defined reductions (waves 6 and 7) and a broad ill defined anodic peak (wave 8) at -1.38V in DMSO are observed. The first reduction in both the solvents is quasi reversible (ΔE_p = 91 mV and 128 mV) and the ratio of the peak current close to unity in DMF and DMSO respectively (Fig.4.9C and D inset). The $E_{1/2}$ values for this reduction is not in the range of first reduction of STPPS in both solvents discarding the possibility of the ring reduction. Alternatively this has to be ascribed to the metal centered reduction corresponding to the formation of $[Ni(I)STPPSCl]^{-5}$. This also is in contrast to that observed for NiTPPS where the first electron addition results in the monoanion formation.[144] It is known from earlier electrochemical studies that the reduction of Ni(II) STPPCl in THF undergoes two one electron reduction process. The first electron addition corresponds to a metal centered reduction (Ni(II)/Ni(I) couple). Two cathodic waves observed at -0.23 V and -0.52V were assigned to the formation of Ni(I)STPP and $[Ni(I)STPPCl]^-$ based on the dependence of peak current on addition of LiCl as source of chloride ligand.[145] Addition of increasing amounts of LiCl increases the peak current at -0.52V while a decrease in peak current was observed at -0.23V. This has been accounted in terms of existence of two types of Ni(I) forms in solution. One corresponding to the four co-ordinate Nickel with fifth axial chloride dissociation while other corresponds to five coordinate nickel without the chloride dissociation. However in the present study only one couple (wave 6) is observed in both solvents for Ni(II)/Ni(I) reduction and the titration of LiCl had no appreciable effect on the peak currents of wave 6 indicating

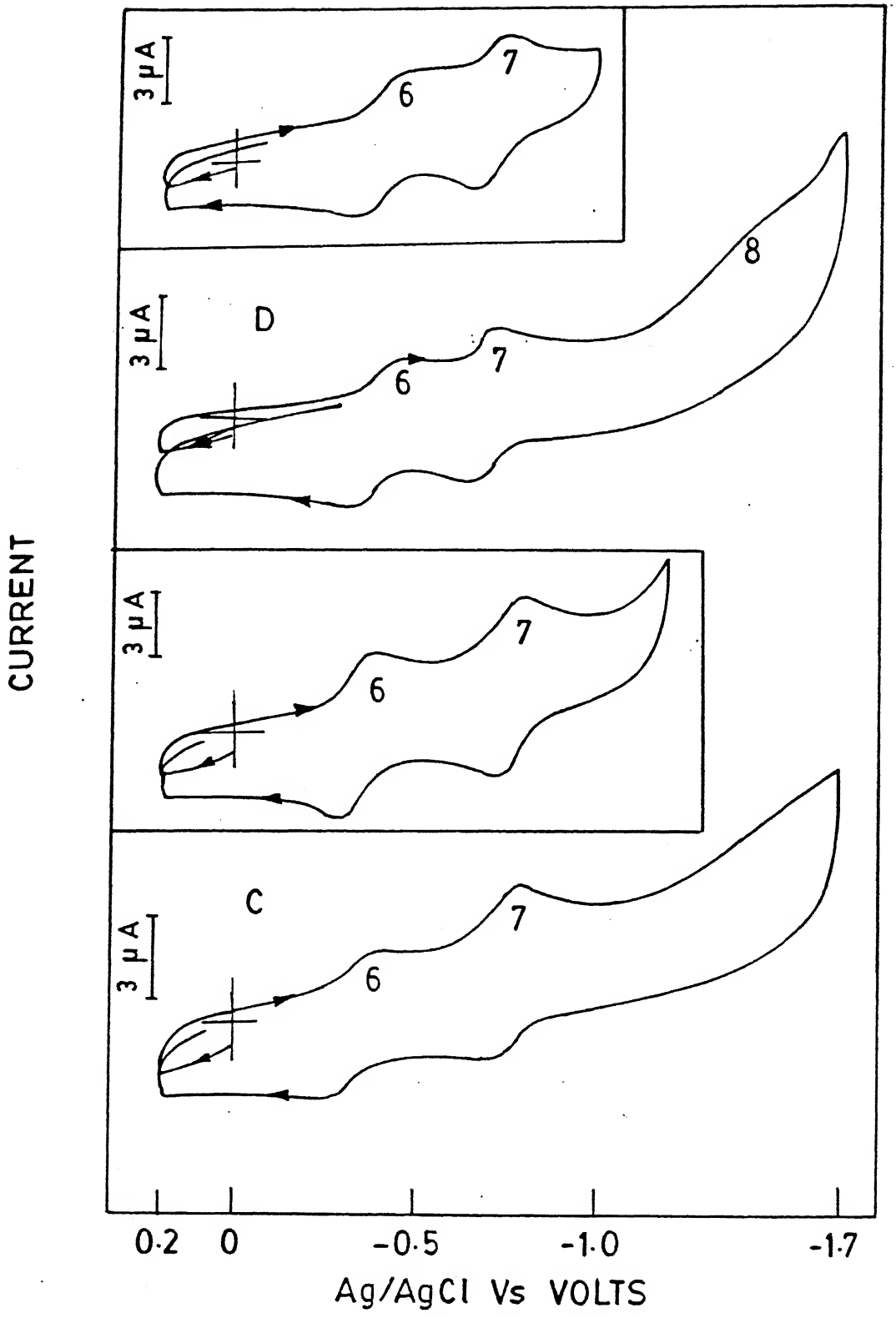

Fig.4.9 Cyclic voltammogram of (C) NiSTPPSCl ($\simeq 5.4 \times 10^{-4}$M) in DMF, ν = 100 mV/s and (D) NiSTPPSCl ($\simeq 6.5 \times 10^{-4}$M) in DMSO, ν = 100 mV/s (inset C and D show the quasi-reversible and reversible nature of wave 6 and 7, respectively).

that the axial chloride ligand is not dissociated under our experimental condition.

The addition of second electron results in the formation of monoanion $[Ni(I)STPPSCl]^{-6}$ and this reduction is reversible in both solvents (wave 7) (ΔE_p = 64 mV, 73 mV and the ratio of peak currents close to unity in DMF and DMSO respectively). Further addition of electron results in the formation of the dianion$[Ni(I)STPPSCl]^{-7}$ (wave 8). The absolute potential difference between the two successive ring reductions is 0.57V which is slightly more than the expected value of 0.45±0.05 V. Because of the broadness and irreversible nature of this peak (wave 8) only peak potentials are reported while for the first ring reductions (wave 7) the $E_{1/2}$ corresponds to mid point of anodic and cathodic peaks. This probably accounts for the small difference observed. A schematic representation of the electrode process are shown below:

$$[NiSTPPSCl]^{-4} \underset{-e}{\overset{+e}{\rightleftharpoons}} [Ni(I)STPPSCl]^{-5}$$

$$-e \uparrow \quad \downarrow +e$$

$$[NiSTPPSCl]^{-7} \underset{-e}{\overset{+e}{\leftarrow}} [Ni(I)STPPSCl]^{-6}$$

It is well known that the site of reduction of the metalloporphyrin complexes with redox active metals depends on the relative energies of the empty $e_g(\pi^*)$ orbitals and the filled metal d-orbitals. Consideration of the first reduction potentials of H_2TPPS and STPPS indicate that the $e_g(\pi^*)$ orbitals of STPPS are lower in energy by about 119 mV relative to that of H_2TPPS. In spite of this, the first electron addition to Cu^{+2}, and Ni^{+2} derivatives of STPPS results in metal centered reduction,

suggesting that the metal $d_{x^2-y^2}$ orbital in both the metals are infact lower in energy than the $e_g(\pi^*)$ orbitals of the porphyrin ring. The reverse is true for CuTPPS and NiTPPS. Lavallee and coworkers have reported that the $CuNCH_3TPPCl$[69] undergoes Cu(II)$\longrightarrow$ Cu(I) reduction process at -0.38V in CH_3CN. The observed metal centered reduction is explained by the ligand field strength. The $CuNCH_3TPPCl$ have three strong metal to nitrogen bonds and therefore, a smaller ligand field strength. The non N-substituted porphyrins have highly planar with four strong metal to ligand bonds and have higher ligand field strength. Thus the stabilisation of Cu(I) in $CuNCH_3TPPCl$ is due to the low ligand field strength relative to non N-substituted porphyrins. The structures of CuSTPPCl[57] and NiSTPPCl[57] have revealed that the porphyrin plane is nonplanar and the thiophene ring is sharply bent out of the plane of the porphyrin. The shape of the porphyrin resembles that in metal complexes of porphyrin N-oxides[146] and N-alkyl porphyrins.[69] The introduction of SO_3^- groups at the p-phenyl rings should not affect the distorted geometry around the metal ion in CuSTPPSCl and NiSTPPSCl. The observed split soret band and a complex pattern of Q-bands in absorption spectra justifies such a conclusion. On the other hand, both NiTPPS and CuTPPS have planar porphyrin core.[147] Thus, this difference in the structures of the porphyrin core around the metal ion probably is responsible for the reversal of order of energy level. A schematic representation of the reversal of empty metal $d_{x^2-y^2}$ orbital is shown below:

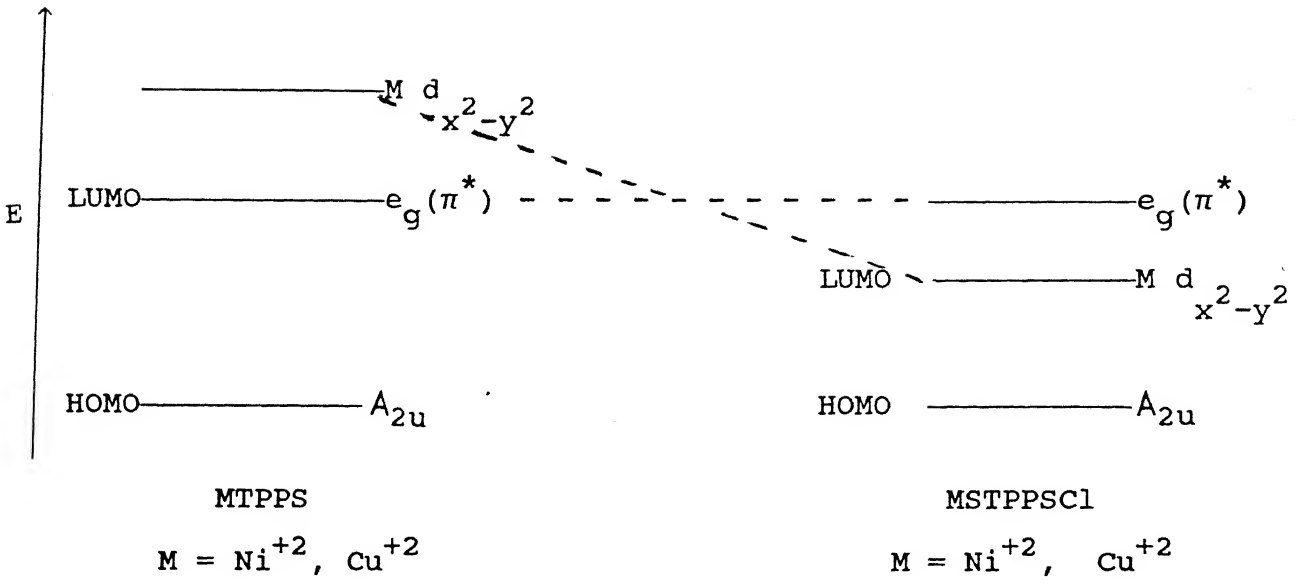

MTPPS

M = Ni^{+2}, Cu^{+2}

MSTPPSCl

M = Ni^{+2}, Cu^{+2}

4.3.5 Fluorescence Spectra:

The free base water soluble thiaporphyrins STPPS and S_2TPPS exhibit room temperature fluorescence in aqueous solution which is shown in Fig. 4.10. The emission data are listed in table 4.5. The fluorescence spectral data (table 4.5) show that the emission maxima are red shifted relative to free base H_2TPPS consistent with the reduction in Δ_{redox}. The magnitude of the red shift and the intensity quenching depends on the number of sulfur atom(s) in the porphyrin core. The fluorescence quantum yield has been calculated by using a comparative method with H_2TPPS as standard[77,148] (ϕ_f = 0.08). The natural radiative lifetime (τ^o) has been estimated from the absorption and the emission spectra using Birks-Dyson[78] modification of Strickler-Berg equation.[79] The details of calculation of natural radiative (τ^o) lifetime is described in Chapter 2. The natural radiative life time (τ^o), the rate of intersystem crossing (K_{isc}) and the rate of fluorescence radiative decay (K_f) are tabulated in table 4.5. The

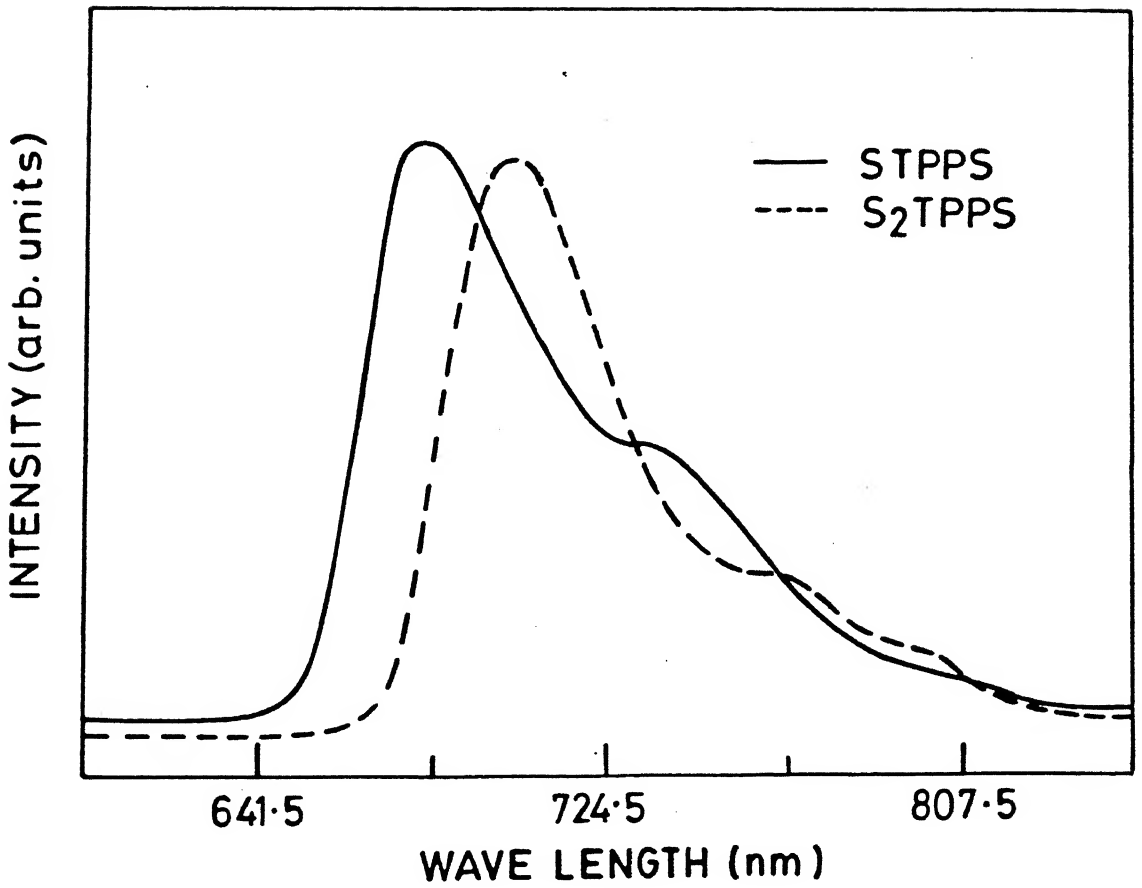

Fig.4.10 Fluorescence spectra of STPPS (——) (4.9×10^{-5}M) and S_2TPPS (-----) (5.2×10^{-5}M) in water.

Table 4.5 Singlet excited state parameters of thiaporphyrins

Porphyrin	Emission band maxima (nm) Q(o,o)	Q(o,1)	Quantum yield ϕ_f	τ^o (ns)	$10^{-6}K_f$ s^{-1}	$10^{-8}K_{isc}$ s^{-1}	E_{o-o} (P-P*) (eV)	$^*E^o$ $^a(P^+/^*P)$ (V)	$^*E^o$ $^b(^*P/P^-)$ (V)
STPPS	678 (686)	742 (766)	0.0055	234	4.3	7.77	1.83	-0.666	+0.985
S_2TPPS	703 (720)	768 (800)	0.0042	278	3.6	8.53	1.76	-0.520	+1.015
H_2TPPS	645 (669)	700 (750)	0.08	203	4.9	0.56	1.92	-0.82	+0.956

The number in parenthesis correspond to emission maxima of dimers.
a : Excited state oxidation potential
b : Excited state reduction potential

general feature of these findings can be summarised as follows: (a) the quantum yield decreases in the series H_2TPPS > STPPS > S_2TPPS, (b) τ^o and K_{isc} increases in the order H_2TPPS < STPPS < S_2TPPS and (c) there is a small decrease in K_f in the order H_2TPPS > STPPS > S_2TPPS. The decrease in quantum yield can be ascribed in part to the increase in the K_{isc} and τ^o due to the introduction of heavy sulfur atom(s) into the porphyrin core. The heavy atom effect[96] is known to increase the K_{isc} and the increase in K_{isc} upon sulfur substitution is consistent with this. However, in porphyrins systems, internal conversion is known to be one of the major decay pathway from S_1 state.[96] A rough estimate of ϕ_{ic} for H_2TPPS from known values of ϕ_f (0.08) and ϕ_T (0.78)[143], internal conversion accounts for about 14% decay. In the absence of ϕ_T values for thiaporphyrins, estimates of contribution of internal conversion to S_1 state is difficult. Nevertheless,contribution from internal conversion to S_1 state decay is expected because theoretical calculations by Gouterman and co-workers predict the absence of any low lying charge transfer state for S_2TPP.[52] Thus, it is reasonable to presume that the combined effect of increase in K_{isc} rates and internal conversion accounts for the decrease in the quantum yield upon substitution of sulfur atoms.

4.3.6 Excited State Potentials

The excited state redox potentials listed in table 4.5 reveal the following features: (a) thiaporphyrins are better oxidants (by 150-200 mV) and poor reductants (60 mV) in the first singlet excited state relative to H_2TPPS. (b) between the two free bases, S_2TPPS is a better oxidant (by 146 mV) than STPPS. It is interesting to note that the $E_{1/2}$ values evaluated both for ground

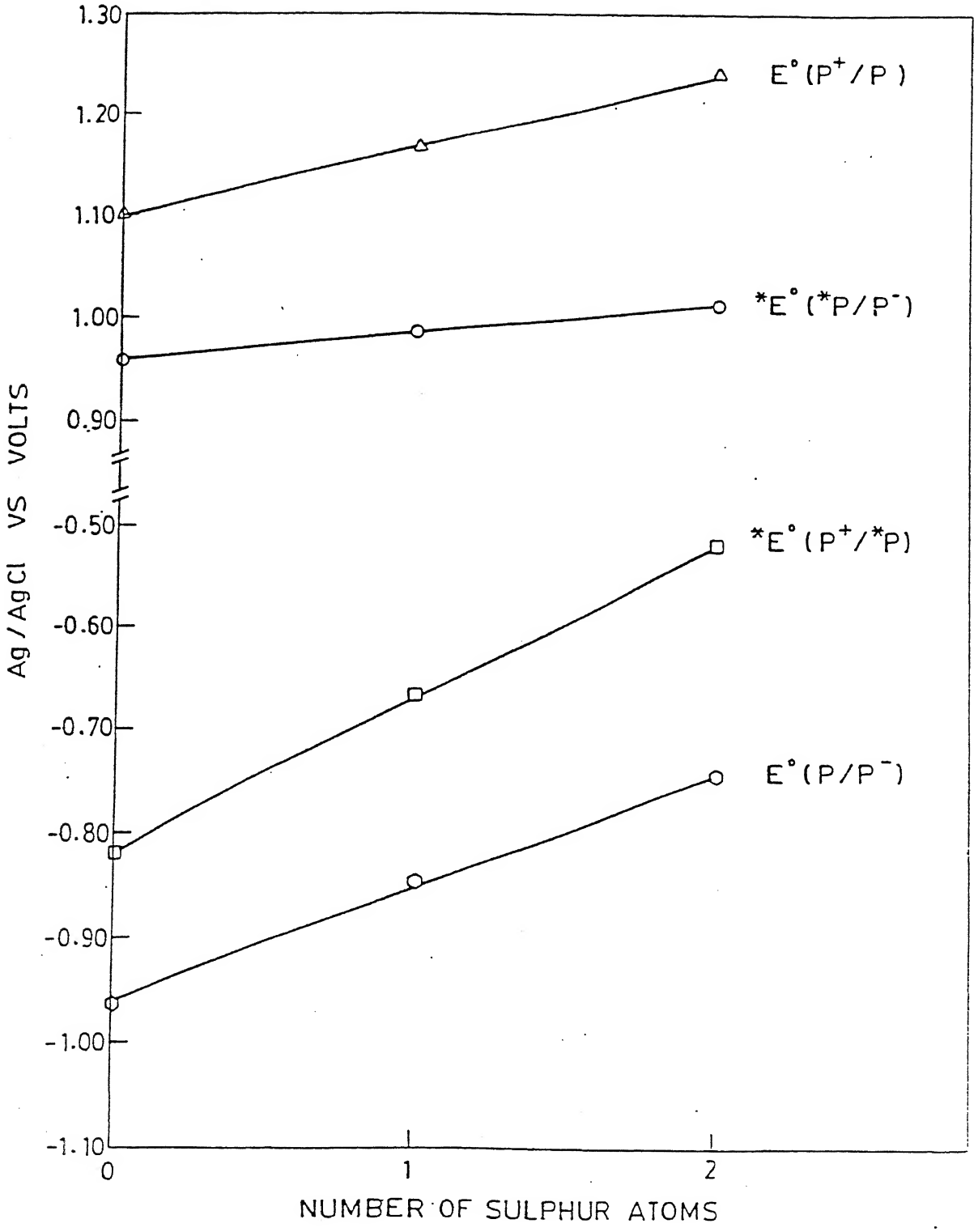

Fig.4.11 Plots of ground state potentials ($E^{o}(P^{+}/P)$, $E^{o}(P/P^{-})$) and excited state potentials ($^{*}E^{o}(P^{+}/^{*}P)$, $^{*}E^{o}(^{*}P/P^{-})$) versus the number of sulfur atoms in the porphyrin core.

(E^{o} (P^{+}/P), $E^{o}(P/P^{-})$ and excited ($^{*}E^{o}(P^{+}/^{*}P)$, $(^{*}E^{o}(^{*}P/P^{-}))^{*}$ states can be correlated with the number of sulfur atoms in the porphyrin core. Such a plot shown in Fig. 4.11 reveals that thiaporphyrins are harder to reduce and easier to oxidise in the excited states. These correlations are best illustrated in the following Latimer type diagrams.

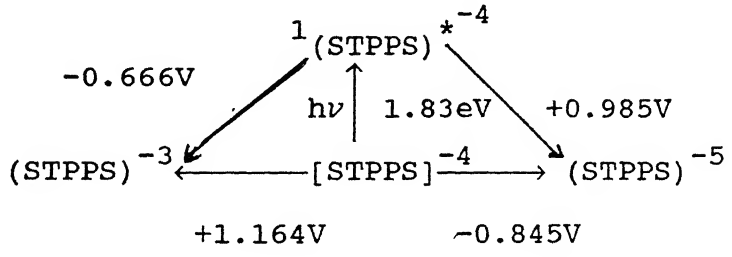

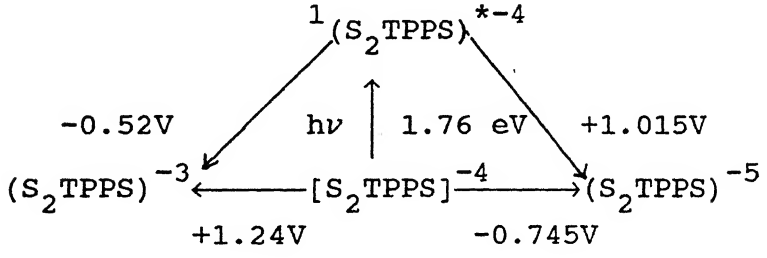

4.3.7 Photoexcited Triplet ESR Studies on Water-Soluble thiaporphyrins

Results and Discussions:

A comparison of low-temperature (100K) ESR of photoexcited triplets of STPPS and S_2TPPS in H_2O : glycerol is shown in Fig.4.12. The zero field splitting parameters of thiaporphyrins are listed in table 4.6. Both the thiaporphyrins exhibit an electron spin polarized triplet (ESP) state indicating that the triplet sublevels are coupled selectively to the singlet manifold.[113] The observed ESP pattern ea ea ea is essentially the

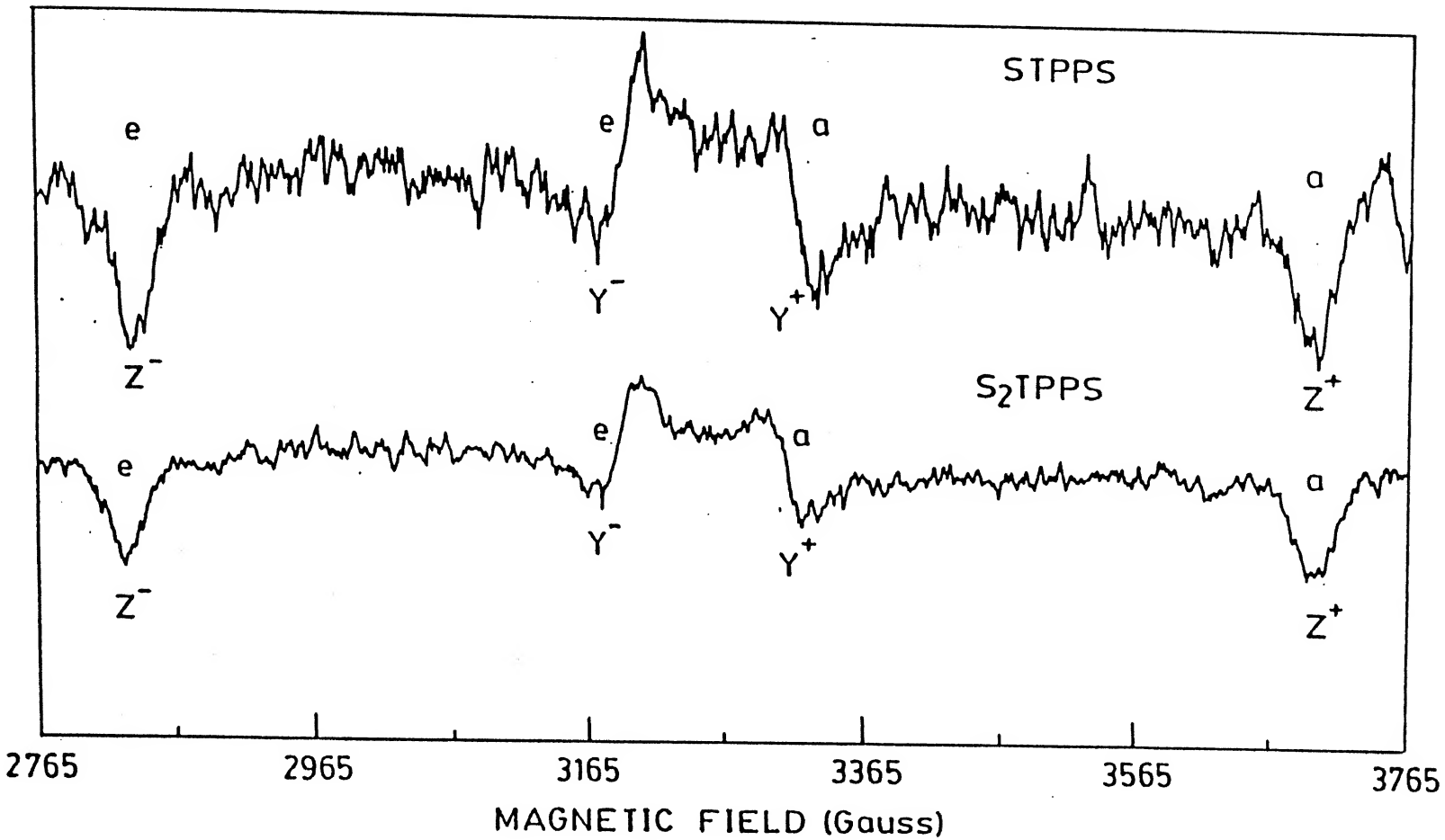

Fig.4.12 ESR spectra of photoexcited triplets of STPPS (~$5x10^{-4}$M), S_2TPPS (~ $5x10^{-4}$M) in water: glycerol (1:1) at about 100K recorded with field and light modulation using CW Argon ion laser. Absorption (a) and emission (e) Peaks have been labelled.

Table 4.6 Zero-field splitting parameters (10^{-4} cm^{-1})[a] of thiaporphyrins

Porphyrin	D	E	X	Y	Z
STPPS	(+)403	(-)96	231	38	-269
$[STPPS]_2$	(+)345	(-)88	203	27	-230
S_2TPPS	(+)405	(-)95	230	40	-270
$[S_2TPPS]_2$	(+)337	--	--	--	-225
H_2TPPS	(+)391	(-)75	205	56	-261
$[H_2TPPS]_2$	(+)334	(-)80	191	31	-223

a : It has been assumed that the out-of-plane ZFS parameter D>0 and the in-plane axes are chosen so that X>Y (estimated uncertainity $\pm 5 \times 10^{-4} cm^{-1}$)

same as found for triplets of H_2TPPS. This signifies that the population and depopulation rates of zero field T_y spin state are larger than those of the other two states (following the convention, the order of energy levels is chosen as $T_x > T_y > T_z$). Furthermore, both a and e lines of each pair have nearly equal intensity suggesting larger deviations from Boltzmann equilibrium at 100K.[116]

The effect of addition of K^+ and 18-crown-6 on the triplets of STPPS and S_2TPPS are shown in Fig.4.13. These spectra were recorded by the pulsed laser excitation method (Chapter 2). It is evident that upon addition of K^+ and 18-crown-6 the original triplet ESR spectrum is replaced by a new spectrum, reflecting a reduction in the value D and E. The addition also leads to a marked reduction in signal amplitude. The triplet spectrum observed for S_2TPPS + 18-crown-6 + K^+ is slightly different from those observed for STPPS + 18-crown-6 + K^+. This probably is due to the presence of a small concentration of higher aggregates in solution.

The triplet spectra from STPPS and S_2TPPS are remarkably similar to that of H_2TPPS with respect to the magnitude of ZFS parameters (table 4.6). In addition, the triplet spectra of STPPS and S_2TPPS are very similar as well (Fig. 4.12). Apparently the introduction of sulfur atoms into the porphyrin core does not alter the triplet characteristics of H_2TPPS. This suggests that neither the structure of the porphyrin core nor the energies of π-molecular orbitals involved in the triplet transitions are altered significantly. It has been pointed out earlier that the porphyrin core in both STPPH[42] and S_2TPP[47] are almost planar (as indicated by X-ray structure) with a small deviation. The

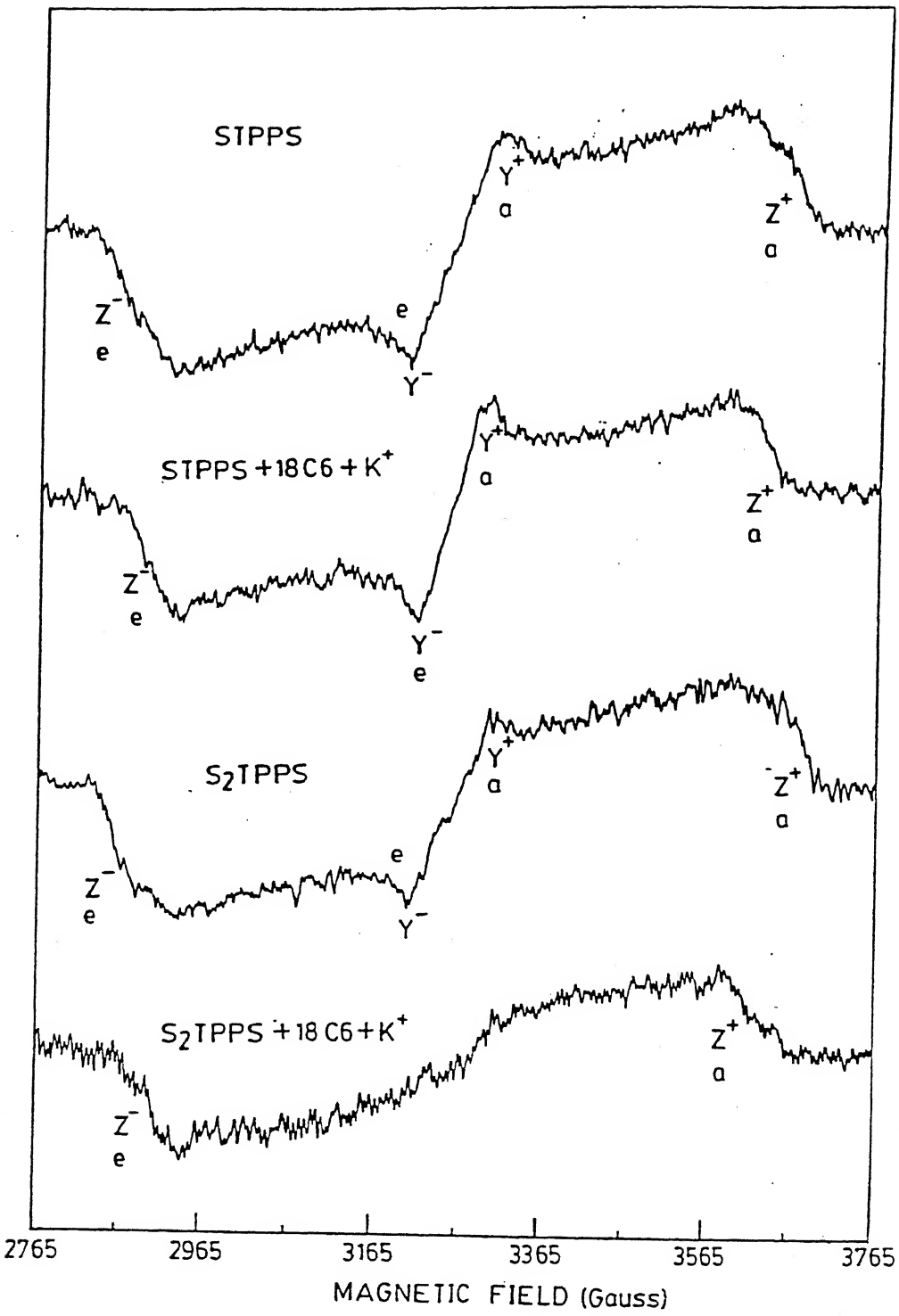

Fig.4.13 ESR spectra of photo excited triplets of monomeric and dimeric STPPS and S_2TPPS in water: Glycerol (1:1) at about 100K recorded with pulsed laser excitation without field modulation (18-crown-6) (0.05 M) and K^+(1.9×10^{-1}M) were added to induce dimerization . ~5×10^{-4}M porphyrin solution was used to record the spectra.

presence of an extra SO_3^- group at the para-phenyl position of water-soluble thiaporphyrins used in the present study is not expected to affect the structure of the porphyrin skeleton significantly.[149,150] Furthermore, MO calculations on S_2TPP[52] indicate the presence of an additional HOMO orbital which is antibonding (p_y) orbital on sulfur atom. Thus the similarities in the structures of the porphyrin cores of H_2TPPS, STPPS, S_2TPPS may explain the similarity in the triplet characteristics.

In the earlier section (4.4.3) it has been shown that both STPPS and S_2TPPS undergo dimerization upon addition of 18-crown-6 and K^+ ions into aqueous solution. The observed reduction in ZFS values upon addition of 18-crown-6 and K^+ can be attributed to the formation of dimers in solution. Earlier studies on H_2TPPS triplets have revealed that dimerization reduces the magnitude of zero field splitting parameters with a change in the triplet kinetics. These data have been used to predict the solution structure of dimers.

The ZFS values of photoexcited triplets of in vivo reaction center of Bacteriochlorophyll a are about 20% smaller than those of in vitro Bacteriochlorophyll a.[151] The reduction has been attributed to the dimerization. As the data in table 4.6 show, dimerization induced changes in D values of the thiaporphyrins triplets are similar to those found for chlorophylls. However, the porphyrin dimers in which the two porphyrin rings are linked together by covalent links do not exhibit such a dimerization effect on ZFS values.[152] Thus, the dimerization effects on the ZFS parameters depends on the relative magnitudes of exchange interaction (J) between the dimer constituents and the ZFS parameters. If $J < D, E$ the triplet excitation energy[75] is

localized (on the time scale of ESR measurement) on one porphyrin ring. The observed reduction in D(14.4% for STPPS, 16.8% S_2TPPS) relative to its corresponding monomer and the fact that the optical absorption bands are shifted to lower energy by several hundred wave numbers [STPPS (335, 454, 293, 513 cm^{-1}), S_2TPPS (336, 505, 126, 452 $cm)^{-1}$] indicate the presence of an appreciable exchange interaction and thus this mechanism is unlikely in the present case. On the other hand if J >> D, a charge transfer to form a radical pair (P_1^-. P_2^+) is expected to change the sign of the D value and to produce a large reduction in the absolute values of ZFS parameters.[75] The values in table 4.6 rule out this possibility. Thirdly, if J ≥ D, a rapid transfer of triplet energy between the dimer constituents (exciton formalism) would affect ZFS parameters only if the ZFS tensor axes of the dimer constituents are not collinear. The values of principal components of the ZFS tensor for the monomer and dimer triplets of thiaporphyrin are given in table 4.6. It is apparent that ZFS tensor of the dimer constituents are not collinear and to account for the observed dimerization induced changes in ZFS parameters, the planes of the two porphyrin rings have to be rotated with respect to each other by some angle θ. It is noteworthy to point out that the exciton model has been used earlier to fit the data for H_2TPPS dimerization.[149,150] However, it has been pointed out that this interpretation may be too simplistic since there could be a significant charge transfer contribution. Thus it is concluded that the exciton model with some contribution from charge transfer can account for the observed dimerization induced changes in the ZFS parameters for the thiaporphyrins.

4.4.0 Conclusions

The traditional "H_2SO_4 method" for sulfonation of meso aryl porphyrins posed many problems such as: (i) harsh reaction conditions, (ii) larger reaction times (~ 48 hours), (iii) probability of formation of di- and trisulfonated products and their difficult separation and (iv) low yield. The chlorosulfonic acid method used in the present study eliminates most of these problems and offers a milder method of sulfonation of variety of porphyrins.

The analysis of the absorption, ^1H NMR, fluorescence, triplet ESR spectral data reveal that many similarities and differences exist between the normal H_2TPPS and its thia analogues. It has been shown that similarities exist between the free base derivatives with respect to dimerization, absorption and emission, characteristics and redox behaviour. Many differences exist between the Cu^{2+} and Ni^{2+} derivatives of STPPS and H_2TPPS in magnetic properties and electrochemical behaviour. In fact the Cu^{2+} and Ni^{2+} derivatives of STPPS shown characteristics of N-substituted metalloporphyrins.[133,134] This clearly suggests that the differences observed in magnetic and electrochemical properties are due to the change in the structure of the metalloporphyrin core rather than change in the electronic structure of the ring.

The similarities in the triplet state characteristics of water soluble thiaporphyrins with respect to zero field splitting parameters and ESP pattern both in monomeric and dimeric state with H_2TPPS is rather surprising.

CHAPTER 5

SYNTHESIS, CHARACTERIZATION, ELECTROCHEMISTRY AND PHOTOPHYSICAL PROPERTIES OF NOVEL DIPORPHYRIN CONTAINING N_4 AND N_3S CORES

5.1.0 Introduction

Chlorophyll and related pigment molecules serve several important functions in the photosynthetic process. Photosynthesis is a process by which light energy is converted via a separation of charge into chemical potential. The potential thus created is used in green plants to reduce CO_2 to sugars. These organisms have two photosystems and it has proven difficult to separate the components of such a system for study. A simpler arrangement can be found in photosynthetic bacteria such as RHODOSPIRILLIUM which have only one photosystem.[153,154] This single photosystem can be divided into two main sections, namely, the light harvesting complex and the reaction center complex. The harvesting complex (P_{870}) present in Bacteriochlorophyll (BChl) is serving to absorb light energy and transfers it to the reaction center. The excitation energy transferred to the reaction center serves to excite the primary donor, p_{870} to the first excited singlet state. p_{870} is believed to consist of a dimer of BChl and is generally called as "special Pair".[155] The excited singlet of primary donor p^*_{870} donates an electron to a molecule of bacteriopheophytin (BPh) which is simply a demetallated BChl. It

is believed that special electronic properties resulting from the excitonic interactions within this dimer contribute to its important role in the charge separation processes. ESR studies of P^{+}_{870} show that P_{870} ESR signal is reduced from that given by isolated monomeric $BChl^{+}$ by a factor $\frac{1}{\sqrt{2}}$ which is indicative of a dimer.[155] Photo excited triplet of P_{870} has zero field splitting parameter 20% smaller than that are in vitro BChl triplet.[156] In vivo BChl has absorption peaks that are 30 nm red shifted with respect to vitro BChl.[157,158,160] These experimental results are in accord with "special pair" model. Thus it is necessary for setting model system which can do photosynthetic energy conversion and from that we can understand the effects of dimeric formation and excitonic interactions on the electronic properties of porphyrin complexes.

Many dimeric porphyrins are synthesised and characterized as models to photosynthetic electron transfer. Dimers can be classified into (a) cofacial dimers of chlorophyll and porphyrins with a fixed geometry, (b) singly covalently linked dimers. These dimers are often rather flexible so that the porphyrin ring can assume a wide range of relative orientations. The synthetic analogue of special pair have two important criteria: (i) an energetically lower S_1 and (ii) a lower one electron oxidation potential.

Electron or energy transfer in a covalently linked dimer ($M-H_2$) can be determined using the free energy changes. The change in free energy values can be calculated from the redox potential data and the excited state energy levels.

One of the proof for energy transfer directly comes from fluorescence spectroscopy. The emission spectroscopy of the mixed dimer [$M-H_2$] is dramatically different from the superposition of the spectra of its constitutive parts. If the singlet state of the metal containing porphyrin is completely quenched whereas emission spectrum corresponding to the non-metallated part is strongly enhanced. This shows that the efficient energy transfer has occurred between the metal porphyrin part (singlet energy donor) and non-metallated subunit (singlet energy acceptor).

In 1970, Birks and coworkers[160] studied the singlet-singlet energy transfer between non-conjugated but covalently linked aromatic chromophores. In 1972 Schwartz and coworkers[161a] demonstrated energy transfer between covalently linked metalloporphyrins. However, the singlet-singlet energy transfer was not observed in this work. In 1978, Govindjee and coworkers[161b] synthesised three covalently-linked hybrid dimers, each containing a metallotetraaryl porphyrin Zn(II),Cu(II) or Ni(II) and a free base tetraaryl porphyrin. Transfer of singlet excitation energy from the metalloporphyrin center to free base porphyrin center was determined by fluorescence measurements. In

this work, zinc hybrid dimer displayed excellent intra molecular transfer of energy (≥ 85%) from the excited singlet state of Zn(II) chromophore to the free base chromophore. No evidence for such transfer of the excited singlet energy was found in the Ni(II) or Cu(II) analogues.

In 1984, Momenteau and coworkers[162] synthesised three covalently linked and "face to face" hybrid zinc and copper bisporphyrins. The excited state life time of these dimers were measured and compared. Their decays are explained by a triplet energy transfer mechanism through an exchange coupling.

In 1984 Benthem et al[163] synthesised mixed metallo-free base TPP dimers linked by a single chain, attached to various positions of the phenyl groups of each porphyrin (ortho-ortho, ortho-para, para-para). They have analysed the singlet-singlet energy transfer between the zinc-containing and free base moieties in TPP dimers by emission spectroscopy and fluorescence kinetics. In this they measured the quantum efficiency for energy transfer (ϕ_{Et}) from the intensities of ZnTPP fluorescence at 613 nm and free base fluorescence at 650 nm of the dimer as compared to a mixture 1:1 of $TPPH_2$ and ZnTPP monomers, when exciting with 431 nm light. The quantum efficiency for energy transfer is given by

$$\phi_{Et} = 1 - \frac{I^{d}(Zn)\ \ I^{m}(H_2)}{I^{m}(Zn)\ \ I^{d}(H_2)}$$

where d stands for the dimer and m for the monomers in the mixture. From this, they calculated rate constant for energy transfer (K_{Et})

$$K_{Et} = \frac{K_f \phi_{Et}}{\phi_f(1-\phi_{Et})}$$

K_f is calculated from experimental life time. ϕ_f is the donor fluorescence quantum yield. The values of ϕ_{Et} and K_{Et} reveals that the energy transfer rate constant is dependent on $<r^{-6}>$ as well as on the relative orientation of the transition dipole moment. The o,p dimer energy transfer rate constant is lower compared to p,p-dimers due to perpendicular position of both porphyrin in o.p-dimer.

In 1986 Harriman and coworkers[164] synthesised a series of covalently linked Zn-H_2 tetraphenyl porphyrin dimers. The linkage consists of a flexible chain of variable length ($-(CH_2)_n-$, n=1-6). The fluorescence spectroscopy shows that ZnTPP unit. transfers singlet state excitation energy to $TPPH_2$. As the length of the alkoxy chain is decreased, the energy transfer is efficient. In the alkoxy chain (n = 2) they observed the maximum singlet energy tranfer from ZnTPP to $TPPH_2$.

In 1989,J.P Sauvage and coworkers[165] synthesised 1,10-phenanthraline covalently linked hybrid dimers each containing zinc tetraphenylporphyrin and a free base tetraaryl

porphyrin. Using the electrochemical and emission data, they proved that efficient singlet energy transfer from zinc porphyrin unit (singlet energy donor) to the free base porphyrin unit.

It is clear from the above survey of literature on TPP type dimers that the dimers studied so for are confined to two porphyrin units having similar cores. The results presented in the earlier chapter clearly indicate that the substitution of nitrogen by sulfur(s) affects the energy levels of the porphyrins and thus affecting the light absorption characteristics. Thus we thought then of an assembly containing a core modified thiaporphyrin and a normal porphyrin can offer an unique diporphyrin with N_4 and N_3S cores. Because the two cores are different it is expected to show some unusual electronic structure. Specifically,metallation of normal porphyrin with Ni^{+2} yields a square planar nickel porphyrin while introduction of Ni^{+2} to thiaporphyrin unit results in the formation of distorted square pyramid nickel with axial chloride. Thus even though the metal is same, the electronic environments around the metal are different in the diporphyrin due to the differing cores of the diporphyrin (Fig. 5.1). Thus in this chapter we have synthesised and studied various diporphyrin containing metals like Zn^{+2}, Cu^{+2} and Ni^{+2} in the porphyrin cavity. It has been shown that the same metal ion can be stabilized in two different oxidation states atleast electrochemically. Thus Ni(II)-Ni(I) and Cu(II)-Cu(I)

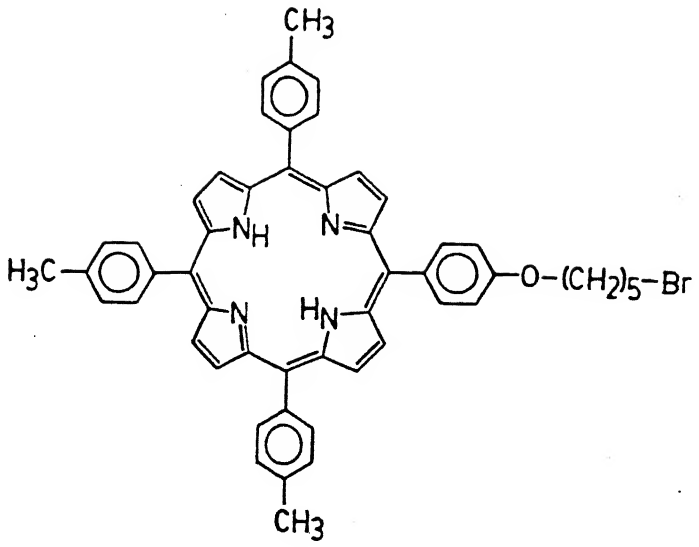

1

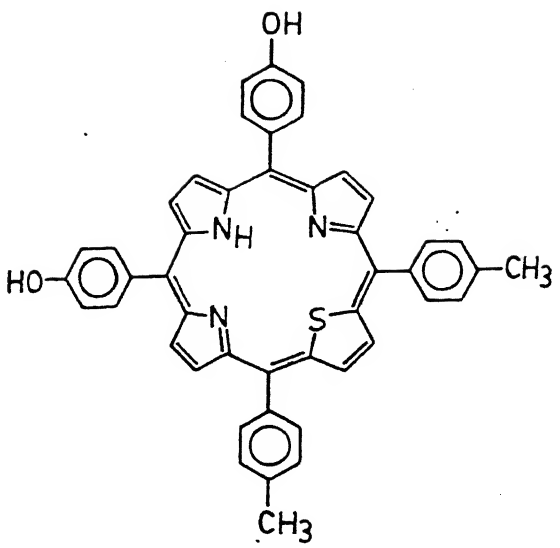

2

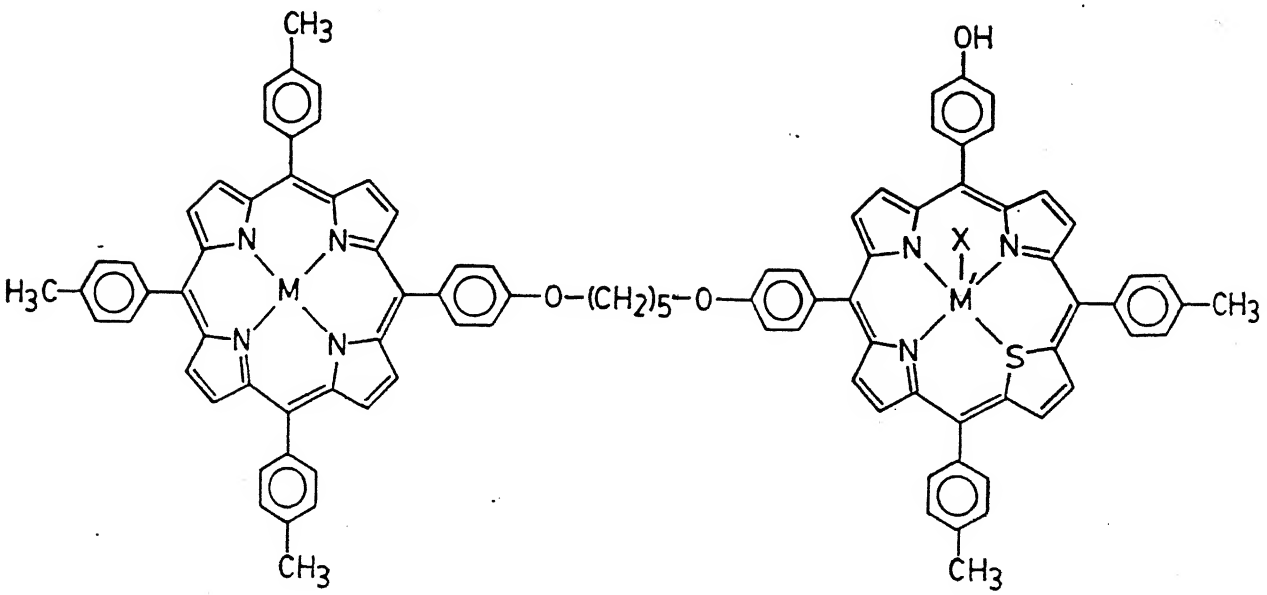

M = 2H ; M′ = H ; H_2 - H Diporphyrin 3

M = Zn^{+2} ; M′ = H ; Zn - H Diporphyrin 4

M = Zn^{+2} ; M′ = Cu^{+2} ; X=Cl ; Zn-Cu Diporphyrin 5

M = Ni^{+2} ; M = Ni^{+2} ; X=Cl ; Ni-Ni Diporphyrin 6

Fig.5.1 Molecular structure of various porphyrin derivatives.

diporphyrins have been characterized using this unique diporphyrin containing heterocores. The emission properties indicate that the two porphyrin units behave independent of each other showing characteristics of individual monomers.

5.2.0 Experimental

The synthesis and purification of compound 1 is described in Chapter 2.

5.2.1 Synthesis of Compound 2

Difunctional tetraaryl monothiaporphyrins were synthesised using the mixed aldehyde approach described by Little et al.[73]

A mixture of two equivalents of P-hydroxy benzaldehyde (6.7848 g,0.0555 mol) and one equivalent of 2,5-bis (p-tolyl hydroxy methyl) thiophene (9 g, 0.02777 mol) and three equivalents of pyrrole (5.583 g, 0.0833 mol) were dissolved in freshly distilled propionic acid (1000 cm^3). The reaction mixture was refluxed for $1\frac{1}{4}$ hours and was left for over night at room temperature. The solvent propionic acid was completely removed under reduced pressure. The black residue obtained was washed several times with hot water and was kept in oven at 100^oC for an hour. Then the crude product was dissolved in $CHCl_3$ and filtered. The crude product was purified by column chromatography over silica gel using $CHCl_3$ as the eluent. The first yellow fraction

obtained was identified as $(CH_3)_4S_2TPP$. Elution with a mixture of chloroform and methanol (100 : 2 V/V) produced a yellow-brown band identified as compound 2. Elution and removal of the solvent afforded compound 2 (0.777 g)in 4.03% yield.

5.2.2 Synthesis of H_2-H Diporphyrin (Compound 3)

A mixture of compound 1 (0.150 g, 0.1824 mmol), compound 2 (0.4032 g,0.585 mmol) and 2.0 g of anhydrous K_2CO_3 were stirred in 30 cm^3 of dry DMF for two weeks at room temperature. The DMF was removed under reduced pressure. The residual solid was washed thoroughly with hot water and dried. It was dissolved in $CHCl_3$ and chromatographed on a silica gel column. The unreacted compound (1) was eluted with $CHCl_3$ as the first (pink) fraction. Further elution with a mixture of $CHCl_3$ and methanol (100: 0.5 V/V) produced yellow pink fraction compound 3 (H_2.H diporphyrin) that was recovered as a solid after evaporation of solvent under vacuum. It was again chromatographed over silica gel column. The compound 3 (H_2-H diporphyrin) (0.071 g) was obtained in 27% yield.

5.2.3 Synthesis of Zn-H Diporphyrin (Compound 4)

Selective metallation of 'normal' porphyrin subunit in compound 3 was achieved as follows.

A solution of 50 mg of zinc acetate in 25 cm^3 of methanol was added to a solution of 30 mg (0.021 mmol) of compound 3 in 125 cm^3

of chloroform. The solution was heated under reflux for 2 hours. It was cooled and then the solvent was removed under reduced pressure. The residue was dissolved in chloroform and washed several times with water. It was dried over anhydrous Na_2SO_4. Then it was chromatographed over silica gel column using mixture of chloroform and methanol (100 : 1 V/V) as a eluent. The yellowish pink fraction (compound 4, Zn-H) recovered as a solid after evaporation of solvent under vacuum. It was twice chromatographed over silica gel column. The compound 4 (0.027 g) obtained in 86% yield.

5.2.4 Synthesis of Zn-Cu Diporphyrin (Compound 5)

A solution of $CuCl_2.2H_2O$ (50 mg, 0.3 mmol) in 20 cm^3 of methanol was added to a solution of compound 4 (0.030 g, 0.021 mmol) in 60 cm^3 of chloroform and then refluxed for 6 hours. It was cooled and then the solvent was removed under reduced pressure. It was dissolved in chloroform and washed several times with water. It was dried over anhydrous Na_2SO_4. Then it was chromatographed over silica gel column using mixture of chloroform :methanol (100 : 1 V/V) as a eluent to get unreacted compound 4. The second greenish pink fraction (compound 5, Zn-Cu) (chloroform: methanol 100:5 V/V) recovered as a solid after evaporation of solvent under vacuum. It was twice chromatographed over silica gel column. The compound 5 (0.023 g) obtained in 70% yield.

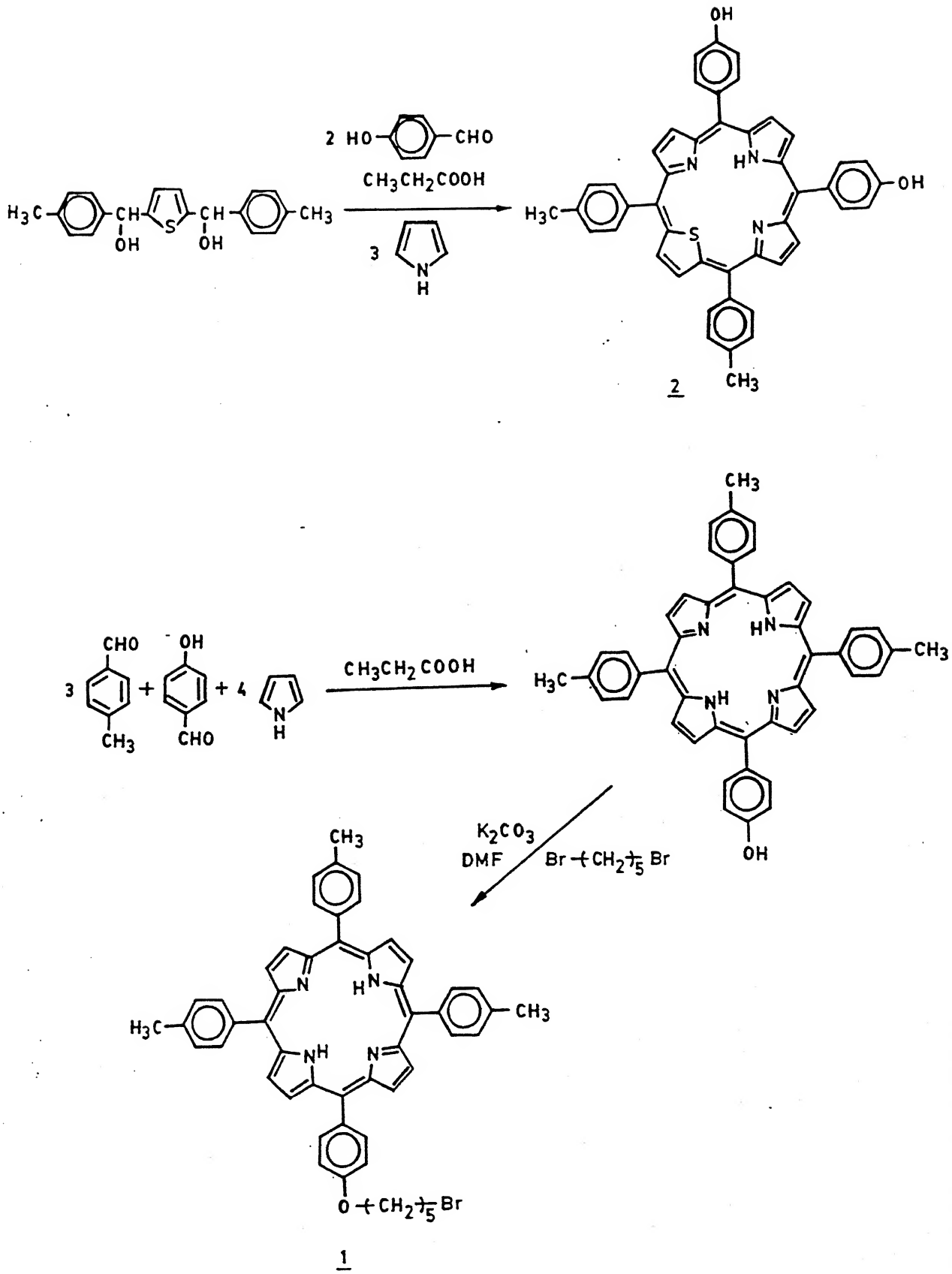

Fig.5.2 Synthetic scheme for compounds 1 and 2.

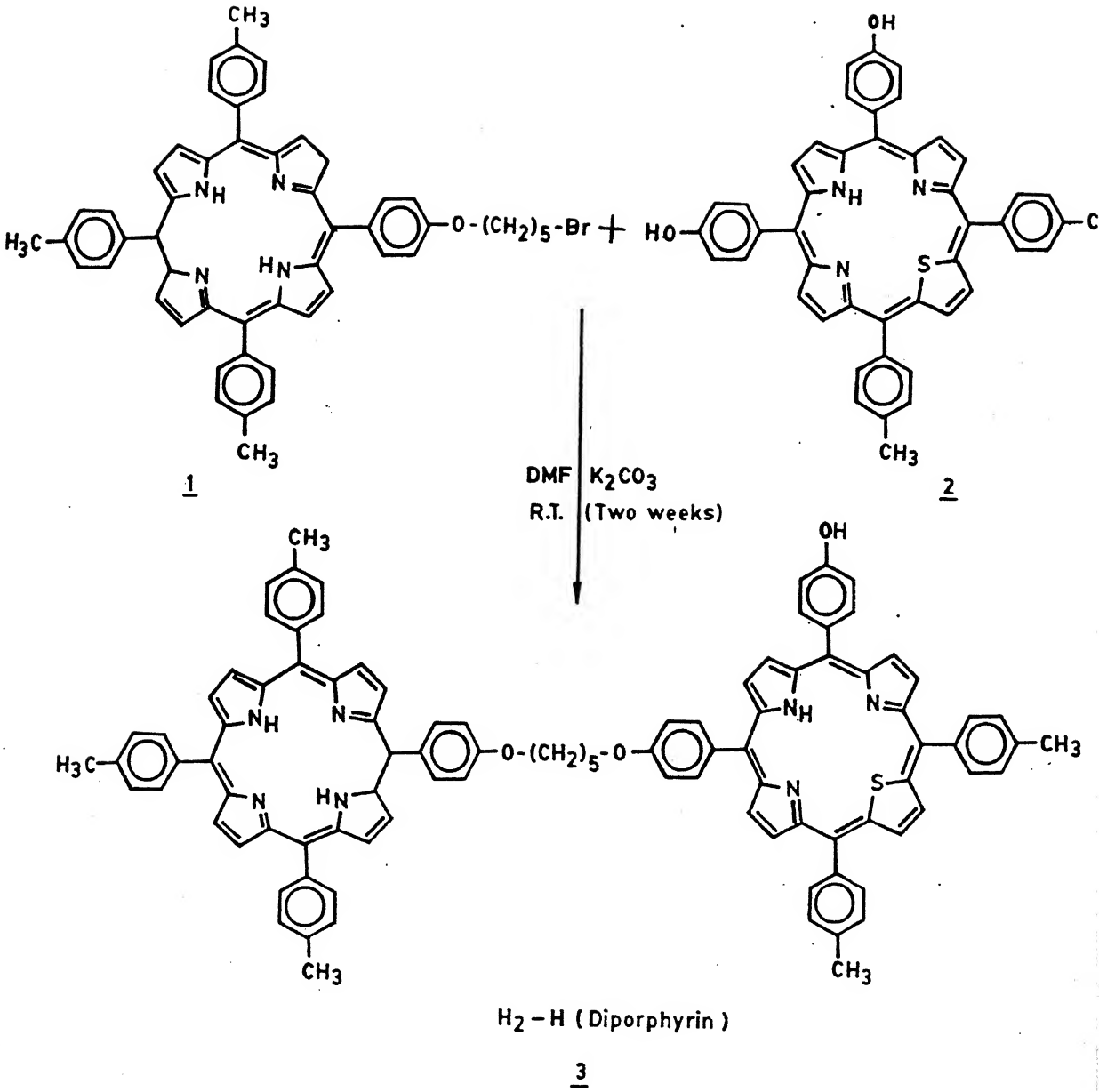

Fig.5.3 Synthetic scheme for diporphyrin containing N_4 and N_3S cores compound 3 (H_2-H diporphyrin)

5.2.5 Synthesis of (Ni-Ni dimer) (Compound 6)

A solution of $NiCl_2.6H_2O$ (125 mg) in 50 cm^3 of methanol was added to a solution of compound 3 (20 mg) in 125 cm^3 of chloroform and then refluxed for 24 hours. It was cooled to room temperature. The solvents were evaporated under reduced pressure. Then it was dissolved in 50 cm^3 of $CHCl_3$ and washed several times with water and dried over anhydrous Na_2SO_4. The solvent $CHCl_3$ was evaporated to 15 cm^3 and chromatographed over silica gel column. The column eluted with $CHCl_3$: MeOH (99 : 1 V/V) gave the compound 3 followed by Ni-H diporphyrin. Then it was eluted with $CHCl_3$: MeOH (92 : 8 V/V) to give the required compound 6 (8.8 mg). It was recovered as solid after vacuum evaporation. It was again chromatographed over silica gel column. Yield 35%.

5.3.0 Results and Discussion

Synthetic scheme for compound 1 and 2 are shown in Fig.5.2 and synthetic scheme for compound 3 (H_2-H diporphyrin) is shown in Fig. 5.3.

5.3.1 ^1H NMR Spectra

The ^1H NMR spectroscopy has been used to identify the monomeric and dimeric porphyrins. Fig. 5.4 and 5.5 give the ^1H NMR spectra of compounds 2 and 3 in $CDCl_3$ and the corresponding

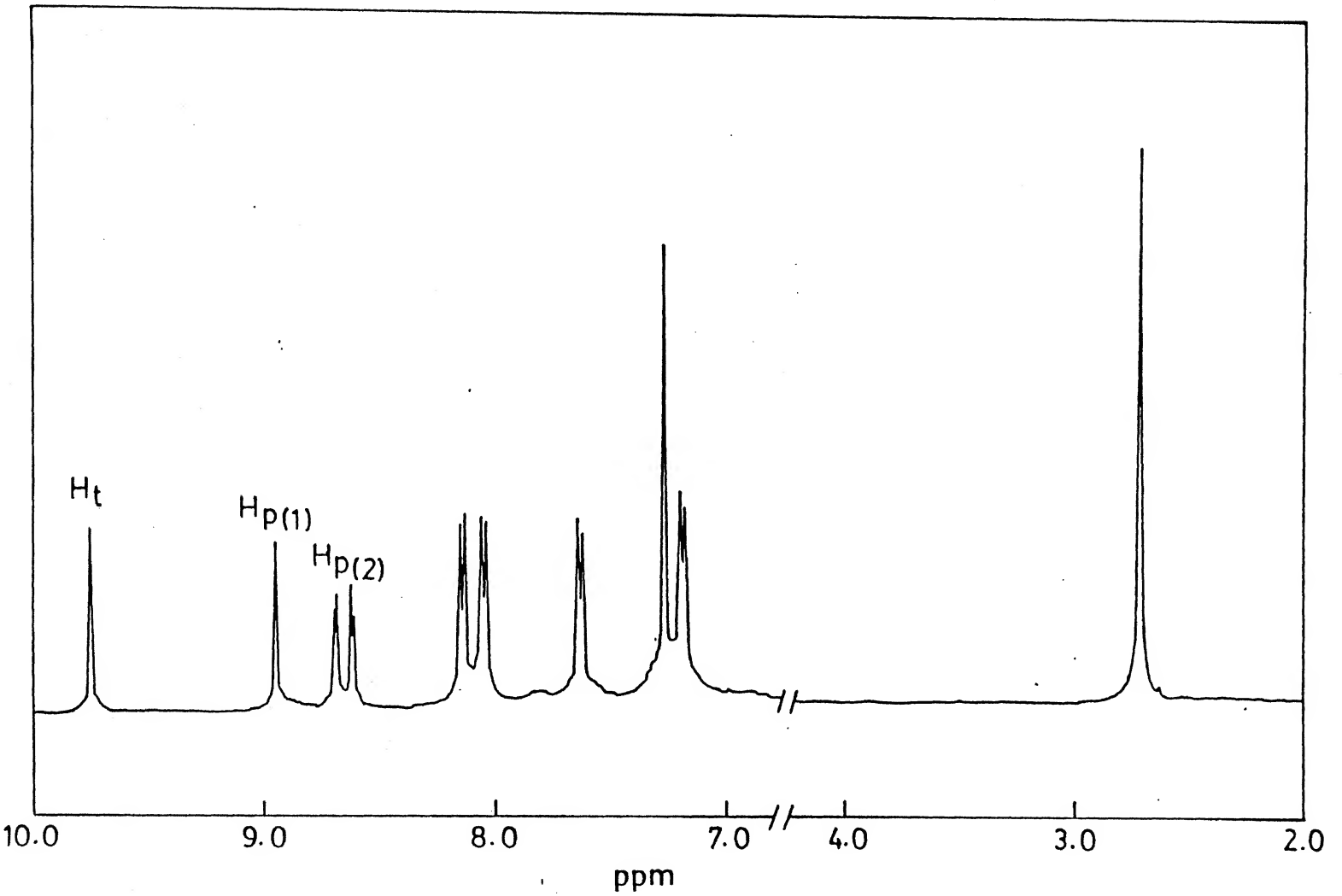

Fig.5.4 ^{1}H NMR spectrum of compound 2 in $CDCl_3$

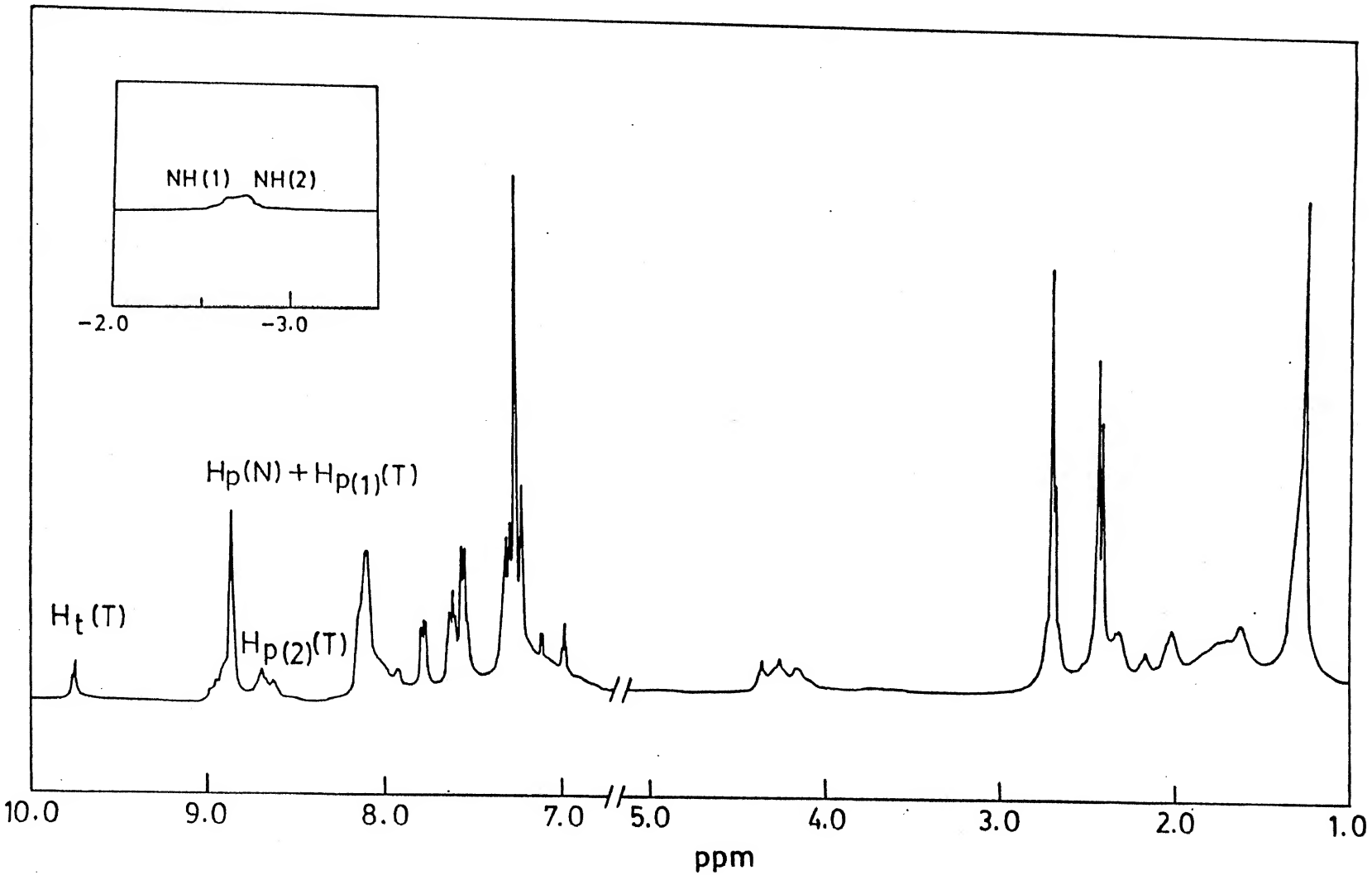

Fig.5.5 ^{1}H NMR spectrum of compound 3 (H_2-H diporphyrin) in $CDCl_3$.

Table 5.1 Chemical shift (ppm) values of monomer and diporphyrins of thiaporphyrins in $CDCl_3$

Porphyrin	Thiophene	Pyrrole	Phenyl protons		$-O-CH_2$	$-CH_2Br$	p-CH_3	$-(CH_2)_3-$
			ortho	meta				
Compound 1	-	8.75(s)	8.11(d)	7.55(d) 7.22(d)	4.20(t)	3.5(t)	2.65(s)	1.43(m)
Compound 2	9.75(s)	8.94(s) 8.65(q)	8.14(d) 8.05(d)	7.62(d) 7.18(d)	-	-	2.7(s)	-
Compound 3	9.75(s)	8.85(s) 8.67(q)	8.11 -	6.98(m)	4.21	-	2.7(s) 2.68(s) 2.44(s) 2.42(s)	1.5(m)
Compound 4	9.71(s)	8.96(s) 8.67(q)	8.18 -	6.98(m)	4.16(m)	-	2.71(s) 2.69(s) 2.45(s) 2.43(s)	1.54(m)

data of all the monomeric and dimeric porphyrins are tabulated in table 5.1. Because of the introduction of the thiophene group the symmetry of the monothiaporphyrin (compound 2) is reduced and this is clearly reflected in the ^1H NMR spectra. Specifically, the pyrrole protons have became inequivalent showing two sets of resonances at 8.94 ppm (singlet, two protons) ($H_{p(1)}$) and at 8.65 ppm (quartet, four protons) $H_{p(2)}$. The two thiophene protons (H_t) are equivalent and resonate as a singlet at 9.75 ppm. The mesophenyl groups have different substituents (-OH, $-CH_3$) at p-positions. This results in inequivalence of phenyl protons and thus ortho and meta protons resonate as a four sets of closely spaced doublets in the region 8.05 to 7.18 ppm. The p-methyl substituent is seen as a singlet at 2.7 ppm. Thus the different substituents at the p-phenyl positions are clearly reflected in the proton NMR spectrum (Fig. 5.4).

The normal tetraphenyl porphyrin unit of the diporphyrin (compound 1) shows a sharp singlet at 8.75 ppm assigned to eight pyrrole protons. The ortho and meta meso phenyl protons appear as doublets at 8.11, 7.55 and 7.22 ppm respectively. The alkoxy chain at the p-phenyl positions appears as two triplets at 4.20 and 3.5 ppm assigned to $-OCH_2$ and $-CH_2Br$ terminal groups respectively. While the middle $-(CH_2)_3-$ group appears as a multiplet at 1.43 ppm. The p-methyl substituent resonates as a singlet at 2.65 ppm.

The ^1H NMR spectra of the dimeric H_2-H diporphyrin (compound 3) obviously should consist of signals attributable to both compound 1 and 2 with the linking groups. Thus one would expect a singlet for two thiophene protons and the peak at 9.75 ppm in Fig.5.5 is assigned to two thiophene protons of thiaporphyrin subunit. The comparison of the chemical shift of these protons with the same protons in the monomer (compound 2) indicate very little interaction between two porphyrins subunits in the diporphyrin.

The pyrrole protons are assigned as follows: there are fourteen pyrrole protons,eight belonging to normal porphyrin subunit and six belonging to thiaporphyrin subunit. The eight protons of normal porphyrin unit is expected to resonate as a singlet while the six protons of the thiaporphyrin subunit should show two resonances (a set of two protons (singlet) and a set of four protons (quartet). This is based on the spectrum observed for the two monomers taken independently. The spectrum shown in Fig. 5.5 shows two sets of pyrrole resonances at 8.85 ppm (singlet) ($H_{(p)}(N) + H_{p(1)}(T)$) and 8.67 ($H_{p(2)}(T)$) ppm (quartet). An analysis of the peak intensity indicate ten protons to the singlet at 8.85 ppm while the four protons to the signal at 8.67 ppm. Obviously the eight pyrrole protons of normal porphyrin subunit and two pyrrole protons of thiaporphyrin subunit are

merged and the singlet at 8.85 ppm (Fig. 5.5) is assigned to these protons. The quartet observed at 8.67 ppm corresponds to four protons, obviously from the thiaporphyrin pyrrole unit.

The meso phenyl ortho and meta protons appear as a complex multiplet in the region 8.11 - 6.98 ppm and it is difficult to make individual assignments without the specific deuteration experiments. No attempts were made in this direction. The linking pentoxy chain protons appear as two multiplets at 4.21 and 1.50 ppm. The multiplet at 4.21 is assigned to $-OCH_2$ protons based on the electronegativity and closeness to the porphyrin π-system while the multiplet at 1.50 ppm is assigned to the $-(CH_2)_3-$ units. The $-O-CH_2$ protons are expected to appear as a triplet if both the porphyrin units have similar aromaticity. However, the observed multiplet structure in the diporphyrin indicate the small difference in the aromaticity of the two individual subunits. This is also supported by the appearance of four closely spaced singlets for p-methyl substituents on the meso phenyl groups. The inner NH protons are expected to resonate as two independent singlets, one corresponding to NH protons of normal porphyrin subunit and the other NH proton corresponding to the NH proton of thiaporphyrin subunit. Thus two singlets at -2.63 (NH(1)) and -2.73 (NH(2)) ppm should correspond to these two NH signals.

In order to specifically assign these signals to individual units, the specific metallation of normal porphyrin subunit was

carried out. Thus introduction of Zn^{+2} ion to the normal unit shows disappearance of -2.73 ppm signal while the signal at -2.63 ppm is still observed in the partially metallated diporphyrin. This clearly suggests that the singlet at -2.63 ppm belongs to thiaporphyrin subunit while the singlet at -2.73 ppm belonging to the nomal porphyrin subunit. A comparison of chemical shifts of the various protons in the diporphyrin (H_2-H) (Compound 3) with those of individual monomeric units indicate only minor differences suggesting that the two porphyrin subunit in the dimer interact very weakly. This is consistent with the earlier reports observed for the covalently linked tetraphenyl porphyrin dimers.[163]

Introduction of Zn^{+2} ion to the normal porphyrin subunit in the dimer should not affect the chemical shifts of the pyrrole and thiophene protons of the thiaporphyrin subunit. While pyrrole protons of the normal porphyrin subunit is expected to show a small deshielding effects. This is clearly reflected in the ^1H NMR spectra of Zn-H diporphyrin (compound 4) (table 5.1). Thus the proton NMR spectra clearly support the proposed structure of the diporphyrin in solution.

5.3.2 FAB Mass Spectra

In order to confirm the molecular weight of the synthesised diporphyrin , the FAB mass spectra of individual monomer as well as diporphyrin were recorded. Theoretically calculated molecular

weight for the compound 1,2 and 3 are 821.8, 691.85 and 1432.8, respectively. The observed FAB mass spectra of the compound 1, 2 and 3 peaks m/z at 822, 692 and 1433 clearly indicating the formulated molecular weights.

Zn-Cu diporphyrin was further characterized by EPR spectroscopy. The EPR spectrum at room temperature in 1:1 ($CHCl_3$: toluene) mixture shows nitrogen hyperfine lines with A^N = 16 G and g value is 2.08. These values resemble that of N-methyl substituted Cu(II)porphyrins indicating a distorted geometry around Cu^{+2} ion thiaporphyrin subunit.[69]

5.3.3 Optical Spectra

Fig. 5.6 shows the absorption spectra of H_2-H, Zn-H and Zn-Cu diporphyrins in $CHCl_3$ in the soret and Q bands regions and the absorption data are tabulated in table 5.2. The absorption spectra of H_2-H dimer appears to be simply the sum of the two free base monomers. A comparison of these with a 1:1 mixture of the compound 1 and 2 in $CHCl_3$ indicate only small shifts (1-2 nm) in the λ_{max} values. However, the molar absorption coefficients of the diporphyrins are only about 70-75% of the corresponding bands, probably suggesting a weak interaction between the two chromophores. Literature studies[163] on covalently linked dimer of $TPPH_2$ with varying chain lengths have shown two bands in the soret region. This has been accounted in terms of two conformers,namely,

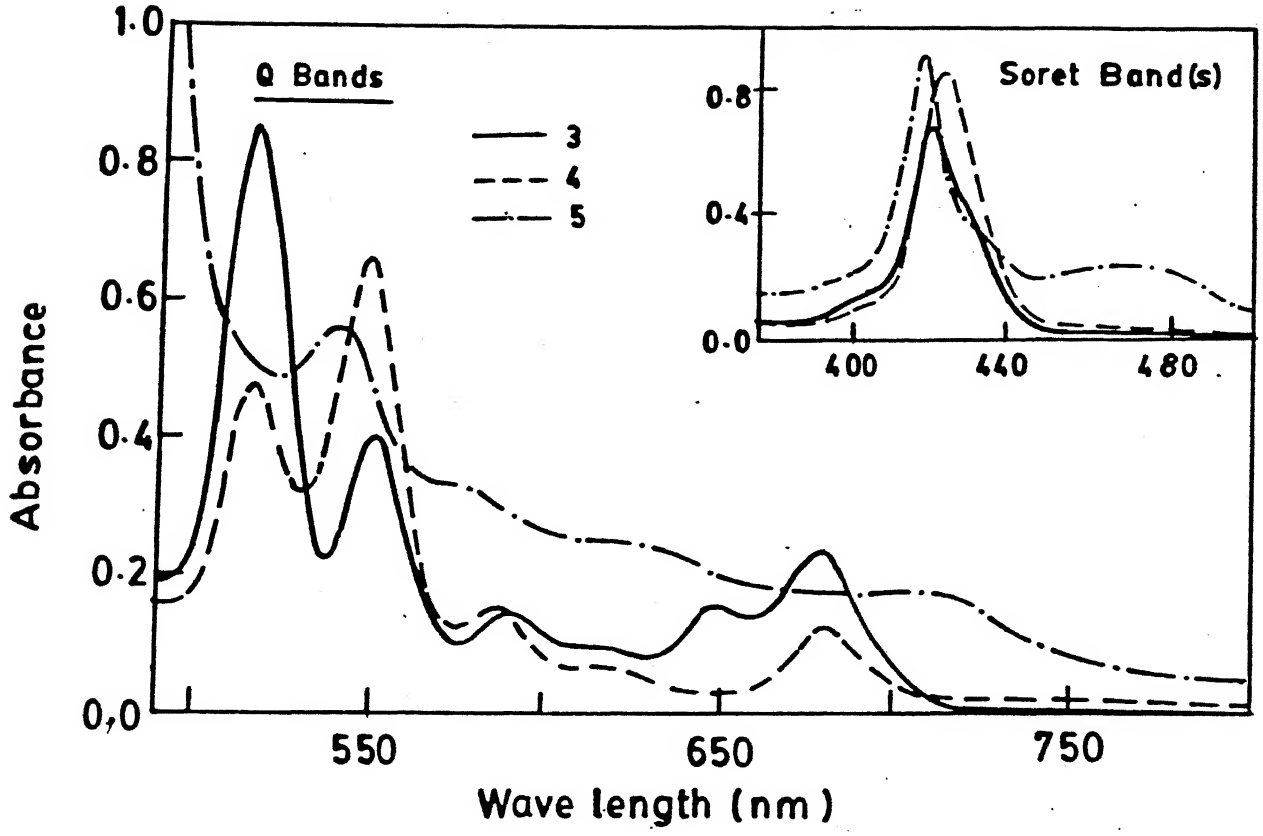

Fig.5.6 Absorption spectra of compounds 3 (———), 4 (- - - -) and 5 (- . - . -) in Q and soret band region in $CHCl_3$ (concentration used $\simeq$ $1x10^{-5}$).

Table 5.2: Absorption spectral data of monomer and diporphyrins of thiaporphyrins

Porphyrin	Soret band(s) (nm) $\varepsilon \times 10^{-4}$	Q bands (nm) $\times \varepsilon \times 10^{-3}$					
		VI	V	IV	III	II	I
Compound 1	420(47.5)	-	-	517(18.71)	553(10.45)	592(5.52)	649(6.22)
Compound 2	430(17.7)	-	-	516(15.24)	551(6.93)	618(3.31)	677(5.23)
Compound 3 (H_2-H)	421(47.89) 430(30.28)	517(31.03)	553(15.07)	591(5.7)	616(3.15)	647(4.98)	680(4.37)
Compound 4 (Zn-H)	423(43.0) 433(24.42)	-	516(16.47)	550(23.56)	587(5.62)	617(2.78)	680(4.54)
Compound 5 (Zn-Cu)	418(5.82) 434(2.08) 469(1.46)	-	540(4.51)	573(2.65)	617(2.04)	675(1.48)	707(1.45)
Compound 6 (Ni-Ni)	419(17.38) 440(6.33) 472(5.26)	-		529(14.57)	558(9.84)	614(4.22)	685(2.74)

"extended and closed conformers".[166] This has been confirmed by recording the spectrum in various solvents of different polarity. However, in the present study no such observations are made ruling out of the existence of two conformers.

Metallation of a porphyrin ring results in collapse of $Q_x(0,0)$ and $Q_y(0,0)$ bands thus showing only two Q bands. Introduction of Zn^{+2} ion to the normal porphyrin in the subunit increases the absorption at ~ 550 nm and 587 nm bands while the other Q bands belonging to the thiaporphyrin subunit remains unaltered in the intensity. Also the peak positions in the diporphyrin match very well with 1:1 mixture of zinc derivative of compound 1 and free base of compound 2, again suggesting a weak interaction between two chromophores. The observation of two well defined Q bands for the zinc porphyrin subunit in the diporphyrin suggests an approximate D_{4h} symmetry around Zn^{+2} ion.

The absorption spectrum of Zn-Cu diporphyrin (Compound 5) is quite revealing. Specifically, the absorption bands belonging to zinc porphyrin part is substantially quenched (table 5.2) with a blue shift of both Q and soret bands of zinc porphyrin subunit. Furthermore the Q band region of the copper thiaporphyrin subunit shows more than two ill defined bands with reduced molar absorption values. The soret bands get splitted into two bands at 434 and 469 nm with substantially quenched molar extinction coefficients relative to Zn-H or H_2-H diporphyrin. This clearly

suggests the distorted geometry around copper thiaporphyrin unit as observed for the monomeric coppermonothiaporphyrin. This change in structure around the copper thiaporphyrin unit induces a change in the zinc porphyrin subunit implying that the two porphyrin subunits interact substantially in the bimetallic diporphyrin. Electrochemical data also support this observation.

The absorption spectrum of Ni-Ni diporphyrin also shows features similar to those observed for Zn-Cu diporphyrin. The absorption data in table 5.2 clearly indicate quenching of intensity of the absorption bands of the Ni^{+2} normal porphyrin subunit with small blue shift absorption bands. The Q bands are of the nickel thiaporphyrin which are broadened and soret bands split again suggesting the reduced symmetry around the nickel thiaporphyrin unit.

5.3.4 Electro Chemistry

The redox chemistry of the various diporphyrins are followed by cyclic voltammetry. Before a discussion on redox reactions of the diporphyrin, the redox reactions of individual monomers are desirable. Fig. 5.7 and Fig. 5.8 give a comparison of the oxidation and reduction processes of individual monomers (compounds 1 and 2). All the cyclic voltammograms were recorded in CH_2Cl_2 using TBAP as the supporting electrolyte unless otherwise

Table 5.3 Redox Potentials[a] (V) of monomer and diporphyrins of thiaporphyri

Porphyrin	Oxidation				Reduction		
	I	II	III	$E_{1/2}(M^{2+}/M^{+})$	I	II	III
Compound 1	0.992 (ir)	1.254 (ir)	-	-	-1.181 (q.r)	-1.59 (ir)	-
Zinc derivative of compound 1	0.735	1.029	-	-	-1.315	-	-
Compound 2	0.93 (ir)	1.376 (ir)	-	-	-1.092 (q.r)	-1.57 (ir)	-
Compound 3 (H_2-H)	0.942 (ir)	1.046 (ir)	1.288 (q.r)	-	-1.10 (ir)	-1.15 (q.r)	-1.57 (q.r)
Compound 4 (Zn-H)	0.735 (q.r)	1.02 (q.r)	1.231 (q.r)	-	-1.1 (q.r)	-1.312	-1.576 (ir)
Compound 5 (Zn-Cu)	0.919	1.173 (q.r)	1.362	-0.0885	-0.854 (ir)	-1.046 (ir)	-
Compound 6 (Ni-Ni)	0.98	1.121 (ir)	1.4 (ir)	-0.280	-0.885 (q.r)	-	-

a Unless indicated otherwise $E_{1/2}$ - values correspond to peak potentials for reversible process; ir - irreversible process; q.r.-quasi reversible

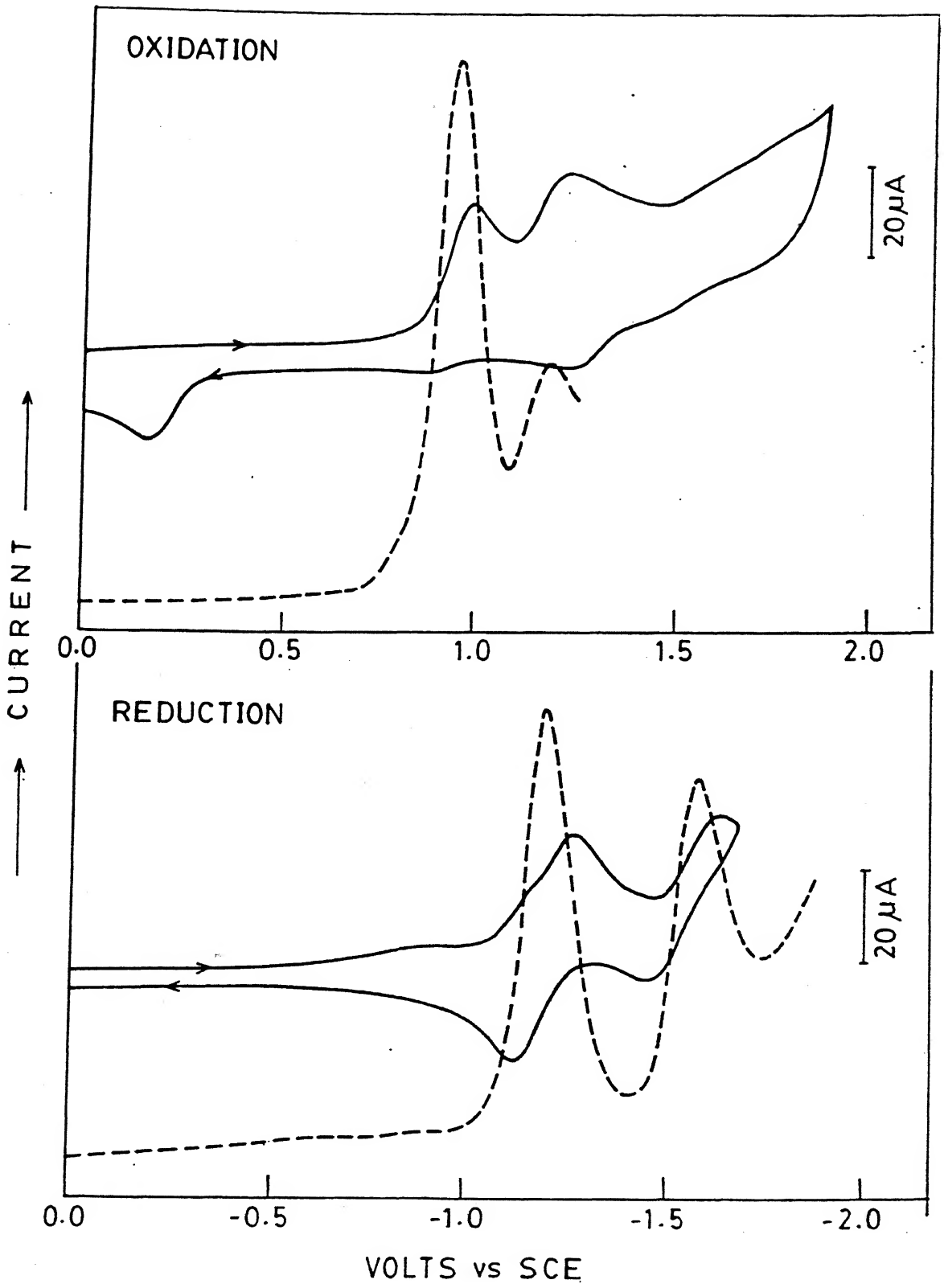

Fig.5.7 The cyclic voltammogram (———) and differential pulse voltammogram (- - -) of compound 1 in CH_2Cl_2. ν = 100 mV/s for cyclic voltammogram and ν = 10 mV/s for differential pulse voltammogram.

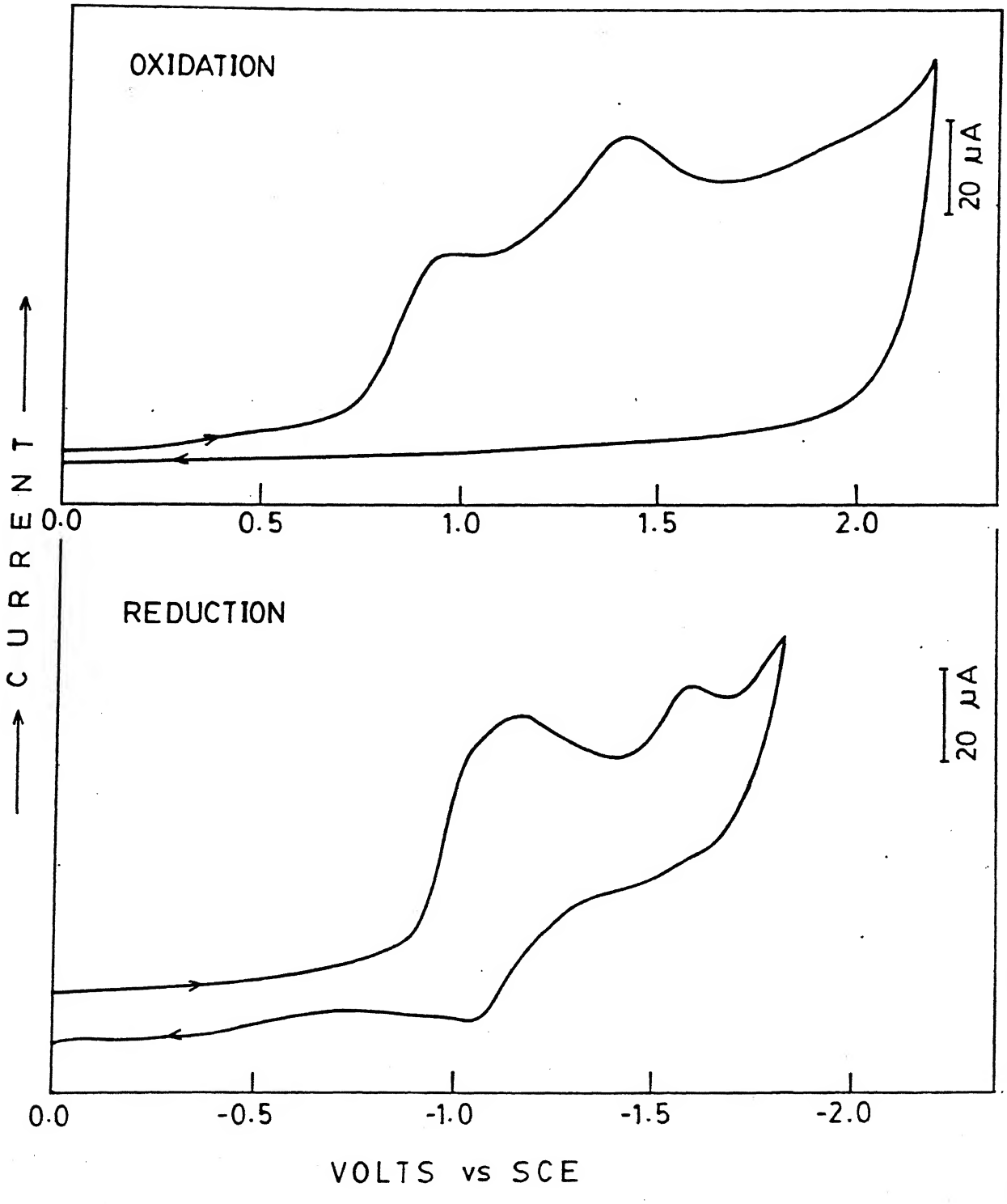

Fig.5.8 Cyclic voltammogram of compound 2 in CH_2Cl_2 and 0.1M TBAP, ν = 100 mV/s.

indicated at a scan rate of 100 mV/s. The voltammogram are not clearly separated, therefore, the differential pulse voltammograms have been recorded for a precise measurement of redox potentials. All the differential pulse voltammograms are recorded at 10 mV/s. The redox potential data of various monomers and diporphyrins are tabulated in table 5.3.

Inspection of the table 5.3 and figures 5.7 and 5.8 indicate that the compound 1 (normal porphyrin) shows two oxidation waves and two reduction waves. The difference between the two oxidation processes lies in the range 0.29 ± 0.05 V which is typical of free base porphyrin[167] ($TPPH_2$). The attachment of alkoxy chain at the p-phenyl position does not seem to have any major effect on the potentials. Upon scanning to negative potential side two separate reductions are observed at -1.181 V and -1.59 V and the difference between these two reduction process are within the range of expected 0.42 ± 0.05 V.[167] These two reductions correspond to the formation of mono and dianions of porphyrin (compound 1) respectively.

Compound 2 (thiaporphyrin monomer) also exhibits two oxidation waves at 0.93 V and 1.376 V respectively. These two oxidation processes are irreversible. The first oxidation is shifted slightly towards less positive values (~ 70 mV) relative to STTPH[70] indicating the effect of substituents (-OH and $-CH_3$) on the phenyl ring. These two oxidations are assigned to the

formation of mono and dications of thiaporphyrin respectively. Reversal of potential direction results in the reduction of the porphyrin ring. Compound 2 also shows two reductions at -1.092 V (quasi reversible, ΔE_p = 92 mV) and -1.57 V (irreversible). A comparison of these potentials with STTPH[70] shows no significant changes in the reduction potential values.

The cyclic voltammogram for the H_2-H diporphyrin (compound 3) is displayed in Fig. 5.9. It is apparent from the figure that there are three oxidation processes at 0.942 V, 1.046 V and 1.288 V. The first two oxidation processes are irreversible while the third oxidation process is quasi reversible (ΔE_p = 100 mV). The oxidation wave at 0.942 V is assigned to the oxidation of the thiaporphyrin subunit based on the fact that this value is close to that observed for the first oxidation of compound 2 (table 5.3). The oxidation waves at 1.046 V and 1.288 V are assigned to the first and second oxidations of normal porphyrin subunit based on the fact that (a) these potentials are more close to that observed first and second oxidation of normal porphyrin monomer (table 5.3) and (b) that the difference in potentials between the oxidation range 0.29 ± 0.05 V.[167] Upon scanning to the negative potentials, the H_2-H diporphyrin shows three reduction processes at -1.10 V, -1.15 V and -1.57 V (Fig.5.9). The first reduction at -1.10 V (seen clearly in differential pulse voltammogram) (Fig.5.9) is assigned to the first reduction of thiaporphyrin

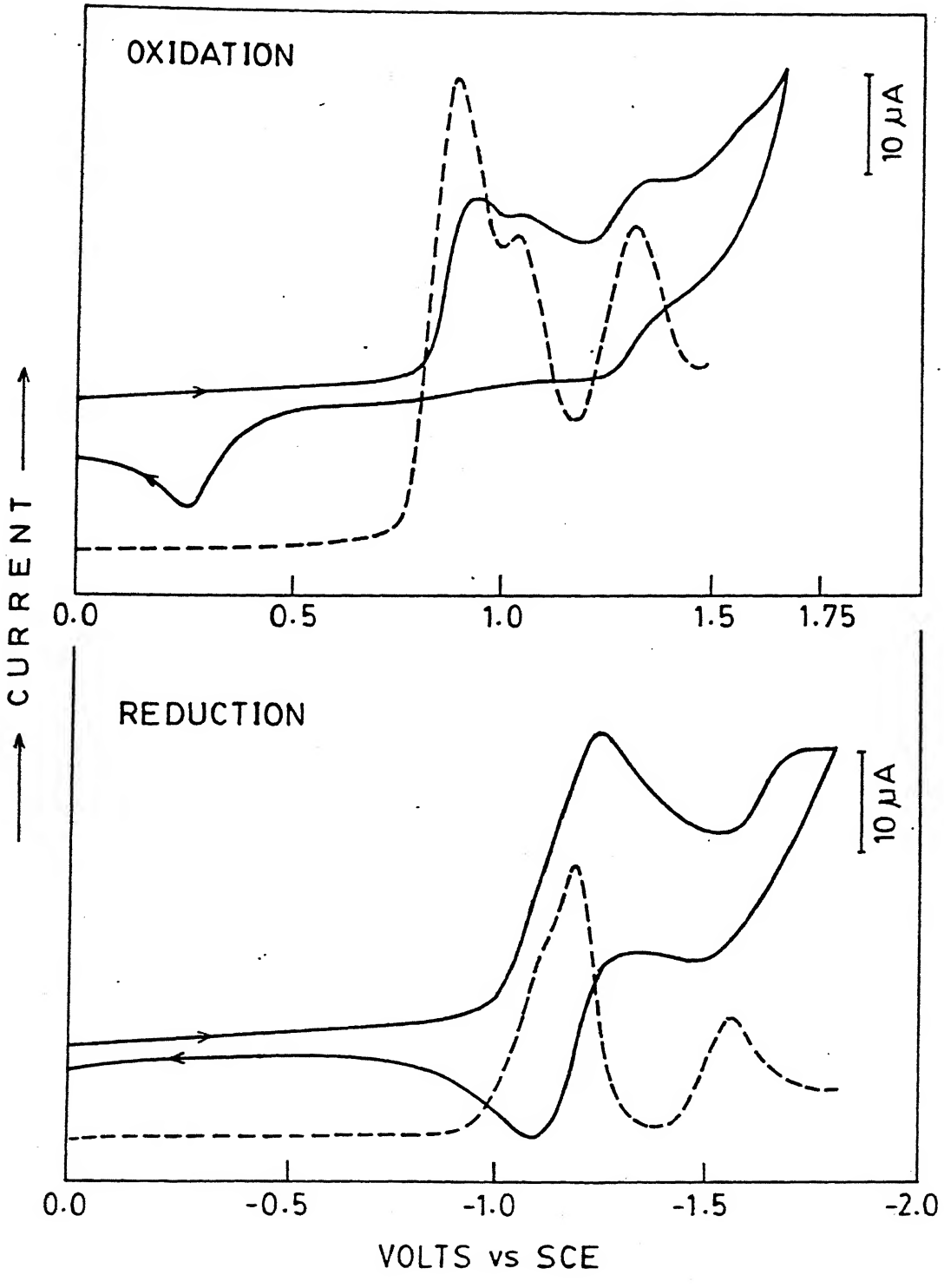

Fig.5.9 Cyclic voltammogram (——) and differential pulse voltammogram (- - - -) of compound 3 in CH_2Cl_2 and 0.1 M TBAP, ν = 100 mV/s for cyclic voltammogram and ν = 10 mV/s differential pulse voltammogram.

subunit based on the fact that thiaporphyrins are easier to reduce relative to normal porphyrins.[70,86] The two reduction waves at -1.15V (ΔE_p = 169 mV) and -1.57 (ΔE_p = 181 mV) are assigned to the first and second reduction of normal porphyrin unit based on the fact that the potential difference between two reductions are in the expected range of 0.42 ± 0.05 V. Thus the redox potentials for the H_2-H diporphyrin (compound 3) indicate very little interaction between two porphyrin subunits as concluded from the ^1H NMR data. A similar conclusion was arrived at by Becker[168] and coworkers on the covalently monolinked zinc porphyrin dimers. They used the saturated carbon chains of various lengths and concluded from the electrochemical studies that the two porphyrin ring in the dimer behave independently with no interaction between them regardless of the length of the hydrocarbon chain joining them together.

Specific metallation (Zn^{+2}) of normal porphyrin subunit results in the formation of Zn-H diporphyrin (compound 4). The cyclic voltammogram of this diporphyrin shown in Fig.5.10 indicate three oxidation waves at 0.735 V, 1.02 V and 1.23 V. All the three oxidations are quasi reversible. The oxidation waves at 0.735 V and 1.02 V correspond to the first and second oxidations of zinc porphyrin subunit. These assignments were confirmed by synthesising Zn^{+2} derivative of compound 1 which also show exhibit two oxidation waves at 0.735 V and 1.029 V in CH_2Cl_2

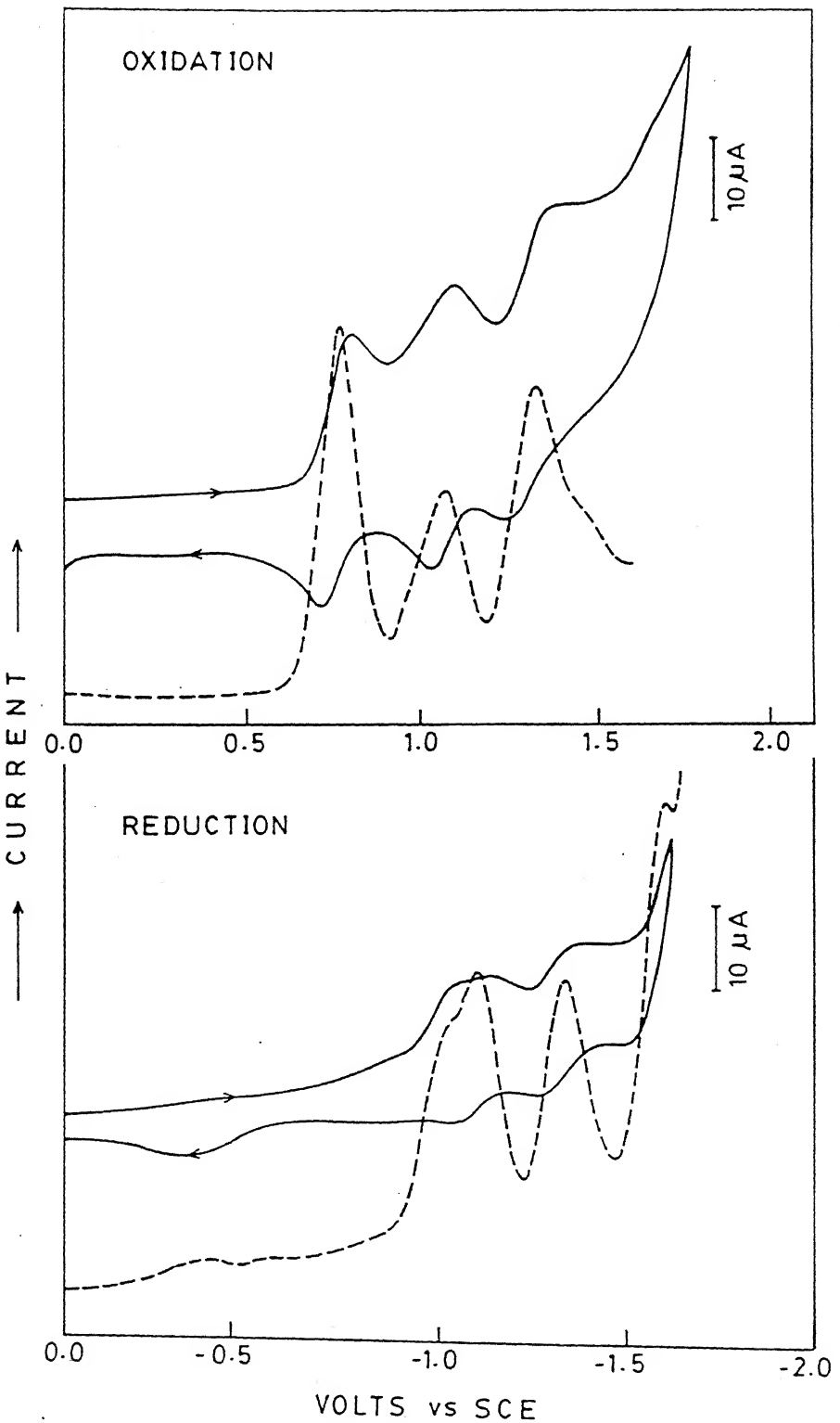

Fig.5.10 Cyclic voltammogram (——) and differential pulse voltammogram (- - -) of compound 4 (Zn-H diporphyrin) in CH_2Cl_2 and 0.1 M TBAP, ν = 100 mV/s for cyclic voltammogram, ν = 10 mV/s for differential pulse voltammogram.

under similar conditions (table 5.3). Furthermore, the difference in potentials between two oxidations also lies in the range 0.29 ± 0.05 V. The oxidation wave at -1.231 V of compound4 (Fig.5.10) is assigned to the first oxidation of thiaporphyrin subunit. This potential is shifted to more +ve value (289 mV) relative to the first oxidation of thiaporphyrin unit in H_2-H diporphyrin (compound 3) indicating harder oxidations upon introduction of Zn^{+2} ion into the normal porphyrin core. This may be probably due to small structural change at the thiaporphyrin pheriphery upon introduction of Zn^{+2} to the normal porphyrin core.

Upon reduction Zn-H diporphyrin (compoud 4) shows three reduction waves at potentials -1.1 V, -1.312 V and -1.576 V. Also there is a ill defined wave (a small shoulder in differential pulse voltammogram) at -1.023 V. This has been attributed to probably small concentration of monomer impurity. The reduction waves at -1.1 V and -1.576 V are assigned to the first and second reduction of thiaporphyrin subunit based on closeness of the potential values to those observed in compound 3 (H_2-H diporphyrin) as well as compound 2. The reduction waves at -1.312 V (reversible reduction) is attributed to the first reduction of zinc porphyrin unit. The zinc derivative of compound 1 also shows this reduction at the same potential.

In order to study a bimetallic diporphyrin, Cu^{+2} ion, was introduced into the thiaporphyrin core by specifically metallating

Zn-H diporphyrin (compound 4). It is known from earlier chapters that the introduction of Cu^{+2} ion into the porphyrin core distorts the geometry around the copper ion due to co-ordination needs of thiophene ring. This structural change is clearly reflected in the cyclic voltammogram of the Zn-Cu diporphyrin (compound 5) shown in Fig. 5.11. It is seen from Figure 5.11 that this exhibits three oxidation waves at 0.919 V (ΔE_p = 69 V), 1.173 V (ΔE_p = 116 mV) and 1.362 V (ΔE_p = 50 mV). The oxidation at 1.173 V is assigned to the oxidation of the copper thiaporphyrin unit based on the fact that this value is similar to that observed for the monomeric copper thiaporphyrin unit.[70] The oxidation waves at 0.919 V and 1.362 V are assiged to the first and second oxidations of zinc porphyrin unit. These two oxidation potentials are shifted to more positive values by 184 mV and 342 mV respectively relative to same oxidations in Zn-H diporphyrin suggesting harder oxidations. This must be attributed to the structural change accompanying the Cu^{+2} insertion. Thus it is seen that in metal diporphyrins (Zn-H and Zn-Cu) the introduction of a metal at one subunit has altered the potential at the other subunit probably suggesting a weak interaction between the two porphyrin centers.

Three reduction waves are seen upon reduction of Zn-Cu dimer at potentials -0.0885 V, -0.854 V and -1.046 V. The first reduction wave is perfectly reversible when scanned separately (Fig.5.11inset) and this potential is completely away from the

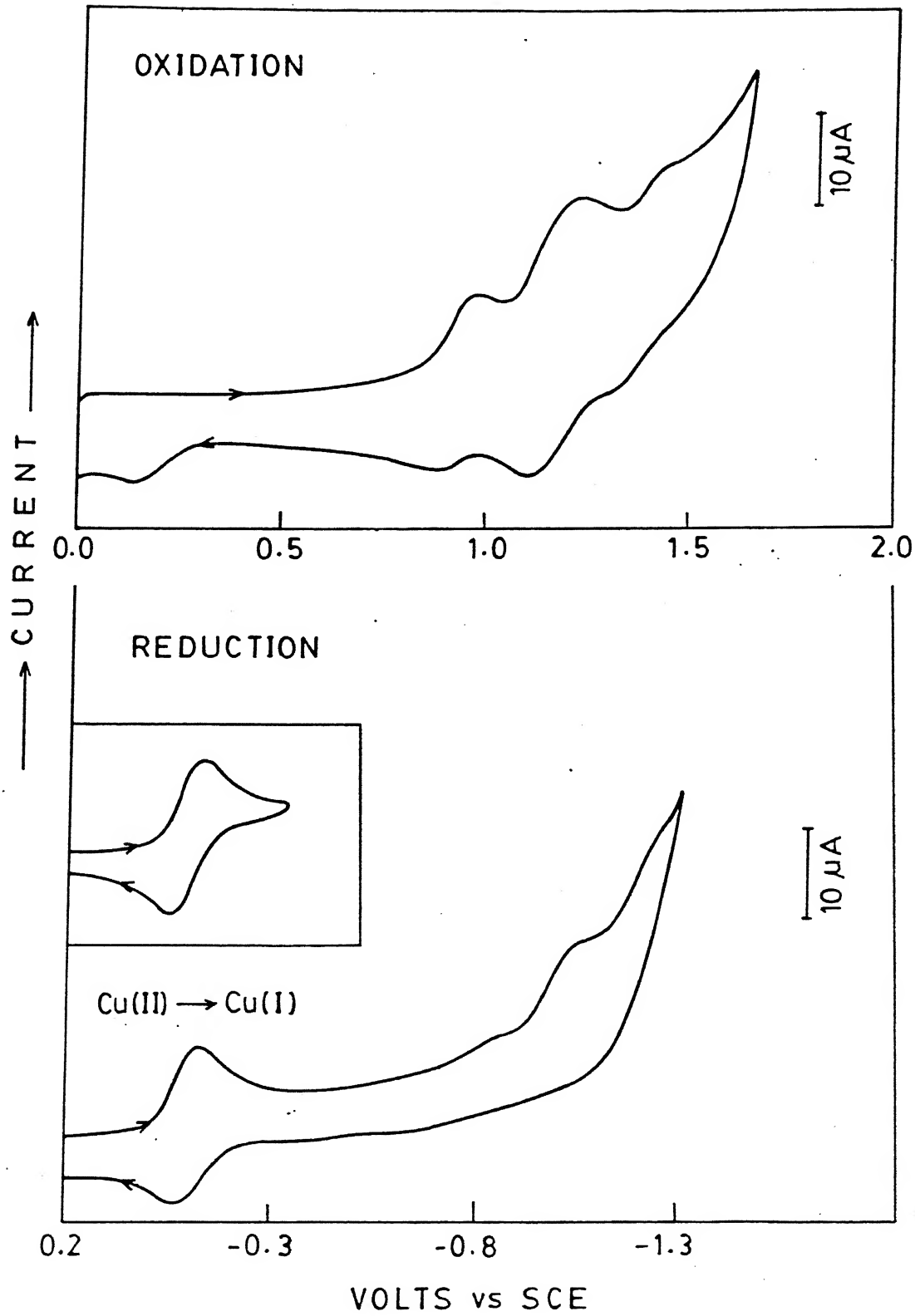

Fig.5.11 Cyclic voltammogram of compound 5 (Zn-Cu diporphyrin) in CH_2Cl_2 and 0.1 M TBAP, ν = 100 mV/s [Inset shows reversible nature of Cu(II) ⟶ Cu(I) reduction].

range of ring reduction potentials of either zinc porphyrin subunit or copper porphyrin subunit. Based on the earlier results on copper derivatives of monothiaporphyrin water soluble porphyrins (Chapter4), this reduction is attributed to metal centered reduction corresponding to the reduction of Cu(II) $\longrightarrow$ Cu(I) in the thiaporphyrin subunit. This is further confirmed by optical absorption spectrum upon addition of about 1.5 equivalent sodium dithionate in water and ethyl acetate. Upon reduction, both Q and soret bands are blue shifted (5-10 nm), typical for metal centered reductions in metalloporphyrins.[169] However, upon standing the demetallation of copper has been observed. This is similar to that observed for the monomeric copper thiaporphyrin described in the earlier chapter.

The second reduction at -0.854 V is assigned to the ring reduction of thiaporphyrin subunit. Again this potential is close to that observed for monomeric copper thiaporphyrin. The reduction waves at -1.046 V is assigned to the reduction of zinc porphyrin subunit. A comparison of this value with that in the Zn-H diporphyrin indicates a less negative shift of approximately 366 mV suggesting easier reductions probably due to the structural change accompanying the metal insertion.

In order to study the behaviour of a bimetallic diporphyrin containing same metal in the diporphyrin cores, Ni(II) - Ni(II) diporphyrin has been synthesised and characterized. The cyclic

voltammogram shown in Fig. 5.12 of this diporphyrin indicates three oxidation waves at 0.98V (ΔE_p = 69 mV), 1.12 V and 1.4V (irreversible oxidations). The oxidations at 0.98 V and 1.4 V are assigned to the first and second oxidations of Ni(II) normal porphyrin subunit on the basis of similarities of these potentials with that of NiTPP.[144] The oxidation at 1.12 V is assigned to the first ring oxidation of Nickel (II) thiaporphyrin.

Upon scanning to negative potentials two reductions at -0.28V (ΔE_p = 64 mV) and -0.885 V (ΔE_p = 77 mV) are observed. The potential range for the first reduction is not in the range expected for the ring reduction of either thiaporphyrin subunit or normal porphyrin subunit. Based on the earlier studies in Chapter 4 this first reduction at -0.288 V has been assigned to the reduction of metal center in the thiaporphyrin subunit corresponding to Ni(II) ⟶ Ni(I) couple. This potential is close to (-0.23V) that observed for the reduction of nickel in the monothiaporphyrin in THF.[145] The second reduction at -0.885 V is assigned to the first ring reduction of the thiaporphyrin subunit. This is based on the following two observations: (i) the ring reduction in nickel thiaporphyrin monochloride is at -0.82 V (ii) normal nickel (II) porphyrins exhibit first ring reduction at -1.2 V thus ruling out the possibility of the reduction of the porphyrin unit. Further scanning above 1.0 V results in the decomposition of the sample probably suggesting a coupled chemical

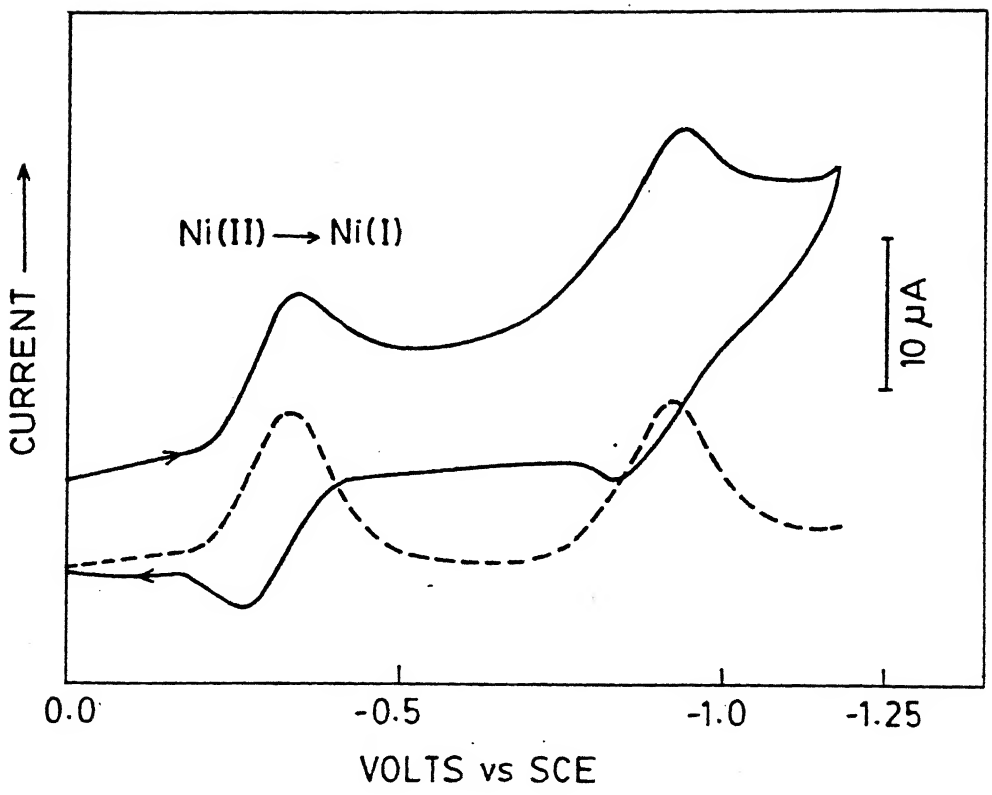

Fig.5.12 Cyclic voltammogram (———) and differential pulse voltammogram (- - -) of compound 6 (Ni-Ni diporphyrin) in CH_2Cl_2 and 0.1 TBAP, ν = 100 mV/s for cyclic voltammogram, ν = 20 mV/s for differential pulse voltammogram.

reaction. Thus it has been shown that Ni(II) - Ni(I) diporphyrin can be atleast observed electrochemically in the diporphyrin porphyrin unit. The summary of the redox processes of various diporphyrins are shown below.

(1) H_2-H dimer (Compound 3)

(a) Oxidation

$$H_2 - H \xrightarrow[0.942V]{-e} H_2 - H^+ \xrightarrow[1.046V]{-e} H_2^+ - H^+ \underset{+e}{\overset{-e}{\rightleftharpoons}} H_2^{2+}-H^+ \quad (1.288V)$$

(b) Reduction

$$H_2-H \xrightarrow[-1.10V]{+e} H_2 - H^- \underset{-e}{\overset{+e}{\rightleftharpoons}} H_2^- - H^- \underset{-e}{\overset{+e}{\rightleftharpoons}} H_2^{2-}-H^- \quad (-1.150;\ -1.57V)$$

(2) Zn-H diporphyrin (compound 4)

(a) Oxidation

$$Zn\ P - H \underset{+e}{\overset{-e}{\rightleftharpoons}} Zn\ P^+ - H \underset{+e}{\overset{-e}{\rightleftharpoons}} ZnP^{+2}-H \underset{+e}{\overset{-e}{\rightleftharpoons}} ZnP^{+2}-H^+ \quad (0.735V;\ 1.02V;\ 1.23V)$$

(b) Reduction

$$ZnP-H \underset{-e}{\overset{+e}{\rightleftharpoons}} ZnP-H^- \underset{-e}{\overset{+e}{\rightleftharpoons}} ZnP^--H^- \xrightarrow{-e} ZnP^--H^{2-} \quad (-1.1V;\ -1.312V;\ -1.576V)$$

(3) Zn-Cu diporphyrin (compound 5)

(a) Oxidation

$$ZnP\text{-}CuP \underset{+e}{\overset{-e}{\rightleftharpoons}} ZnP^{+} - CuP \underset{+e}{\overset{-e}{\rightleftharpoons}} ZnP^{+} - CuP^{+} \underset{+e}{\overset{-e}{\rightleftharpoons}} ZnP^{2+}\text{-}CuP^{+}$$

0.919V 1.173V 1.362V

(b) Reduction

$$ZnP\text{-}CuP \underset{-e}{\overset{+e}{\rightleftharpoons}} ZnP\text{-}CuP^{-}(I) \xrightarrow[-0.854V]{+e} ZnP\text{-}CuP(I)^{2-} \xrightarrow[-1.046V]{+e} ZnP^{-}\text{-}CuP(I)$$

-0.0885V

(4) Ni-Ni Diporphyrin (compound 6)

(a) Oxidation

$$NiP\text{-}NiP \underset{+e}{\overset{-e}{\rightleftharpoons}} NiP^{+}\text{-}NiP \xrightarrow[1.121V]{-e} NiP^{+}\text{-}NiP^{+} \xrightarrow[1.4V]{-e} NiP^{+2}\text{-}NiP^{+}$$

0.98V

(b) Reduction

$$NiP\text{-}NiP \underset{-e}{\overset{+e}{\rightleftharpoons}} NiP\text{-}NiP(I)^{-} \underset{-e}{\overset{+e}{\rightleftharpoons}} Ni\text{-}Ni(I)^{2-}$$

-0.28V -0.885V

5.3.5. Emission Spectra

The singlet excited state characteristics of H_2-H diporphyrin and Zn-H diporphyrin were evaluated by emission spectroscopy. Fig. 5.13 shows a comparison of emission spectra of H_2-H diporphyrin along with 1:1 mixture of the two monomers dissolved in $CHCl_3$ at various excitation wavelengths. The

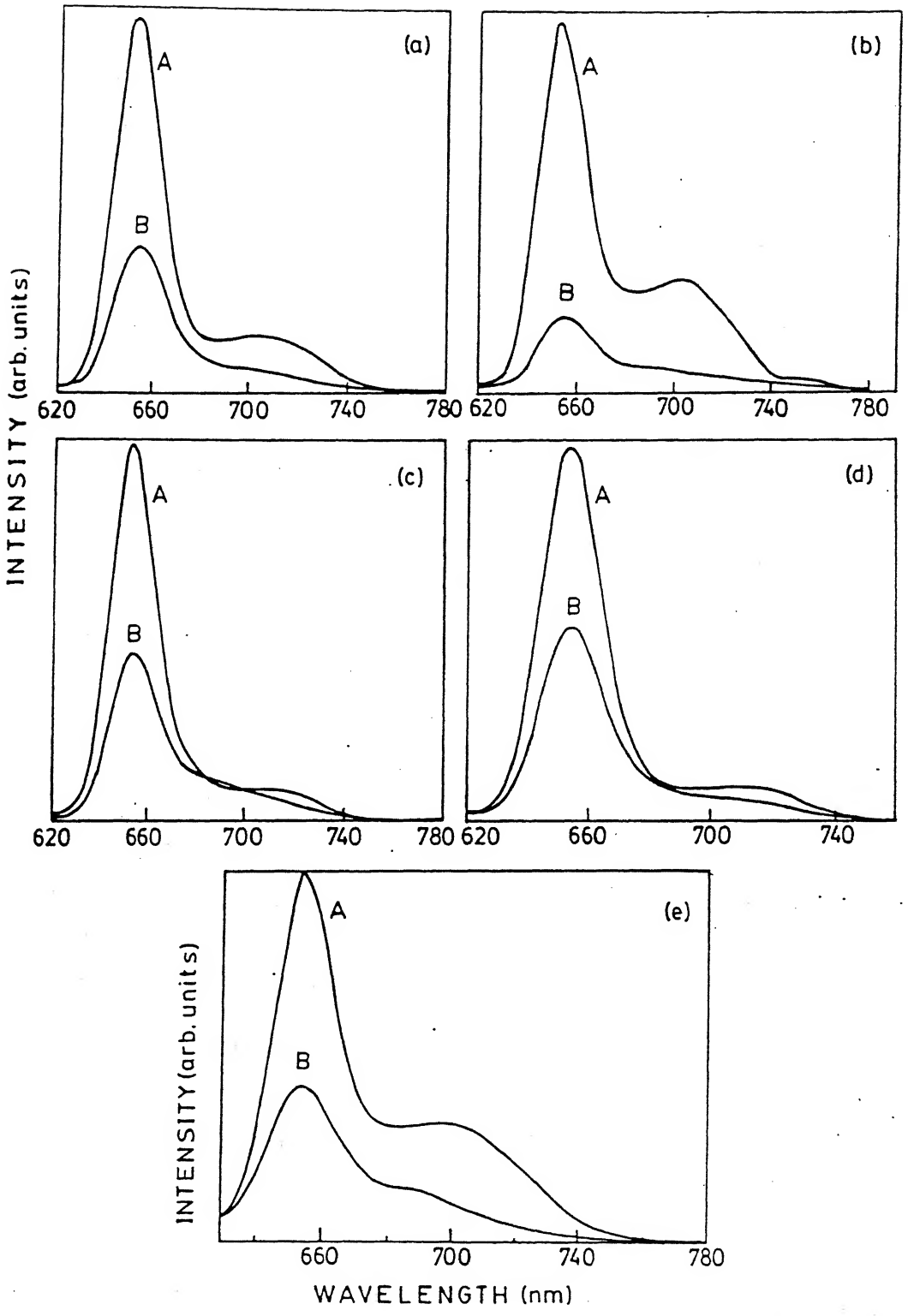

Fig.5.13 Comparison of emission spectra of compound 3 (H_2-H diporphyrin) (B) with 1:1 mixture of corresponding monomeric subunits (A) at constant concentration 2.7933×10^{-5}M (excitation wavelengths (a) 420 nm, (b) 430 nm, (c) 515 nm (d) 592 nm and (e) 616 nm).

Table 5.4: Emission data of monomer and diporphyrins of thiaporphyrins in $CHCl_3$

Porphyrin	Emissision maxima at 515 nm excitation (nm)	Quantum yield ϕ_f
Compound 1	655,710	8.58×10^{-2}
Compound 2	683.0	1.85×10^{-3}
Compound 3 (H_2-H)	654, 691.0	1.33×10^{-2}
1:1 mixture of (Compound 1 and 2)	654, 709	2.29×10^{-2}
Compound 4 (Zn-H)	601, 644, 689	2.04×10^{-2}
1:1 mixture of zinc derivative of Compound 1 and Compound 2	607,641,682	2.62×10^{-2}

excitation wavelengths were chosen to make sure of specific excitations at normal porphyrin part and thiaporphyrin part. The concentrations are kept constant [2.7933×10^{-5}M]. It is clear from figure that the emission bands of the H_2-H diporphyrin have a profile similar to that observed for the 1:1 mixture of the corresponding individual subunits at all the excitation wavelengths. However, the emission spectrum of 1:1 mixture has a greater intensity compared to the dimeric species suggesting that the fluorescence intensity is quenched in the diporphyrins relative to 1:1 mixture. The emission spectrum of the H_2-H diporphyrin predominatly shows the emission spectrum of normal TPP part (655 nm) while the emission spectrum of thiaporphyrin part at (683 nm) is much weaker because of the quenching of porphyrin fluorescence upon sulfur substitution.

The quantum yield data indicate quenching of fluorescence in the diporphyrins relative to individual monomers as well as to the 1:1 mixture. An inspection of table 5.4 indicates almost about 50% reduction in quantum yield between compound 1 and 2 showing effect of sulfur substitution. The quantum yield data indicate further quenching of fluorescence in the diporphyrin relative to 1:1 mixture. This is consistent with the earlier literature reports on covalently linked TPP dimers.[161,163,164]

The fluorescence of Zn-H diporphyrin is dominated by the zinc porphyrin subunit. Fig. 5.14 shows the emission spectra of Zn-H

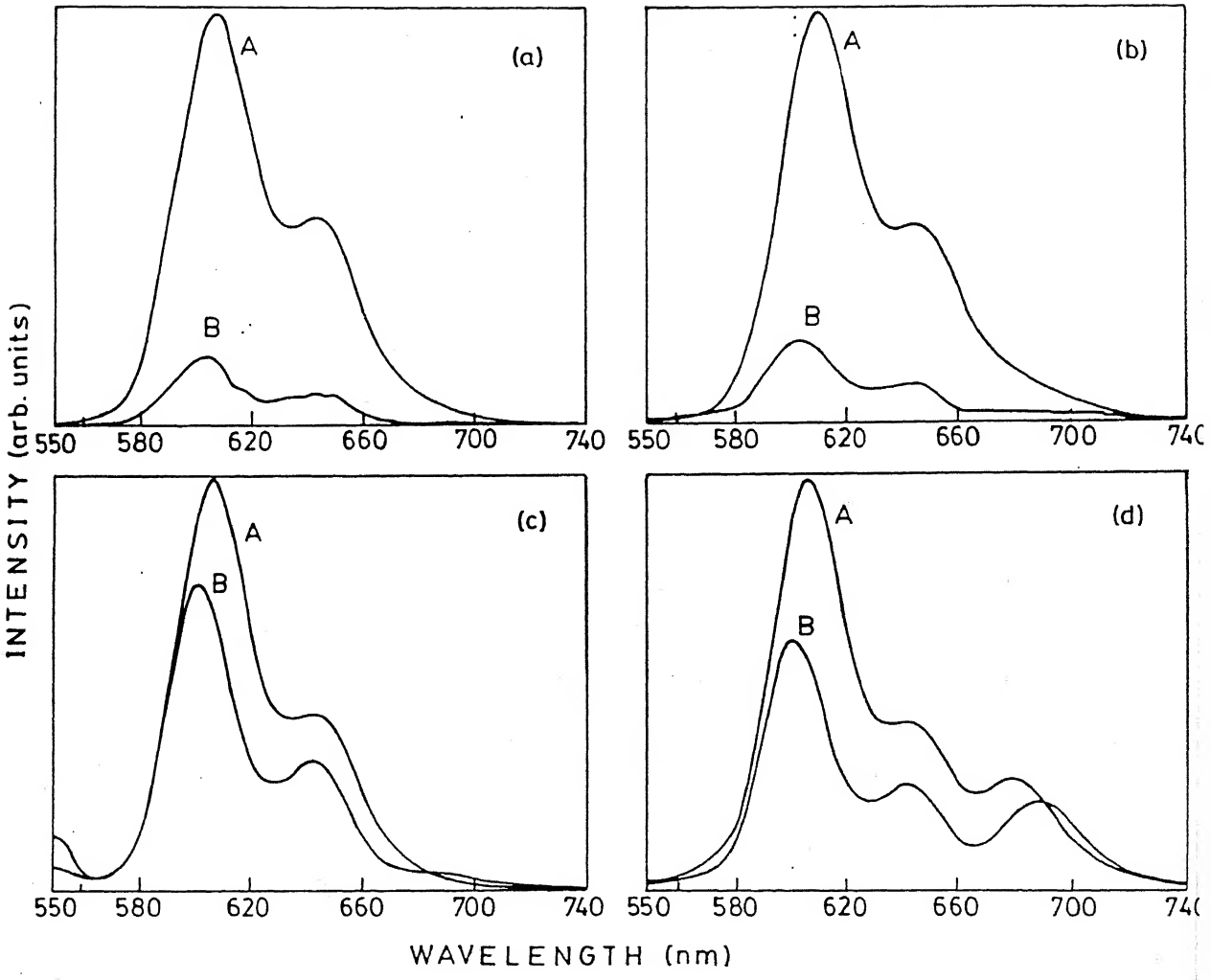

Fig.5.14 Comparison of emission spectra of compound 4 (Zn-H diporphyrin) (B) with 1:1 mixture of corresponding monomeric subunits [A] at constant concentration 3.3445×10^{-5} (excitation wavelengths (a) 420 nm, (b) 430 nm, (c) 550 nm and (d) 515 nm).

diporphyrin excited at specifically at zinc porphyrin absorption and thiaporphyrin absorption. The spectra shown in Fig.5.14 gives a comparison of emission spectra of Zn-H diporphyrin with that of a 1:1 mixture of normal zinc porphyrin and free base thiaporphyrin. It is clear (figure 5.14) that the excitation at 420 and 550 nm at the zinc porphyrin unit essentially gives an emission spectrum corresponding to ZnTPP (601 and 644 nm) while the excitation at thiaporphyrin Q bands (515 nm) shows the emission bands of thiaporphyrin at 682 nm. A persal of literature on Zn-freebase diporphyrins reveals that the transfer of energy from zinc porphyrin part to the free base part because of the favourable energetics. However, in the Zn-H diporphyrin we did not observe any energy transfer from the zinc porphyrin part to thiaporphyrin. This is probably due to the tough competition between the energy transfer and the electron transfer processes.An attempt has been made to calculate the energy levels of charge transfer state (Zn^{+}-H) of the lowest singlet excited state of zinc porphyrin subunit (S_{Zn}-H) and the lowest singlet excited state of thiaporphyrin subunit (Zn-S_{H}) from the electrochemical and the emission data.[165] A schematic diagram of the energy levels are shown below.

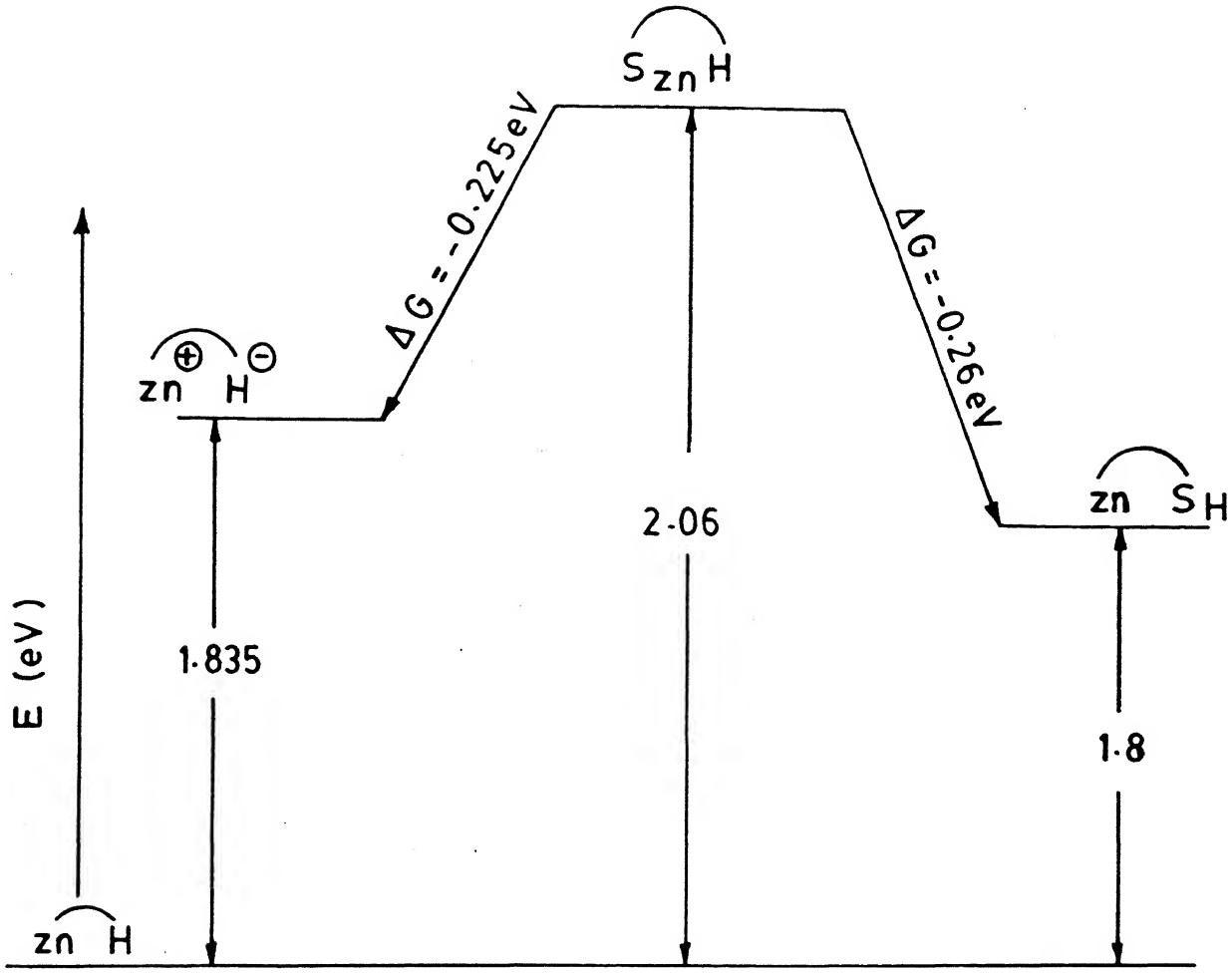

Thus it is clear from the data shown above that indeed, electron transfer and energy transfer compete with each other in the present case.

The quantum yields of the Zn-H diporphyrin are also calculated with respect to $TPPH_2$. An inspection of data in the

table 5.4 indicate considerable quenching of fluorescence in the Zn-H diporphyrin relative to 1:1 mixture consistent with the literature reports.[161,163,164]

5.4.0 Conclusions

Synthesis of an unique diporphyrin containing N_4 and N_3S cores have been achieved. Metals ion such as Zn^{+2}, Cu^{+2} and Ni^{+2} present in the porphyrin cores yield both homo and hetero bimetallic diporphyrins. The ^1H NMR, FAB mass, EPR and optical absorption and emission spectroscopy have been used to characterize these diphorphyrins. The redox chemistry have been followed by cyclic voltammetry as well as by differential pulse voltaammetry. The spectral studies reveal only weak interaction between the two diporphyrin subunits in the free base diporphyrin and Zn-H diporphyrin. However, introduction of a metal to the thiaporphyrin subunit results in a substantial interaction between normal and thiaporphyrin subunits. A blue shift and quenching absorbance of Q and soret bands of zinc normal porphyrin subunit in Zn-Cu diporphyrin, a positive shift for oxidation and reduction potentials of zinc normal porphyrin subunit in Zn-Cu diporphyrin justifies such a conclusion. However, the electrochemistry data for H_2-H diporphyrin reveal the characteristics of the corresponding monomeric subunits. In Zn-Cu and Ni-Ni diporphyrins the observation that the first reduction is metal centered (the

metal present in thiaporphyrin subunit) indicate the reversal of order of energy levels of metal $d_{x^2-y^2}$ and the porphyrin $e_g(\pi^*)$ similar to that observed for individual metallo thiaporphyrins. The emission characteristics also shows that two subunits in the diporphyrin behave independently in the first excited singlet state. However, it has been observed that the quantum yield is considerably decreased in the diporphyrins relative to the corresponding 1:1 mixture of monomers. Surprisingly, no energy transfer has been observed for Zn-H diporphyrin. The electrochemical data on Zn-Cu and Ni-Ni diporphyrins have revealed the possibility of stabilisation of two different oxidation states of the metal using this bisporphyrin unit. Preliminary studies on chemical reduction of Ni(II)-Ni(II) diporphyrin and Cu(II) - Cu(II) diporphyrin using mild reducing agents reveal the presence of Ni(II) - Ni(I) and Cu(II)-Cu(I) in N_4 and N_3S cores respectively. We think the easy synthetic accessibility and stability of this unique diporphyrin merits further investigation.

CHAPTER 6

SUMMARY

The present study has characterized, spectral characteristics of core modified thiaporphyrins and their metal derivatives in ground, excited singlet and triplet states. Eventhough, the synthetic methodolgies for synthesis of thiaporphyrins were known some time back there were no systematic studies on their spectral behaviour. The structural characterization of some of these thiaporphyrins were reported recently.[57a,60] The results reported in this thesis provide systematic data evaluated from various spectral techniques such as optical absorption, emission, ^{1}H NMR, ESR and photoexcited triplet ESR.

The first part of the thesis describes the spectral studies of various thiaporphyrins and their protonated derivatives both in ground and excited states. It has been shown that the thiaporphyrins behaves almost in a similar fashion upon protonation compared to corresponding tetraphenylporphyrin indicating similar structural change. The expected structural change upon protonation is clearly reflected in the shift of the structurally sensitive Raman modes. The direction of the shifts of these Raman modes suggest core expansion upon protonation.

Theoretical analysis by IEH Model[52] on S_2TPP predicted that the triplet state should be populated for both S_2TPP and its dication which show weak fluorescence. The experimental proof for such a prediction is provided by the following observations: (a) the decrease in rate of fluorescence decay and simultaneous

increase of rate of intersystem crossing (table 3.5) (b) the observation of triplet ESR signals for all the thiaporphyrins reported here.

The soret transition is the major π-π^* transition in the optical spectra of porphyrins and it is the only transition containing x,y and z components, it thus may serve as the best expression for various effects of sulfur substitution has on the outer orbital of the porphyrin molecule. Experimentally this band shows gradual red shift upon sulfur substitution. The figure 6.1 shows how this red shifts relates to $\Delta_{redox}(E_{1/2(ox)}-E_{1/2(red)})$, thus suggesting a decrease in Δ_{redox} upon sulfur substitution. In order to see the effect of sulfur substitution on Δ_{redox}, a plot of Δ_{redox} (excited state) versus the emission maxima in Fig. 6.2. A linear correlation is observed when there are no substituents on the phenyl ring. The deviation for the methyl and methoxy substituted derivatives reflects the participation of substituents in the π-conjugation in the excited state.

It has been shown before[56] that the linear relationship exists between the chemical shifts in the ^1H and ^{13}C NMR of the heterocycles, thiophene, selenophene, furan and the electronegativities of the hetero atoms. No such correlation was found in the present study. However, it has been suggested that the first reduction potential may serve as the measure for the molecular "electron affinity" in these systems instead of the individual electronegativities which do not take into account the bonding interactions in the core. Thus a plot of first reduction potential versus the chemical shifts of the pyrrole protons shows

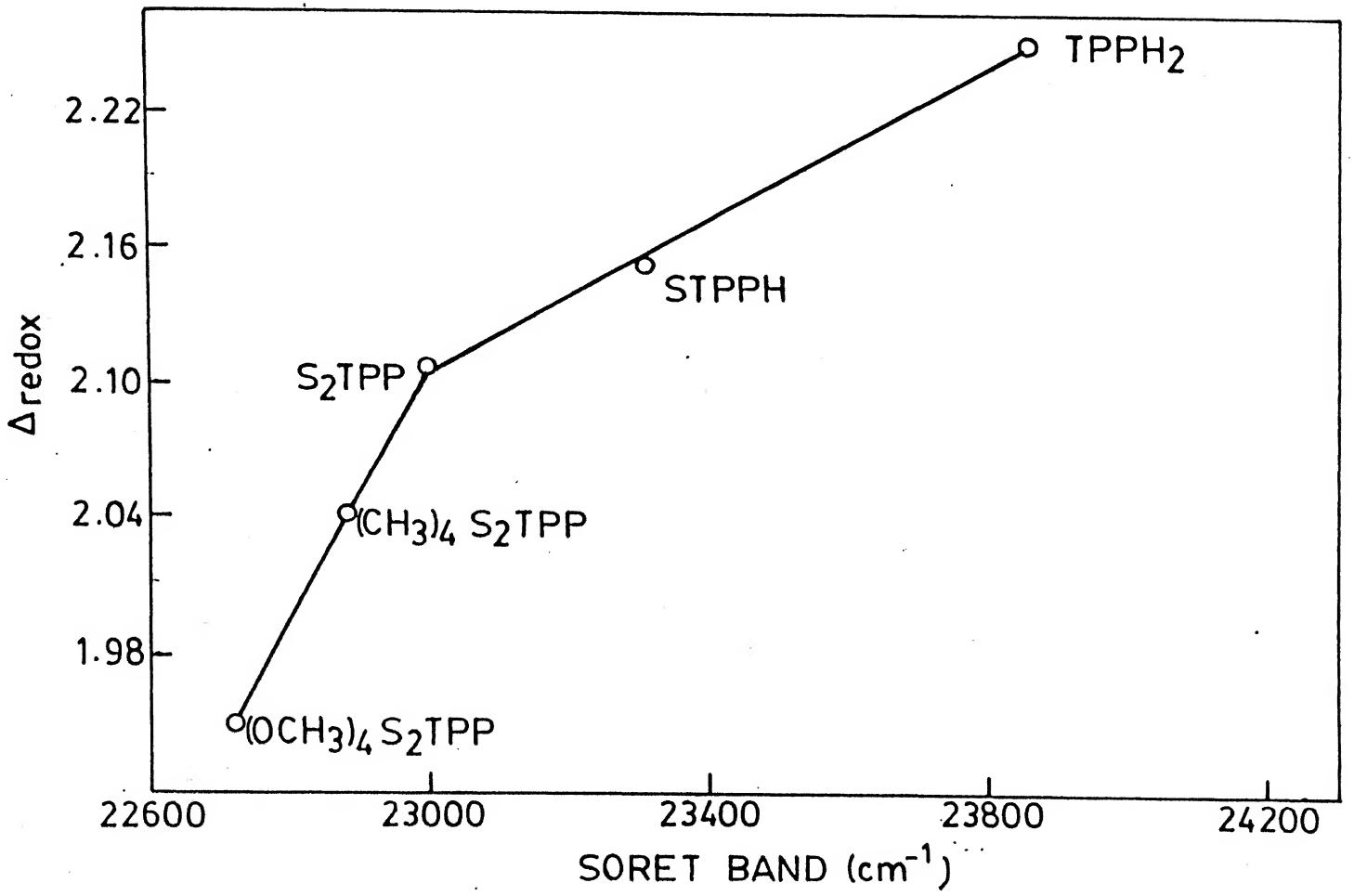

Fig.6.1 A plot of Δ_{redox} [$E^1_{1/2}$ (ox) - $E^1_{1/2}$ (red)] versus the energy of soret band of various thiaporphyrins and $TPPH_2$.

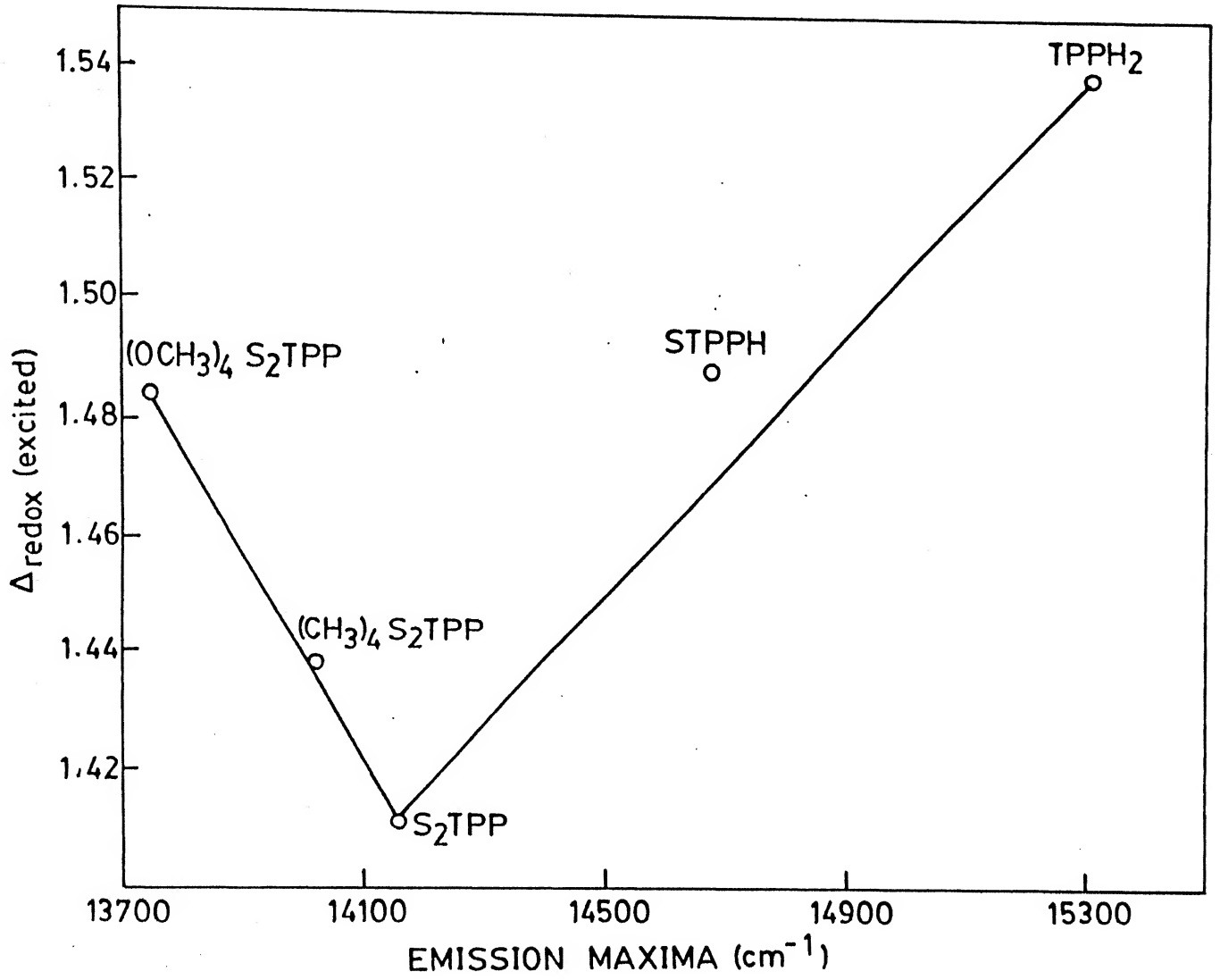

Fig.6.2 A plot of Δ_{redox} (excited) versus energy of the Q(0,0) emission band of various thiaporphyrins and $TPPH_2$.

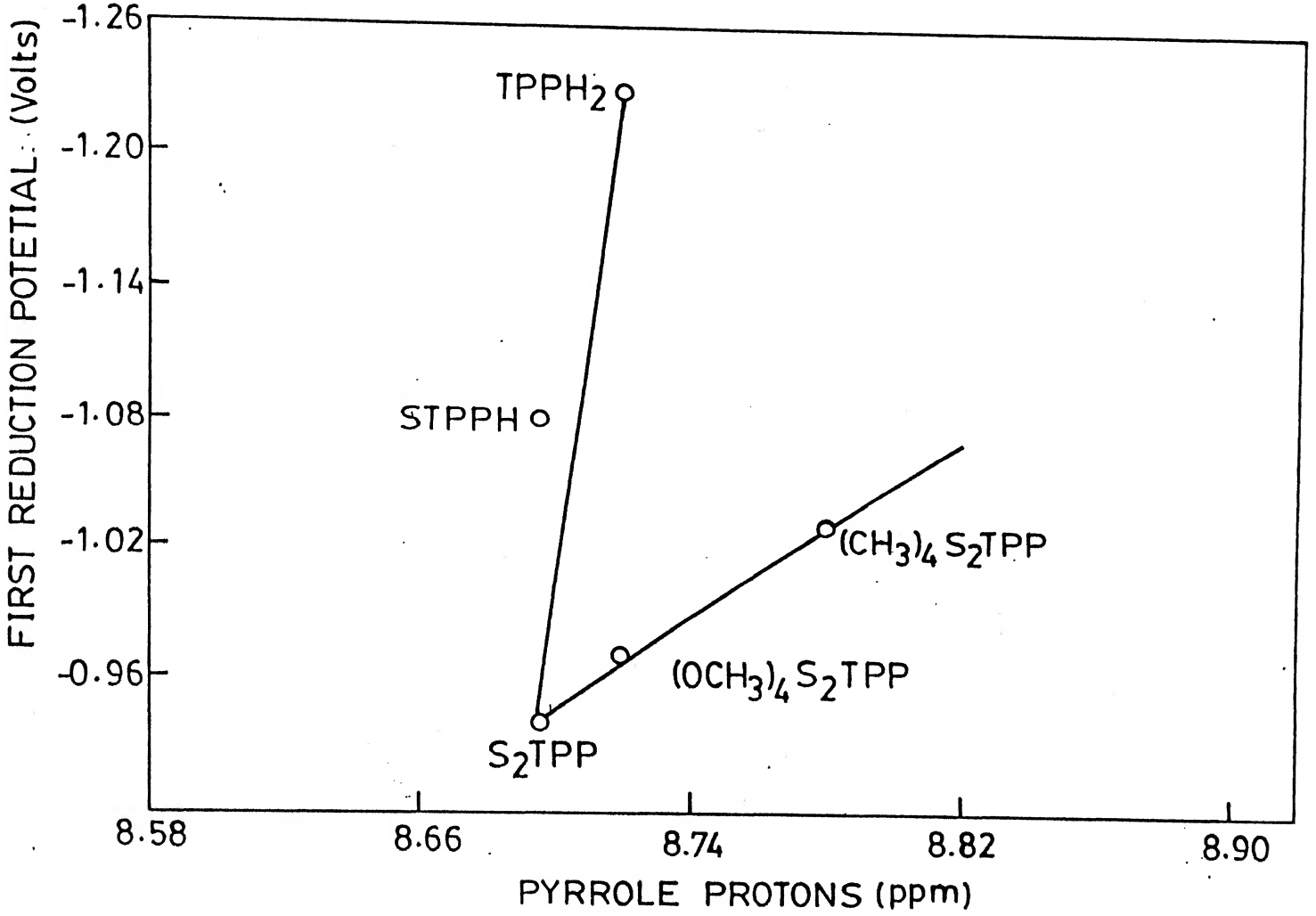

Fig.6.3 A plot of first reduction potential versus chemical shift of pyrrole protons of various thiaporphyrins and $TPPH_2$.

a linear correlation for the unsubstituted derivatives. Again, deviations are observed for the methoxy and methyl substituted derivatives, probably reflecting the participation of the substituents in the π-system.

It was surprising to see that the zero field splitting parameters D and E as well as ESP pattern remain same as that of $TPPH_2$. However, the structural change accompanying protonation is clearly reflected in the drastic reduction of ZFS parameters and the change in the ESP pattern. The different ESP pattern observed for monothia (**aa ae ee**) and dithia (**aa ea ee**) porphyrins upon protonation reflects the difference in the population and depopulation rates among triplet sublevels.

The water soluble thiaporphyrins have been prepared for the first time with milder method. This method has advantage over the traditional H_2SO_4 method in many ways.[132] It has been shown that the free base thiaporphyrins behave exactly similar to that of H_2TPPS (5,10,15,20(4-sulfonato phenyl) porphyrin) with respect to aggregation behaviour. Addition of 18-Crown-6 and K^+ ions to a dilute monomeric solution of both STPPS and S_2TPPS results in the formation of cofacial dimer similar to those observed for water soluble anionic porphyrins.[138] However, the magnitude of dimerization constant decreases upon sulfur substitution in linear fashion. A plot of dimerization constant evaluated from spectral methods for H_2TCPP (5,10,15,20-tetrakis (4-carboxy phenyl) porphyrin),[138] STPPS and S_2TPPS is shown in Fig.6.4. The metal derivatives (Cu^{+2} and Ni^{+2}) of STPPS however, behave quite differently from those established for Cu^{+2} and Ni^{+2} regular

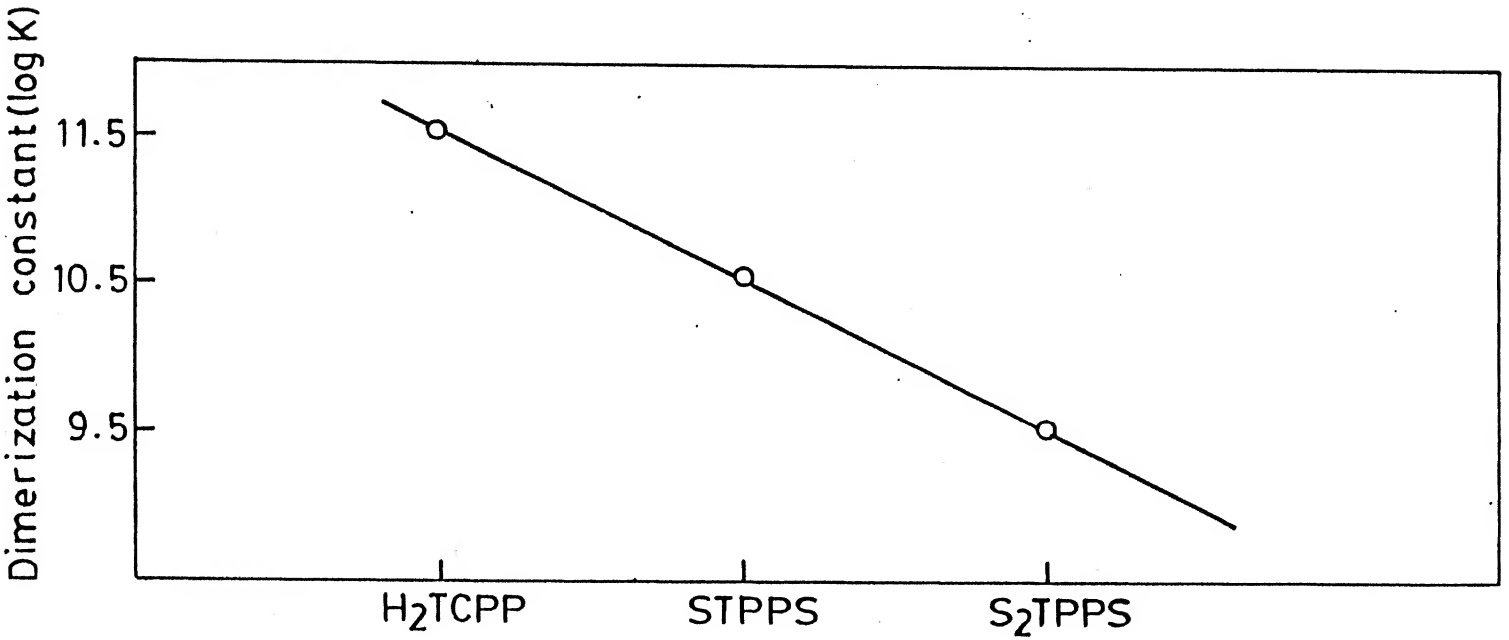

Fig.6.4 A plot of dimerization constant versus H_2TCCP, STPPS and S_2TPPS.

porphyrins. For example, (a) the electronic absorption spectra show the split soret band and a complex pattern of Q-bands (b) a well defined M(II)/M(I) reduction (c) the metal derivatives are highly distorted with a approximate square pyramid geometry. It should be noted that the magnetic properties, redox potentials and the structure show a straight forward simlarity with the metallo N-substituted porphyrins. The altered electrochemical (reversal of metal $d_{x^2-y^2}$ and porphyrin $e_g(\pi^*)$ orbital energies) and the magnetic properties is attributed to the structural change upon metal coordination to STPPS rather than to the change in the electronic structure due to the sulfur substitution.Strong justification for such a conclusion is provided by the similarities in structures of CuSTPPX[57a] and $CuNCH_3TPPX$[57b] systems reported recently. The easier reduction of metal (Cu^{+2} and Ni^{+2}) is attributed to the fact that M(II) ions in STPPS is probably displaced from the porphyrin plane unlike in planar CuTPP and NiTPP.

The photoexcited triplet ESR spectrum of water soluble thiaporphyrins show many similarities in terms of zero field splitting parameters (D and E) and electron spin polarization pattern. The observed ESP pattern (ea ea ea) signifies that the population and depopulation rates of zero field Ty spin state are larger than those of other two states. The dimerization results in decrease in D values (~ 16%) similar to those observed for photo excited triplets of in vivo reaction centre of Baterio chlorophylla. This represents the first photoexcited triplet ESR study on thiaporphyrins.

The preliminary studies reported in chapter 5 offer many interesting features. The unique diporphyrin reported here has different electronic cores [N_4 and N_3S] thus offering different environments for metal coordination. Since both the free base porphyrins are almost planar there is only weak interaction between the two porphyrin ring systems. However introduction of the metal to the thiaporphyrin core drastically alters the planarity of the thiaporphyrin core due to the co-ordination requirement of thiophene ring. This distorted metallothiaporphyrin core induces electronic changes in the normal porphyrin subunit. This is clearly reflected in the blue shift of zinc normal porphyrin absorption bands upon metallation of the thiaporphyrin unit and the shifts of the redox potential of normal porphyrin unit upon metallation in the thiaporphyrin unit. The electrochemical data of bimetallic derivatives have given a clue for chemical reduction of metal center in thiaporphyrin subunit. The metal reduction potentials are clearly well separated from the porphyrin ring redox potentials. Thus the mild reducing agents should be able to reduce specifically the metal center in bimetallic derivatives (Ni-Ni, Cu-Cu) giving Ni(II)/Ni(I), Cu(II)/Cu(I) bimetallic diporphyrins. Studies in this direction are in progress. It is hoped that the investigations reported in this thesis has added a new dimension in the chemistry of thiaporphyrins and will be a useful database for an understanding of electronic structure of porphyrin skeleton. Another aspect of the thiaporphyrin chemistry which is not been studied so for is their catalytic ability towards some simple organic conversions.

Synthetic porphyrins are now meeting point for inorganic chemistry, catalysis and pharmacology. Combined efforts in such a interdisplinary area will probably produce new application of thiaporphyrins and metallothiaporphyrins. It is hoped that some of the catalytic reactions for simple organic conversions using the metallothiaporphyrins synthesised in the present study will be taken up in this laboratory soon.

References

1. Hemoglobin and oxygen binding, ed. C.Ho, (Elsevier Biomedical, New York, 1982).
2. F.S. Mathews, *Prog. Biophys. Mol. Biol.*, **45**, 1, 1985.
3. Y. Hatefi, *Ann. Rev. Biochem.*, **54**, 1015, 1985.
4. J.E. Frew and P. Jones, *Adv. Inorg. Bioinorg. Mech.*, **3**, 175, 1984.
5. (a) Cytochrome P-450: Structure, Mechanism and Biochemistry, ed. portiz de Montellano (Plenum press, New York, 1985).
   (b) V. Ullrich, *Top. Curr. Chem.*, **83**, 67, 1979.
   (c) T.D. Porter and M.J. Coon, *J. Biol. Chem.*, **266**, 13469, 1991
   (d) J.T. Groves and G.A. McClusky, *J. Am. Chem. Soc.*, **98**, 859, 1976.
6. (a) Peroxidases in Chemistry and Biology, Vol. I & II, eds. J. Everse; K.E. Everse and M.B. Grishom (CRC Press, Boca Raton, 1991).
   (b) H.P. Dunford, *Adv. Inorg. Biochem.*, **4**, 41, 1982.
7. (a) L.P. Hager; D.R. Morris; F.S. Brown and H. Eberwein, *J. Biol. Chem.*, **241**, 1769, 1966.
   (b) S.R. Blanke and L.P. Hager, *J. Biol. Chem.*, **263**, 18739, 1988.
8. I. Fita and M.G. Rossmann, *J. Mol. Biol.*, **185**, 21, 1985.
9. C.K. Chang, *J. Am. Chem. Soc.*, **101**, 3413, 1979.
10. J.T. Groves and W.J. Kruper, *J. Am. Chem. Soc.*, **101**, 7613,

1979.

11. C.L.Hill and B.C. Schardt, *J. Am. Chem. Soc.*, **102**, 6374, 1980.

12. J.T. Groves; W.J. Kruper and R.C. Haushalter, *J. Am. Chem. Soc.*, **102**, 6375, 1980.

13. C.K. Chang and F. Ebina, *J. Chem. Soc., Chem. Comm.*, 778, 1981.

14. J.T. Groves and T.E. Nemo, *J. Am. Chem. Soc.*, **105**, 5786, 1983.

15. O. Bortolini and B. Meunier, *J. Chem. Soc. Chem. Comm.*, 1364, 1983.

16. P.S. Traylor; D. Dolphin and T.G. Traylor, *J. Chem. Soc., Chem. Comm.*, 279, 1984.

17. B. De Poorter and B. Meunier, *Tetrahedron Lett.*, **25**, 1895, 1984.

18. T.G. Traylor and S. Tsuchiya, *Inorg. Chem.*, **26**, 1338, 1987.

19(a) D.H. Dolphin; T. Nakano;T.K. Kirk; T.E. Maroni; R.L. Farrell and T.P. Wijesekera, *Patent PCT Int. Appl. WO 88/07988*, 1988

(b) T. Wijesekera; A. Matsumoto; D. Dolphin and D. Lexa, *Angew. Chem.Int. Ed. Engl.*, **29**, 1028, 1990.

20(a) G. Labat; P. Hoffmann; J.L. Series and B. Meunier, *Fr. Patent Appl. 89.10762*, 1989; *Chem. Abstr.* **115**, 1991, 114269t

(b) P. Hoffmann; G. Labat; A. Robbert and B. Meunier, *Tetrahedron Lett.*, **31**, 1991, 1990.

21. S. Tsuchiya and M. Seno, *Chem. Lett.*, **263**, 1989.

22(a) M.J. Broadhurst; R. Grigg and A.W. Johnson, *J. Chem. Soc., Perkin Trans. 1*, 2111, 1972.

(b) A.K. Burrel; J.L. Sessler; M.J. Cyr; E.McGhee and J.A. Ibers, *Angew. Chem. Int. Ed. Engl.*, **30**, 91, 1990.

23. H. Rexhausen and A. Gossauer, *J. Chem. Soc., Chem. Comm.*, **275**, 1983.

24. V.W. Day; T.J. Marks and W.A. Wachter, *J. Am. Chem. Soc.*, **97**, 4519, 1975.

25(a) R.A. Berger and E. LeGoff, *Tetrahedron Lett.*, 4225, 1978.

(b) E. LeGoff and O.G. Weaver, *J. Org. Chem.*, **52**, 710, 1987.

26(a) M. Gosmann and B. Franck, *Angew. Chem. Int. Ed. Engl.*, **25**, 1100, 1986.

(b) H. Konig; C. Eickemeier; M. Moller; U. Rodewald and B. Franck, *Angew. Chem. Int. Ed. Engl.*, **29**, 1393, 1990.

27(a) N. Jux; P. Koch; H. Schmicker; J. Lex and E. Vogel, *Angew. Chem. Int. Ed. Engl.*, **29**, 1385, 1990.

(b) E. Vogel, N. Jux, E. Rodriguez-Val, J. Lex and H. Schmicker, *Angew. Chem. Int. Ed. Engl.*, **29**, 1387, 1990.

28(a) J.L. Sessler; T. Murai; V. Lynch and M. Cyr, *J. Am. Chem. Soc.*, **110**, 5586, 1988.

(b) J.L. Sessler; T. Murai and G. Hemmi, *Inorg. Chem.*, **28**, 3390, 1989

(c) B.G. Maiya; T.E. Mallouk; G. Hemmi and J.L. sessler, *Inorg. Chem.*, **29**, 3738, 1990.

29(a) F.V. Acholla and K.B. Mertes, *Tetrahedron Lett.*, **25**, 3269, 1984.

(b) F.V. Acholla; F. Takusagawa and K.B. Mertes, *J. Am. Chem. Soc.*, **107**, 6902, 1985.

(c) H. Singer, *J. Organomet. Chem.*, **9**,135, 1967.

(d) J.D. Goodrich; P. N. Nickias and J.P. Selegue, *Inorg. Chem.*, **26**, 3426, 1987.

30. A.D. Adler; F.R. Longo and J.D. Finarelli, *J. Org. Chem.*, **32**, 476, 1967.

31. A.D. Adler; L. Sklar; F.R. Longo; J.D. Finarelli and M.G. Finarelli, *J. Hetercycl. Chem.*, **5**, 669, 1968.

32. R.G. Little; J.A. Anton; P.A. Loach and J.A. Ibers, *J. Heterocyclic. Chem.*, **12**, 343, 1975.

33. R.L.N. Harris; A.W. Johnson and I.T. Kay, *J. Chem. Soc. (C)*, 22, 1966.

34. M.J. Broadhurst; R. Grigg and A.W. Johnson, *J. Chem. Soc.(C)*, 3681, 1971.

35. R.L.N. Harris; A.W. Johnson and I.T. Kay, *Quart. Rev.* **20**, 211, 1966.

36. V.B. Math, *Ph.D. Thesis*, Univ. of Nottingham, Nottingham, 1969.

37. G.P. Arsenault; E. Bullock and S.F. MacDonald, *J. Amer. Chem. Soc.*, **82**, 4384, 1960.

38. A. Ulman and J. Manassen, *J. Am. Chem. Soc.*, **97**, 6540, 1975.

39. A. Ulman; J. Manassen; F. Frolow and D. Rabinovich, *Tetrahedron Lett.*, 167, 1978.

40. A. Ulman; J. Manassen; F. Frolow and D. Rabinovich, *Tetrahedron Lett.*, 1885, 1978.

41. A. Ulman and J. Manassen, *J. Chem. Soc., Perkin Trans. 1*, 1066, 1979.

42. L. L. Grazynski; J. Lisowski; M.M. Olmstead and A.L. Balch, *J. Am. Chem. Soc.*, **109**, 4428, 1987.

43(a) W. Haas; B. Knipp; M. Sicken; J.Lex and E. Vogel, *Angew. Chem. Int. ed. Engl.*, **27**, 409, 1988.

(b) E. Vogel; W. Haas; B. Knipp; J. Lex and H. Schmickler, *Angew. Chem. Int. Ed. Engl.*, **27**, 406, 1988.

44. E. Vogel; M. Sicken; P. Rohrig; H. Schmickler, J. Lex and O. Ermer, *Angew. Chem. Int. ed. Engl.*, **27**, 411, 1988.

45. E. Vogel; P. Rohrig; M. Sicken; B. Knipp, A. Herrmann;M. Pohl; H. Schmickler and J. Lex, *Angew. Chem. Int. ed. Engl.*, **28**, 1651, 1989.

46. S.J. Silvers and M. Tulinsky, *J. Am. Chem. Soc.*, **89**, 3331, 1967.

47. L. L. Grazynski; J. Lisowski; L. Szterenberg; M.M. Olmstead and A.L. Balch, *J. Org. Chem.*, **56**, 4043, 1991.

48. F. Frolow; D. Rabinovich; A. Ulman and J. Manassen (unpublished results).

49. Hand Book of Chemistry and Physics, ed. R.C. Weast (CRC Press, Cleveland, Ohio, 1975-76), p.178.

50. F.A. Cotton and G. Wilkinson, Advanced Inorganic Chemistry, (3rd ed., John Wiley Interscience, 1972), p. 117.

51. M.B. Hall and R.F. Fenske, *Inorg. Chem.*, **11**, 768, 1972.

52 L. Hill and M. Gouterman and A. Ulman, *Inorg. Chem.*, **21**, 1450, 1982.

53(a) D. Bak; D. Christensen; L. Hansen-Nygard and J. Rastrup-Andersen, *J. Mol. Spectrosc.*, **7**, 58, 1961.

(b) R.A. Bonham and F.A. Momany, *J. Chem. Phys.*, **67**, 2474, 1963.

(c) W.R. Harsbarger and S.H. Bauer, *Acta Crystallogr.*, **26**, 1010, 1970.

54. I. Cohen, *J. Chem. Phys.* **57**, 5076, 1972.

55. P. Stein; A. Ulman and T.G. Spiro, *J. Phys. Chem.*, **88**, 369, 1984.

56(a) A. Ulman; J. Manassen; F. Frolow and D. Rabinovich, *J. Am. Chem. Soc.*, **101**, 7055, 1979.

(b) R.J. Abraham; P. Leonard and A. Ulman, *Org. Magn. Resonance*, **22**, 561, 1984.

(c) R.J. Abraham; G.E. Hawkes and K.M. Smith, *Tetrahedron Lett.*, 1483, 1974.

57(a) L. L. Grazynski; J. Lisowski; M.M. Olmstead and A.L. Balch, *Inorg. Chem.*, **28**, 1183, 1989.

(b) O.P. Anderson; A.B. Kopelove and D.K. Lavallee, *Inorg. Chem.*, **19**, 2101, 1980.

58. L. L. Grazynski; M.M. Olmstead and A.L. Balch, *Inorg. Chem.*, **28**, 4065, 1989.

59(a) A. Gleizes; M. Dartiguenave; Y. Dartiguenave; J. Galy and H.F. Klein, *J. Am. Chem. Soc.*, **99**, 5187, 1977.

(b) M.M. Olmstead; W.K. Musker and R.M. kessler, *Inorg. Chem.*, **20**, 151,1 1981.

60. L. L. Grazynski; J. Lisowski; M.M. Olmstead and A.L. Balch, *Inorg. Chem.*, **28**, 3328, 1989.

61. J. Lisowski; L. L. Grazynski and L. Szterenberg, *Inorg. Chem.*, **31**, 1933, 1992.

62. P.J. Chimelewski and L. Latos-Grazynski, *Inorg. Chem.*, **31**, 5231, 1992.

53(a) G.N. La Mar; W.D. Horrocks, Jr.; R.H. Holm, In: "NMR of Paramagnetic Molecules", ed. W.D. Horrocks, Jr. (Academic Press: New York, 1973) Chapter 4, p. 172.

(b) W.D. Horrocks,Jr. and D.L. Johnson, Jr.; *Inorg. Chem.*, **10** 1835, 1971.

64(a) D. Laneon; P. Cocolios; R. Guilard and K.M. Kadish, *J. Am. Chem. Soc.*, **106**, 4472, 1984.

(b) A.L. Balch; G.N. La Mar; L. L. Grazynski and M.W. Renner, *Inorg. Chem.*, **24**, 2432, 1985.

65. A.L. Balch; Y.W. Chen; M.M. Olmstead and M.W. Renner, *J. Am. Chem. Soc.*, **105**, 2393, 1985.

66(a) D. Mansuy; I. Morgenstern-Badaran; M. Lange and P. Gans, *Inorg. Chem.*, **21**, 1427, 1982.

(b) H.J. Callot; B. Chevrier and R. Weiss, *J. Am. Chem. Soc.*, **100**, 1324, 1978.

67(a) S. Saito and H.A. Itano, *Proc. Natl. Acad. Sci., USA*, **78**, 5508, 1981.

(b) G. Augusto; K.L. Kunze and P.R. Ortiz de Montellano, *J. Biol. Chem.*, **257**, 6231, 1982.

68(a) L. L. Grazynski; R.J. Cheng; G.N. La Mar and A.L. Balch, *J. Am. Chem. Soc.*, **103**, 4200, 1981.

(b) B. Chevrier; R. Weiss; M. Lange; J.C. Chottard and D. Mansuy, *J. Am. Chem. Soc.*, **103**, 2899, 1981.

69. D. Kuila; A.B. Kopelove and D.K. Lavallee, *Inorg. Chem.*, **24**, 1445, 1985.

70. J. Lisowski; M. Grzeszczuk and L. L. Grazynski, *Inorganica Chimca Acta*, **161**, 153, 1989.

71. K. Drabent; L.L. Grazynski and A. Wyslouch (unpublished results).

72(a) Vogel's Text Book of Practical Organic Chemistry, ed. B.S. Furniss (ELBS and Longman, Fourth edition, 1978) Chapter-2.

(b) A. Weissberger; E.S. Proskaner; J.A. Riddick; E.F. Toppos Jr., "Organic Solvents in Techniques of Organic Chemistry", Vol. IV (Third Edition, Inc. N.Y., 1970).

73. R.G. Little, *J. Heterocyclic Chem.*, **15**, 203, 1978.

74. H. Levanon and S.I. Weissman, *J. Am. Chem. Soc.*, **93**, 4309, 1971.

75. H. Levanon and J.R. Norris, *Chem. Rev.* **78**, 185, 1975.

76. H. Van Willigen; M. Vuolle and K.P. Dinse, *J. Phys. Chem.*, **93**, 2441, 1989.

77. P.G. Seybold and M. Gouterman, *J. Mol. Spectrosc.*, **31**, 1, 1969..

78. J.B. Birks and D.J. Dyson, *Proc. Roy. Soc. (London)*, **A275**, 135, 1963.

79. S.J. Strickler and R.A. Berg, *J. Chem. Phys.*, **37**, 814, 1962.

80. V. Balzani; F. Bolletta; M.T. Gandolfi and M. Maestri, *Topics in Current Chemistry*, **75**, 1, 1978.

81. D.F. Evans, *J. Chem. Soc.*, 2003, 1959.

82. W.Gerger; U. Mayer and V. Gutmann; *Monatsh. Chem.*, **108**, 417, 1977.

83. M. Gouterman, *J. Mol. Spectros.*, **6**, 138, 1961.

84. A. Stone and E.B. Fleischer, *J. Am. Chem. Soc.* **90**, 2735,

1968.

85. C.B. Storm and Y. Teklu, *J. Am. Chem. Soc.*, **94**, 1745, 1972.

86 A. Ulman; J. Manassen; F. Frolow and D. Rabinovich, *Inorg. Chem.*, **20**, 1987, 1981.

87(a) J.H. Fuhrhop; K.M. Kadish and D.G. Davis, *J. Am. Chem. Soc.*, **95**, 5140, 1973.

(b) K.M. Kadish and M.M. Morrison, *J. Am. Chem. Soc.*, **98**, 3326, 1976.

88. X.Y.Li; R.S. Czernuszewicz; J.R. Kincaid; O. Su and T.G. Spiro, *J. Phys. Chem.*, **94**, 31, 1990.

89(a) T. Kitagawa and Y. Ozaki, *Struct. Bond.*, **64**, 71, 1984.

(b) R.S. Czernuszewicz; K.A. Macor; X.Y. Li; J.R. Kincaid and T.G. Spiro, *J. Am. Chem. Soc.*, **111**, 3860, 1989.

90. T. Kitagawa; H. Ogoshi; Ellichinwatanabe and Z. Ichiyoshida, *J. Phys. Chem.*, **79**, 2629, 1975.

91(a) J.A. Shelnutt; K. Alston; E.W. Findsen; M.R. Ondrias, and J.M. Rifkind, *ACS Symposium Series*, **321**, 232, 1986.

(b) D. Kim; Lisamillar; O. Su; J. Terner and T.G. Spiro, *ACS Symposium Series*, **321**, 248, 1986.

92. *T.G.* Spiro; J.D. Stong and P. Stein, *J. Am. Chem. Soc.*, **101**, 2648, 1979.

93(a) J.M. Burka; J.R. Kincaid and T.G. Spiro, *J. Am. Chem. Soc.*, **100**, 6077, 1978.

(b) W.H. Fuchsman; Q.R. Smith and M.M. Stein, *J. Am. Chem. Soc.*, **99**, 4190, 1977.

(c) M. Kozuka and M. Iwaizumi, *Bull. Chem. Soc., Japan*, **56**, 3165, 1983.

(d) G.S.S. Saini; N.K. Chaudhury and A.L. Verma, *Photochem. Photobiol.*, **55**, 815, 1992.

94(a) H. Kashiwagi and S. Obara, *Int. J. of Quantum Chem.*, **20**, 843, 1981.

(b) D.Spangler; G.M. Maggiora; L.L. Shipmen and R.E. Christoffersen, *J. Am. Chem. Soc.*, **99**, 7470, 1977.

(c) D.Spangler; G.M. Maggiora; L.L. Shipmen and R.E. Christoffersen, *J. Am. Chem. Soc.*, **99**, 7478, 1977.

95. W.A. Oertling; A. Salehi; Y.C. Chung; G.E. Lerorn; C.K. Chang and G.T. Babcock, *J. Phys. Chem.*, **91**, 5887, 1987.

96. M. Gouterman, "The Porphyrins",Vol. III, ed. D. Dolphin (Academic Press, New York, 1978), Chapter 1, p. 1.

97. C.A. Hutchison, Jr., in "The Triplet State", ed. A.B. Zahlan, (Cambridge University Press, New York, 1967), p. 63.

98. A.M.P. Goncalves and R.P. Burgner, *J. Chem. Phys.*, **61**, 2975, 1974.

99. S.D. McGlynn; J. Azumi and M. Kinoshita, "Molecular Spectroscopy of the Triplet State" (Prentice-Hall, Englewood

Cliffs, N.J., 1969).

100. M.A. El-Sayeed and S. Siegel, *J. Chem. Phys.*, **44**, 1416, 1966.

101. S. Siegel and H.S. Judeikis, *J. Phys. Chem.*, **70**, 2205, 1966.

102(a) E. L. Frankevich; A.I. Pristupa and V.I. Lesin, *Chem. Phys. Lett.*, **47**, 304, 1977.

(b) S.S. Kim and S.I. Weissman, *J. Mag. Reson.*, **24**, 167, 1976.

103. S.I. Weissman, *J. Chem. Phys.*, **29**, 1189, 1958.

104. H. Levanon, in: "Multiple Electronic Resonance", eds. M. Dorio and J.H. Freed (Plenum, New York, 1978), Chapter 13.

105. N.M. Atherton, in: "Electron Spin Resonance: Theory and Applications" (Wiley, New York, 1973), p. 158.

106. K.H. Hausser and H.C. Wolf, *Adv. Magn. Reson.*, **8**, 85, 1976.

107. H. Levanon and S.I. Weissman, *Isr. J. Chem.*, **10**, 1, 1972.

108(a) *P.* L. Dutton; J.S. Leigh and M. Seibert, *Biochem. Bio. Phys. Res. Comm.*, **46**, 406, 1972.

(b) P.L. Dutton; J.S. Leigh and D.W. Reed. *Biochim. Biophy. Acta,* **292**, 654, 1973.

(c) C.A. Wraight; J.S. Leigh; P.L. Dutton and R.K. Clayton, *Biochim. Biophys. Acta,* **333**, 401, 1974.

109(a) R.A. Uphaus; J.R. Norris and J.J. Katz, *Biochim. Biophys. Res. Comm.*, **61**, 1057, 1974.

(b) R. Norris; R.A. Uphaus and J.J. Katz, *Chem. Phys. Lett.*, **31**, 157, 1975.

110(a) T.J. Schaafsma; J.F. Kleibenka; R.J. Plantenkamp and P. Geerso,in: Proceedings of the 12th European Congress on Molecular Spectroscopy, eds. M. Grossman, S.G. Elkmoss and J. Kingeissen (Elsevier, Amsterdam, 1976), p. 491.

(b) J.F. Kleibenkar; R.J. Plantenkamp and T.J. Schaafasma, *Chem. Phys. Lett.*, **41**, 557, 1976.

111. M.C. Thurnauer; J.J. Katz and J.R. Norris, *Proc. Natl. Acad. Sci., U.S.A.* **72**, 3270, 1975.

112. H. Levanon and A. Wolberg, *Chem. Phys. Lett.*, **24**, 96, 1974.

113. J.H. Van der Waals; W.G. VanDorp and T.J. Schaafsma in: The Porphyrins, Vol. 4, ed. D. Dolphin (Academic Press, New York, 1979), p. 257.

114. A.M. P. Goncalves and R.P. Burgner, *J. Chem. Phy.* **65**, 1976, 1221.

115(a) H. Levanon and S. Vega, *J. Chem. Phys.* **61**, 2265, 1974.

(b) J.F. Kleibeuker and T.J. Schaafsma, *Chem. Phys. Lett.*, **29**, 1974, 116.

116(a) H. Sixl and M. Schwoerer, *Z. Naturforsch*, **24a**, 952, 1969.

(b) H. Sixl and M. Schwoerer, *Z. Naturforsch*, **25a**, 1383, 1970.

117. A.M. P. Goncalves and W.U. Spendel, *Chem. Phys. Lett.*, **54**, 1978, 611.

118. M.K. Bowman, *Chem. Phys. Lett.*, **48**, 17, 1977.

119. A.M.P. Goncalves and R. P. Burgner, *J. Chem. Phys.*, **60**, 2942, 1974.

120. Z.P. Gribova and L.P. Kayushin, *Russian Chem. Rev.* **41**, 1221, 1974.

121(a) A. Regev; S. Michaeli; H. Levanon; M. Cyr and J.L. Sessler, *J. Phys. Chem.*, **95**, 9121, 1991.

(b) H. Levanon; A. Regev; S. Michaeli; T. Galili; M. Cyr and J.L. Sessler, *Chem. Phys. Lett.*, **174**, 235, 1990.

122 R.H. Clarke; R.E. Connors; T.J. Schaafsma; J.F. Kleibeuker and R.J. Platenkamp, *J. Am. Chem. Soc.*, **98**, 3674, 1976.

123(a) P. Hambright, *Coordination Chem. Rev.*, **6**, 247, 1971.

(b) M. Krishnamurthy; J.R. Sutter and P. Hambright, *J. Chem. Soc., Chem. Comm.*, 13, 1975.

124. J.R. Darwent; P. Douglas; A. Harriman; G. Porter and M.L. Richoux, *Coordination Chem. Rev.*, **44**, 83, 1982.

125. G.R. Seely, *Photochem. Photobiol.*, **27**, 639, 1978.

126. D. Holten; M. Gouterman; W.W. Parson; M.W. Windsor and M.G. Rockley, *Photochem. Photobiol.*, **23**, 415, 1976.

127 M. Gouterman and D. Holten, *Photochem. Photobiol.*, **25**, 85, 1977.

128. D. Holten; M.W. Windsor; W.W. Parson and M. Gouterman, *Photochem. Photobiol.*, **28**, 951, 1978.

129. K. Kalyanasundaram and M. Gratzel, *Helv. Chim. Acta.*, **63**, 478, 1980.

130. G. McLendon and D.S. Miller, *J. Chem. Soc. Chem. Comm.*, 533, 1980.

131. A. Harriman; G. Porter and M.C. Richoux, *J. Chem. Soc Faraday Trans. 2*, **77**, 833, 1981.

132 E.B. Fleischer; J.M. Palmer; T.S. Srivastava and A. Chatterjee, *J. Am. Chem. Soc.*, **93**, 3162, 1971.

133. M. Guldi; P. Neta; P. Hambright and R. Rahimi, *Inorg. Chem.*, **31**, 4849, 1992.

134. L.L. Grazynski and A. Jezierski, *Inorganica Chimica Acta*, **106**, 13,1985.

135. L.L. Grazynski, *Inorg. Chem.*, **24**, 1681, 1985.

136. R.F. Pasternack; P.R. Huber; P. Boyd; G. Engasser; L. Francesconi; E. Gibbs; P. Fasella; G. Cerio Venturo and L. dec. Hinds, *J. Am. Chem. Soc.*, **94**, 4511, 1972.

137. R.F. Pasternack; L. Francesconi; D. Raff and E. Spiro, *Inorg.Chem.*, **12**, 2606, 1973.

138. M. Ravikanth; D. Reddy and T.K. Chandrashekar, *J. Chem. Soc. Dalton Trans.*, 2103, 1991.

139. N. Kobayashi and A.B.P. Lever, *J. Am. Chem. Soc.*, **109**, 7433, 1987.

140(a) J.K.M. Sanders, *J. Am. Chem. Soc.*, **112**, 5525, 1990.

(b) A. Warshel, *J. Am. Chem. Soc.*, **101**, 744, 1979.

141. V. Thanabal and V. Krishnan, *Inorg. Chem.*, **21**, 3606, 1982.

142. P. Worthington; P. Hambright; R.F.X. Williams; J. Reid; C. Burnham; A. Shamim; J. Turay; D.M. Bell; R. Kirkland; R.G. Little; N. Datta Gupta and V. Eisner, *J. Inorg. Bio Chem.*, **12**, 281, 1980.

143 K. Kalyanasundaram and N. Spallart, *J. Phys. Chem.*, **86**, 5163, 1982.

144. K.M. Kadish; D. Sazou; Y.M. Liu; A. Saoibi; M. Ferhat and R. Guilard, *Inorg. Chem.*, **27**, 1198, 1988.

145. P. Chimelewski; M. Grzeszczuk; L.L. Grazynski and J. Lisowski, *Inorg. Chem.*, **28**, 3546, 1989.

146. A.L. Balch; Y.W. Chan and M.M. Olmstead, *J. Am. Chem. Soc.*, **107**, 6510, 1987.

147. W.R. Scheidt, in : The Porphyrins", Vol. 3, ed. by D. Dolphin (Academic Press, New York, 1978), Chapter 10.

148 O. Ohno; Y. Kaizu and H. Kobayashi, *J. Chem. Phys.*, **82**, 1779, 1985.

149. T. K. Chandrashekar; H. Van Willigen and M.H. Ebersole, *J. Phys. Chem.*, **88**, 4326, 1984; *ibid,* **89**, 3453, 1985.

150(a) T.K. Chandrashekar and H. Van Willigen, *Chem. Phys. Lett.*, **106**, 237, 1984.

(b) H. Van Willigen; T.K. Chandrashekar; U. Das and M.H. Ebersole, *Am. Chem. Soc. Sym. Ser.*, **321**, 140, 1985.

151(a) J.S. Leigh and P.L. Dutton, *Biochim. Biophys. Acta*, **357**, 67, 1974.

(b) M.C. Thurnauer and J.R. Norris, *Chem. Phys. Lett.*, **47**, 100, 1977.

152(a) K.J. Kaufmann and M.R. Wasielewski, *Advan. Chem. Phys.* **47**, 579, 1981.

(b) R.E. Overfield; A. Schenz; K.J. Kaufmann and M.R. Wasielewski, *J. Am. Chem. Soc.*, **105**, 4256; 5747, 1983.

153. J.J. Katz; J.R. Norris; L.L. Shipman; M.C. Thurnauer and M.A. Wasielewski, *Ann. Rev. Biophys. Bioengg.*, **7**,393,1976.

154. *W.W.* Parson R.J.and Cogdell, *Biochem. Biophys. Acta.*,**416**, 105, 1975.

155. J.A. Norris; R. A. Uphaus; H.L. Crespi and J.J Katz, *Proc. Natl.Acad. Sci., U.S.A.*, **68**, 1971, 625.

156. A.J. Hoff and H.G. Devries, *Biochem. Biophys. Acta*, **503**, 94, 1978.

157. L.N.M. Duysens; W.J. Huiskamp; J.J. Vos and J.M. Van der Hart, *Biochem. Biophys. Acta,* **19**, 188, 1956.

158. J.C. Goedheer and Brookhaven, *Symps. Biol.*, **11**, 325,1958.

159. J.H. Fuhrhop and D. Mauzerall, *J. Am. Chem. Soc.*, **91**, 4174, 1969.

160. Photophysics of Aromatic Molecules, ed. J.B. Birks (Wiley Interscience, New York, 1970), p. 518.

161(a) F.P. Schwartz; M. Gouterman; Z. Muljiani and D.H. Dolphin, *Bioorg. Chem.*, **2**, 1, 1972.

(b) J.A.Anton; P.A. Loach and Govindjee, *Photochem. Photobiol.*, **28**, 235, 1978.

162. J.C. Mialocq; C. Giannotti; P. Maillard and M. Momenteau, *Chem. Phys. Lett.*,**112**, 87, 1984.

163(a) L. Benthem, *Ph.D. Thesis*, Agricultural University, Wageningen, 1984.

(b) L. Benthem; R.B.M. Koehorst and T.J. Schaafsma, *Magn. Reson. Chem.*, **23**, 732,1985.

164 R.L. Brookfield; H. Ellul; A. Harriman and G. Porter, *J. Chem. Soc., Faraday Trans. 2*, **82**, 219, 1986.

165. S.C. Noblat; J.P. Sauvage and P. Mathis, *Angew. Chem, Int. Ed. Engl.*, **28**, 593, 1989.

166. O. Ohno; Y. Ogasawara; M. Asano; Y. Kajii; Y.Kaizu; K. Obi and H. Kobayashi, *J. Phys. Chem.*, **91**, 4269, 1987.

167. K.M. Kadish in "Progress in Inorganic Chemistry", Vol-XXXIV, ed. Lippard (Johnwiley Interscience, New York, 1988).

168. J. Y. Becker; D. Dolphin; J.B. Paine and T. Wijesekera, *J. Electroanal. Chem.*, **164**, 335, 1984.

169(a) A.M. Stolzenberg and M.T. Stershic, *Inorg. Chem.*, **26**, 3082, 1987.

(b) A.M. Stolzenberg and M.T. Stershic, *J. Am. Chem. Soc.*, **110**, 6391, 1988.

List of Publications

Most of the work reported in this thesis has been published in the following Journals:

(1) Spectroscopic studies on monomers and dimers of thiaporphyrins.

Proc. Indian Acad. Sci. (Chem. Sci.), **102**, 307, 1990.

(2) Photoexcited Triplet ESR studies on water soluble thiaporphyrins.

Chem. Phys. Lett., **198**, 163, 1991.

(3) Photoexcited Triplet ESR studies on thiaporphyrins and their protonated derivatives.

Chem. Phys. Lett., **202**, 127, 1993.

(4) Water soluble thiaporphyrins and Metallothiaporphyrins: Synthesis, characterization, ground and excited state properties.

J. Chem. Soc. Dalton Trans., 119, 1993.

(5) Excited state properties of thiaporphyrins and their dications

J. Chem. Soc. Faraday Trans., **89**, 677, 1993.

(6)* Non-metal porphyrins - Reactions of PCl_3, $POCl_3$ and $PhPOCl_2$ with tetraphenyl porphyrin: Spectroscopic and electrochemical studies

Ind. J. Chem., **30A**, 579, 1991.

(7) A novel diporphyrin with N_4, N_3S cores; Synthesis, characterization, ground and excited state properties

Communicated, 1993.

* This work is not included in the thesis.